Universität Rostock Traditio et Innovatio

Characterization and Utilization of Zinc-based Ring-Opening-Polymerization Catalysts

Dissertation

zur

Erlangung des akademischen Grades

doctor rerum naturalium (Dr. rer. nat.)

der Mathematisch-Naturwissenschaftlichen Fakultät

der Universität Rostock

vorgelegt von **Lea Rebecca Grefe**,

geb. am 21.10.1993 in Uelzen

Rostock, 2023

https://doi.org/10.18453/rosdok_id00005044

Die vorliegende Arbeit wurde in der Zeit von Oktober 2018 bis Dezember 2021 am Leibniz Institut für Katalyse an der Universität Rostock unter der Betreuung von Prof. Dr. Udo Kragl angefertigt.

1. Gutachter: Prof. Dr. Udo Kragl, Universität Rostock, Institut für Chemie

2. Gutachter: Prof. Dr. Thomas Werner, Universität Paderborn, Department Chemie

Jahr der Einreichung: 2023

Datum der Verteidigung: 20.06.2023

Erklärung

1. Die Gelegenheit zum vorliegenden Promotionsvorhaben ist mir nicht kommerziell vermittelt worden. Insbesondere habe ich keine Organisation eingeschaltet, die gegen Entgelt Betreuerinnen/Betreuer für die Anfertigung von Dissertationen sucht oder die mir obliegenden Pflichten hinsichtlich der Prüfungsleistungen für mich ganz oder teilweise erledigt.

2. Ich versichere hiermit an Eides statt, dass ich die vorliegende Arbeit selbstständig angefertigt und ohne fremde Hilfe verfasst habe. Dazu habe ich keine außer den von mir angegebenen Hilfsmitteln und Quellen verwendet und die den benutzten Werken inhaltlich und wörtlich entnommenen Stellen habe ich als solche kenntlich gemacht.

Düsseldorf, den …….. ……

Lea Rebecca Grefe

Abstract

The present work focusses on zinc-based heterogeneous catalysts for the polymerization of epoxides. The sum formula of the catalyst and the effects of the complexing agents on the structure were determined. Next to this the structure of the active site and the polymerization mechanism of the epoxide homopolymerization of the catalyst was proposed based on a comprehensive analysis. Additionally, a heterogeneous catalyst was used to prepare novel homotelechelic diol copolymers. This catalyst was also shown for the first time to be active in the terpolymerization of epoxides, cyclic esters, and CO_2 without the need of initiators, cocatalysts or quenching.

Inspired by this knowledge, molecular zinc-based catalysts were prepared, characterized, and tested for their catalytic activity in (co)polymerizations of epoxides, cyclic esters, and CO_2. These molecular catalysts were shown to be of high activity in the ring-opening-polymerization of *rac*-lactide.

Kurzzusammenfassung

Die vorliegende Arbeit befasst sich mit zinkbasierten heterogenen Katalysatoren für die Polymerisation von Epoxiden. Die Summenformel des Katalysators wurde ermittelt und der Effekt der eingesetzten Komplexbildner auf dessen Beschaffenheit untersucht. Neben diesem wurde basierend auf umfassenden Analysen ein Vorschlag zur Struktur des aktiven Zentrums und zum Mechanismus der Homopolymerisation von Epoxiden durch den Katalysator erarbeitet. Überdies wurden neuartige homotelechelische Diol-Copolymere mit diesem Katalysator hergestellt. Der Katalysator erwies sich ebenfalls erstmalig als aktiv in Terpolymerisationen von Epoxiden, cyclischen Estern und CO_2 ohne Bedarf an Initiatoren, Co-Katalysatoren oder Quenching.

Auf Basis des erlangten Wissens wurden molekulare zinkbasierte Katalysatoren synthetisiert, charakterisiert und auf ihre Aktivität in der (Co-)Polymerisation von Epoxiden, CO_2 und cyclischen Estern getestet. Besonders hohe Aktivität zeigten diese Katalysatoren in der ringöffnenden Polymerisation von racemischem Lactid.

Danksagung

An dieser Stelle möchte ich mich bei allen bedanken, die mich während meiner Promotion begleitet und unterstützt haben.

Mein besonderer Dank gilt Prof. Dr. Udo Kragl, der mich zum Masterstudium in seine Arbeitsgruppe aufgenommen hat und mich auch in der darauffolgenden Promotion sehr gut beraten und begleitet hat. Prof. Kragl fand trotz vollem Kalender immer eine Möglichkeit sich meinen Fragen und Problemen anzunehmen und erarbeitete mit mir stets eine Lösung, die im Sinne meiner beruflichen, aber auch persönlichen Weiterentwicklung war.

Prof. Dr. Thomas Werner möchte ich für die Übernahme des Zweitgutachtens danken.

Großer Dank gebührt ebenfalls Dr. habil. Esteban Mejía für die fachliche und zwischenmenschliche Unterstützung meiner Promotion und die vielen Herausforderungen, vor die er mich über die Jahre gestellt hat. Esteban hat mir stets zur Seite gestanden, aber auch gewusst, welche Kämpfe ich allein kämpfen muss, um zu wachsen.

Ich danke ebenfalls der Henkel AG und Co. KGaA für ein Promotionsthema mit industrieller Anwendung und dessen Finanzierung. Die vielen Diskussionen und Anregungen durch meine Kooperationspartner Dr. Jan-Erik Damke, Dr. Ligang Zhao und Dr. Johann Klein haben mich sehr gut auf meinen weiteren beruflichen Werdegang vorbereitet und meine Vorstellung davon, was für eine Chemikerin ich sein will, geformt. Großer Dank gilt ebenfalls Dr. Marc Hamm für die Unterstützung der Modellrechnungen und die fruchtbaren Diskussionen. Nicht zuletzt möchte ich mich auch bei Dr. Kang Wei Chou und Dr. Clara Anduix für ihre großartige Unterstützung bei meinem Besuch des Henkel-Labors am ALBA Synchrotron Barcelona bedanken.

Für die Anfertigung unzähliger Analysen bedanke ich mich bei der Analytik-Abteilung des LIKATs und der Analytik der AG Kragl. Ebenfalls danke ich der Arbeitsgruppe von Professor Corzilius für die Festkörper-NMR Messungen, Dr. Stephan Bartling für die XPS-Messungen, Dr. Kevin Oldenburg für die TEM-Messungen, Dr. Dirk Michalik für die DOSY NMR, dem Institut für Gerätesysteme und Schaltungstechnik und Dr.-Ing. Fred Lange für die Möglichkeit REM-Aufnahmen anzufertigen und Dr. Anke Spannenberg für die Einkristallstrukturanalyse. Mein Dank gilt auch Herrn Hutter für die schnelle Lösung jeglichen technischen Problems.

Ich danke den aktuellen und ehemaligen Mitgliedern der Arbeitsgruppe Polymerchemie & Katalyse, besonders Niklas, Paul, Nayereh, Felix und Abel, für die freundschaftliche Atmosphäre und den Zusammenhalt. Meinen Student*innen Leo Gräber, Wilko Fokken, Laura Kraußer, Yannik Thaens und Joshua Meinshausen danke ich für ihre tatkräftige Unterstützung. Prof. Hung Huy Nguyen and Angél Andres Castro Ruiz danke ich für die jeweils gute Kooperation auf dem Feld der homogenen Katalyse.

Ich möchte mich bei meiner Familie für die Unterstützung meines Studiums und der Promotion bedanken. Danke an meine Freund*innen, insbesondere den Chor Celebrate, die Power-Gang und Juri für die tollen Unternehmungen und die dringend benötigte Ablenkung von der Promotion. Danke Mareike für den allwöchentlichen Frittwoch!

Danke Mama, Papa und Gordon. Danke Mareike N und Robert. Danke Mareike H und danke Niklas. Danke, dass ihr für mich da wart und seid. Ohne Euch hätte ich diese Arbeit vielleicht niemals fertig schreiben können.

»If you base medicine on science, you cure people.
If you base the design of planes on science, they fly.
If you base the design of rockets on science, they reach the moon.
*It works... b*tches.«*

Richard Dawkins

Table of Contents

List of Abbreviations

AC	atomic concentration
AMM	activated monomer mechanism
ATR	attenuated total reflection
BE	bond energy
CA	complexing agent
CHO	cyclohexene oxide
co-CA	co-complexing agent
COSY	correlated spectroscopy (NMR)
CP	copolymer
CTA	chain transfer agent
D_3	hexamethylcyclotrisiloxane
D_4	octamethylcyclotrisiloxane
DFT	density-functional theory
DMC	double metal cyanide (catalyst)
DNA	deoxyribonucleic acid
DNP-SENS	dynamic nuclear polarization surface enhanced NMR spectroscopy
DOSY	diffusion ordered spectroscopy (NMR)
EA	elemental analysis
ED	electron density
EDX	energy dispersive X-ray
EO	ethylene oxide
ESI-MS	electrospray ionization mass spectrometry
EXAFS	extended X-ray absorption fine structure
FTIR	Fourier-transform infrared
GC	gas chromatography
GPC	gel permeation chromatography
HMBC	heteronuclear multiple bond correlation (NMR)
HPLC	high performance liquid chromatography
IR	infrared
IUPAC	International Union of Pure and Applied Chemistry
$L_{NN}1$	2,6-dipicolinoylbis(N,N-diethylthiourea) ligand
$L_{NN}2$	2,6-bis(acetobenzoyl)pyridine ligand
MALDI-MS	matrix assisted laser desorption/ionization mass spectrometry
MAS	magic angle spinning (NMR)
M_n	number average molecular weight
M_w	weight average molecular weight
MWD	molecular weight distribution
N/S	not significant
NMR	nuclear magnetic resonance
NOESY	nuclear overhauser enhancement and exchange spectroscopy (NMR)
PCHCCL	polycyclohexene carbonate polycaprolactone
PCHCLA	polycyclohexene carbonate polylactic acid
PDI	polydispersity index
PDMS	polydimethylsiloxane
PEG	polyethylene glycol
PLA	polylactic acid
PO	propylene oxide
PPCCL	polypropylene carbonate polycaprolactone
PPCLA	polypropylene carbonate polylactic acid
PPG	polypropylene glycol
PPG-CL	polypropylene glycol polycaprolactone
PPG-PLA	polypropylene glycol polylactic acid
ppm	parts per million
PPNCl	μ-Nitrido-bis(triphenylphosphan)-chlorid
PPO	polypropylene oxide
ROCOP	ring-opening-copolymerization
ROP	ring-opening-polymerization
SEM	scanning electron microscopy
SR-XRPD	synchrotron radiation X-ray powder diffraction
TEM	transmission electron microscopy
T_G	glass transition temperature
t_{ind}	induction time
TOF	turnover frequency
TPP-AlCl	(5,10,15,20-tetraphenylporphinato)aluminum chloride
wt	weight
XANES	X-Ray absorption near edge structure
XAS	X-ray absorption spectroscopy
XPS	X-ray photoelectron spectroscopy
XRPD	X-ray powder diffraction
ε-CL	ε-caprolactone

Index of Tables

Index of Figures

1 Introduction

Polyether polyols are a well-known class of polymers with high industrial demand. They are mainly used as building blocks in polyurethanes which find applications in insulation material, coatings, adhesives, and sealants but can also be found in household products, furniture, personal care products or the medicinal sector.[1-4] Within the polyurethane market that was worth 70.67 billion US$ in 2020, approximately 60 % of the products were covered by polyols in 2016.[1,4]

One typically used polyether polyol in adhesive products is polypropylene glycol (PPG) produced from propylene oxide (PO). Importantly, the conventionally used anionic ring-opening-polymerization of propylene oxide is accompanied by undesired reactions leading to unsaturated side products. Therefore, the PPG production is facing an upper limit in molecular weight of the polymers.[3] In conclusion, it is of great interest to produce high quality polyether polyols, especially PPG with narrow polydispersity index and high molecular weight in a controlled manner.

Double metal cyanide (DMC) complexes are a family of heterogeneous catalysts used for the ring-opening-polymerization (ROP) of epoxides (Figure 1**a**), especially propylene oxide. They were first described in a patent by General Tire and Rubber in 1966.[5-7] Later, the catalysts were also found to be active in the copolymerization of epoxide/CO_2 in industry labs (Figure 1**b**),[8] before academic research was started in the early 2000s by Chen *et al*.[9]

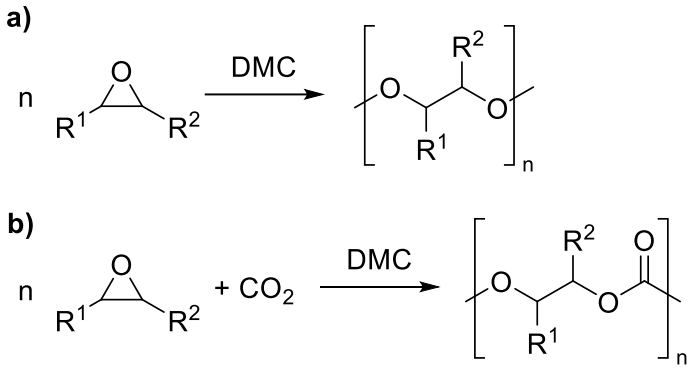

Figure 1: Homopolymerization of epoxides (**a**) and copolymerization of epoxides and CO_2 (**b**) with DMC catalysts.

Compared to the typically used basic catalyst for the ROP of epoxides (i.e. KOH), DMC catalysts allow for the reduction of purification steps, due to their high activity and low formation of unsaturated side products. The small amount of DMC catalyst that is needed for the polymerization of propylene oxide (15-50 ppm) can stay in the polymer and therefore no residual metal salt has to be removed.[10-12] Next to this, the polyethers that are produced using DMC catalysts rather than KOH show an improvement in performance of the polyurethane elastomers manufactured with them.[13]

In the copolymerization of epoxides and CO_2, DMC catalysts allow for the incorporation of polyether blocks within the copolymers. This leads to a lower glass transition temperature (T_G) in comparison to strictly alternating copolymers obtained with zinc dicarboxylates or molecular catalysts.[14-15] These low T_G polyether carbonates can be used to replace polyether polyols in polyurethane production to obtain polymers with lower petrochemical content, which is desirable regarding the current climate crisis.[16]

Nevertheless, DMC catalyzed polymerization reactions have some challenging characteristics:

- The activity of the catalyst is highly dependent on the synthesis procedure and the reaction conditions during its preparation.[17-19]
- The polymerization reaction does not start immediately after the addition of monomer but shows an induction time.[11,20-21]
- To obtain a polymer with the desired molecular weight and a narrow molecular weight distribution (MWD) a chain transfer agent (CTA) has to be added to the reaction. The CTA is thus incorporated into the product and leads to longer induction times.[11,21-22]
- In epoxide/CO_2 copolymerizations the activity of the catalyst is lowered. The carbon content is not easily controllable and it is challenging to obtain high polycarbonate yields using propylene oxide as comonomer.[23]

2 Objective and Proposal

To conquer the challenges in the industrial production of polyethers mentioned above, an in-depth knowledge about the DMC catalyst's structure and the catalytic mechanism is needed. However, despite long years of research, there are still many open questions and ambiguities to resolve to be able to prepare the catalyst and perform the catalysis in a fully reproducible manner.

This thesis aims to elucidate the structure of DMC catalysts in order to better understand the effects of the chosen reactants on the catalytic activity. Solid state analyses will be used to elucidate the catalyst's bulk and surface structure and the influence that different metal centers, complexing agents and co-complexing agents have.

Next to this, mechanistic studies of a DMC catalyzed homopolymerization of propylene oxide will be performed. *In operando* monitoring of the polymerization and kinetic measurements will help to understand the polymerization reaction further. The aim of these studies is to shed light on the activation of the catalyst and its polymerization mechanism to enable future optimization towards the production of higher quality polyethers.

Moreover, the polyether-containing products need to be constantly developed towards higher performance, lower content in fossil derived carbon and biodegradability to stay competitive in

the market. Therefore, catalysts used in the polymer production need to be able to polymerize a wide range of monomers and comonomers. In this thesis a DMC catalyst will be evaluated towards its ability to copolymerize epoxides, especially propylene oxide, with cyclic siloxanes, cyclic esters, and CO_2 as comonomers.

Additionally, molecular catalysts will be prepared inspired by the results of the structural characterization of the DMC catalysts and tested for their catalytic activity in the ROP and ROCOP (ring-opening-copolymerization) of heterocyclic monomers.

This thesis proposal is shown schematically in Figure 2.

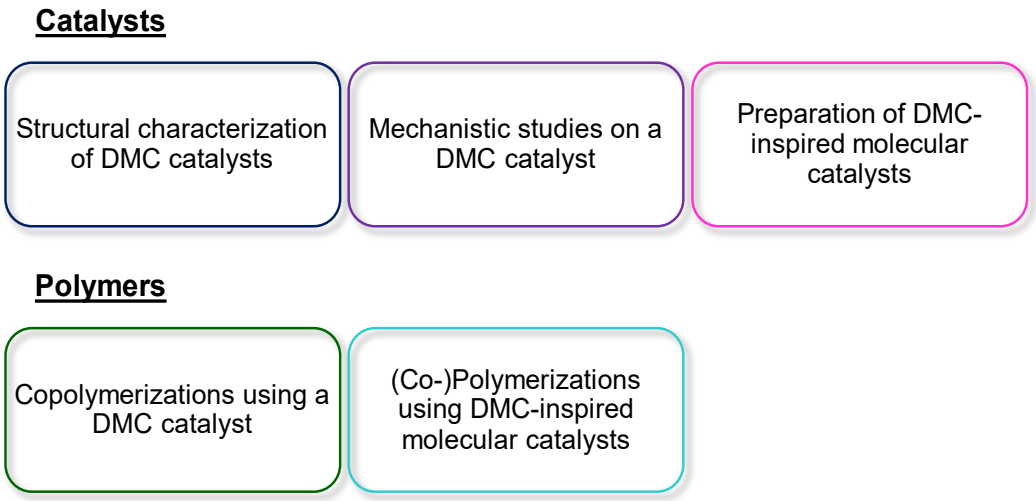

Figure 2: Schematic overview of the proposal of the thesis.

3 Theoretical Background

Polymers are a widely used class of material with special properties that find application in nearly every field. They range from natural macromolecules like cellulose, keratin, or proteins over ubiquitous synthetic polymers like polyolefins, nylon or silicones to specialty polymers designed for a specific application in e.g., the medicinal sector.

This broad application spectrum of polymers is due to their unique properties. Their high molecular weight, that ranges from hundreds to millions of Daltons, enables polymers to have special mechanical properties. Examples of these properties are elasticity, hardness, and tensile strength as well as broad-ranging physical properties that make them useful as thermal insulators or cooling media, electronic properties ranging from acting as an insulator to a conductor and even information storage properties e.g., DNA.[24-26]

Tailoring a polymer to its specific application, however, is only made possible by polymerization catalysis, which allows for cost efficient production of very defined and also complex polymers. In 1963 Karl Ziegler and Giulio Natta were awarded the Nobel Prize in chemistry for their development of metal-organic catalysts performing coordination polymerization of ethylene

and propylene in a controlled manner. Their invention laid the fundament for further catalysts that make the production of very defined polymers with controllable mechanistic properties at mild reaction conditions possible.[27]

3.1 Polyethers

After the first polyether – polyethylene oxide – was prepared using alkali metal hydroxide or zinc chloride by C. A. Wurtz in 1863,[28] H. Staudinger and O. Schweitzer performed several polymerizations of ethylene oxide of varying molecular weight in 1929.[29] These studies marked the start of the development of industrial processes to produce polyethylene glycol and later also polypropylene glycol polyethers.[3,10]

The first patents issued on this matter claim a reaction using various bases with alcoholates as initiators,[3,10] various halide salts,[30] or iron(III)oxide hydroxide[31] for the polymerization of propylene oxide.

Polypropylene oxide (PPO, Figure 3), which this thesis lays its main focus on, is a flexible polymer with glass transition temperatures around -70 °C. These polymers are often referred in industry to as polypropylene glycol (PPG), whereas in scientific literature a PPG is defined as a shorter chain PPO with molecular weights of up to 4000 g/mol.[32]

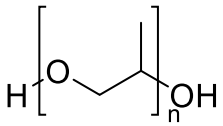

Figure 3: Polypropylene oxide

Due to the methyl group in the repeating unit, the polymer can show different stereo- and regioregularities. The PPG repeating unit can be found in either the (*R*)- or the (*S*)-conformation within the polymer. As exemplarily shown in Figure 4, a polymer is called “isotactic” if only one conformation can be found throughout the whole polymer chain, it is called “syndiotactic” if the (*R*)- and the (*S*)- conformation alternate, and it is “atactic” if the stereocenters are ordered randomly.[33]

Regarding the regioregularity of the PPG chain, the repeating units can be ordered in a head-to-head, tail-to-tail and a head-to-tail fashion as shown in Figure 5. In a regioirregular polymer chain these are randomly arranged.[34]

PPG is usually found in an atactic conformation when prepared from racemic monomer but can also be produced in an isotactic or syndiotactic conformation using stereoselective catalysts.[35-36] Whether the polymer is regioregular depends on the catalyst and type of polymerization reaction it is produced by.[32]

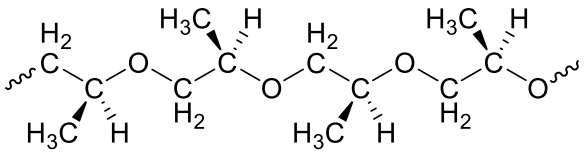

isotactic PPG

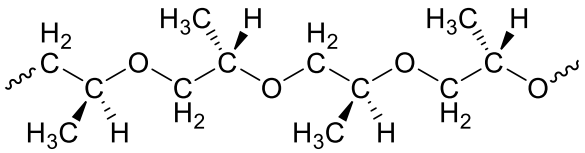

syndiotactic PPG

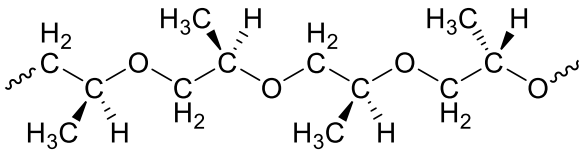

atactic PPG

Figure 4: Tacticity of PPG chains.

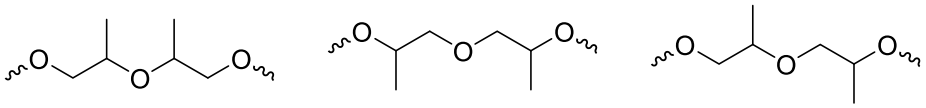

head-to-head tail-to-tail head-to-tail

Figure 5: Regioregularity of PPG chains.

3.2 Polymerization reactions

The different types of polymers can be either classified based on their structure or on the polymerization process they have been prepared by. Structure-based classifications divide polymers in homochains, with only identical atoms in the polymer chain, and heterochains, in which multiple elements can occur in the chain. Next to this, polymers can be structurally classified by their polydispersity index (PDI). The PDI is the quotient of the weight average molecular weight $\overline{M}_w$ and the number average molecular weight $\overline{M}_n$ of the obtained polymer (**Equation 1**). The number and weight average molecular weights are defined in **Equation 2** and **Equation 3**, respectively. In these definitions N_i is the number of molecules with the molecular weight M_i and N is the total number of molecules in the sample. A PDI of 1 depicts a monodisperse polymer. A polymer that is producible with a PDI close to the unit is generally regarded as being of higher quality due to a better control over the polymer's properties.[37]

$$\mathrm{PDI} = \frac{\bar{M}_w}{\bar{M}_n} \qquad \textbf{Equation 1}$$

$$\bar{M}_n = \frac{\sum N_i M_i}{\sum N_i} \qquad \textbf{Equation 2}$$

$$\bar{M}_w = \frac{\sum N_i M_i^2}{\sum N_i M_i} \qquad \textbf{Equation 3}$$

When classifying polymers by the polymerization process, the two main types of polymerization reactions considered are the addition polymerization and the condensation polymerization. In the addition polymerization the sum formula of the repeating unit of the polymer is the same as in the monomer whilst in condensation polymerization the sum formula differs between monomer and repeating unit.

Condensation polymerizations are oftentimes catalyzed, meaning the catalyst appears unchanged after running a full catalytic cycle. It is important to note that in polymerization reactions a full catalytic cycle usually is completed over the addition of one monomer to the polymeric chain and not over the full synthesis of the desired macromolecule. Addition polymerizations on the other hand are usually initiated and parts of the initiator become part of the polymer.[38] Despite this, initiators are commonly labeled as catalysts in literature covering polymerization reactions.

As shown in Figure 6, PPG can – in theory – be obtained via both polymerization routes. However, a polycondensation of propylene glycol to form PPG has not been successfully conducted to date. Diols with six or less methylene units were observed to intra-condensate under ring-formation rather than inter-condensate with other diol molecules when presented to the catalytic conditions necessary for self-condensation.[39-40]

The addition polymerization of propylene oxide (PO) to form PPG is called ring-opening-polymerization (ROP). Due to the high ring-strain and polarization of the PO molecule, various initiators are able to perform the polymerization following different addition polymerization pathways. The different subtypes of the ROP of PO known to date are anionic ROP, cationic ROP, the activated monomer mechanism, and coordination polymerization.[3,10,41]

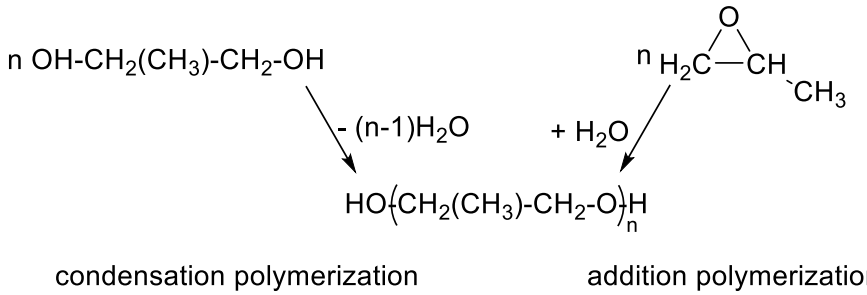

Figure 6: Theoretical polymerization pathways to obtain polypropylene glycol.[38]

3.2.1 Anionic ring-opening-polymerization

The anionic ring-opening-polymerization is characterized by the nucleophilic attack from an anionic initiator to the monomer. This happens under dissociation of the initiator and formation of an active polymer chain carrying a negative charge or strong polarization.[42-43]
Commonly, anionic ROP reactions are initiated by Brønsted or Lewis bases, e.g., alkali metals, phosphines, alcoholates or amines.[43] For the initiation of the anionic ROP of epoxides, alkali metal salts, especially those of sodium, potassium and cesium are the most used reactants. The initiator attacks the propylene oxide monomer selectively on the methylene carbon undergoing an S_N2 type mechanism, leading to PPG chains with only head-to-tail order.[44] As shown in Figure 7, the initiation is followed by the nucleophilic attack of the generated alkoxide on another PO molecule leading to chain elongation. This process is called propagation. Finally, the polymerization can be terminated by addition of an electrophilic compound. In order to control the molecular weight during the anionic ROP, water and other nucleophilic impurities have to be strictly excluded. This procedure can also be used to introduce functional terminal groups to the polymer.[43-44]

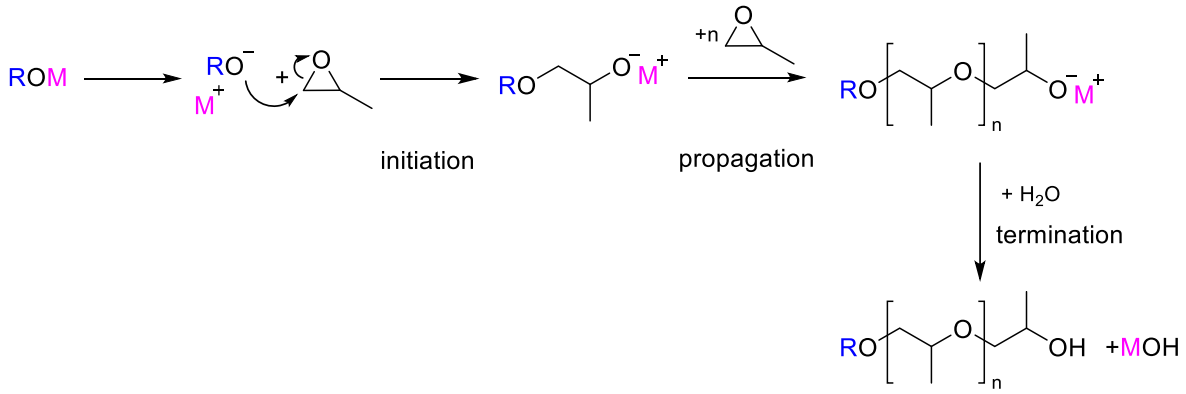

Figure 7: Anionic polymerization mechanism of propylene oxide.

The anionic polymerization of propylene oxide is limited to a maximum molecular weight of approx. 6000 g/mol due to the possible proton abstraction from the monomer by the propagating species. A chain transfer reaction to the PO monomer takes place (Figure 8).[10,44] This side reaction is influenced by the counterion M^+ and the frequency of its occurrence decreases in the order $Na^+ > K^+ > Cs^+$.[10,44] Because of its high toxicity, cesium is not used in the large scale polymerization of propylene oxide. This makes potassium hydroxide the most used initiator in the preparation of low molecular weight PPG in chemical industry. Additionally, crown ethers can be used to complex the counterion to obtain molecular weights up to 15000 g/mol due to the reduction of aggregates and a larger charge separation.[10,44]

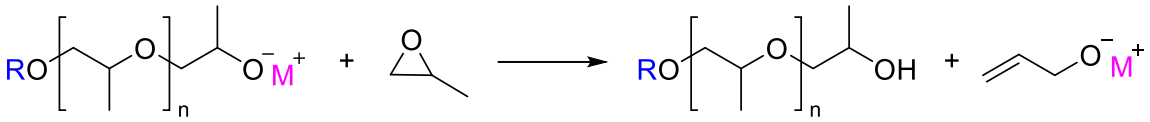

Figure 8: Proton abstraction of the methyl proton during the anionic ROP of PO.

An anionic ROP was the first reaction described as a “living polymerization” by Szwarc *et al.*[45-46] Living polymerizations do not self-terminate and can be revived after reaching the equilibrium monomer concentration by addition of fresh monomer. This leads, in theory, to all polymer chains growing simultaneously which allows for very narrow polydispersity indexes and therefore, very high quality polymers can be obtained.[43]

A living polymerization is defined as chain polymerization in which irreversible chain transfer and chain termination are not present.[47-48] Ideally, this type of polymerization shows a high initiation rate constant k_i compared to the propagation rate constant k_p (**Equation 4**) and the monomer conversion u equals approx. 1 (**Equation 5**).

$$k_i \gg k_p \qquad \textbf{Equation 4}$$

$$u = ([M]_0 - [M])/[M]_0 \approx 1 \qquad \textbf{Equation 5}$$

After early reports for anionic polymerizations, living polymerizations were also observed in pseudoanionic coordination polymerizations as well as cationic polymerizations and have been lately mainly reported for radical polymerizations.[47]

3.2.2 Cationic ring-opening-polymerization

Another type of ionic ROP is the cationic ROP, in which electrophiles act as initiators. Similar to the anionic polymerization, monomers that are able to undergo cationic ROP have polarized bonds with the addition that a lone pair of electrons is needed in order to be attacked by the initiator. Hence, olefins, ketones, aldehydes, cyclic ethers, lactones, and lactates are the most common monomers in cationic ROP; common initiators are found in the groups of Brønsted acids, Lewis acids, well-defined Lewis-acidic metal cations, carbenium salts, onium ions and photoinitiators.[41,43,49-50]

The growing polymer chain possesses a cationic center resulting from the nucleophilic attack on the initiator by the monomer (Figure 9). The mechanism of this nucleophilic attack is dependent on the stability of the cationic center. In case of a stabilization by electron donating neighbors, the S_N1 mechanism shown in Figure 9, characterized by a spontaneous ring-opening of the monomer after initiation, is dominant.[41,43] Otherwise, a second monomer attacks the initiated species to form the active polymer chain in the S_N2 mechanism. The propagation reaction proceeds via further nucleophilic attacks of the monomer on the growing

polymeric chain. Many cationic ROPs can be classified as living polymerizations when water and other nucleophilic impurities are excluded. Hence, termination of the polymerization needs to be induced by the addition of terminating agents, e.g. water, alcohols, amines or carboxylic acids.[49]

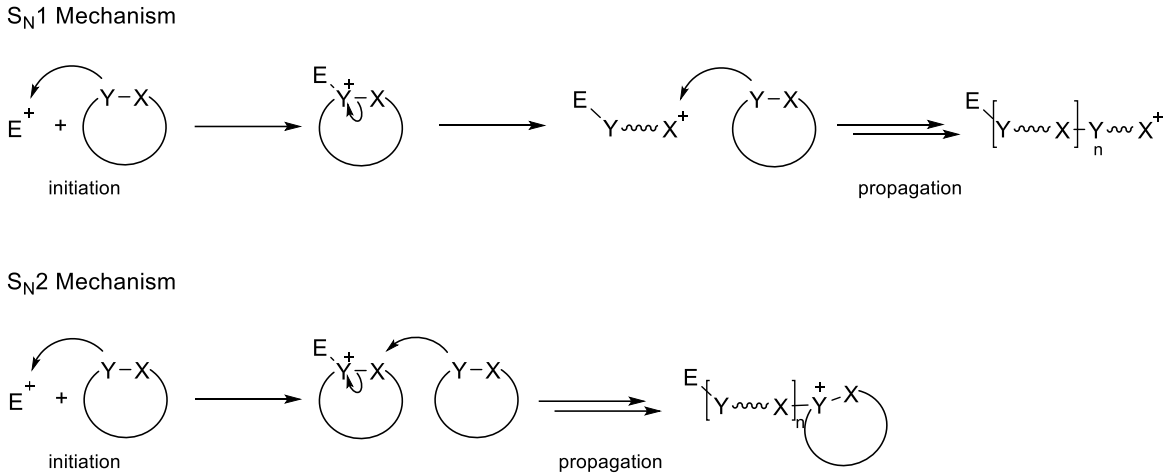

Figure 9: Initiation and propagation mechanisms of the cationic ring-opening polymerization (E: electrophilic initiator).[41]

Important industrial polymers prepared by cationic ROP are e.g., polyacetals, poly tetrahydrofuran and polysiloxanes.[49] Nevertheless, this type of ROP is oftentimes regarded as too expensive to be used in industry. This is, *inter alia*, due to the fact that solvents can change the nucleophilicity of the counterion and therefore only a small selection of solvents is suitable for this polymerization.[43] Next to the high costs of the necessary solvents, the large amount of unwanted side products makes the cationic ROP less economic than other polymerization processes. The many side reactions occur because the polymer's repeating units consist of the same nucleophilic groups as the monomer which opens up the possibility of a nucleophilic attack on the chain end by the polymer chain itself. This type of side reaction is called back-biting (Figure 10). It depends on steric factors and on the nucleophilicity of the heteroatoms in the polymer compared to the monomer.[43,48-49]

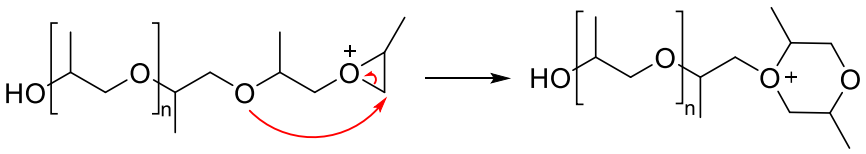

Figure 10: Back-biting reaction in the cationic ROP of PO.

Because of the nucleophilic oxygen in the PPG chain, inter- and intramolecular chain transfer reactions take place which creates many cyclic byproducts in the cationic ROP of PO. Hence, cationic ROP is not commonly used for the polymerization of propylene oxide.

3.2.3 Activated monomer mechanism

Both anionic and cationic ROP are accompanied by undesired cyclisation reactions. The ionic species is located at the end of the polymeric chain which therefore can easily attack itself. To circumvent this back-biting reaction, most polymerizations can be conducted via the activated monomer mechanism (AMM) in which the monomer carries the reactive ionic site. This activation of monomer, extensively described by the group of Penczek *et al.,* is usually achieved by an upstream acid-base reaction.[10,41,44,51-52]

The ”cationic” or “electrophilic” activated monomer mechanism for the polymerization of PO was first described in 1988 by Kubisa *et al.*[52] As it is shown in Figure 11, HBF_4 is used to protonate the PO monomer which then reacts with the hydroxyl group of the alcohol initiator or the neutral growing polymer chain. Subsequently, another monomer is activated by rapid proton exchange. This AMM competes with the active chain end mechanism but is dominant in the presence of an excess in hydroxyl groups. Therefore, the continuous addition of monomer during the reaction can be used to push it towards the AMM.[49,51,53] Nevertheless, the cationic activated chain end mechanism is rarely used for the large scale production of PPG due to difficulties of introducing the desired end groups and the still high amounts of cyclisation side reactions.[10]

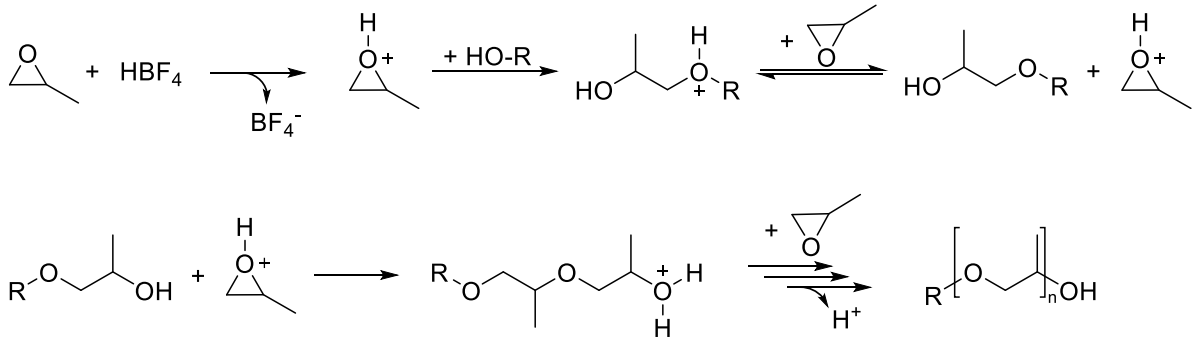

Figure 11: Electrophilic activated monomer mechanism of the PO polymerization.

In case of the “anionic” or “nucleophilic” activated monomer mechanism for the polymerization of PO a Lewis acidic species is needed to complex the monomer together with a nucleophilic species to perform the ring-opening. Complexation of the monomer makes it more reactive towards the nucleophilic initiator and therefore increases the reaction speed. The AMM also improves the living character of the polymerization.[44]

This type of reaction involves the formation of a complex with coordination of the monomer and can therefore also be considered a coordination polymerization.

3.2.4 Coordination polymerization

In coordination polymerizations monomers are inserted between a catalyst's active site and a growing polymer chain. For this kind of ROP, a metal complex acting as initiating species is inevitable.

The mechanism of the coordination polymerization is often referred to as coordination-insertion mechanism, because the monomer is coordinated and pre-oriented at the transition metal before it is inserted into the bond between the metal and the initiating group of the complex.

The first coordination polymerization catalyst reported is the Ziegler catalyst for the Ziegler-Natta polymerization of olefins shown in Figure 12 (illustration of the first steps of the coordination polymerization mechanism proposed by P. Cossee and E. Arlman).[33,54] The Ziegler-Natta catalyst however, does not perform ring-opening-polymerization.

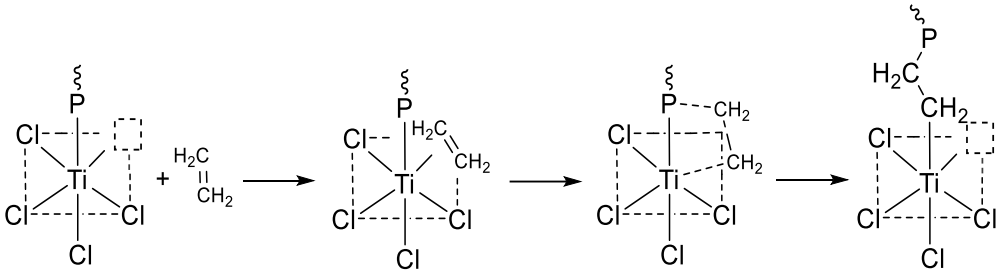

Figure 12: Cossee-Arlman mechanism for the Ziegler-Natta polymerization.

Even though the initiating species in a coordination polymerization is commonly called "catalyst" it is not a catalyst by definition, because it is necessary for the reaction to proceed. Additionally, it stays bonded to the reacting site over the cause of many propagation steps and does not stay unchanged undergoing the reaction.[33,54]

The coordination polymerization of epoxide monomers differs from the polymerization of the vinyl monomers shown above. In epoxide polymerizations the heteroatom of the monomer coordinates to the metal center via σ-bond formation which is followed by a ring-opening-reaction. This ring-opening-reaction is induced through a nucleophilic attack by an initiator, initiating group or the active polymer chain.[10]

The coordination polymerization of propylene oxide is of anionic nature and involves the activation of the monomer (*vide supra*). Therefore, it is also referred to as pseudoanionic polymerization.[55] Various aluminum complexes can be used as initiator in the ROP of PO. Examples are the (5,10,15,20-tetraphenylporphinato)aluminum chloride (TPP-AlCl) system by Aida *et al.*[56-58], the combination of TPP-AlCl and bulky Lewis acids like methylaluminum bis(2,5,6-trialkylphenlate) as developed by Sugimoto *et al*.[59] and triisobutylaluminum together with different alcoholates by Billouard *et al.*[10,60] The latter initiating system yields high molecular weights of 170000 g/mol with simultaneous narrow PDI of 1.34.[10,60] The system

was further improved by the combination of noncoordinating cations (phosphonium salts, tetraalkylammonium halides) with the triisobutylaluminum.[10,61-62]

The coordination polymerization of propylene oxide follows a bimetallic mechanism (exemplarily shown in Figure 13) in which the propylene oxide coordinates to one Lewis acidic initiator which subsequently lowers the electron density in the α-carbons of the oxirane ring. This makes the PO more susceptible to ring-opening by an initiator that is either the same or another molecule.

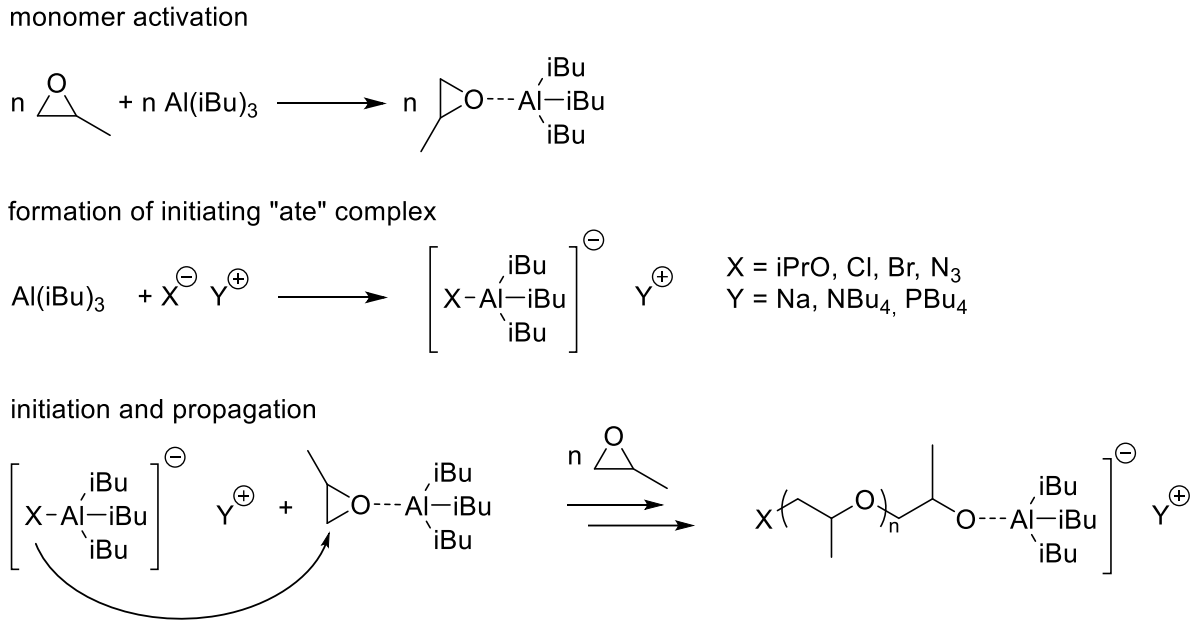

Figure 13: Coordination polymerization mechanism of PO using the monomer-activation technique.[10,60]

Due to the coordination of the monomer, the second initiating molecule only needs to be a weak nucleophile. Next to this, proton abstraction is not prominent since the electron withdrawing effect on the β-hydrogens is small. The activated monomer is attacked by the initiating group of the second molecule, ring-opened and inserted in the bond between said second metal center and the initiating group. Propagation proceeds in a similar manner as it can be seen in Figure 13. The shown mechanism is specifically characterized by the formation of an “ate” complex of the triisobutylaluminum and the alcoholate. This “ate” complex attacks the heteroatom of the coordinated monomer which is followed by the ring-opening.

Coordination polymerizations are usually terminated by the addition of a nucleophile that detaches the growing polymer chain from the complex and forms its end group.[10,60,63]

3.2.5 Copolymerization

IUPAC defines copolymers as polymers “derived from more than one species of monomer”.[64] In a copolymerization two or more so-called comonomers react with each other to form a

copolymer. Copolymerizations proceed via many different mechanisms including the above mentioned ionic ring-opening polymerization, an activated monomer strategy or coordination insertion pathways.

A type of copolymer that only consists of two comonomers called bipolymer. These monomers can be arranged in various ways resulting in the copolymer being categorized as alternating bipolymer, periodic bipolymer, graded copolymer, block copolymer, statistical copolymer or random copolymer. These different structure-based categories are further described in Table 1.[33,54,64] A copolymer containing three different monomers is called terpolymer and can also be classified by the same categories.

Table 1: Structure-based copolymer categories.[33,54,64]

copolymer category	specification
periodic bipolymer	copolymer of two comonomers in which their sequences are repeated periodically
alternating bipolymer	a copolymer that consists of two comonomers that are arranged strictly alternating
graded copolymer	copolymers of two or more comonomers that are arranged following a gradient along the polymer chain
block copolymer	copolymers of two or more comonomers that are arranged in block sequences each consisting of the same comonomer
statistical copolymer	copolymer of two or more comonomers in which the comonomers are arranged in a way that follows a statistic law
random copolymer	copolymer of two or more comonomers arranged in a way that cannot be attributed to the nature of the adjacent comonomer

3.3 DMC Catalysts[1]

The specific catalyst investigated in this thesis is the heterogeneous DMC catalyst that is used by chemical industry for PO homopolymerization and copolymerization of epoxides and CO_2.[65-70]

DMC catalysts are commonly prepared by a precipitation reaction between metal-cyanide and metal-halide salts in the presence of one or more complexing agents (CAs) in aqueous solution. The complexes thus produced are structural analogues of $Fe_4[Fe(CN)_6]_3$, the oldest known pigment, commonly named Prussian blue. These mixed valence cyanides are described in various patents with the general formula:

$$M_a^I[M^{II}(CN)_b] \times wM^IX_c \times xL^I \times yL^{II} \times zH_2O$$

wherein M^I is, *inter alia*, one of the earth-abundant metals Zn, Fe, Ni or Co, with X being one of the halides Cl, I or Br and M^{II} being Co, Fe, Ni, Cr, Pd or Pt.[68,71-76] The most common metals incorporated into DMC catalysts are Zn(II) as M^I and Co(III) and Fe(III) as M^{II}[12,14,77] since they lead to a higher concentration of vacancies throughout the structure.[78-79] A proposed structure of this Zn(II)/Co(III) DMC catalyst is shown in Figure 14.

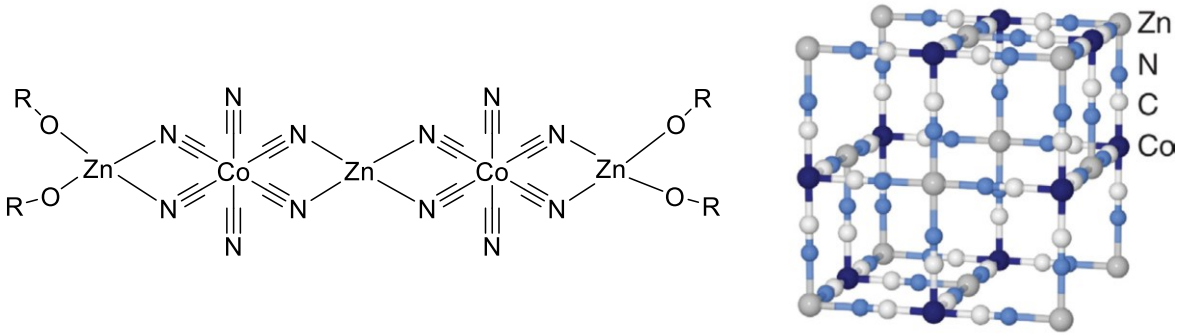

Figure 14: Schematic depiction of DMC catalyst (left) and cubic crystal structure of a Zn-Co-DMC (right). Reprinted with permission from P. Valvekens, D. De Vos in *New Materials for Catalytic Applications*, Copyright (2016) Elsevier, Amsterdam

Remarkably, due to the inorganic polymeric nature of the heterogeneous DMC catalysts and their amorphous character, full structure elucidation of these type of complexes has not been achieved yet and analytical reports deem the currently "accepted" sum formula as it is stated above as dubious.[80-81] One reason for this is the observation that the activity of the DMC catalysts is introduced (to the otherwise inactive Prussian blue analogues)[12,76,82] by incorporation of the complexing agents (L^I) and co-complexing agents (co-CAs, L^{II}): by acting as Lewis bases, these potential ligands can enter the metals' coordination sphere, resulting in novel complexes structurally different from the classic Prussian blue notation that is currently

[1] Parts of this chapter have been previously published in L. Grefe, E. Mejía, *Tetrahedron* **2021**, *98*, 132433.

used to describe DMC catalysts. Another reason is the necessity of an excess in M^{I}-halide salt to achieve a sufficient catalytic activity (depicted as $wM^{I}X_c$ in the traditional sum formula of the catalyst). However, no crystalline metal salt was detected in DMC catalysts so far.[81]

The catalyst's activity was found to be highly dependent on the choice of complexing agent, choice of M^{I} and M^{II} salt, the preparation procedure, and its morphology.[12,81,83]

The ideal polymerization temperature depends on the used type of DMC catalyst, but ranges generally between 90 °C and 145 °C. The higher the catalyst concentration, the shorter the polymerization time and the higher the monomer conversion.[84-86] The polydispersity of the product decreases with an increase in catalyst concentration.[11]

Multiple attempts have been conducted to elucidate the structure of DMCs, as well as the mechanism of the homopolymerization of epoxides and the copolymerization of epoxides and CO_2. Darensbourg *et al.* successfully prepared homogeneous model structures (an example is shown in Figure 15) resembling the active site of a Zn(II) and Fe(III) containing DMC catalyst. They found that the epoxide most likely binds to the tetrahedrally coordinated Zn atom that is connected to Fe atoms via two bridging cyanide groups. However, they could not reproduce the catalytic activity of the heterogeneous compounds within their homogeneous systems for the PO/CO_2 ROCOP that predominantly produced cyclic carbonate.[87-88] Efforts to prepare the corresponding cobalt-containing homogeneous structures only lead to the formation of insoluble cyanide bridged structures that showed no activity for the copolymerization of CO_2 and cyclohexene oxide.[89]

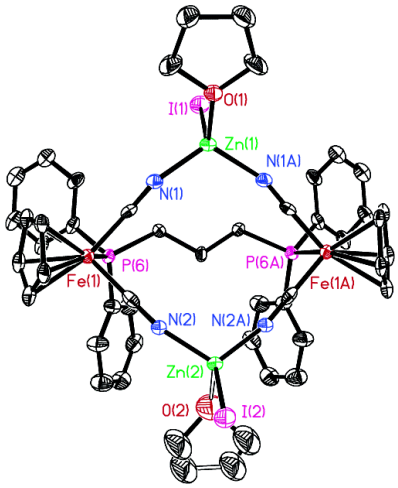

Figure 15: X-ray structure of a homogeneous model structure of a DMC catalyst. Reprinted with permission from D. J. Darensbourg et. al, *Inorg. Chem.* **2003**, *42*, 7809-7818. Copyright (2003) American Chemical Society.

The most recent research on the structure of DMC catalysts surrounds the copolymerization of epoxides and CO_2 and focusses on DFT calculations. Wojdeł *et al.* calculated a model of the active site of DMC catalysts in 2007 that includes both, single center and double metal center.[90] Further calculations were done by Almora-Barrios *et al.* in 2015 focusing on the effect

of the full replacement of the bridging chloride ions in the Prussian blue analogues structure by the complexing agents water, ethanol and *tert*-butanol. They showed that the bulkier CAs lead to lower energies required to create an active surface.[91] Next to the structural investigations, also mechanistic calculations were conducted by the same group, but only for the homopolymerization of ethylene oxide, as later supported by Kim *et al*.[91-92]

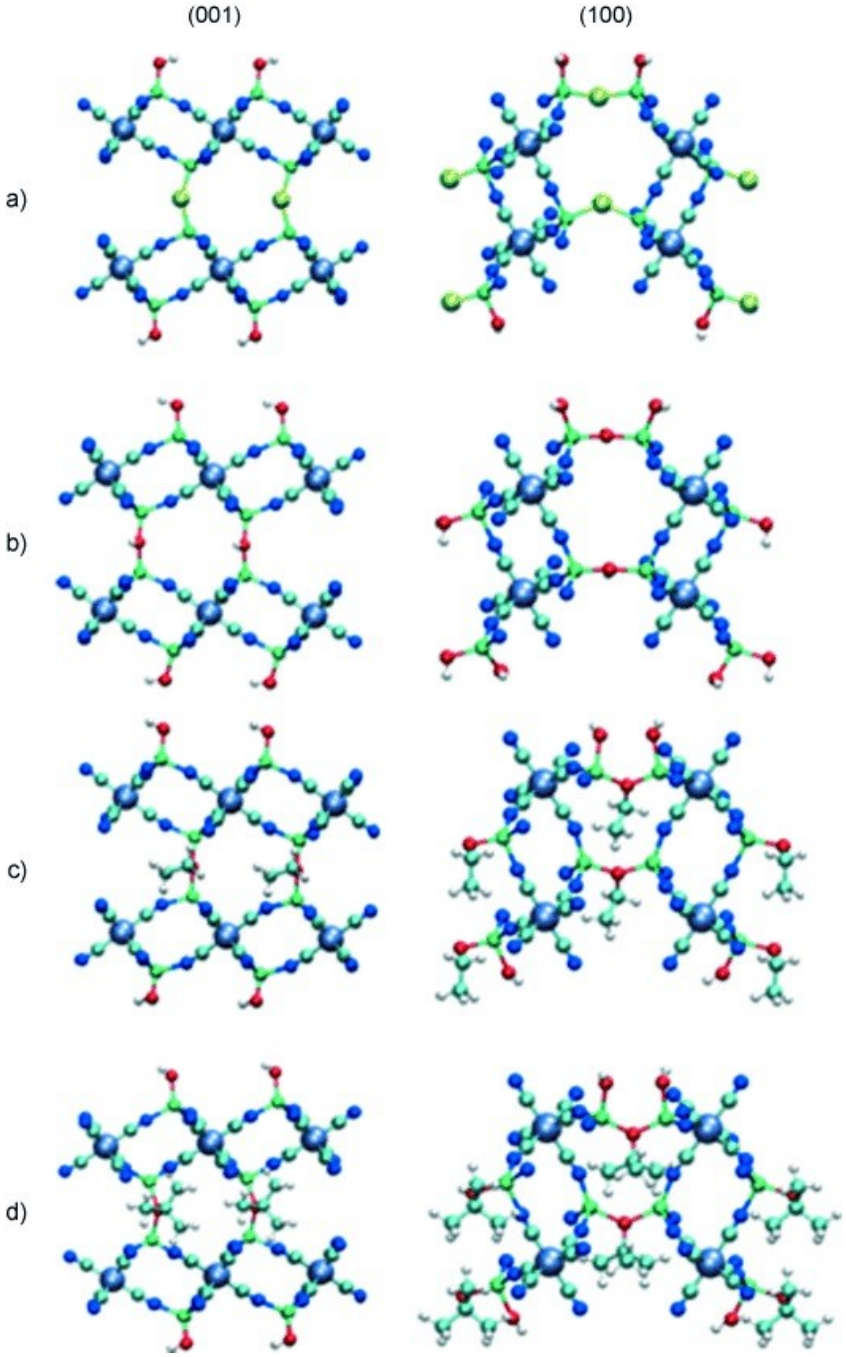

Figure 16: Lowest energy surfaces of DMC with different CAs: a) Cl, b) OH, c) OEt, d) O*t*Bu. Color code: Co centers (large gray/blue) Zn centers (green), Cl (yellow), C (cyan), N (blue), O (red) and H (white) atoms. Reprinted with permission from N. Almora-Barrios, S. Pogodin, L. Bellarosa et al., *ChemCatChem* **2015**, *7*, 928-935. Copyright (2015) John Wiley and Sons

3.3.1 Complexing- and co-complexing agents

(Co-)complexing agents are known to lower the crystallinity of the catalyst and influence its porosity.[9,78] Despite the fact that in the pure $Zn_3[Co(CN)_6]_2$ one third of the hexacyanocobaltate sites are vacant, no catalytic activity was observed using this complex, because the pore size is too small to allow diffusion of the reactants.[83,93] The lacking mesoporosity is necessary for catalytic activity.

An active and partly amorphous catalyst for the homopolymerization of PO was first prepared by the addition of 1,2-dimethoxyethane during the precipitation, which was then improved by replacement with *tert*-butanol.[94-95] *Tert*-butanol is overall regarded as the CA leading to the highest activity of DMC catalysts for both, ROP and ROCOP reactions of epoxides.[78,82,96-97] However, Tran *et al.* found that the incorporation of dicarbonyls leads to an increased amorphousness and higher activity of the DMC catalysts in comparison to *tert*-butanol for the ROP of PO[22] as well as achieving a higher CO_2 incorporation than by using α-dicarbonyls for the ROCOP of PO and CO_2.[98]

Usually, complexing agents have to be used in great quantities during the preparation procedure to obtain sufficient activity. This creates great amounts of wastewater and therefore poses a threat to the environment, but can be circumvented by either using lactate esters as complexing agents[78] or by mechanochemical preparation procedures with a ball mill. This mechanochemical method developed by Guo *et al.* and Shi *et al.* avoids the extensive use of solvents throughout the preparation.[99-102]

Further improvement of catalytic activity was achieved by addition of co-complexing agents in small quantities. These co-CAs lower the crystallinity further and have, similar to the complexing agents, a great influence on the mesoporosity of the catalysts.[18-19]

The employed co-CAs in DMC catalysts for the ROP and ROCOP of epoxides range from short chained alcohols to highly branched polymers and are commonly only employed in very small amounts compared with the portion of complexing agent used.[98] In 2009 Lee *et al*. investigated the influence of co-CAs on the catalytic activity of DMCs in the copolymerization of cyclohexene oxide (CHO) and CO_2 and found that these are most likely providing steric stabilization throughout the precipitation process in the catalyst preparation and therefore protect the particles from growing too big and losing surface area. This is supported by findings of Zhou *et al*. who stated that with increasing molecular mass of the co-CA, the content of monoclinic phase inside the catalyst structure, which is found to be of smaller overall crystal size, increases.[103] Additionally, this change in crystallites leads to a change in pore structure and therefore to different surface areas. The highest catalytic efficiency in the PO/CO_2 ROCOP of 4725 $g_{Polymer}/g_{zinc}$ was achieved by incorporation of a polyethylene glycol (PEG) with a molar mass of 4000 g/mol into the DMC catalyst which consecutively lead to the highest surface area

measured.[103] However, it was also found that an excessive use of co-CAs can lead to deactivation of the catalyst.[104]

In 2014, Sebastian and Srinivas showed that not only the variation of the components of the DMC complex, but also the method of preparation influences the catalytic activity, because of its influence on the morphology.[17] It was shown that, contrary to the cubic structure of pure $Zn_3[Co(CN)_6]_2$, the active catalysts shows either a mixture of cubic and monoclinic, monoclinic and rhombohedral or solely rhombohedral phases in powder XRD analysis.[17,92,99-100,103,105-107] Interestingly, a rhombohedral phase content was only found when co-complexing agents (co-CAs) were introduced.[107]

3.3.2 M^I and M^{II} salt

Another important parameter influencing the activity of the DMC complexes is the usage of excess M^I halide salt during their precipitation.[12,105] Chen *et al.* found that the CAs help retain an excess of the halide salt inside the catalyst, inducing anisotropy (or amorphous domains) in the otherwise perfect crystals, as later supported by Zhang *et al*.[81-82] Moreover, the complexing agent *tert*-butanol does not complex if no excess of $ZnCl_2$ is used.[81]

The combination of zinc and cobalt as M^I and M^{II} in a DMC catalyst is regarded as the most effective combination for the homopolymerization of propylene oxide.[22,77]

In 2007, Zhang *et al.* investigated the influence of the metal of the cyanide salt M^{II} on the catalytic activity of DMC catalysts in the ROCOP of PO and CO_2. M^{II} was either Co(III), Fe(III), Fe(II), Cr(III), Mo(IV), Mn(III) or Ni(II). Co(III) was found to lead to the highest product yield of 1466 $g_{Polymer}/g_{catalyst}$. Ni(II) lead to a higher polycarbonate selectivity and a higher carbonate fraction, but only 438.7 $g_{Polymer}/g_{catalyst}$ could be achieved at 130 °C. All other metals tested showed lower catalytic activity compared to Co(III). The conclusion drawn by Zhang *et al*. to explain these results is that the octahedral coordination structure of the hexacyanocobaltate is crucial for high catalytic activity, which was supported by other experiments distorting its coordination structure that lead to a decrease in activity.[108] Yu *et al.* combined $CoCl_2$ as the M^I metal salt with various M^{II} and compared catalytic activities for the ROP of PO. They found that the combination of Co(II) as M^I and Ni(II) as M^{II} show similar catalytic activity of 9900 $g_{polymer}/g_{catalyst}$ to the Zn(II)/Co(III) combination and that the unsaturation of the final polyether can be influenced by the chosen metal.[76] In 2005, Kim *et al*. demonstrated that, next to the metals M^I and M^{II} themselves, also the counterion of M^I shows to influence the catalytic reaction. They tested DMC catalysts prepared using ZnF_2, $ZnCl_2$, $ZnBr_2$, and ZnI_2 and found that the counterions Cl, Br, and I yield similar TOFs (turnover frequencies) in the PO/CO_2 ROCOP (131.55 – 133.7 $g_{polymer}/(g_{Zn}*h)$ for CHO/CO_2 and 21.11 – 21.69 for PO/CO_2 $g_{polymer}/(g_{Zn}*h)$ copolymerization) but lead to the formation of products with varying CO_2

fractions and molecular weights. For the PO homopolymerization a clear increase of catalytic activity and decrease in induction time was observed when using $ZnBr_2$ (1667 $g_{polymer}/g_{catalyst}$, t_{ind} = 5 min) instead of $ZnCl_2$ (889 $g_{polymer}/g_{catalyst}$, t_{ind} = 53 min). When using ZnF_2 however, no conversion of the raw materials into DMC complexes was observed.[86,109]
Varghese *et al.* changed the counterion of M^I from the commonly employed potassium (which is known to poison the catalysis) to hydrogen, using $H_3Co(CN)_6$ as raw material. With this a great improvement in PO/CO_2 ROCOP was achieved compared to the conventionally prepared DMC catalyst.[110]

3.3.3 Induction time

In general, DMC catalysts have to be activated by addition of a defined amount of monomer before the process can continue by (constantly) adding monomer. After the initial portion of monomer is added to the reactor, a certain induction time is observed, which depends on the type of DMC catalyst as well as on the reaction temperature, catalyst concentration and monomer concentration. An increase in one or more of the latter three factors leads to a decrease in induction time.[11,20-22,111-114] The induction time can also be influenced by the choice of (co-)complexing agent. In a comparison of *tert*-butanol with β- and γ-dicarbonyls, the shortest induction time was obtained with 2,5-dihexanone as CA in combination with a poloxamer as co-CA by Tran *et al*.[20,92] Wu *et al.* showed that the induction time is longer with CAs having more hydroxyl groups.[112] Additionally, Kim *et al.* concluded that the time can be decreased by using weakly coordinating CAs.[97,113] However, it was later shown by the same group that if a CA coordinates too weakly, no catalytic activity can be observed.[92]

3.3.4 (Co-)Polymerization mechanism of DMC catalysts

Multiple different reaction mechanisms have been proposed for the homopolymerization of epoxides using a DMC catalyst. Earlier proposals by Kim *et al.*, Huang *et. al.* and Zhang *et al.* present the chain transfer agent (CTA) as initiator in the activation step of the reaction.[20-21,81] However, the presence of the CTA is not needed to initiate the reaction.[21,92,111] Therefore, these proposals do not describe the reaction mechanism properly.
Huang *et al*. suggested a coordinative cationic active site due to its opposing properties to the KOH catalysis.[111] Kim *et al.* suggest a monomer insertion mechanism and that the active site has both, cationic and coordinative characters.[20,113] The latest mechanistic proposal by Tran *et al.* combines these suggestions and describes active sites at the surface of the catalyst that perform a cationic ROP mechanism (Figure 17a) whilst an activated chain-end mechanism takes place in the bulk of the catalyst (Figure 17b), *inter alia*, due to the finding of head-to-head

and tail-to-tail configurations. Next to this, a fragmentation behavior of the DMC catalysts similar to the one of Ziegler-Natta catalysts is described.[92] Anyhow, this mechanism by Tran *et al.* still shows the inessential involvement of the chain transfer agent (L) in the surface mechanism (a).

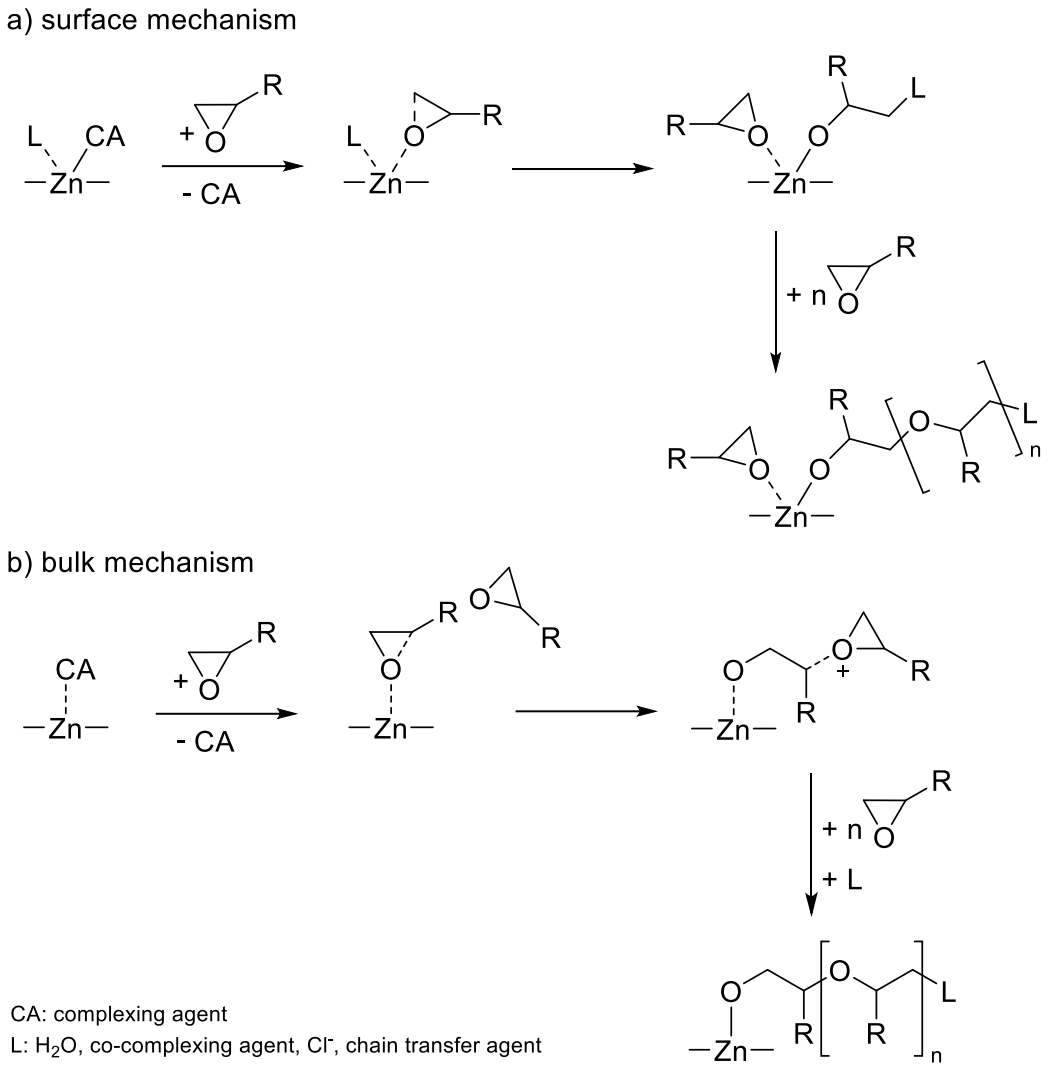

Figure 17: Polymerization mechanism of an epoxide homopolymerization using DMC catalysts according to Tran *et. al.*[92]

Additionally, Chruściel *et al.* analyzed the behavior of the CA *tert*-butanol using thermogravimetric analysis and found that this CA has a very stable bond towards the catalyst and therefore doubt the exchange of *tert*-butanol with the epoxide monomer.[96] Hence, further mechanistic investigations are still needed to elucidate the homopolymerization mechanism of DMC catalysts.

Mechanistic insight on the copolymerization of epoxides and CO_2 was gained by the group of Sun *et al*. by analyzing the resulting polycyclohexene carbonate copolymers using ESI-MS. They showed that consecutive enchainment of epoxide molecules most probably occurs only at the start of the polymerization reaction until a first CO_2 insertion takes place. This is followed

by alternating copolymerization. This fact and the finding that all copolymers bear OH end-groups lead to the conclusion that the initiation of the copolymerization occurs via ring-opening of the epoxide at a Zn-OH site (Figure 18).[115] A similar mechanism was also proposed by Dharman *et al*.[116]

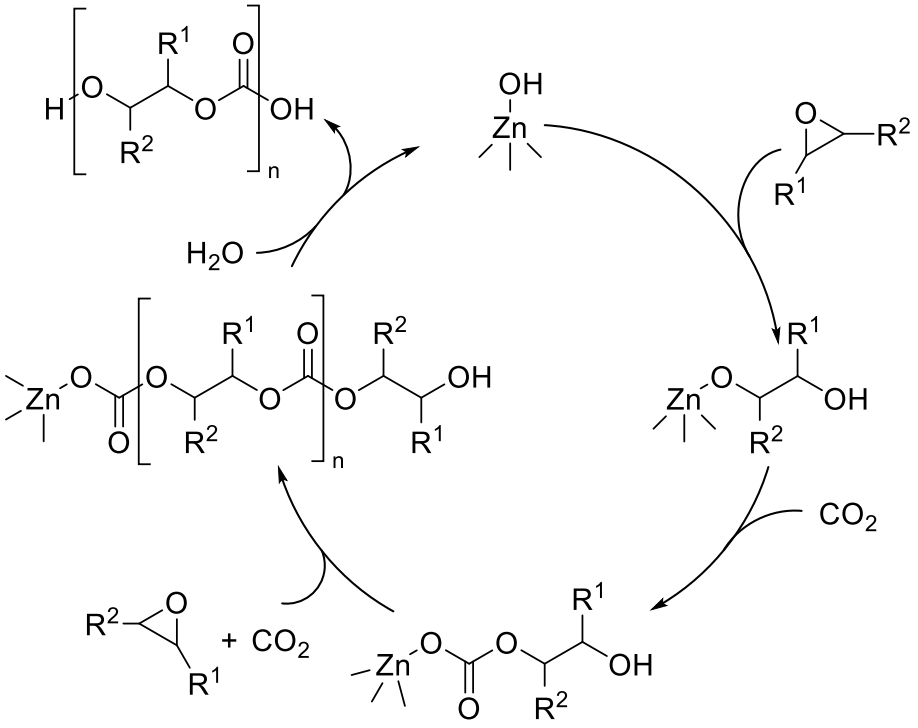

Figure 18: Proposed reaction mechanism for the ROCOP of CO_2 and epoxides, catalyzed by DMC.[115]

The ring-opening-copolymerization itself is not only controlled by varying the catalyst composition, but also the reaction conditions employed. The dependency of polymer yield, amount of cyclic carbonate formed as unwanted side product, CO_2 incorporation into the polycarbonate and molecular weight distribution, however, is consistent throughout the various DMC catalysts developed.[107,110,117-120]

In both types of reaction, ROP and ROCOP, a chain transfer agent can be added to control molecular weights and molecular weight distributions. CTAs are usually polymeric diols (e.g., PPG or PEG) with molecular weights below 1000 g/mol, although various carboxylic acids or bisphenols are also reported.[121] These CTAs need to be added to the reaction to achieve control over the molecular weight and obtain a narrow molecular weight distribution similar to the “immortal” polymerizations described by Inoue for metalloporphyrin catalysts.[122] For a long time, the CTAs were regarded as “initiators” or “starters” similar to the necessary initiating alcohols in the traditional KOH catalysis.[20-21,111] However, as stated above, it was found by Huang *et al.* that the addition of the commonly used hydroxy-functional polyethers is not necessary to start the reaction which led to the suggestion of a living polymerization mechanism. Because the moles of obtained polymer molecules are nearly equivalent to the moles of chain transfer agent added, a rapid exchange of active polymerization sites and

dormant species (**Equation 6,** active species marked with an asterisk) must be present to achieve the observed narrow PDIs.[111,113]

$$DMC\text{-}P_n^* + P_m \rightleftharpoons DMC\text{-}P_m^* + P_n \qquad \textbf{Equation 6}$$

Gao *et al.* concluded that increasing amounts of CTA lead to lower molecular weight, carbonate content and molecular weight distribution in epoxide/CO_2 copolymerization. A decrease of molecular weight of the chain transfer agent lead to a decrease of catalytic activity and a longer induction time of the reaction was observed.[123] Nevertheless, a high CTA concentration also decreases catalytic activity.[21] The CTAs can be used to influence the glass transition temperature of the product or to introduce special properties, as reported by Ma *et al*. who used Bisphenol A to produce flame-retarding oligomers.[121]

3.3.5 DMC variations

In other developments, Huang *et al*. showed that the addition of calcium ions during the precipitation of the DMC catalyst enhances its catalytic activity.[21,124] Next to this, the addition of small amounts of modified montmorillonite, quaternary ammonium salts, ionic liquids or tris(pentafluoro)borane as nucleophilic ring-opening agent increases the activity of Zn/Co DMC catalysts.[114,125-127] DMC catalyst can be supported on carrier materials like SiO_2, by co-precipitation, ball milling or physical mixing.[65,83] Developments in the area of ROCOP of epoxides and CO_2 include the induction of the copolymerization by microwaves, leading to shorter reaction times and lower CO_2 pressures needed,[116] as well as supporting the DMC complexes on TiO_2 to suppress formation of cyclic carbonate byproduct.[128]
Additionally, Sebastian *et. al.* reported the terpolymerization of PO, CHO and CO_2 using DMC catalysts in 2015.[106-107] DMC catalysts have also been shown to be active for copolymerizations of epoxides with CO_2, cyclic esters, cyclic siloxanes and anhydrides next to ring-opening of epoxides with amines, transesterification, hydroamination, condensation, and hydrolysis reactions.[8,14,74,94,129-137] Copolymerizations are described in more detail in chapter 4.2. Next to polymerizations involving epoxides, DMC catalysts can be used in the copolymerization of glycerol and succinic acid[18-19], hydroamination[93], reduction of CO_2 to formic acid[138] and photocatalytic wastewater treatment.[139]

4 Results and Discussion

4.1 Characterization of DMC catalysts

In this chapter, the structure and polymerization mechanism of DMC catalysts are investigated. This analysis aims towards further understanding of the dependence of catalytic activity on the catalyst preparation and the reaction course of a propylene oxide homopolymerization.

4.1.1 Assessment of catalytic activity

The evaluation of the catalytic activity of DMC catalysts in the homopolymerization of propylene oxide represents a complex combination of various evaluation parameters. While the reaction itself can be parametrized by its induction time, reaction rate and lifetime of catalyst, the polymeric product of the reaction has to also be considered. A narrow polydispersity index and therefore low viscosity as well as coherence of the calculated and observed average molecular weight indicate a fast chain transfer reaction and therefore good activity of the catalyst. Hence, catalytic activity of a DMC catalyst cannot only be described by one parameter, e.g., reaction rate. An empiric method to assess the catalytic activity of DMC catalysts based on the polymerization reaction and product has been developed in our group. A decision tree (Figure 19) is followed to decide whether the respective catalyst is of high, medium to low or no activity. In a 32 g scale reaction with 450 ppm (wt.) of DMC catalyst, the induction time, maximum reaction temperature, and the product's PDI as well as molecular weight are evaluated. The induction time depicts the time between PO addition and reaction start, indicated by a strong increase in temperature and decrease in pressure. The maximum temperature (ϑ_{max}) during this reaction was also found to be an important factor to determine the catalytic activity.
The collected parameters are influenced not only by the catalyst itself, but also by many other factors like pressure and temperature inside the reaction vessel or impurities in the reactants. Following the decision tree in Figure 19 however, has proven to be a reliable way to evaluate catalytic activity in our group.
To be classified as of "high activity", the DMC complexes have to show an induction time below 8 min and an exothermic reaction with temperatures above 150 °C. The PDI has to be 1.3 or lower and the observed molecular mass needs to coincide with the calculated molecular mass (see appendix, chapter A-2.1). A DMC has "no activity" if the induction time is longer than two hours or the ϑ_{max} is below 130 °C. Intermediate results are in the "medium to low activity" range depending on the observed trend.
Additionally, the lifetime of the catalyst and final product can be evaluated in a 500 g scale reaction with continuous propylene oxide dosing and the double bond content in the PPG

product can be analyzed. High quality DMC catalysts show a long lifetime and a low product unsaturation.

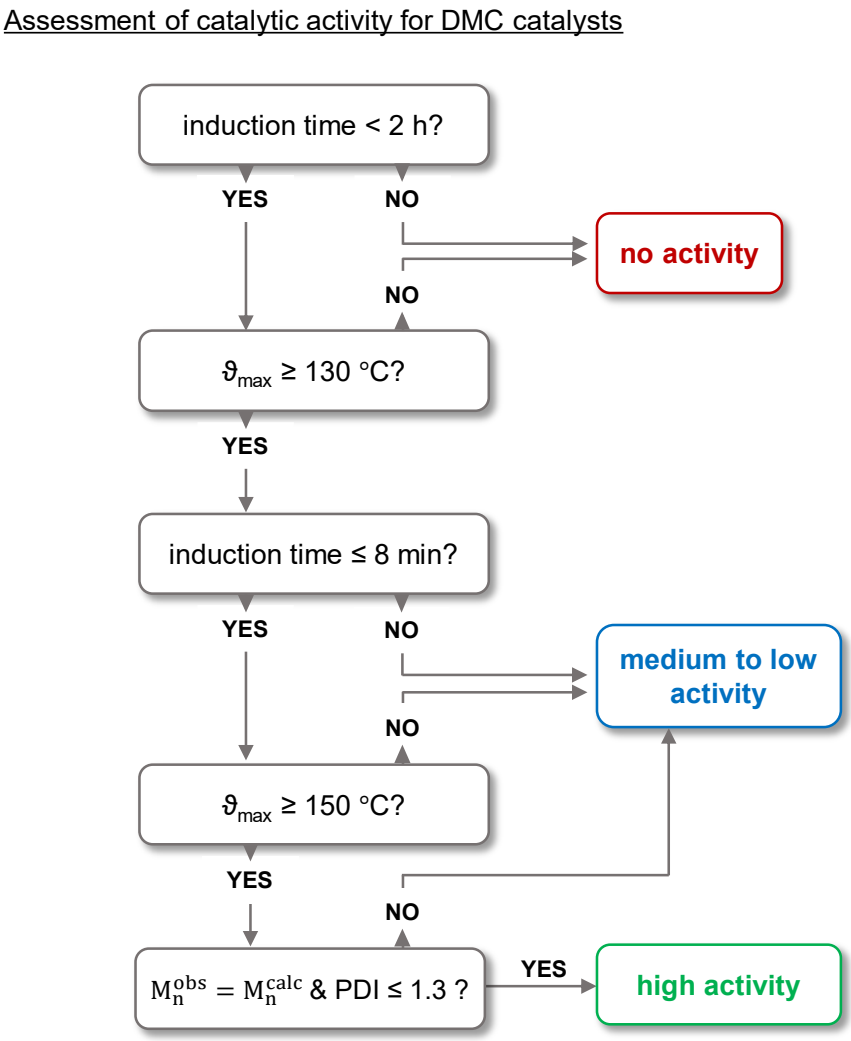

Figure 19: Decision tree for the empiric assessment of catalytic activity of a DMC catalyst.

4.1.2 Structure elucidation of DMC catalysts

Despite the long-standing development of DMC catalysts in chemical industry, the exact structure of the partly amorphous inorganic material is not known (*vide supra*). Therefore, various analytic techniques and DFT calculations were conducted in this thesis to not only get further insights into the DMC catalysts structure, but also to help with subsequent mechanistic understanding of the ring-opening-polymerization of propylene oxide.

For structural investigations multiple DMC catalyst variants were prepared following previously developed synthetic routes and variations thereof (Table 2) as described in the experimental section (appendix, chapter A-1.4). These were then submitted to a series of analytical tests, which are considered in the following.

Table 2: DMC variants prepared.

catalyst	salt 1	salt 2	CA	co-CA	catalytic activity
DMC0	$ZnCl_2$	$K_3[Co(CN)_6]$	-	-	inactive
DMC1	$ZnCl_2$	$K_3[Co(CN)_6]$	*tert*-butanol	-	medium/high
DMC2	$ZnCl_2$	$K_3[Co(CN)_6]$	*tert*-butanol	2-octyl-1-dodecanol	high
DMC3	$ZnCl_2$	$K_3[Co(CN)_6]$	*tert*-butanol	PPG4000	medium
DMC4	$ZnCl_2$	$K_3[Co(CN)_6]$	dimethoxyethane	-	medium/low
DMC5	$ZnCl_2$	$K_3[Co(CN)_6]$	tripropylene-glycol	-	low
DMC6	$ZnCl_2$	$K_3[Co(CN)_6]$	*tert*-butanol	PEG380-420	low
DMC7	$ZnCl_2$	$K_4[Fe(CN)_6]$	*tert*-butanol	-	inactive
DMC8	$ZnCl_2$	$K_4[Fe(CN)_6]$	*tert*-butanol	2-octyl-1-dodecanol	inactive

(co-)CA: (co-)complexing agent | catalytic activity determined by the assessment decision tree in Figure 19.

The DMC complex is a heterogeneous catalyst with the catalytic reaction expected to be happening on the catalyst surface, its structural characterization can be divided into the bulk and the surface structure. Hence, these are regarded separately in the following chapter.

4.1.2.1 Bulk structure of DMC catalysts

The catalytic activity of a DMC complex is induced by addition of a (co-)CA during its preparation (see chapter 3.3), therefore a first comparison of the inactive **DMC0** to **DMC1** containing *tert*-butanol as CA and **DMC2** additionally comprising 2-octyldodecan-1-ol as co-CA was conducted.

Synchrotron radiation was used to record powder XRD spectra (SR-XRPD) to ensure a low detection limit. When comparing the SR-XRPD spectra of **DMC0**, **DMC1** and **DMC2** (Figure 20) it can be observed that under addition of complexing agent the characteristic reflexes of $Zn_3[Co(CN)_6]_2 \times zH_2O$ (2Θ = 6.01°, 6.94°,9.82°, 11.52°, 13.90°, 15.55°, 17.05°, 18.09°, 19.70°, 20.91°, 22.05°, 23.15°, 24.19°, 25.19°, 28.88°) are not detectable in **DMC1** and a new set of broad peaks appears (2Θ = 5.60°, 7.34°, 9.44°, 12.46°, 14.59°, 15.10°, 16.37°, 18.94°, 20.56°). The observed signals do not correspond with the signals observed when analyzing the reactants or the reactants mixed with the complexing agent (see appendix, Figure A 2, Figure A 3). They are therefore assigned to a structurally new complex, the DMC catalyst. The newly formed DMC structure can be described as containing crystalline parts with a monoclinic P11m structure, due to the reflexes at 2Θ = 14.59°, 16.37° and 20.56°.[93] However, it also contains an amorphous phase, recognizable by the broadness of the signals. This is in contrary to the traditional DMC sum formula that describes the complex as an unvaried Prussian blue analogue containing complexing agents, water, and a metal halide salt. This amorphous phase can also be seen in TEM analysis of the catalyst particles where small crystallites of 2-5 nm diameter dispersed in an amorphous surrounding become visible (Figure 32 *infra*).

It has to be mentioned that **DMC2** shows signals that can be assigned to $Zn_3[Co(CN)_6]_2 \times zH_2O$ and to the DMC catalyst, which shows that the coexistence of a crystalline $Zn_3[Co(CN)_6]_2 \times zH_2O$ phase and a partly amorphous DMC catalyst phase is possible. This is accompanied by a decrease in crystallinity compared to **DMC1**. In conclusion, the sum formula of the DMC catalyst has to be extended by a term for the new crystalline DMC structure and by an amorphous phase.

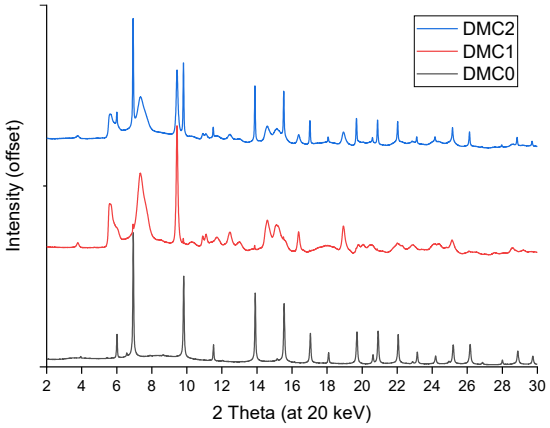

Figure 20: XRD spectra of **DMC0**, **DMC1** and **DMC2**.

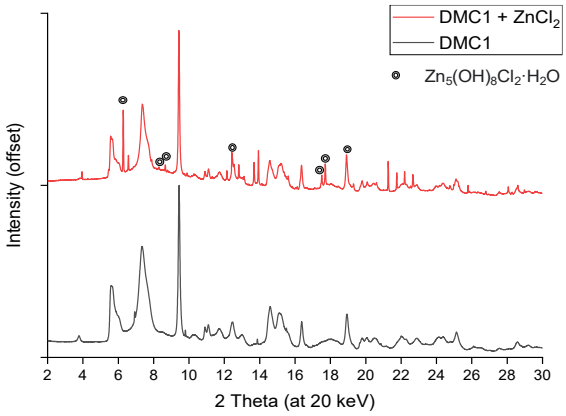

Figure 21: XRD spectra of **DMC1** and a ground mixture of **DMC1** and $ZnCl_2$.

The amorphous phase is known to arise from the incorporation of complexing agents and can be enhanced by the utilization of an excess in zinc chloride during the preparation of the catalyst[81] and by the incorporation of co-CA.[9,20,78] However, it is not known whether the amorphous phase is the reason for catalytic activity or a consequence of other features leading to activity. A clear correlation between crystallinity and catalytic activity could not be derived from the existing literature or observed over the course of this thesis. Moreover, the amorphous phase of an insoluble solid is challenging to analyze since conventional solid-state analysis, e.g., XRPD only works on crystalline phases and there is hardly any analytical method regarding the amorphous phase only and neglecting the crystalline parts of the solid. Therefore, only conclusions from analyses regarding the bulk of the catalyst can be drawn in this chapter.

Additionally, characteristic reflexes of crystalline zinc chloride were not found in the catalyst's spectra. By analyzing the spectrum of **DMC2** to which a crystalline zinc chloride phase was added through grinding it becomes apparent that, when in contact with the DMC catalyst, $ZnCl_2$ is converted to its hydroxide form (Figure 21). Subsequently, the measured SR-XRPD spectra were analyzed for characteristic signal of zinc chloride hydroxide, but no matching signals were detected. Thus, it can be concluded from the SR-XRPD measurements that the crystalline M^I halide salt must not be included in the DMC's sum formula. However, the highly hygroscopic

$ZnCl_2$ could be contained in the amorphous phase of the catalyst and therefore not detectable with the used methods.

For elucidation of the structure of the so far unknown DMC-catalyst-phase, Synchrotron XAS (X-Ray absorption spectroscopy) spectra of the catalysts **DMC0** and **DMC2** were recorded to analyze the coordination sphere of the metal centers zinc and cobalt. X-ray absorption near edge structure spectroscopy (XANES) and extended x-ray absorption fine structure spectroscopy (EXAFS) were conducted at the Co and the Zn absorption edge. The samples are compared to reference materials to gather information about the atoms surrounding the metal centers. The references used are $Zn_3[Co(CN)_6]_2$ (**DMC0**), $Co(OH)_2$, Co_3O_4, $Co(NO)_3$ and Co foil for cobalt and $Zn_3[Co(CN)_6]_2$ (**DMC0**), ZnO, $ZnCO_3$, $Zn(NO_3)_2$, $ZnCl_2$, ZnS and Zn foil for zinc.

As it can be seen in Figure 22, **DMC0** and **DMC2** only differ slightly from each other concerning the near edge and the EXAFS area. Additionally, the Fourier transformed spectra in Figure 23 shows no major difference in the location of atoms around the cobalt center.

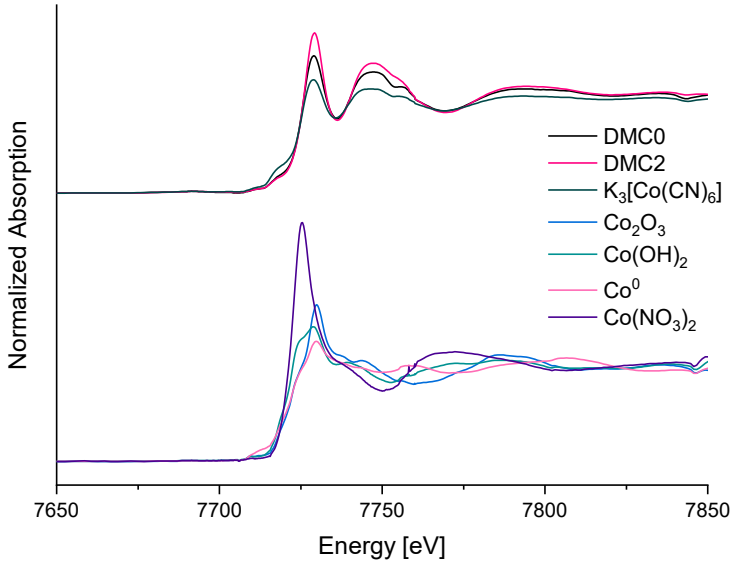

Figure 22: XA-Spectra of the different DMC catalysts recorded at the Co K-edge.

This goes in line with proposed structures of the catalyst in literature in which the cobalt atom functions as a structural element.[140] The complex $Co(CN)_6$ is known to be highly stable and not easily hydrolysable. Therefore, it is expected to show no coordination to the added complexing agents, and not to be involved in the catalytic reaction. However, previous reports show that exchanging cobalt with another metal of similar coordination properties leads to a change in catalytic activity of the catalyst.[108] Moreover, in the activity assessment of the DMC catalysts, the complexes that were prepared using potassium hexacyanoferrate instead of potassium hexacyanocobaltate, **DMC7** and **DMC8**, were inactive (see Table 2). Consequently, cobalt influences the catalytic reaction in spite of not being the catalytically active site. The

minor differences between the distances of the atoms surrounding the cobalt center in $K_3[Co(CN)_6]$, **DMC0** and **DMC2** visible in Figure 23 may account for these observations.

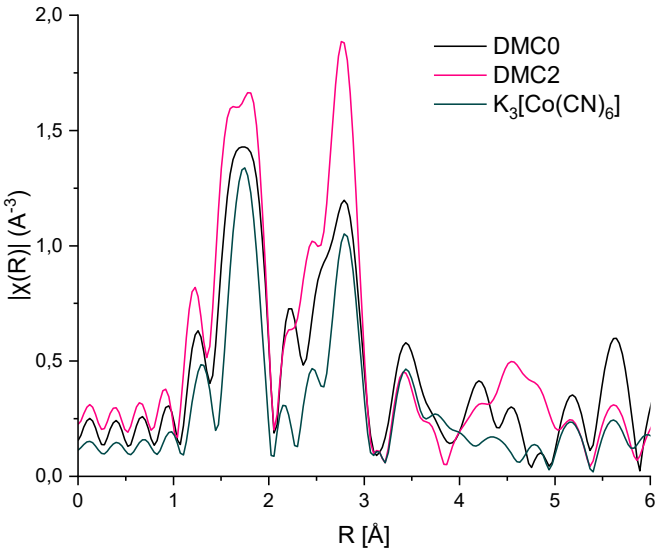

Figure 23: Comparison of Fourier transformed spectra of **DMC0**, **DMC2** and $K_3[Co(CN)_6]$ for Co.

The X-ray absorption patterns of the samples regarding the zinc K-edge, on the other hand, show differences between **DMC0** and **DMC2** (Figure 24), especially in the EXAFS area. This indicates that the adjacent atoms of the zinc center change under addition of CA. Since the CA induces catalytic activity, the active sites of the catalyst are expected to be the Zn-atoms coordinating the complexing agent molecules.

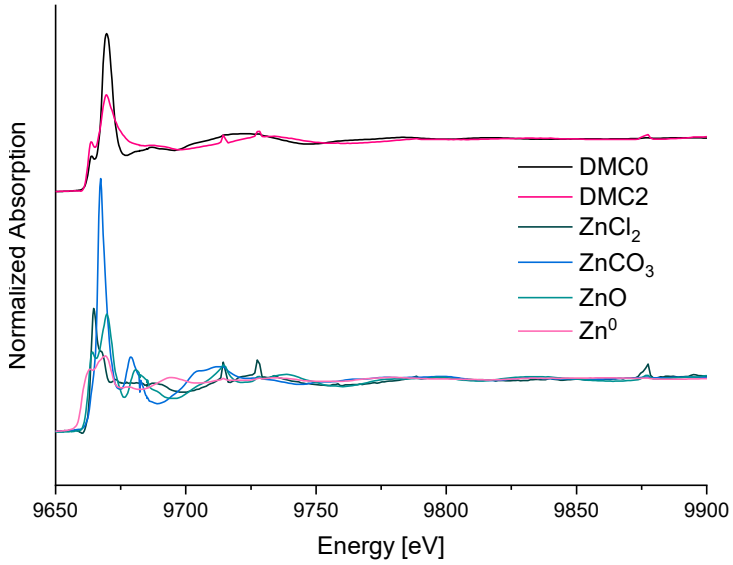

Figure 24: XA-Spectra of the different DMC catalysts recorded at the Zn K-edge.

Figure 25 underlines this change in coordination sphere of the Zn-atoms under addition of CAs and co-CAs when comparing **DMC0** and **DMC2**. Additionally, it becomes obvious that while the coordination sphere of **DMC0** still contains some characteristics of the reactant $ZnCl_2$, these features are not visible in **DMC2**.

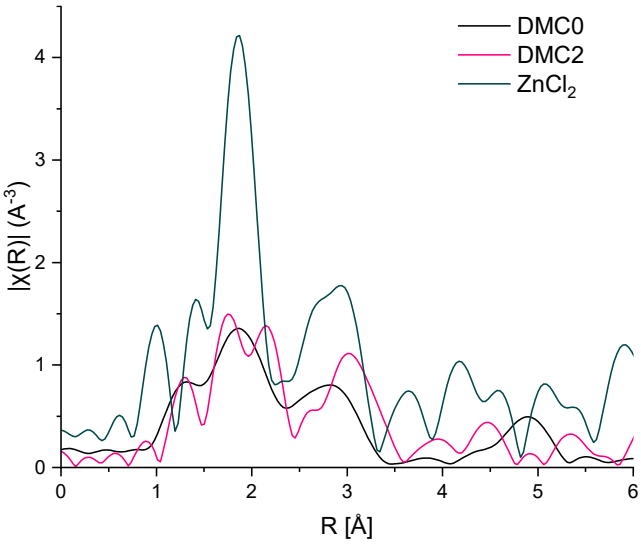

Figure 25: Comparison of Fourier transformed spectra of **DMC0**, **DMC2** and $ZnCl_2$ for Zn.

The elemental composition of the complexes changes when CA is incorporated, not only towards a higher carbon content indicating incorporation of the CA into the catalyst structure, but also towards a higher chloride and zinc content (Table 3), which further supports the formation of a new crystal phase. The incorporation of the CA *tert*-butanol and the co-CA 2-octyldodecan-1-ol could additionally be proven by GC and HPLC analysis after microwave extraction of the catalysts as described in experimental (appendix, chapter A-1.3).

Table 3: Elemental composition of **DMC0**, **DMC1** and **DMC2**.

sample	Elemental Analysis /wt%							tert-butanol /wt%	2-octyldodecan-1-ol /wt%
	C	H	N	K	Cl	Zn	Co		
DMC0	16.05	3.074	19.55	0.2320	0.352	24.308	13.815	-	-
DMC1	23.05	2.666	18.53	0.2666	6.354	28.398	12.090	10.65	-
DMC2	25.27	2.745	19.32	0.3077	5.768	27.443	12.483	8.41	0.49

Analytical methods used for elemental analysis and determination of CA and co-CA are described in experimental (appendix, chapter A-1.3).

When compared to **DMC0**, elemental analysis reveals an increase of the molar zinc-to-cobalt ratio from 1.5 to 2.1 and 2.0 in the bulk of **DMC1** and **DMC2**, respectively. Next to this, a significant increase of chloride is found in the active catalysts whilst **DMC0** shows only traces of this element. The additional amount of zinc and chloride atoms in **DMC1** and **DMC2** compared to **DMC0** appear in the molar ratio 1:2, seemingly supporting the hypothesis by Zhang *et al.* of crystalline $ZnCl_2$ being withhold in the catalyst bulk due to the addition of CAs.[81] As mentioned before, there was no crystalline $ZnCl_2$ detected in SR-XRPD and XAS analysis in catalytically active DMC complexes. As a result, the newly proposed structure of the DMC

catalyst needs to consider the higher amount of Zn and Cl atoms either in a new crystallite structure, the amorphous phase, or the surface of the active catalyst.

Additional chloride atoms in the structure of the crystalline phase could be present as previously proposed by Wojdeł *et al.*[90] and Almora-Barrios *et. al.*[91] in form of a bridge between the zinc atoms in the lattice layers as shown in Figure 26. However, the layers can be also connected through the complexing agent as simulated by Almora-Barrios *et al.* is (Figure 16 *supra*).[91]

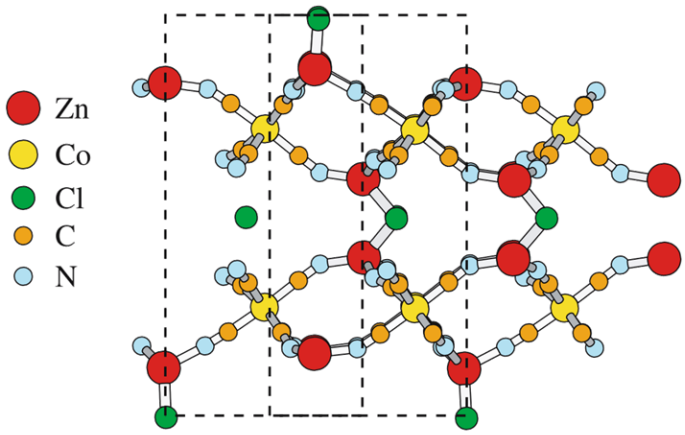

Figure 26: Model of DMC catalyst by Wojdeł et al.[90] Reprinted with permission from J. C. Wojdeł, S. T. Bromley, F. Illas, J. C. Jansen, *J. Mol. Model.* **2007**, *13*, 751-756. Copyright (2007) Springer Nature

To test whether the complexing agent *tert*-butanol is incorporated in the bulk of the DMC catalyst ^{13}C cross polarization MAS-NMR spectra of variations of **DMC1** were recorded. In the ^{13}C cross polarization experiments the magnetization of the ^{1}H nuclei is transferred to the ^{13}C nuclei. Therefore, carbon signals can only be observed when ^{1}H nuclei are contained in the sample.[141] After the recording of a spectra of the unvaried **DMC1** (^{1}H-**DMC1** in Figure 27), the catalyst was immersed in a mixture of deuterated *tert*-butanol-d10 and D_2O, dried in vacuum and another ^{13}C MAS-NMR measurement was performed. The same was done for a DMC catalyst prepared in the same way as **DMC1** with the exception that all reagents were dried and fully deuterated (^{2}H-**DMC1**). ^{2}H-**DMC1** was subsequently immersed in a protic solvent mixture (*tert*-butanol/H_2O). In both cases, a full exchange of *tert*-butanol could be observed in the ^{13}C cross polarization MAS-NMR spectra by either appearance or disappearance of the *tert*-butanol signals (Figure 27). This leads to the conclusion that the complexing agent is not part of the DMC catalyst bulk and therefore only located on the surface of the catalyst's particles. Concludingly, the crystalline part of the bulk structure of a Zn/Co DMC catalyst is expected to have the sum formula $Zn_4[Co(CN)_6]_2Cl_2$ as previously suggested by by Wojdeł *et al.*[90]

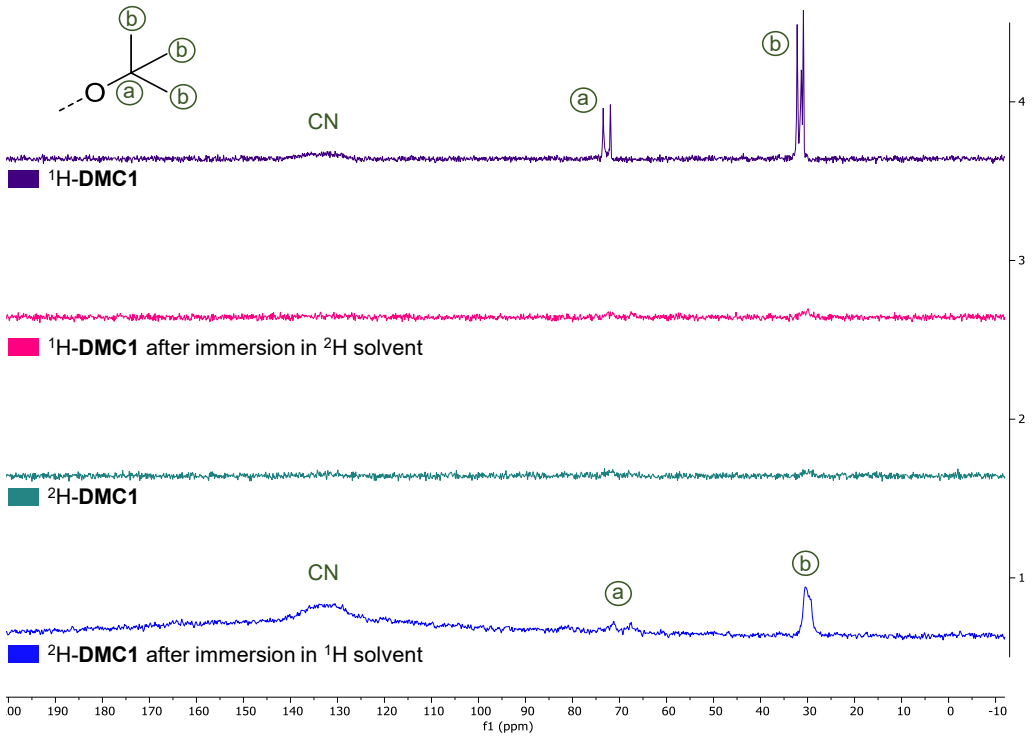

Figure 27: ^{13}C MAS-NMR ^{1}H cross polarization spectra of **DMC1** variations (100 MHz, 298.6 K).

Next to this, the ^{13}C MAS-NMR spectrum of the **DMC2** (Figure 28) shows signals related to both the CA *tert*-butanol (δ = 73.31 ppm, 71.95 ppm (HO**C**$(CH_3)_2$), 30.20-32.07 ppm (HOC(**C**$H_3)_2$) and the co-CA 2-octyl-1-dodecanol (δ = 65.84 ppm (-**C**-OH), 40.68 ppm (-**C**H$(CH_2)_3$-), 27.34 ppm (-CH(**C**$H_2)_3$-), 23.23 ppm (-**C**H_2-CH_3), 14.38 ppm (-CH_2-**C**H_3)). Compared to the free form of *tert*-butanol (^{13}C NMR signals at 68.8 and 32.0 ppm) a downfield shift of the CA's signals can be observed, which suggests a coordination of the complexing agent to the metal center as previously reported by Sebastian *et al.*[17] Next to this, the appearance of the methyl group signal of the CA as multiplet indicates anisotropy, thus the coordinated *tert*-butanol exists under different environments at the catalyst's surface. The 2-octyldodecan-1-ol signals on the other hand, appear at a similar shift to the signals of its free form. This suggests that 2-octyldodecan-1-ol does not coordinate to the metal center and therefore is most likely not involved in the catalytic reaction, which was not known previously. In conclusion, a sum formula of DMC catalysts needs to show coordinated CA only on the surface and free co-CA in case of 2-octyl-dodecan-1-ol.

Since it can be seen that the activity of the catalyst changes when incorporating the co-CA, it was assumed that it solely has an effect on the morphology of the catalyst during the particle formation.[18-19,98] However, when comparing the ^{13}C MAS-NMR spectra of **DMC1** and **DMC2**, as well as ^{2}H-**DMC1** and a ^{2}H-**DMC2** it becomes apparent that the co-CA might play a more crucial role than previously assumed.

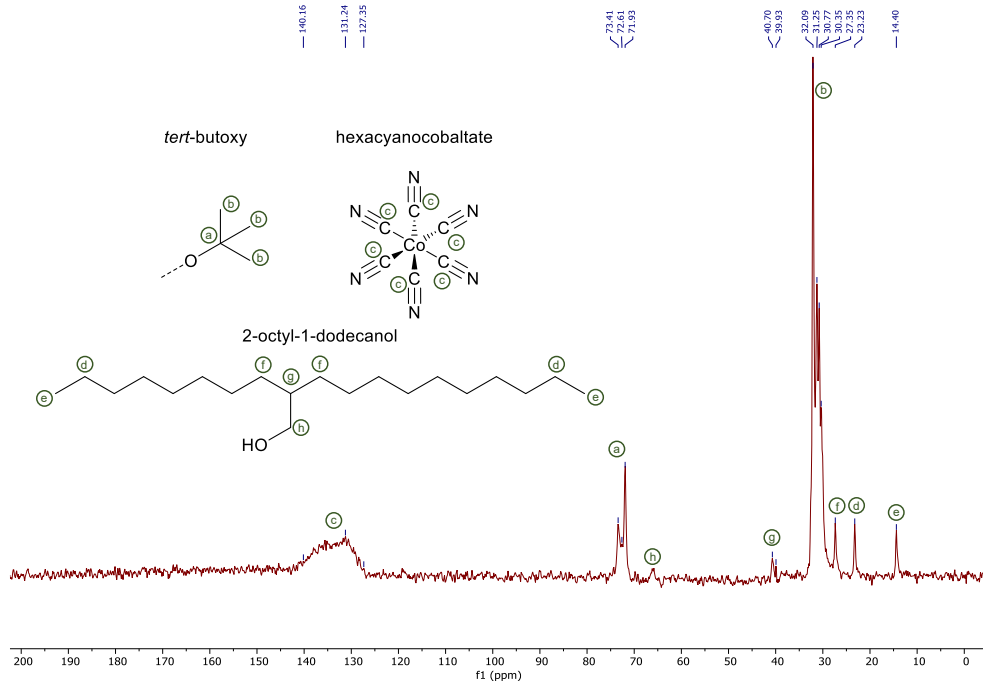

Figure 28: ^{13}C MAS-NMR spectrum of **DMC2** (100.62 MHz, 298.6 K).

When comparing the *tert*-butoxy resonances of **DMC1** and **DMC2** in the ^{13}C cross polarization MAS-NMR spectra, clear differences are noticeable (Figure 29). **DMC1** (without co-CA) shows one resonance for the methyl carbon region and one resonance for the methine carbon region with slight “shoulders” flanking the methyl carbon peak. **DMC2** (with co-CA) shows three resonances for the methyl carbons and two resonances for the methine carbons. This difference is also visible in the ^{13}C direct polarization spectra ^{2}H-**DMC1** and ^{2}H-**DMC2** samples (see appendix, Figure A 17).

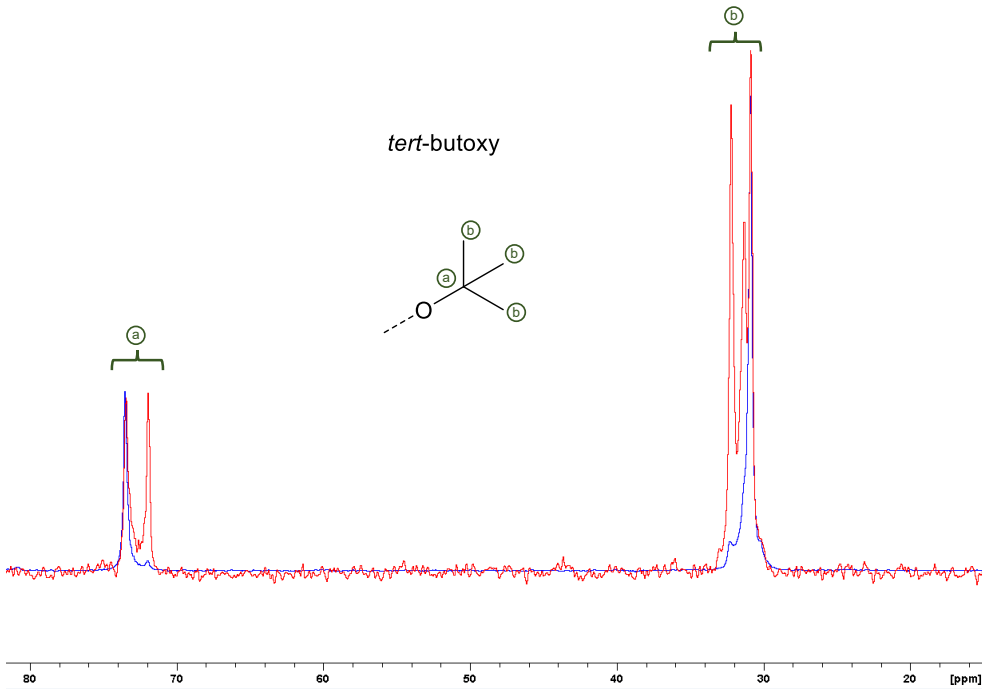

Figure 29: ^{13}C CP MAS-NMR of **DMC1** (blue) and **DMC2** (red) (14 kHz MAS, 297 K).

This observation led to the hypothesis that the co-CA has not only an influence on the morphology of the sample, but also on the coordination mode of *tert*-butanol, leading to a second “type” of *tert*-butanol within the DMC catalyst. This assumption was reinforced by the recording of a ^{13}C MAS-NMR spectrum of **DMC3**, that shows another different set of resonances for the *tert*-butanol signals (see appendix, Figure A 18). The two types of CA are suspected to result from different coordination modes, one being an exchangeable, loosely coordinated form of *tert*-butanol (only found in **DMC1**) and the other a non-exchangeable, strongly coordinated substate (found alongside the loosely coordinated state in **DMC2**). However, these observations can also stem from anisotropy, caused by a morphological effect of 2-octyldodecan-1-ol alone. Therefore, further measurements have to be conducted to investigate this hypothesis.

Because there was only one reflex set found in PXRD for **DMC1**, **DMC2** and **DMC3** it can be concluded that the surface of the catalyst – that is now found to differ between the three – is part of the amorphous phase or depicts a crossover area to the amorphous phase. This crossover area is suspected to be of high catalytic activity due to its structural vulnerability against interaction with the reactants.

The effect of the co-CA was also observed in the TEM pictures as well as the EDX spectra of the catalysts **DMC1**, **DMC2** and **DMC3**. In the TEM pictures (upper panel of Figure 30) the crystallites that are scattered within the amorphous phase that was observed in SR-XRPD analysis (Figure 20) are clearly visible. Here, qualitatively smaller crystallite sizes under the addition of co-CA can be observed. The ordered structure of the atoms in the crystallites becomes better visible in the lower panel of Figure 30.

Table 4: Elemental composition (in relative atomic concentration) as determined by EDX analysis of **DMC1**, **DMC2** and **DMC3**.

catalyst	relative atomic concentration [%]			
	Zn	Co	Cl	O
DMC1	39.45	28.77	18.28	13.49
DMC2	39.99	41.38	2.65	15.98
DMC3	38.13	37.13	1.78	22.96

The relative atom concentrations determined by EDX analysis (Table 4) can be compared to each other and to their respective elemental analysis by the ratios of zinc to cobalt and zinc to chlorine atoms. It becomes apparent, that the zinc to cobalt ratio is approximately 1:1 in **DMC2** and **DMC3** and 1:0.8 in **DMC1,** indicating a change in coordination. Possibly less $Co(CN)_6$ units are bond to one zinc atom in favor of the additional strongly coordinated *tert*-butanol molecules on the surface of the particles. The strongly bound complexing agent might lead to smaller crystallite sizes by inhibiting the crystallite growth during the precipitation of the catalyst and therefore creating more “crossover points” of the crystalline and the amorphous phase

leading to higher activity. This needs to be further be investigated, e.g., by using Pair Distribution Function Analysis on SR-XRPD especially during the early stages of the catalyst preparation.

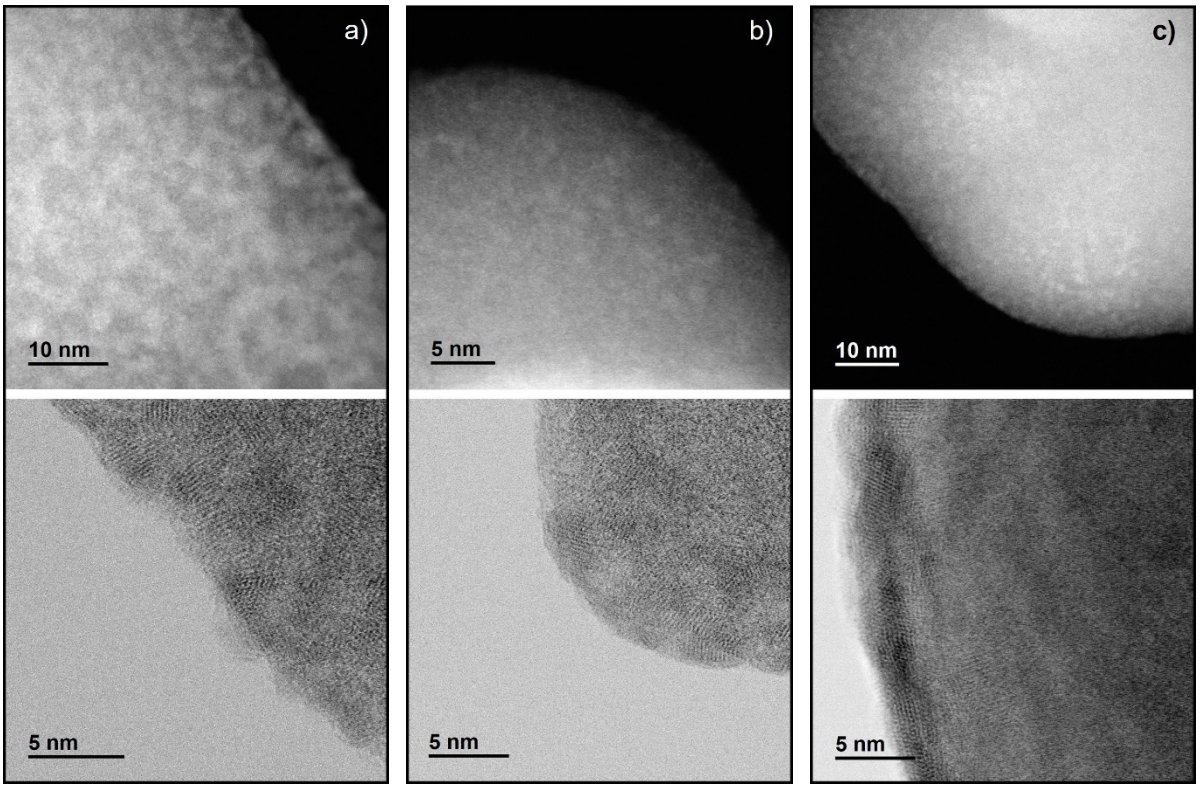

Figure 30: Bright field and dark field TEM recordings at different magnitudes of a) **DMC1**, b) **DMC2** and c) **DMC3**.

Next to this, **DMC2** and **DMC3** contain more oxygen than **DMC1**, which can be assigned to crystal water and most prominent, **DMC1** has a significantly higher amount of chlorine. This is contrary to observations in elemental analysis, where similar amounts of chlorine were found in all three samples (see appendix, Table A 4). This could be attributed to the fact that only a small particle of the sample is used in the EDX analysis and therefore has no statistical significance. The high content in chlorine and the possibility that this particle differs in composition from the bulk of the catalyst powder needs to be statistically validated by conducting more measurements.

A subsequent trial of using DNP-SENS (dynamic nuclear polarization surface enhanced NMR spectrscopy) for further solid state NMR analysis of the DMC catalyst was conducted. This technique can distinguish between the bulk and the surface of the catalyst and hence can help with elucidation of the active surface structure of the catalyst.[142-143] Unfortunately, the analyzed DMC catalysts acted as a radical scavenger for the radical additives used in this method. Therefore, a method to enhance radical concentration needs to be developed to use DNP-SENS.

4.1.2.2 Surface structure of DMC catalysts

It is known that reactions in heterogeneous catalysis commonly take place on the surface of the catalyst's particles. Therefore, the surface structure is of great interest when trying to understand catalytically active materials. In SEM and TEM measurements of DMC catalysts, the particles can be observed at the nanometer scale. In Figure 31 it can be seen that the catalyst powder of **DMC2** is of a layered nanoscale lamella-like structure in which the small plates are distributed around a size of 200-800 nm. This structure consists further of nanoscale crystallites with a diameter of approx. 1-3 nm as shown in the TEM recording in Figure 32. This is consistent for other analyzed DMC catalysts (see Figure 30).

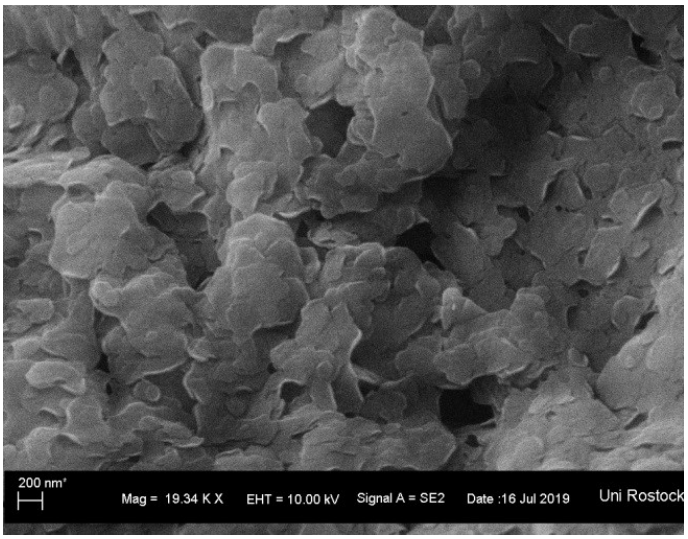

Figure 31: SEM picture of **DMC2**.

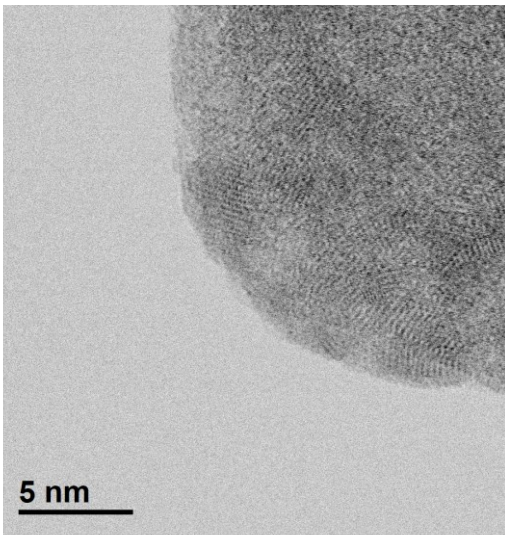

Figure 32: TEM picture of **DMC2.**

The arrangement leads to a high surface area, e.g., **DMC2** has a surface area of 249.0294 m^2/g with micropores with an average volume of 0.102760 cm^3/g. Nevertheless, optical methods of the catalytically active surface cannot give insight into the actual surface structure, including the active sites of the catalyst, because zinc and cobalt cannot be distinguished with a satisfactory resolution using electron microscopy.

As mentioned above, the coordination of the *tert*-butoxy complexing agent was confirmed using ^{13}C (cross polarization) MAS NMR spectroscopy and was found to be exclusively located on the surface of the catalyst. Because the addition of the CA introduces activity into the Prussian blue analogue's structure, the hypothesis is that the complexing agent is located at the active sites. However, as described in chapter 3.3.3 the polymerization reaction starts after an induction time that only appears for the first dose of monomer. This indicates the formation of the active site only under reaction conditions and a dormant active site being present beforehand. In chapter 4.1.2.1 it was suggested by results of XAS spectroscopy of the dormant catalyst that the CA coordinates to the zinc atoms. This goes in line with the measured content of zinc atoms in elemental analysis that exceeds the amount needed to fulfill the above

proposed structure $Zn_4[Co(CN)_6]_2Cl_2$. The excess in zinc atoms could be located on the surface of the catalyst acting as the active sites.

In previous reports various dormant active sites were proposed, namely $(CN)_2ZnCl_2$[21], $(CN)_2ZnCl$, $(CN)_2$-Zn-CA and $(CN)_2$-Zn-OH_2[81], Zn^{2+}, Cl^-[9] and Zn-OH-R.[116] However, it was not yet possible to observe the reaction at the active site analytically. The surface analyses described in this chapter aim to elucidate this structure and its relation to the catalytic activity of the DMC complex. The analytical methods chosen are X-ray photoelectron spectroscopy and ATR FTIR spectroscopy. Due to their *ex operando* mode, only the dormant active sites of the catalysts can be observed.

FTIR analysis of all DMC complexes was performed to confirm coordination and compare the coordination strength of the used complexing agents. The ν(CN) band frequency can be taken as an indicator for valance and electronic configuration of the metals bonded to the cyanide group.[144] Changes in the ν(CN) band frequency most likely indicate changes in the electronic configuration and valance of the zinc atoms, since cobalt atoms bonded to cyanide groups are expected to remain constant upon addition of different (co-)CAs. The cyanide ions donate electrons to Zn^{2+} by acting as a σ-donor, which causes a higher ν(CN) value in **DMC0** (ν(CN)=2174.5 cm^{-1}, Figure 33) when compared to reported values for $K_3[Co(CN)_6]$ (ν(CN)= 2131 cm^{-1}).[17,81,86,104] In case of a complexing agent or a chlorine coordinating to the zinc an even lower electron density (ED) is present at the metal center. Therefore, the ED at the cyanide group is decreased further, leading to an increase in ν(CN) band wavenumber.[20] Using this knowledge, the coordination strength of the different CAs can be compared by the ν(CN) band positions. If a CA has a weaker coordination, the ν(CN) band wavenumber gets lowered due to less ED moving towards the CA from the zinc and therefore higher ED in the cyanide bond.[20] The ν(CN) bands for **DMC0**, **DMC1**, **DMC4** and **DMC5** are located at the wavenumbers 2174.5 cm^{-1}, 2193.9 cm^{-1}, 2191.7 cm^{-1} and 2191.0 cm^{-1}, respectively. The clear shift of approximately 20 cm^{-1} of the ν(CN) band in **DMC1**, **DMC4** and **DMC5** compared to **DMC0** confirms the coordination for all of the used complexing agents.

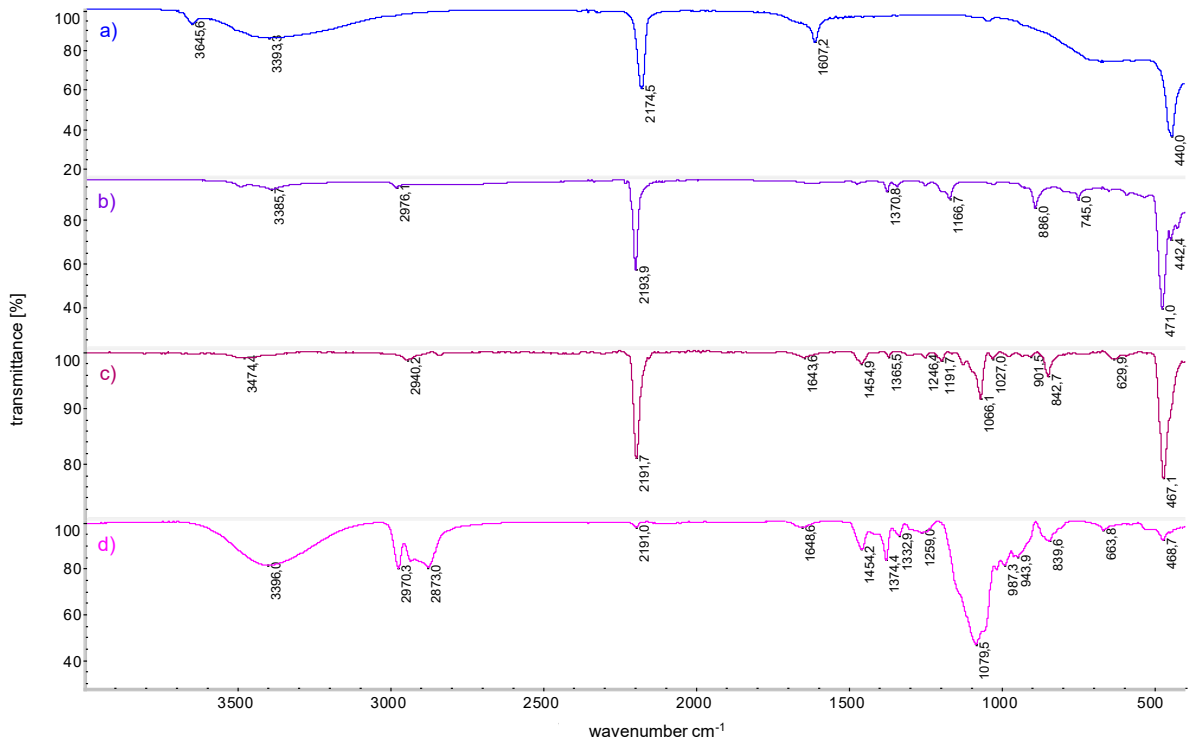

Figure 33: ATR IR spectra of a) **DMC0**, b) **DMC1**, c) **DMC4** and d) **DMC5**.

The coordination strength of the used CAs can be estimated to increase in the order tripropylene glycol ≤ 1,2-dimethoxyethane < *tert*-butanol, which does correlate to the catalytic activity of the regarded complexes (Table 2 *supra*). It can therefore be concluded that the coordination strength of the CA has an important influence in the DMC complexes' catalytic activity, which agrees with previous reports by Tran *et al.* stating that the CA must not coordinate neither too strong nor too weak.[92] In this study no CA with "too strong coordination" was investigated. Next to this, there is only one ν(CN) band visible for each catalyst leading to the conclusion that most zinc atoms on the surface exist in the same coordination state.

The ν(Co-C) stretching band shifts towards higher wavenumbers from ν(Co-C)=440.0 cm^{-1} in **DMC0** to 471.0 cm^{-1}, 467.1 cm^{-1} and 468 cm^{-1} in **DMC1**, **DMC4** and **DMC5**, respectively. This indicates that the influence on electronic configuration of the complexing agent also influences the surrounding of the cobalt atoms close to the surface (Figure 33). This underlines the possibility of an electronic influence of cobalt on the catalysis and arises the question if cobalt exists, in contrary to previous assumptions, in differing coordination than $Co(CN)_6$ on the catalyst's surface. It is noteworthy that under the ancillary addition of co-complexing agent, a shift towards lower wavenumbers of the ν(CN) band is observed in Figure 34 from 2139.9 cm^{-1} in **DMC1** (without co-CAs) to 2193.4 cm^{-1} in **DMC-2** (with 2-octyl-1-dodecanol), 2192.1 cm^{-1} in **DMC3** (with PPG4000) and 2189.9 cm^{-1} in **DMC6** (with PEG380-420).

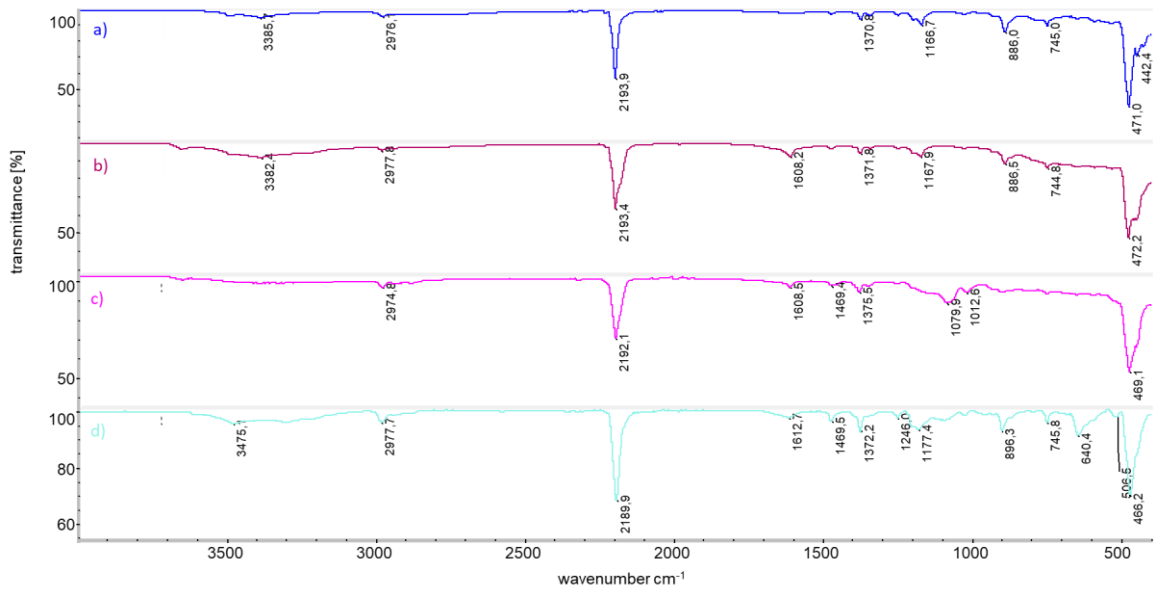

Figure 34: ATR IR spectra of a) **DMC1**, b) **DMC2**, c) **DMC3** and d) **DMC6**.

This supports the hypothesis made upon the MAS-NMR study (*vide supra*) that the presence of co-CA not only influences the morphology of the catalyst, but also the coordination of the zinc atom leading to higher catalytic activity. The addition of the co-CAs in **DMC3** (PPG4000) and **DMC6** (PEG380-420) causes a lowering of the ν(CN) band and ν(Co-C) band wavenumber, which was also observed by Kim et al.[20] This on one hand suggests that the co-CAs with a lower basicity coordinate to the zinc atom and therefore the CN-ligand is left with more electron density or on the other hand that the addition of the co-CAs leads to the coordination of less Cl^- to the surface also leading to a lower electron pulling of the ligands. 2-octyl-dodecanol in **DMC2**, which was shown not to be coordinated to the complex (see chapter 4.1.2.1), however, seems to have a marked influence on the catalyst. It shows a very small shift towards lower wavenumbers in the ν(CN) band and a shift towards higher wavenumbers in the ν(Co-C) band. This indicates that the addition of 2-octyl-dodecanol influences the coordination of the zinc only slightly while also influencing the cobalt center. Even though this specific co-CA is not coordinated it might be associated via hydrogens bonds to the metal.

To investigate the influence of 2-octyl-dodecanol on the CAs located at the catalyst's surface and on the M^{II} metal further, XPS was conducted on **DMC1**, **DMC2**, **DMC7** and **DMC8** (Figure 35). The XPS survey spectra of **DMC1** and **DMC2** show that C, N, Zn and Cl are the main atoms present. In **DMC7** and **DMC8** C, N, Zn and Fe are the most common atoms on the surface of the particles, but not chlorine (Table 5). The concentration of chlorine in **DMC2** is nearly half of the concentration in **DMC1**, which supports the hypothesis proposed on the basis of the ATR IR spectra: The addition of co-CA leads to the coordination of less chlorine to the catalyst's surface and therefore possibly increases the catalytic activity. The suspected

strongly coordinating substate of the CA in ^{13}C MAS-NMR could replace the chlorine atoms on the surface in **DMC2** leading to slightly higher carbon content on the surface.

The exchange of cobalt to iron leads to a significantly lower amount of chlorine on the catalyst's surface. However, this goes in line with a lowered amount of chlorine in the bulk and is accompanied by a lowered amount of CA (Appendix, Table A 4) and a strong loss in activity.

Table 5: Bond energies and atomic concentration of elements on selected DMC catalysts' surfaces by XPS.

	Zn 2p3		Co 2p3		Fe 2p3		O 1s		N 1s[a]		C 1s		Cl 2p	
	BE [eV]	AC [%]	BE [eV]	AC [%]	BE [eV]	AC [%]	BE [eV]	AC [%]	BE [eV]	AC [%]	BE [eV]	AC [%]	BE [eV]	AC [%]
DMC1	1022.75	12.18	782.70	5.13	-	-	533.33	4.41	399.1	26.22	286.52	45.65	198.86	6.42
DMC2	1022.78	11.13	782.49	5.76	-	-	532.87	3.59	399.1	29.52	285.36	46.38	198.985	3.63
DMC7[b]	1023.32	12.34	-	-	710.06	4.89	531.30	5.94	399.1	30.38	287.03	44.6	200.15	1.1
DMC8[b]	1022.77	11.66	-	-	709.82	4.77	533.55	6.07	399.1	6.07	287.07	45.69	200.27	1.11

BE: Bond Energy; AC: Atomic concentration | a: Cyanide nitrogen signal was used as reference at 399.1 eV[140] | b: In **DMC7** and **DMC8** impurities of potassium were found (0.76 % and 0.91 %)

This finding suggests that the coordination sphere of zinc is different for a cobalt-containing DMC and an iron-containing DMC catalyst. The lower overall chlorine content implies that iron forms less of the active $M^{I}_4[M^{II}(CN)_6]_2Cl_2$ phase and therefore fewer active sites are found on the surface of the catalyst. This supports the finding by Zhang *et al.* for an epoxide/CO_2 ROCOP stating that the octahedral coordination structure and donation of electrons introduced by a cobalt metal center is crucial for high catalytic activity and that other metals show lower performance in the copolymerization reaction.[108]

The analyses mentioned above imply that the dormant active site of the investigated **DMC1** and **DMC2** contain zinc atoms as well as chlorine and the complexing agent. Deconvoluted XPS-spectra of the chlorine and zinc signals of **DMC1** show that multiple chemical states of these atoms are present on the catalyst's surface (Figure 36 and Figure 37). The positions of the bond energies of zinc suggest, according to Lawniczak-Jablonska *et al*, the existence of Zn-O and Zn-Cl bonds.[140] The splitting of the signal into a duplet (Figure 35) indicates the interaction of the zinc atoms with the oxygen atom of the CA according to Tran *et al*.[98] However, the resolution of the used equipment to record the XPS spectra shown is not sufficient to fully confirm the existence of two different chemical states of zinc. Nevertheless, the resolution of the system allows to separate the two chemical states of chlorine (BE 199.47 eV and 198.25 eV) shown in Figure 37. These multiple states of chlorine are not visible when using iron instead of cobalt (see appendix, Figure A 9) underlining the effect of the M^{II} metal of DMC catalysts on the active site.

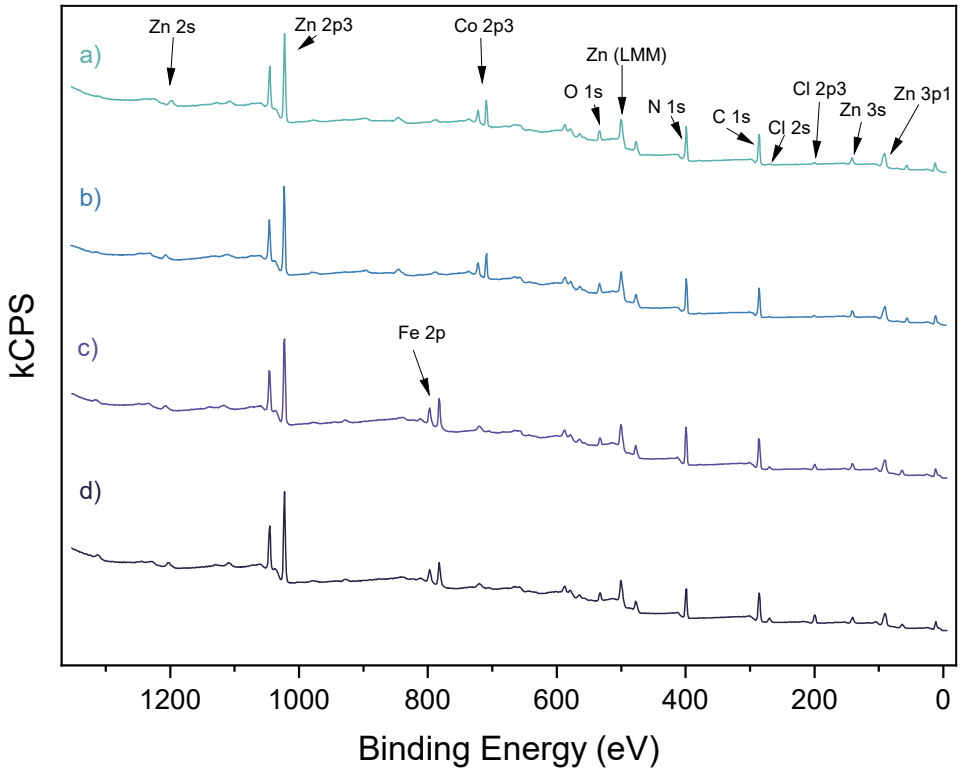

Figure 35: XPS survey spectra of a) **DMC1**, b) **DMC2**, c) **DMC7**, d) **DMC8**.

Surprisingly, two chemical states of the M^{II} metal cobalt are visible in the Co 2p spectrum of **DMC1** and **DMC2** (Figure 38) indicating the existence of both, bonds to cyanide groups (BE≈782 eV) and bonds to oxygen atoms (BE≈781 eV).[140]

Further measurements including reference materials have to be conducted to investigate whether these two chemical states of cobalt are caused by one of the following suggestions: differing groups bond to a cobalt atom, crystal water, varying electron density of the cyanide group due to different groups bond to the coordinated zinc atom or simply aging and therefore oxidizing of the sample while stored on air.

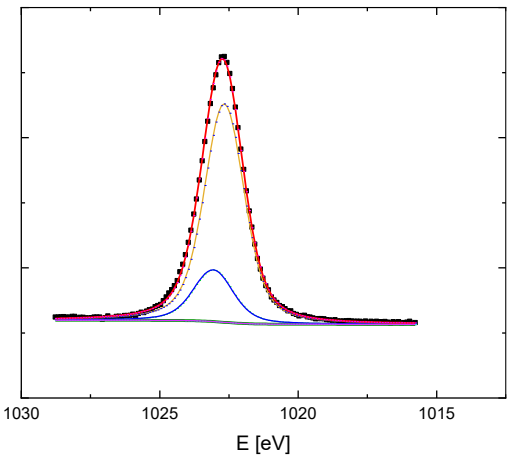

Figure 36: Deconvoluted Zn 2p spectrum of **DMC1** at 1022.75 eV (one of the two duplet signals).

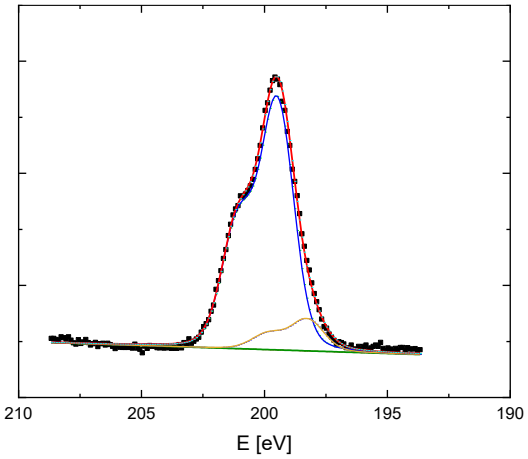

Figure 37: Deconvoluted Cl 2p spectrum of **DMC1** at 199.48 eV (one of the two duplet signals).

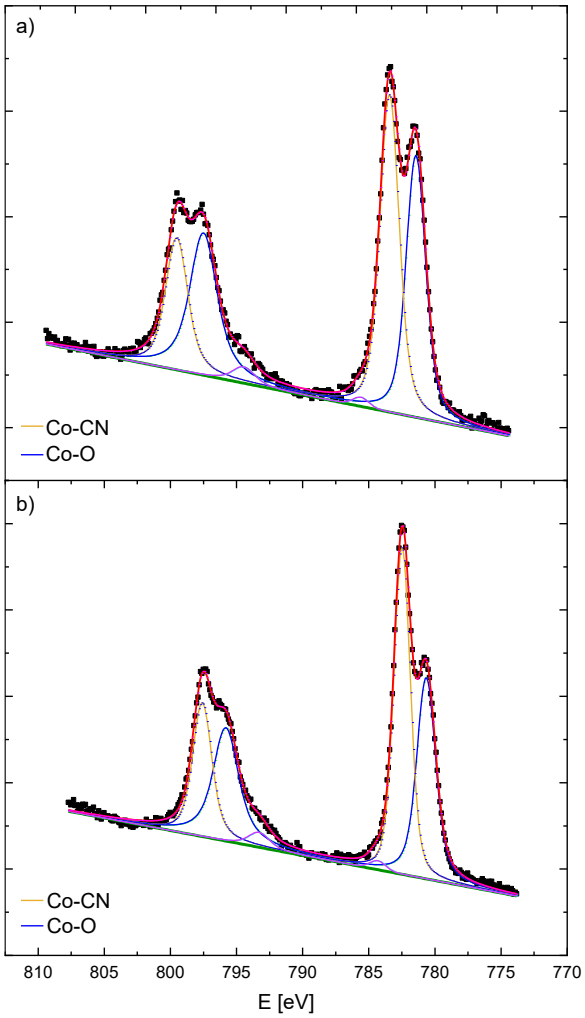

Figure 38: Deconvoluted Co 2p spectra of a) **DMC1** and b) **DMC2**.

4.1.2.3 Conclusion: Structure of DMC catalysts

From the solid state analysis of the DMC bulk (SR-XRPD, XAS and elemental analysis) it can be concluded that the crystalline DMC structure most likely resembles the chlorine-containing model proposed by Wojdeł *et. al.*[90] shown in Figure 26. Therefore, the crystalline part of an updated sum formula for DMC catalysts has to be $M^{I}_4[M^{II}(CN)_6]_2Cl_2$ with possible traces of $M^{I}_3[M^{II}(CN)_6]_2$ x H_2O. The CA is only found on the surface of the catalyst and is likely present, in case of a catalyst with co-CA, in two substate-types: One strongly and one loosely coordinated form. The strongly coordinated form of the CA might be the reason for smaller crystallite sizes and therefore increased active surface. The structures in the amorphous phase remain however, largely unknown. It is possible that the surface of the crystallites represents a great part of the amorphous phase, which should be further investigated using pair distribution analysis or wide angle XRD since these techniques are more suited towards amorphous solids.

It can further be concluded that a combination of zinc and chlorine atoms on the catalyst's surface results in catalytic activity of the DMC complex when a sufficient amount of $M^{I}_4[M^{II}(CN)_6]_2Cl_2$ phase is present in the bulk of the inorganic polymeric structure. Using ATR IR spectroscopy, the coordination of complexing agent to the catalyst is confirmed. This coordination takes place on the zinc atoms since the interaction of the CA with this metal is visible in the deconvoluted XPS spectrum, but a coordination to cobalt atoms cannot be excluded. The electronic state of cobalt seems to play a crucial role in catalytic activity, because catalysts that contain another metal show lower overall activity and miss the variation in zinc and chlorine chemical state. Under the addition of co-CA, the chlorine content on the surface gets lowered with a simultaneous increase in catalytic activity. In conclusion, the dormant active site is most probably comprised of one or multiple zinc atoms bound to complexing agent molecules as shown in Figure 39 with a chlorine atom in close proximity. If chlorine is bound to the same zinc atom as the CA, the electron withdrawing effect of the Cl results in a less nucleophilic character of the latter and could also facilitate monomer insertion.

Figure 39: Proposed structure of the active site of a DMC catalyst.

Under the assumption that the surface of the catalyst comprises the amorphous phase of the particles, the sum formula of this phase needs to include the complexing agent and chlorine bond to the zinc atom. The two coordination states of the CA are usually not expressed in a sum formula. Co-CAs can exist in a coordinated and - in case of 2-octyl-dodecan-1-ol – in a not coordinated form and are therefore to be mentioned separately from the crystalline and the amorphous phase. Additionally, it was found that the catalyst does not contain a crystalline halide salt but is still expected to contain crystal water. Thus, an updated sum formula is proposed in **Equation 7**.

$$M_a^I[M^{II}(CN)_b]X_c \times [M_d^I L_e^I L_f^{II} X_g] \times yL^{II} \times zH_2O \qquad \textbf{Equation 7}$$

4.1.3 Reaction mechanism of Zn/Co DMC catalyzed homopolymerization of PO

Based on the analysis of the DMC catalyst's structure, the polymerization mechanism is investigated. Because there was no activity observed in the Zn/Fe catalysts **DMC7** and **DMC8**, the mechanistic studies are limited to Zn/Co catalysts, focusing on **DMC1** and **DMC2**.
As mentioned above, the polymerization reaction of a DMC catalyst shows an induction time and therefore processes using these catalysts need a special reaction regimen: After the

addition of a first defined portion of monomer, the end of the induction time is awaited (indicated by a sudden increase in temperature, followed by a decrease of pressure). Then additional monomer is added. Any monomer additions after the induction time do not seem to need a second induction period; an immediate reaction is observed. Hence, the reaction monitoring was divided into an “initiation” and a “propagation” phase.
Nevertheless, not only the activation reaction but also polymerization reactions take place during the initiation phase. This makes it necessary to analyze the formation of the active DMC catalyst *ex situ*.

4.1.3.1 Activation of Zn/Co DMC catalysts with PO monomer

Theoretical Calculations

The DMC catalyst is transformed into its active form in the presence of the monomer. With the induction time in mind, the active $Zn_4[Co(CN)_6]_2Cl_2$ phase of the catalyst was modelled according to previous reports by Wojdeł *et al.*[90] The involved molecules of the CA, water and propylene oxide were investigated regarding their adsorption and bonding energy to the surface. For the calculations performed in this work, the atom coordinates of a Zn-Co DMC catalyst’s unit cell published by Wojdeł *et al.*[90] were used. This is the structure of the active phase found in chapter 4.1.2.1. To find the configuration that is lowest in energy and therefore resembles the most likely structure of the catalyst the geometry of the unit cell was modelled from these coordinates and optimized using the generalized gradient functional PW91.[145] This refined unit cell can be seen in Figure 40.
Subsequently, a super-cell was calculated, containing two layers of cobalt atoms and four layers of zinc atoms. This was then followed with forming a slab by cutting the supercell along the [001] surface to obtain an exposed layer of Zn centers with constant distances to a 10 Å vacuum.[90] Two Cl atoms were added to each side of the slab to quench the electrostatic dipole that would otherwise occur alongside it. The obtained structure is subsequently subjected to another geometry optimization to ensure obtaining a realistic model. The model, in which the Zn-Zn distances were found to be 7.632 Å - 7.662 Å, is shown in Figure 41. Using this model, one water molecule and one propylene oxide molecule were each bound to its surface and compared to the total energy of a system bound to one *tert*-butanol molecule (Figure 42). The obtained values shown in Table 6 are only valid to be used for comparison between the different calculations and do not resemble realistic energies. This is due to the inability of the DMC model to portray the whole polymeric nature of the DMC catalyst and only one molecule being present in each of the calculations. However, the informational value by comparison is sufficient for the intended use.

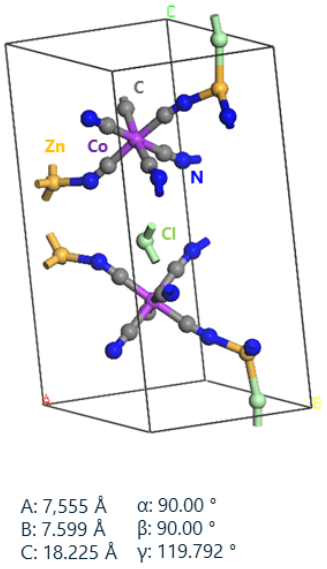

Figure 40: Refined model of the Zn/Co DMC catalyst unit cell based on the atom coordinates published by Wojdeł *et al.*[90]

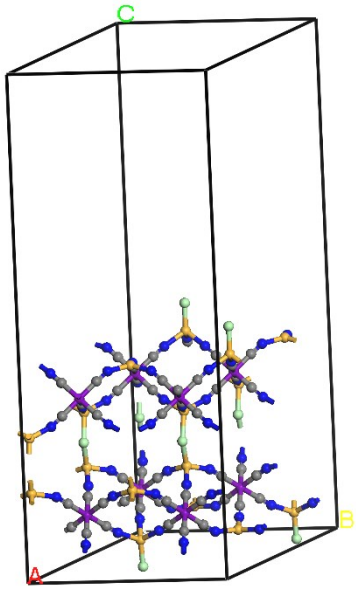

Figure 41: Refined model of the crystalline DMC phase based on the procedure published by Wojdeł *et al.*[90]

The calculated total energies in Table 6 do not differ strongly from each other. It can be observed that the most stable combination is the DMC *tert*-butanol combination. An exchange with propylene oxide and water is possible when presented with a sufficient excess of the respective coordination partner. The complexing agent bound to a zinc atom on the catalyst's surface being the most stable form of the DMC might be the reason for the observed induction time. The catalyst has to be forced into an energetically less stable state before the reaction can start. However, if this would not be the case, the DMC catalysts would likely lose its long shelf-life due to exchange of the complexing agent with water. Next to this, the observed differences in energies are likely too small to have such an effect.

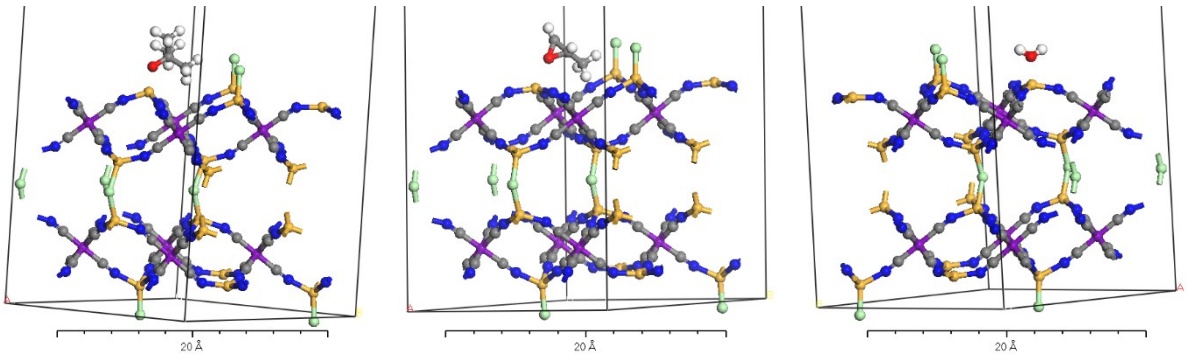

Figure 42: Refined models of *tert*-butanol (left), PO (middle) and H_2O (right) on the DMC catalyst's surface.

Table 6: Total energies of different molecules calculated on the DMC catalyst's surface.

Modeled Compound	E_{total} [kJ/mol]
DMC with ***tert*-butanol**	-18.249
DMC with **propylene oxide**	-18.233
DMC with **water**	-18.189

Calculated using the Dmol^3 module of Biovia Materials Studio.

Experimental Observations

To elucidate the activation of the catalyst, an experiment was performed, in which **DMC2** was heated to 180 °C in vacuum for 5 h to expose adsorption sites followed by venting the activation chamber with gaseous PO after the catalyst had cooled to room temperature. Polymerization of propylene oxide on the catalyst surface was visible, showing that the catalyst remained active after the heating procedure.

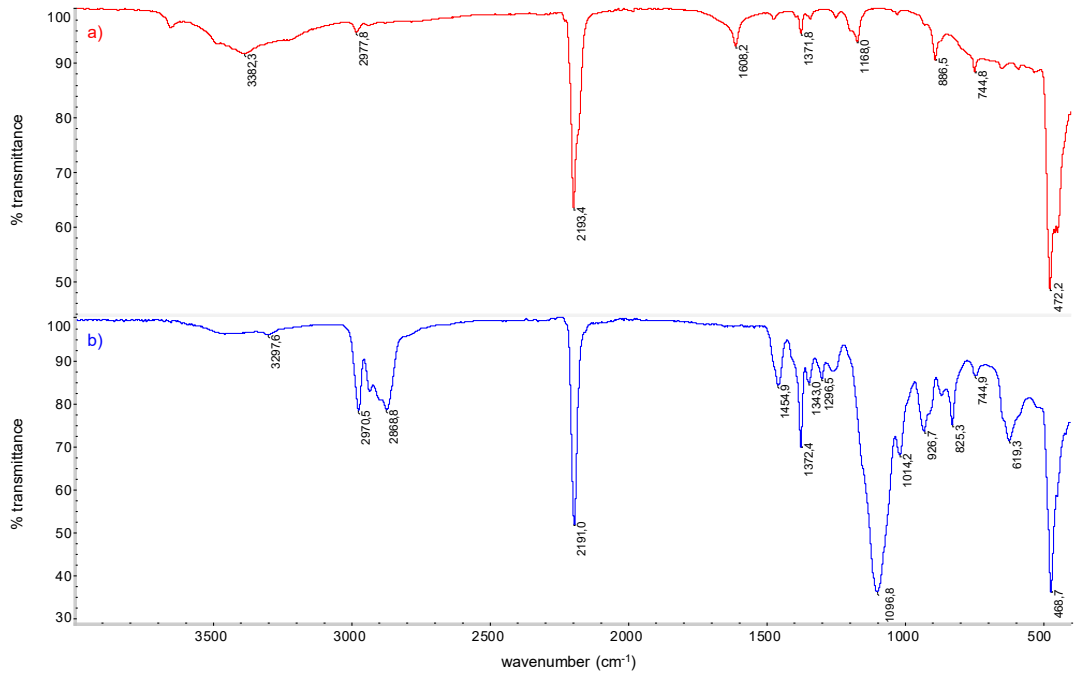

Figure 43: ATR IR spectra of **DMC2** a) before and b) after an *ex operando* activation procedure.

ATR IR of the catalyst was recorded before (Figure 43a) and after (Figure 43b) this activation process. A shift of the ν(CN) band towards lower wavenumbers can be observed after the activation of the catalyst suggesting a change in the zinc's coordination sphere, probably by the change of the *tert*-butanol ligands. The observed wavenumber of ν(CN) = 2191 cm^{-1} in the activated **DMC2** indicates a short chain of polypropylene oxide oligomer being bound to the zinc center. This wavenumber was also observed in **DMC5** (Figure 33) which contains tripropylene glycol as CA. The C-O stretching of the formed ether bond is clearly visible at 1096.8 cm^{-1}, accompanied by the C-H bending of the alkane chain (1372.4 cm^{-1}) and the

methyl group (1454.9 cm^{-1}). Additionally, a shift in the ν(Co-C) band from 472.2 cm^{-1} to 468.7 cm^{-1} upon activation of the catalyst is observed. This shows that the electron density at the cobalt atom is changed by the reaction of the catalyst with PO monomer indicating that cobalt plays not only a structural, but also an electronically important role in the DMC catalyst. In conclusion, the activation of the catalyst appears by either insertion of a propylene oxide monomer into the Zn-CA bond or by exchange of the CA with a monomer molecule as depicted in Figure 44. ^{1}H NMR analysis of the liquid phase forming on the catalyst's surface upon activation reveals that only propylene oxide and polypropylene glycol are present, but no propylene glycol (see appendix, Figure A 10). This shows that the ring-opened monomer is not released from the active site of the catalyst unless it further reacts into an oligomer product.

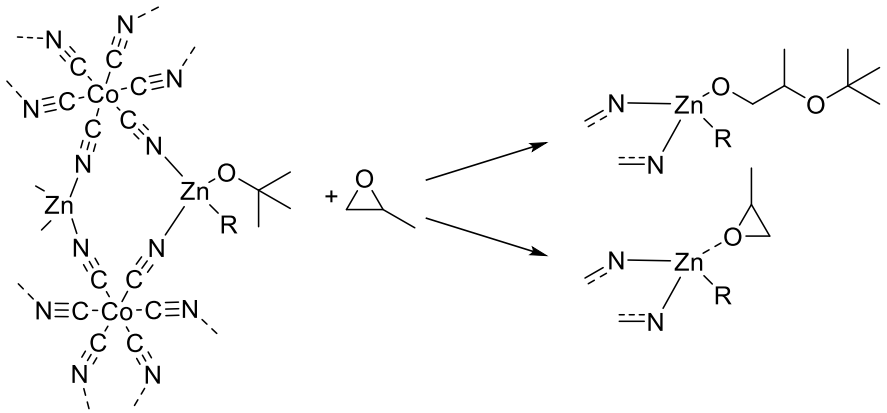

Figure 44: The two possible activation pathways of the DMC catalyst (insertion (top) and exchange (bottom) of monomer).

MALDI-MS of a polypropylene glycol prepared using **DMC2** and PPG2000 as CTA (Figure 45) was performed to investigate which of the two pathways appears more likely. Figure 45 shows the formation of low molecular weight polymers with a *tert*-butoxy end-group. Neither polymers bound to a chlorine atom nor the co-CA could be detected, which might be due to overlay of the matrix and signals corresponding to a molecular weight of below 600 g/mol. The full list of detected signals can be found in Table A 5 (appendix). This finding goes in line with previous investigations of polypropylene glycol as well as polycarbonates using CO_2 as a comonomer to an epoxide.[92,115] Figure 45 also shows the formation of double bonds in the polymers of lower molecular weight. The appearance of double bonds at the end of polymer chains in the molecular weight range of 700 – 1400 g/mol indicates the presence of a transfer reaction on the active site similar to those reported for the anionic ring-opening polymerization of PO using KOH (Figure 8 *supra*).[146-147] All polymer chains with a *tert*-butoxy end-group are of a molecular weight below 800 g/mol which means they did not undergo a chain transfer reaction, because the CTA is of 2000 g/mol average molecular weight. An initiation reaction can be expected in which the CA is involved, but the chain transfer agent is not.

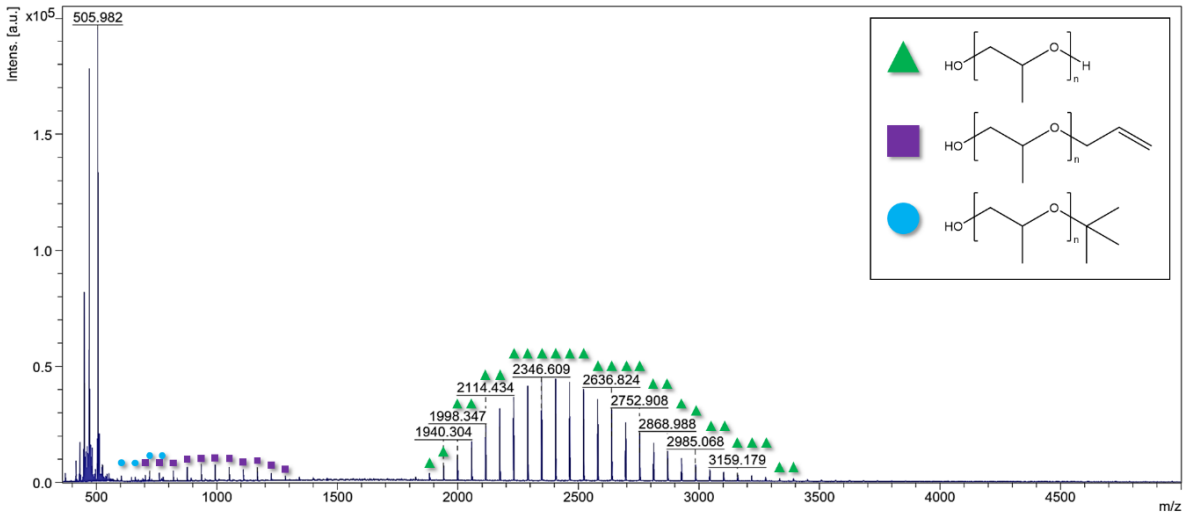

Figure 45: MALDI-MS spectrum of a PPG prepared using DMC2 and a PPG2000 as CTA (Dithranol+LiCl Matrix).

Since *tert*-butoxy end-groups exclusively appear for low molecular weight polymers, a random termination by free *tert*-butanol stemming from an exchange reaction is very unlikely. Consequently, the activation of the DMC catalyst appears via an insertion of the monomer molecule and not by release of CA. Short polymer chains with *tert*-butoxy end groups might terminate themselves by proton transfer similar to other back-biting reactions in ring-opening polymerization (Figure 46). This self-termination seems to be absent above a molecular weight of approx. 750 g/mol, which means that the growing polymer needs a chain length of at least 12 consecutive PO molecules for this reaction to be suppressed.

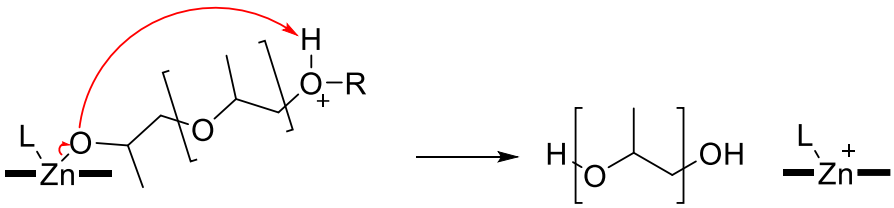

Figure 46: Self-termination of short polymer chains by proton transfer.

4.1.3.2 Kinetic investigations on a DMC catalyzed polymerization reaction

The polymerization reaction of PO using a DMC catalyst encompasses multiple possible elementary reactions. The previously reported proposals are that DMC catalysts follow a coordination-insertion ring-opening-polymerization mechanism,[21,92] and are expected to perform living polymerization, because of the ability of the reaction to be continued upon adding additional monomer.[12,81,111,113]

Based on the mentioned premises for living polymerizations in chapter 3.2 and several examples of anionic[53] and coordination[148] polymerizations, the reaction using DMC catalysts is proposed to comprise the following steps:

- transformation of the DMC catalyst into its active form (activation, **Equation 8**),
- chain elongation by monomer addition (propagation, **Equation 9**),
- chain transfer with dormant polymer species (**Equation 10** and **Equation 12**),
- segmental exchange with chain rupture, as it is typically reported for living polymerizations (**Equation 11**)[48]
- reaction with a terminating agent (**Equation 13**).

Additionally, the polymerization products show a small amount of unsaturation (see Figure 45). Therefore, a proton abstraction side reaction (similar to the one in PO ROP catalyzed by KOH) is expected (**Equation 14**).[146]

activation	$DMC + M \xrightarrow{k_a} DMC\text{-}P_1^*$	**Equation 8**
propagation	$DMC\text{-}P_n^* + M \underset{k_d}{\overset{k_p}{\rightleftharpoons}} DMC\text{-}P_{n+1}^*$	**Equation 9**
chain transfer (exchange)	$DMC\text{-}P_n^* + P_a \underset{k_{tr1}}{\overset{k_{tr1}}{\rightleftharpoons}} DMC\text{-}P_a^* + P_n$	**Equation 10**
segmental exchange	$DMC\text{-}P_b^* + P_d \underset{k_{tr2}}{\overset{k_{tr2}}{\rightleftharpoons}} DMC\text{-}P_{b\text{-}c}^* + P_{d+c}$	**Equation 11**
chain transfer	$DMC\text{-}P_n^* + P_a \underset{k_{tr3}}{\overset{k_{tr3}}{\rightleftharpoons}} DMC^* + P_{n+a}$	**Equation 12**
termination	$DMC\text{-}P_n^* + T \underset{k_{a2}}{\overset{k_t}{\rightleftharpoons}} DMC + P_n$	**Equation 13**
proton abstraction	$DMC\text{-}P_n\text{-}CH_3^* + PO \xrightarrow{k_{tr4}} OH\text{-}P_n\text{-}CH_3 + DMC\text{-}O\text{-}CH_2CH{=}CH_2$	**Equation 14**

: activated species; M: monomer; P_n: living macromolecule; P_n: dormant macromolecule; T: terminating agent; P_a, P_b, P_c: macromolecules with various chain length; k: rate constant

In case of a living polymerization all reactions terminating the propagation and transferring the macromolecule in a dormant state need to be reversible.[47] This criterion is fulfilled when the activation is equally fast or faster than the propagation reaction ($k_a, k_{a2} \geq k_p[M]$). Assuming that no irreversible chain termination takes place, the rate equation for the polymerization (**Equation 15**) can be integrated to find a semilogarithmic dependence of the monomer concentration on the polymerization time with M_{eq} being the monomer concentration when reaching the equilibrium state (**Equation 16**).[48]

$$v_p = -\frac{d[M]}{dt} = k_p \sum [DMC{-}P_n^*][M] - k_d \sum [DMC - P_n^*] \qquad \textbf{Equation 15}$$

$$ln\frac{[M]_0 - [M]_{eq}}{[M] - [M]_{eq}} = k_p \sum [P_n^*]t \qquad \textbf{Equation 16}$$

To gather information on the monomer concentration during a Zn/Co DMC catalyzed homopolymerization of propylene oxide in situ FTIR studies were performed. The reaction conditions were adjusted to slow down the polymerization reaction since the used spectrometer is only able to record one datapoint every 15 s. Preliminary experiments (data not shown) resulted in a variation of catalyst concentration in a range between 0.01 % and 0.5 % (calculated as molar percentage of zinc atoms contained in the catalyst per mol of PO, see appendix chapter A-1.1.1) and a reaction temperature of 85 °C during the activation of the catalyst. A temperature of 70 °C was used in the subsequent propagation reactions. It is possible to follow the epoxide absorbance of PO at a wavenumber of 829 cm^{-1} and 749 cm^{-1}.[149] Within this, these bands represent the ring deformation of propylene oxide and CH_2 rocking, respectively.[150] The $\delta(CH_2)$ band at 749 cm^{-1} was found to be most suitable for monitoring PO consumption, because it is not overlayed by any other interfering IR band and presented a linear dependence between moles of PO and absorbance in a calibration measurement (see appendix, Figure A 14).

Figure 47 shows an exemplary presentation of the PO build-up inside the reactor after dosing and the consumption of PO during the initiation reaction conducted at 85 °C. Because the reaction is conducted without the use of solvent and the used CTA showing the same IR bands as the product it is difficult to transform the obtained data into concentration values in form of substance amount per volume. However, FTIR is an integral method, hence, the absorption A of the $\delta(CH_2)$ band of PO is directly proportional to its concentration and can directly be used without converting it to concentration values.[149,151]

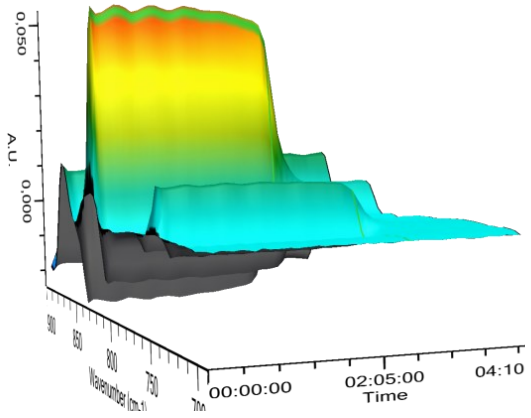

Figure 47: 3D FTIR spectra recorded during the reaction.

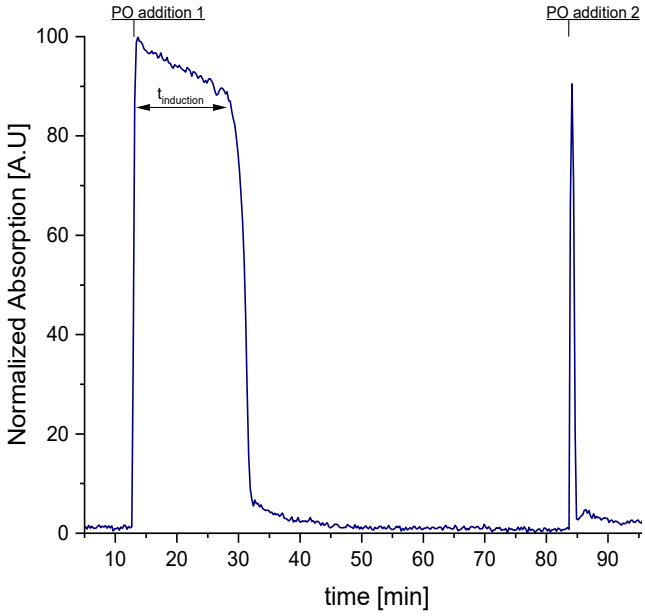

Figure 48: Reaction course followed by the evolution of the $\delta(CH_2)$ band at 749 cm^{-1} (0.025 % **DMC2**).

In the recorded reaction profile (Figure 48) the induction time followed by a sudden monomer consumption can be observed. During the induction time the absorption of the $\delta(CH_2)$ band is slowly decreasing. This observation can be made for various catalyst concentrations in differing strengths but is not reproducible. Since the reaction profile is also monitored via the reactor pressure, which is not decreasing over the induction time, the observed decrease is attributed to measurement inaccuracy.

When a second portion of monomer is added, the induction time is not observed again, which indicates the formation of a stable active catalyst in the first reaction step. As mentioned above, the reaction was divided into the activation phase and the propagation phase for evaluation of the catalyst.

Livingness of the polymerization

To elucidate whether the polymerization is “living”, the semilogarithmic dependence of the monomer concentration (here the absorbance was used directly) and the polymerization time as shown in **Equation 16** is plotted in Figure 49. Because of the high ring strain of propylene oxide the depolymerization reaction is generally regarded as inexistent (i.e., $[M]_{eq}=0$).[48] After the induction period - in which no conversion is observed - the polymerization starts, and a good linear fit can be found. It can be suspected that the polymerization is living, meaning the activation of DMC is fast and no chain termination takes place.

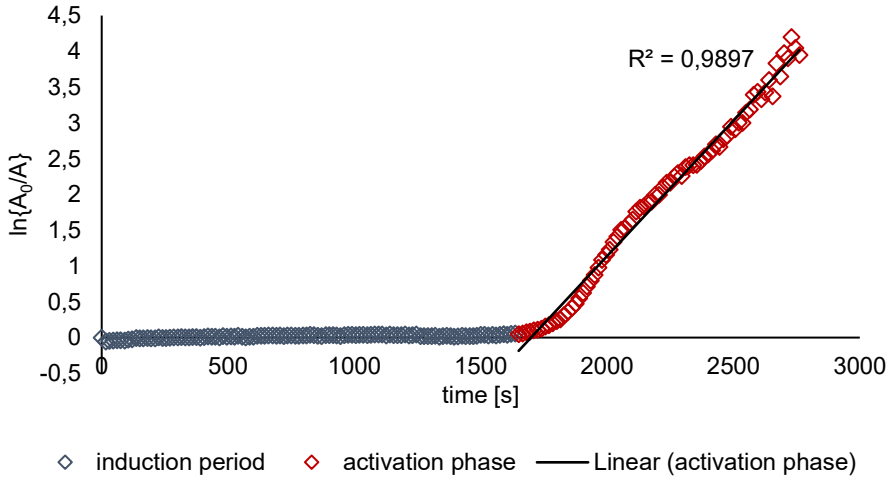

Figure 49: Semilogarithmic kinetic plot of the induction period and activation phase of a PO polymerization using **DMC2** (0.025 mol%$_{DMC,Zn}$), 85 °C, concentration of [PO] depicted as absorbance measured using FTIR.

When varying the DMC concentration, it can be observed that the living character of the polymerization is less prominent at concentrations above 0.025 mol%$_{DMC,Zn}$. The early reaction stages in particular show deviation from linearity (Figure 50). Next to this, the recorded PO consumption profiles in Figure 51 (depicted as of the beginning of the activation phase) show that the consumption rate increases with increasing catalyst concentration.

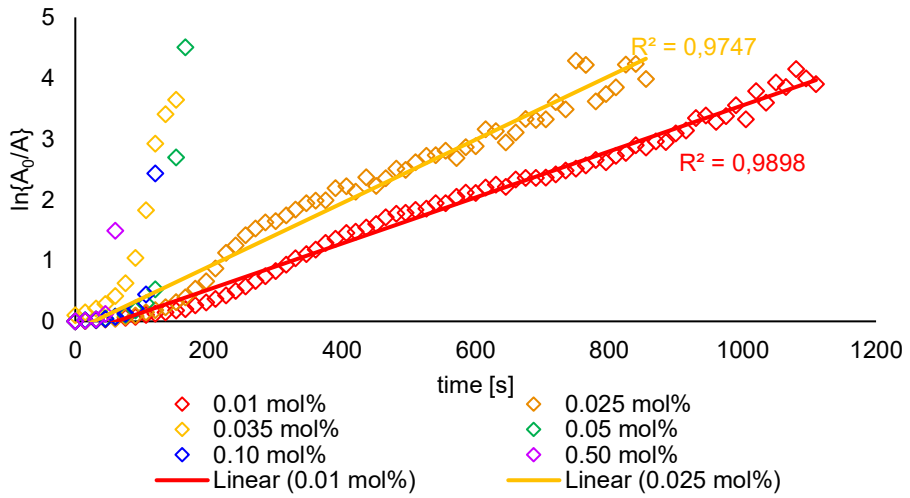

Figure 50: Semilogarithmic kinetic plot of the activation phase of a PO polymerization with varying [**DMC2**], 85 °C, concentration of [PO] depicted as absorbance measured using FTIR (mol% = mol%$_{DMC,Zn}$).

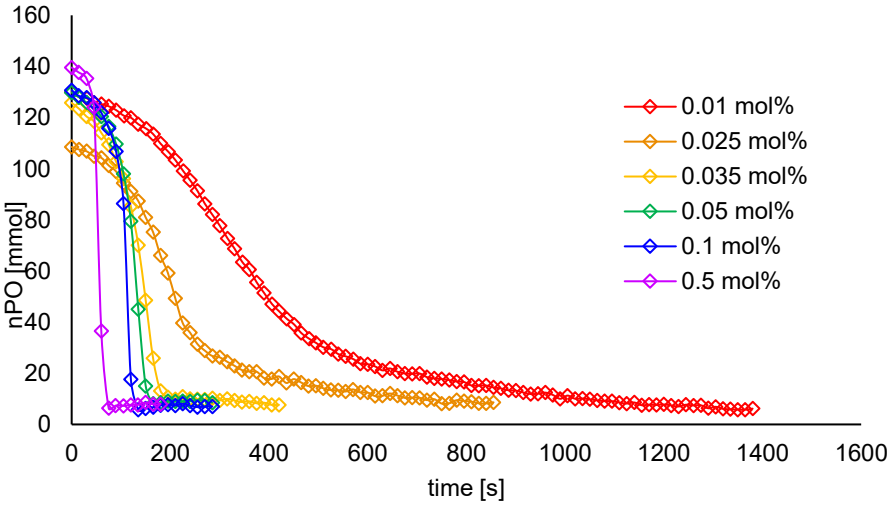

Figure 51: PO consumption in the activation reaction after end of t_{ind} at varying [**DMC2**] (mol% = mol%$_{DMC,Zn}$), 85 °C.

The exact reaction rate varies throughout the activation reaction. Figure 52 shows the fractional conversion and the reaction rate (calculated as shown in **Equation 15**) at a concentration of 0.025 mol%$_{DMC,Zn}$ of **DMC2** over the course of the induction time and the activation of the catalyst. The reaction rate fluctuates around zero before the activation starts due to minor measurement inaccuracy. Once the activation takes place and fractional conversion rises, the reaction rate rapidly increases until a fractional conversion of nearly 100 % is achieved.

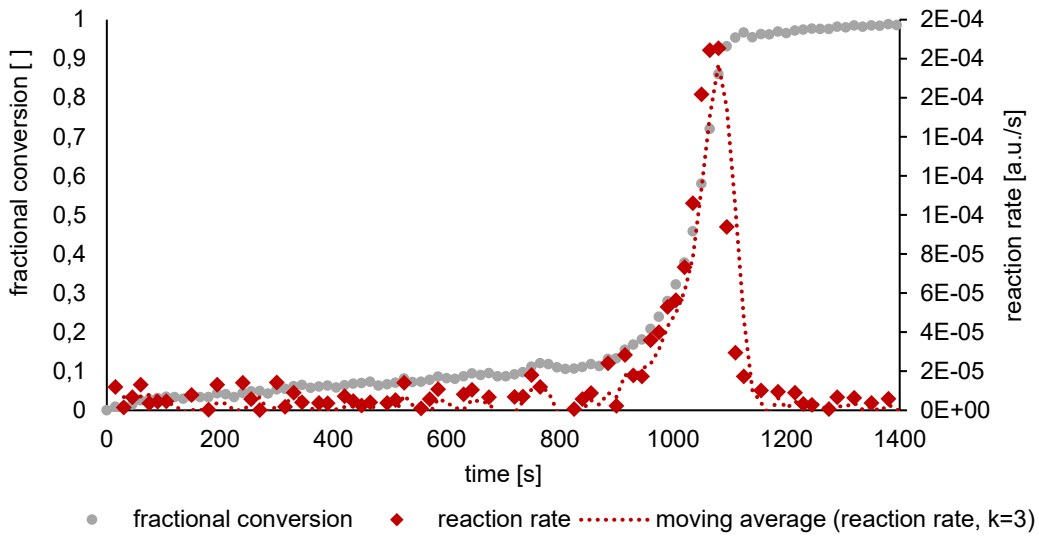

Figure 52: Fractional conversion ($conv._{fract} = \frac{n_{converted}}{n_{fed}}$) and reaction rate ($v_p = -\frac{d[M]}{dt}$) during the activation phase of **DMC2** (0.025 mol%$_{DMC,Zn}$).

When the catalyst concentration is lowered to 0.01 mol%$_{DMC,Zn}$ it becomes apparent that the reaction rate increases until a fractional conversion of 0.5 is reached, followed by a decrease to zero up to a fractional conversion of approximately 1 (Figure 53). The induction time, the sigmoidal shape of the conversion course and the increasing reaction rates indicate that the activation of the DMC catalyst is a self-accelerating reaction.[152-154]

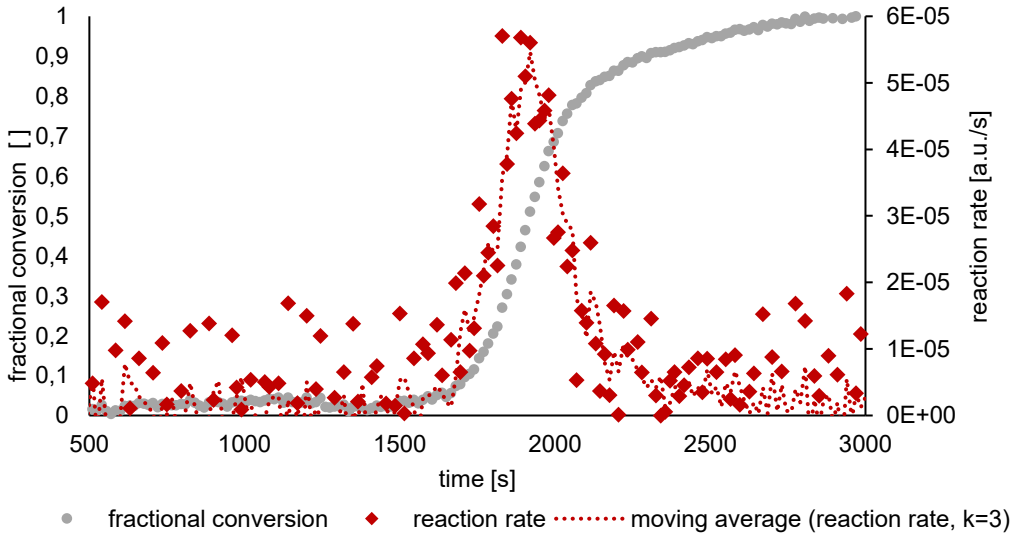

Figure 53: Fractional conversion ($conv._{fract} = \frac{n_{converted}}{n_{fed}}$) and reaction rate ($v_p = -\frac{d[M]}{dt}$) during the activation phase of **DMC2** (0.01 mol%$_{DMC,Zn}$).

An autocatalytic effect of the polymer product could be ruled out by the observation that the reaction proceeds slower under the addition of additional PPG (Figure A 15, appendix). Moreover, the ring-opening of propylene oxide is an exothermic reaction, meaning the rapid increase in temperature accompanying the activation reaction leads to a shift of the reaction

equilibrium towards the reactant side. Therefore, this is also not the reason for the observed acceleration. The fragmentation of the DMC particles and concurrent generation of additional active sites as observed by Tran *et al.*[92] and Huang *et al.*[21] is most likely the culprit of the auto-acceleration mechanism. Such fragmentation of particles is well described for heterogeneous catalysts for polyolefin synthesis. It is caused by the hydraulic forces exerted by the growing polymer chains and can already be observed for the first filling of the pores.[155-156] The discovered auto-acceleration leads to the assumption that this fragmentation process is also occurring under the use of **DMC2,** leading to the expansion of the DMC particles into unconnected substructures immersed in the polymer. This expansion facilitates diffusion of the monomers to the active sites and therefore accelerates the reaction.[155] The extend of this fragmentation of DMC catalysts was not further investigated within this thesis.

The propagation reaction of the catalyst **DMC2** was studied regarding the consumption of a second portion of PO added to the reaction after the activation over time. The same catalyst concentration as in the activation reaction was used, but the reaction temperature was further lowered to 70 °C as mentioned above. Figure 54 shows that the propagation reaction rate increases with increasing catalyst concentration to a point where PO is already consumed before the first measurement was collected at concentrations of 0.05 mol%$_{DMC,Zn}$ and above. Due to this fast reaction, only up to 3 datapoints could be collected above a catalyst concentration of 0.025 mol%$_{DMC,Zn}$ which reduces the significance of the measurements drastically. Therefore, these measurements were excluded from the following considerations. The only possible observation here is that a maximum conversion speed seems to be reached at a catalyst concentration of 0.05 mol%$_{DMC,Zn}$.

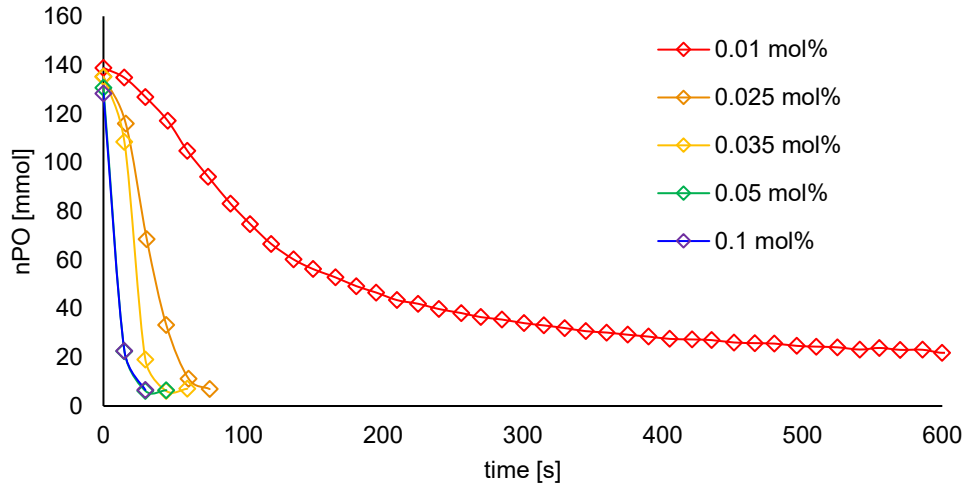

Figure 54: PO consumption in the propagation reaction at varying [**DMC2**] (70 °C, mol% = mol%$_{DMC,Zn}$).

The semilogarithmic kinetic plots of the PO concentration during the propagation phase of the two concentrations considered for **DMC2** show a pronounced lower fit to the linear model of a

living polymerization than during the activation phase (comparison of Figure 50 and Figure 55). This suggests that a coordination polymerization mechanism operates in the DMC catalyst with the formation of stable active polymerization centers during the activation phase that are capable of fast polymerization (i.e., $k_p > k_a$) in the propagation phase. The shape of the obtained graphs additionally indicates the existence of termination reactions and slow initiation.[54]

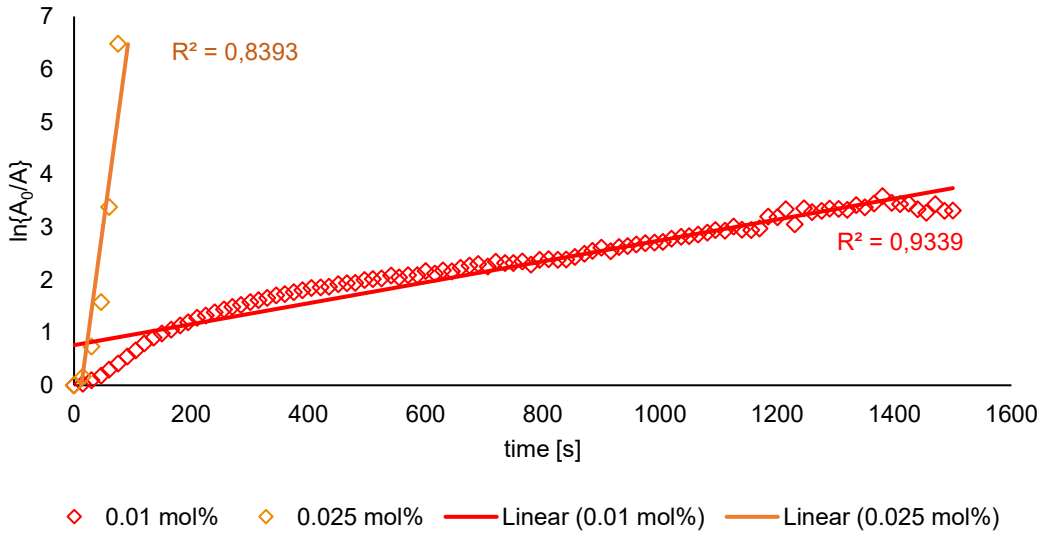

Figure 55: Semilogarithmic kinetic plot of multiple consecutive PO doses in the propagation phase using **DMC2** (70 °C, mol% = mol%$_{DMC,Zn}$).

For the propagation phase of the reaction no induction time was, to the best of our knowledge, mentioned in previously reported studies. However, when analyzing the propagation phase using in situ FTIR it becomes apparent that indeed a short induction period exists in which the reaction rate rapidly increases before it slowly decreases like a reaction with positive-order kinetics would (Figure 56). This shortened induction period (>100 s in activation phase, <50 s in propagation phase) can be reproduced in all four consecutive PO doses investigated. Concludingly, with each addition of monomer new active sites are generated. This is most likely explained by the above-mentioned fragmentation of the catalyst unveiling particle surface that was previously contained in pores that were too small for the monomer to reach. When further investigating the propagation phase reaction kinetics, the newly found induction period needs to be excluded, because it does not show steady-state behavior.[151]

These observations lead to the conclusion that the DMC catalyst **DMC2** actually does not follow a living polymerization mechanism, since activation is not consistently faster than chain elongation over the course of the polymerization. The conversion of the catalyst in its active state mimics a living behavior due to the rapid conversion of the reaction. However, this extensive conversion cannot be maintained by the proposed new exposure of active sites via fragmentation. Moreover, products of a chain transfer to monomer are detectable in MALDI MS (Figure 45).

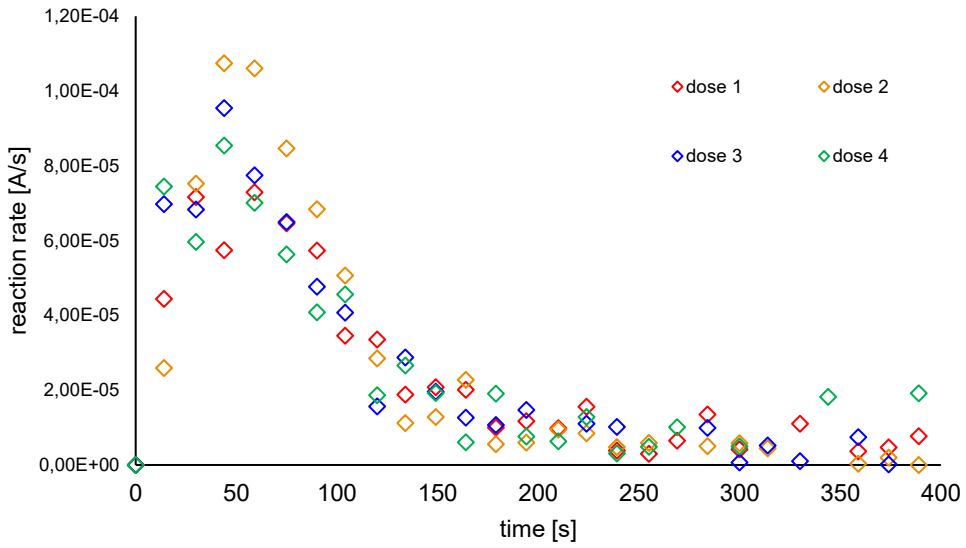

Figure 56: Reaction rate ($v_p = -\frac{d[M]}{dt}$) plotted on time of multiple consecutive PO doses in the propagation phase ([**DMC2**] = 0.035 mol%$_{DMC,Zn}$ 70 °C).

For further kinetic analysis of the propagation phase, its temperature dependency was investigated using an Arrhenius plot. The natural logarithm of the initial effective rate constants $k_{e,initial}$ (Figure 57, left) and initial reaction rates $r_{e,initial}$ (Figure 57, right) at different temperatures of the propagation phase (induction phase discarded) are plotted against the inverse absolute reaction temperature.

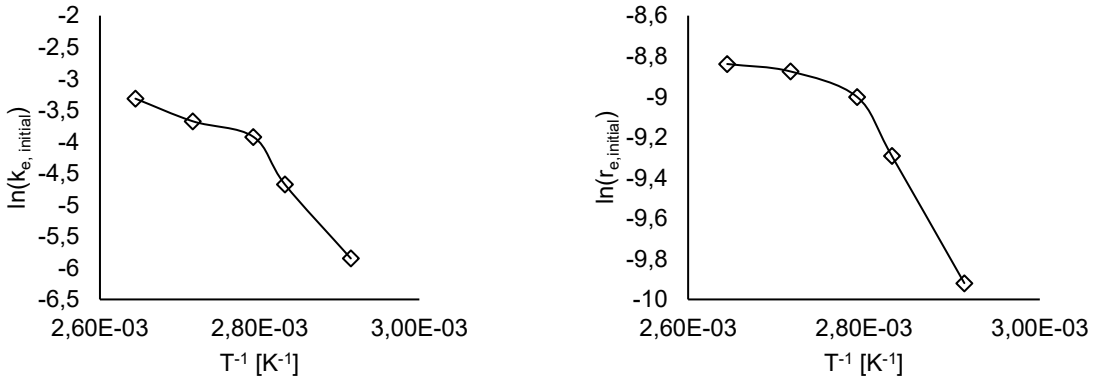

Figure 57: Arrhenius plots of the polymerization's propagation phase (**DMC2**, 0.05 mol%$_{DMC,Zn}$)

A convex shape of the plot for ln($k_{e,initial}$) against reciprocal temperature was observed, meaning the activation energy E_A decreases from lower reaction temperatures (70 °C – 85 °C, $E_{A,obs}$= 129 kJ/mol) to higher temperatures (85 °C – 105 °C, $E_{A,obs}$= 34 kJ/mol).[157-158] This can be an indication that Knudsen diffusion is the rate determining step at high temperatures.[157,159] However, Knudsen diffusion cannot be the only influence since it would only lower the observed E_A by half.[159] The shape of the Arrhenius plot for ln($r_{e,initial}$) additionally indicates prominent external mass transfer control at temperatures above 95 °C.[157] Despite the small

amount of available datapoints at low temperatures, kinetic control can be assumed for the lowest temperature of 70 °C.

Mass transfer control was then investigated by varying the amount of monomer added to the reaction at the transition temperature between kinetic control and mass transfer control: 85 °C (Figure 58).

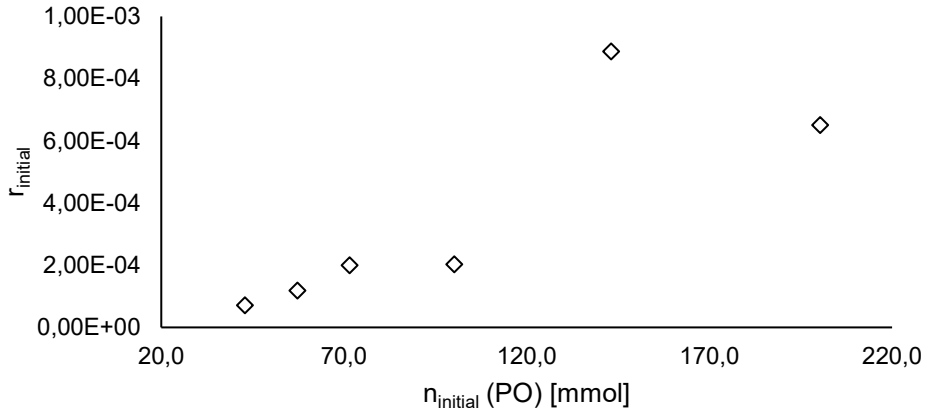

Figure 58: Dependency of the initial reaction rate ($v_p = -\frac{d[M]}{dt}, induction\ phase\ discarded$) on the initial PO amount in the propagation phase [**DMC2**, 85°C]

The initial reaction rate $r_{initial}$ rises with increasing initial PO amount due to the rate of diffusion being proportional to the concentration gradient as stated in Fick's first law.[160] It can also be observed that the reaction switches from first order to second order towards the lower amounts of PO (57.2 and 42.9 mmol). This indicates that the rate limiting step at such low monomer concentrations is the coordination to the active site of the DMC catalyst, supporting a coordinative mechanism.[54] This coordination of monomer seems to be facilitated when an increased amount of monomer is present.

To gain deeper insight, the order in catalyst during the propagation reaction was determined using the graphical "time normalization analysis" by Burés.[161-162] The reaction rates on time were investigated for the existence of an induction period and the respective data was discarded. It was assumed that the catalyst concentration stays constant after the induction takes place. As it can already be assumed from Figure 54, the reaction is not proceeding faster above [**DMC2**] = 0.025 mol%$_{DMC,Zn}$. This brief assumption is supported by the finding of the time normalization analysis in Figure 59 showing that the reaction is of zero order in catalyst except for the lowest catalyst concentration, which was also previously observed by Chruściel *et al*.[11]

This shows that not all active sites are occupied. Therefore, an increase in active sites (increase in catalyst concentration) does not increase reaction rate in the propagation. This can also be the explanation for the increasing reaction rates at increasing monomer concentration shown in Figure 58.

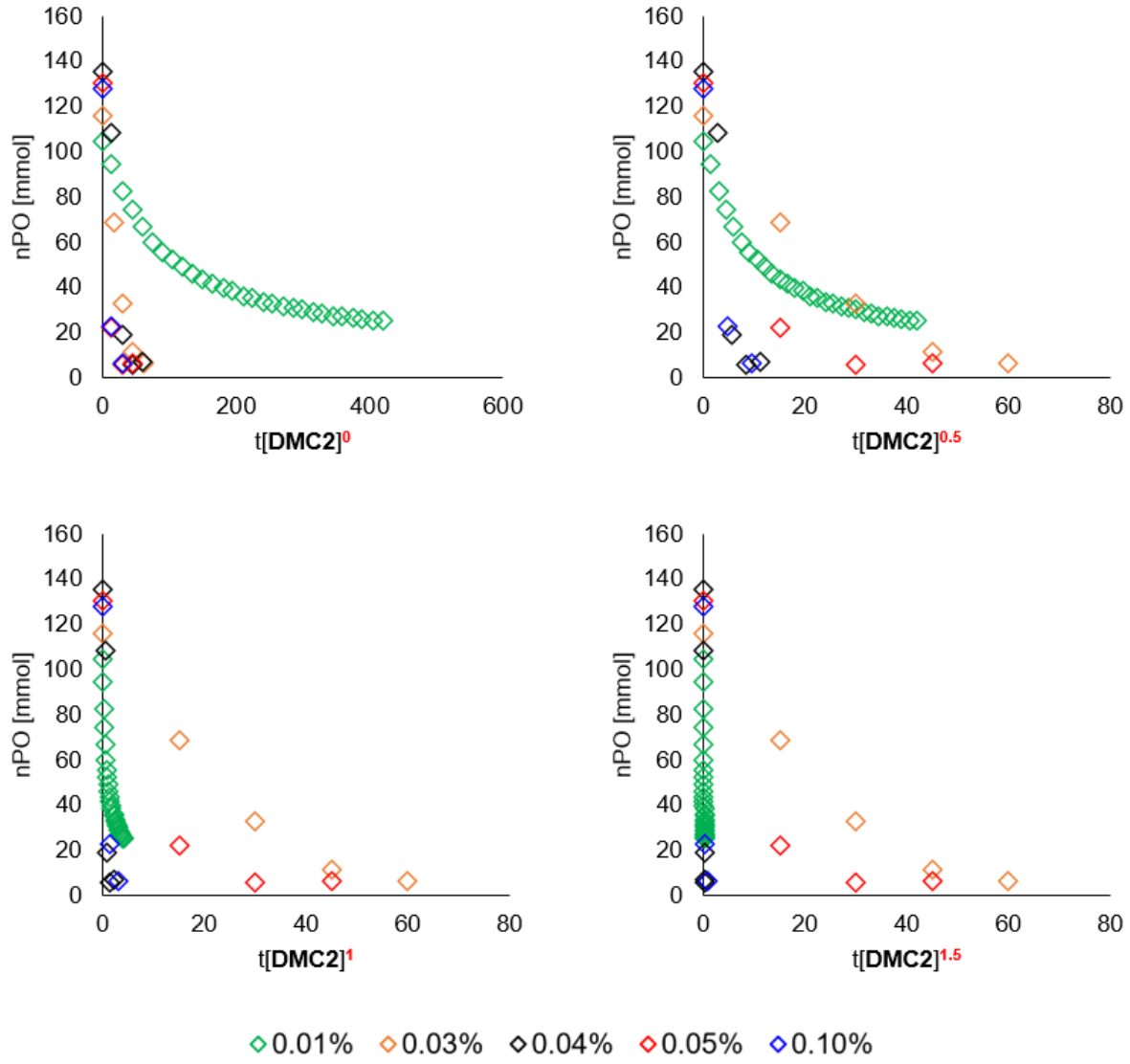

Figure 59: Variable time normalization analysis of the order in catalyst during the propagation phase (induction corrected, 70 °C). In this graphical method the entirety of the reaction concentration profiles is used to determine the order in catalyst by plotting the measured monomer concentration against a normalized time scale $t[DMC]^n$. An overlay of the different concentration's plots marks the correct order in catalyst n. No rate data is needed

When there are more free active sites available than are used at low monomer concentrations, a higher amount of monomer leads to an apparent higher amount of catalyst. It can therefore be concluded that the **DMC2** catalyst is of very high density of active sites after its activation during the induction period. When assuming that fragmentation takes place right at the end of the induction time, a continuous polymer phase with dispersed catalytic sites similar to a Ziegler-Natta catalyst[155] can be proposed. Because of the observed mass transfer limitations at high temperatures, the dispersed active sites are still assumed to be located on defined particles, possibly of nanoscale size.

Another possible reason for these observations is a very fast non-terminating chain transfer reaction taking place leading to the low PDI of the products. If the rate constant of chain transfer is at least ten times higher than the propagation constant, the propagating macromolecule is exchanged before two consecutive monomer molecules can be added to

the polymer chain.[20] Then, the reaction is not dependent on the catalyst concentration, but on the CTA concentration which was kept constant over the course of the these experiments. However, as mentioned above, a higher CTA concentration does not lead to a faster PO consumption. This might indicate a limitation of chain transfer rate by the reaction temperature, used chain transfer agent or catalyst type. This was not investigated in this work and needs to be further explored.

A mechanistic cycle with one active site undergoing more than one chain elongation reaction can only be observed for the catalyst concentration 0.01 mol%$_{DMC,Zn}$. This reaction shows an overall second order, determined by the integral method. Therefore, the rate determining step is of second order and dependent on both, catalyst and monomer concentration.

This clearly indicates that the propagation reaction is composed of a coordination of monomer followed by its insertion into the zinc-polymer bond. ^{13}C NMR analysis of the polymer products microstructure supports this hypothesis by revealing that the polypropylene glycol predominantly consists of head-to-tail bonds. Only few signals observed in ^{13}C NMR DEPT spectra can be assigned according to Schilling *et al*.[163] to either T-T defect structures or end groups of the PPG as it is shown on an exemplary PPG in Figure 60. A coordination polymerization catalyst prefers to ring-open the O-CH_2 bond of the PO leading to regioregular products.[10,163-164]

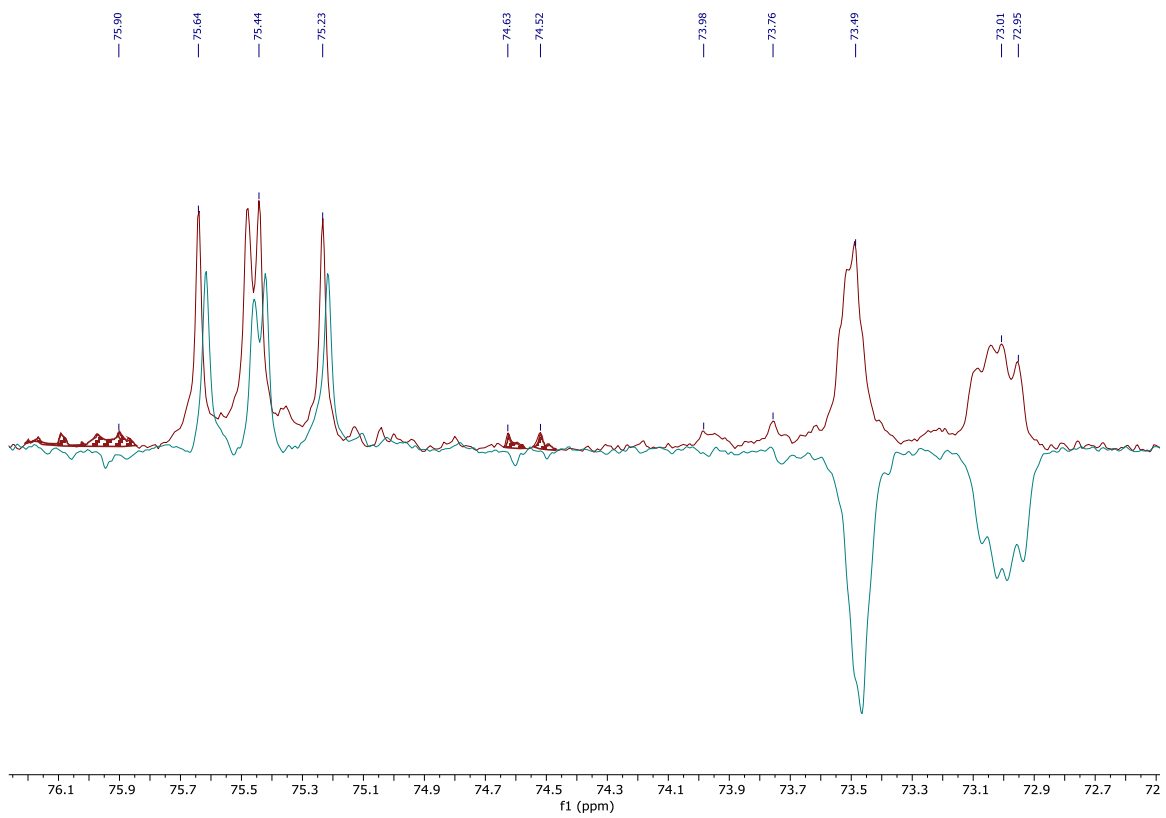

Figure 60: ^{13}C NMR spectrum (red) and ^{13}C NMR DEPT spectrum (blue) of the methine and methylene region of a 3500 g/mol PPG prepared with 0.5 mol%$_{DMC,Zn}$, crosshatched signals can be assigned to T-T defect structures and/or end groups of the polymer ($CDCl_3$, 100 MHz, 297.0 K).

Considering all discussed observations and previous studies on DMC catalysts by other groups, the mechanism shown in Figure 61 is proposed for **DMC2**.

In contrary to the suggestion by Kim *et al*,[20] the transformation of the DMC catalyst precursor into its catalytically active form was found to happen by an insertion of ring-opened propylene oxide monomer into the Zn-CA bond (Figure 61 **A**). This is reasoned in finding low molecular weight polymer chains with CA end groups only in MALDI MS and the detection of oligomeric PPG chains attached to the active site in FTIR experiments.

Since the reaction can be conducted without CTA and polymer chains of a molecular weight below the CTA's weight are observed, it can be assumed that the CTA is not involved in the activation reaction. Moreover, no chlorine end groups were detected on the macromolecules, therefore, a direct participation of the chlorine in the reaction is not considered. However, the electronic and structural effect of the contained halogen is indispensable for catalytic activity. Determination of the catalysts structure revealed that the complexing agent *tert*-butanol is only located on the surface of the catalyst and exists, in case of highly active catalysts, in two different states. The strongly coordinated substate might act as a nucleophilic aid for ring-opening the propylene oxide molecule before it inserts into the bond between the zinc atom and the weakly coordinated *tert*-butanol, similar to the nucleophilic co-catalysts employed in propylene oxide/CO_2 copolymerization. This additionally indicates the existence of a binuclear mechanism, that is however not necessary for the reaction to proceed but leads to a higher reaction rate.

After the activation of the catalyst, the propagation proceeds fast via a cationic activated chain end mechanism (**B**) and a competing coordination insertion mechanism (**C**) as it was previously suggested by Tran *et al.*[92] and Kim *et al.*[20]

An activated chain end mechanism competing with an activated monomer mechanism (AMM) was also described for other cationic polymerizations of cyclic ethers involving alcohol CTAs by Penczek *et al.*[47,51,53] with the difference that in these cases the AMM was not of a coordination insertion nature. However, Penczek *et al.* found that the reaction can be pushed towards the AMM by a high concentration in hydroxyl groups. Accordingly, addition of diol CTA and continuous addition of monomer was found to enhance the performance of DMC catalysts in our group. This likely explains the lack of back-biting or proton transfer products with high molecular weight. These side reactions seem to happen primarily during the initiation phase of the DMC catalyst where a high concentration of monomer is necessary and are then suppressed in the propagation by the continuous addition of monomer. Therefore, it is proposed that the coordination insertion mechanism (**C**) is dominating the propagation reaction leading to regioregular homotelechelic PPG with narrow molecular weight and low unsaturation.

Contrary to the previous suggestion by Kim *et al.*, our observations suggest that the reaction is only activated by the CA on the surface of the catalyst and no monomer activation in the bulk occurs. The catalyst particle's porous morphology most likely allows for fragmentation without the need of a reaction within the bulk of the catalyst.
A self-termination reaction (**D**) can occur during the activated chain end mechanism by proton transfer and leads to short polymer chains with CA end groups. The non-terminating chain transfer reaction leads to fast exchange of the growing macromolecules on the active sites. Therefore, a monomodal MWD below 1.3 is achieved despite two competing propagation mechanisms. With higher reaction temperatures an increase in mass transport limitations can be observed, which is typical for surface reactions on a heterogeneous catalyst and proves that the catalyst is not turning into a homogeneous phase of active sites in polymer over the course of the reaction. However, with every addition of monomer to the catalyst an induction time was detected, indicating activation of more dormant catalytic sites possibly through fragmentation and therefore finer dispersion of the catalyst. Hence, fragmentation behavior of the catalyst should further be studied in detail.

4.1.3.3 Conclusion: Reaction mechanism of Zn/Co DMC catalysts

The reaction mechanism was elucidated using kinetic data obtained by online FTIR measurements and investigating the catalyst's activation by DFT calculations and an *ex situ* activation experiment. The investigated **DMC2** was found to be activated by monomer insertion and to follow a coordination insertion mechanism and a cationic activated chain end mechanism in parallel during propagation. Both reaction pathways take place at the surface of the catalyst only, which makes a big surface area crucial for good catalytic activity. A high concentration of hydroxyl groups seems to push the catalyst towards the coordination insertion mechanism which is why side reactions are suppressed under addition of a CTA and by keeping the PO concentration low by continuous addition of monomer. Contrary to previous assumptions the cobalt atoms on the catalyst's surface appear to be involved in this activation which needs to be further investigated.
Additionally, the pore sizes of the heterogeneous DMC catalyst need to allow for diffusion of PO monomer. The growing polymer chains in the pores seem to break down the catalyst particles and expose more surface area for the monomer to react. Hence, a short induction time can be observed for every addition of monomer to the reactor, even after activation. Moreover, the polymerization reaction is accompanied by a fast chain transfer with the chain transfer agent, making possible to obtain narrow molecular weight distributions.
The catalyst only mimics a living polymerization behavior in the activation phase due to the fast unveiling of fresh surface area and fast chain transfer. However, during the propagation

phase, the polymerization does not seem to have a living character. To understand the catalytic reaction in more detail, the fragmentation of the particles and the chain transfer reaction need to be investigated aiming towards designing a more active and long-living catalyst.

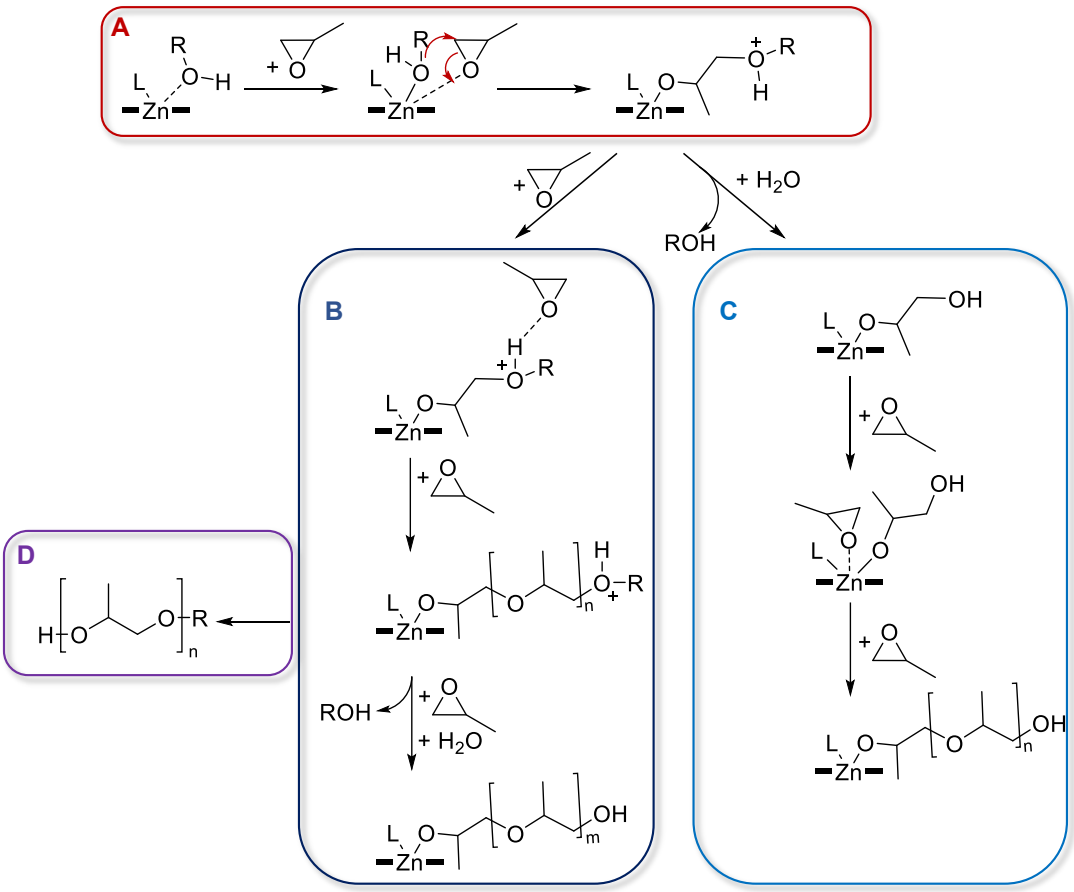

Chain Transfer (Chain Exchange)

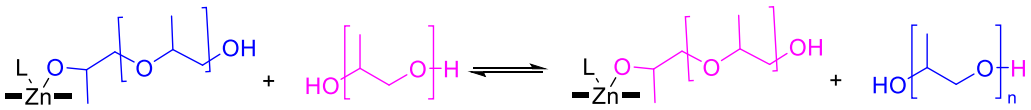

Chain Termination

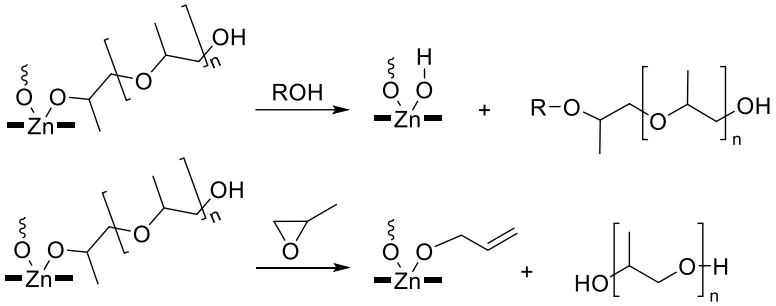

L: H_2O, (co-)complexing agent
ROH: complexing agent

Figure 61: Proposed mechanism of the homopolymerization of propylene oxide using **DMC2** (A: activation of the catalyst | B: activated chain end mechanism | C: coordination insertion mechanism | D: self-termination.

4.2 DMC-catalyzed copolymerization reactions

Next to polypropylene glycol, copolymers of propylene oxide and various comonomers are of high interest for industrial application. By copolymerization of PO with one or multiple comonomers the product's properties can be changed and controlled towards the desired application. An example of such copolymers are Poloxamers, block-copolymers of PO and ethylene oxide (EO), that combine the hydrophobic character of PO with the hydrophilic properties of EO and therefore can be used as amphiphilic nonionic surfactants.[165-166]

Since propylene oxide is produced from petrochemicals, it has a big global warming impact.[16,167] Synthesis of PO from biomass-derived propylene is not yet economically applicable.[168-169] In order to reduce the environmental footprint of products containing PPG, **DMC2** catalyst was tested for activity in the bipolymerization of propylene oxide and cyclic ester monomers (*rac*-lactide and ε-caprolactone) as well as terpolymerization of epoxides, cyclic esters, and CO_2. With this, parts of the PO are replaced by more environmentally friendly comonomers, which are readily derived from biomass[170-173], introduce biodegradable groups into the macromolecules and improve thermal stability.[174-176]

While only few catalytic systems are known to copolymerize propylene oxide and cyclic esters directly into statistic or gradient copolymers,[177-179] many more catalysts and catalytic systems are active for the polyether-polyester copolymerization under the addition of carbon dioxide.[130,132-133,174-176,180-190]

Catalytic activity of double metal cyanide catalysts towards the ROCOP of PO and other cyclic monomers was previously reported in a patent by "Arco Chemical Technology" for ε-caprolactone, δ-valerolactone and β-propiolactone as comonomers.[137] Next to this, the group of Frey reported the activity of DMC catalysts for the ROCOP of hexamethylcyclotrisiloxane (D_3) and PO.[129] Even though it does not depict an ecological advantage, the PO/D_3 copolymer is of high industrial interest, since it combines the beneficial properties of a PDMS[191] - low glass T_G and high stability - with the easier implementable and less expensive polyether PPG in one copolymer.

Other reported PPG/PDMS copolymerization procedures focus on hydrosilylation of prepolymerized polyethers and polysiloxanes (Figure 62**A**),[192-194] or use PDMS as a chain transfer agent for propoxylation or ethoxylation reactions with,[195-196] or without previous functionalization (Figure 62**B**).[197] These procedures generally yield ABA-type block copolymers with polyether blocks as end groups.

For the application of polyether-polysiloxane copolymers in low viscosity consumer adhesive products, a gradient copolymer is preferred. This type of macromolecule shows less interchain repulsion and therefore better miscibility of components as well as lower turbidity than a block-copolymer due to a less pronounced microphase separation.[198-200]

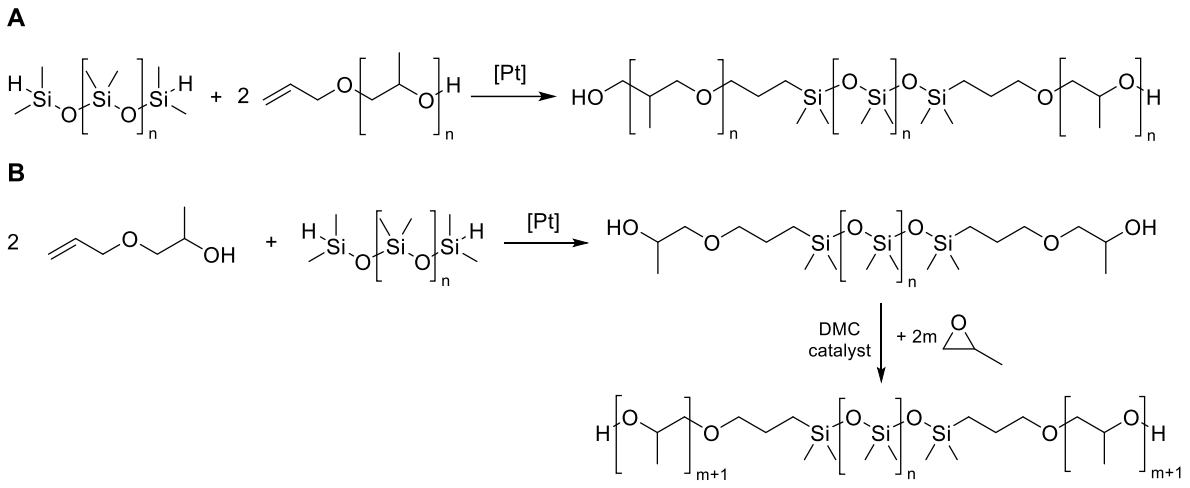

Figure 62: Preparation of PDMS-PPG block-copolymers by hydrosilylation (**A**) and by using a pre-endcapped PDMS as CTA (**B**).[195].

Surprisingly, the preparation of bifunctional PO/D_3 gradient type copolymers in an applicable process by industry has not been reported so far. Therefore, the development of new polymer products using DMC catalyst became objective of this part of the dissertation. Polymers with novel homotelechelic reverse (BAB) silicone polyether structures in which the polypropylene oxide represents the middle unit of the polymer were produced. The PDMS and PPG units are ordered in a gradient copolymer fashion towards -Si$(CH_3)_2$-OH end groups. A visual comparison between the previously reported ABA block-copolymers and new BAB gradient-copolymers can be seen in Figure 63.

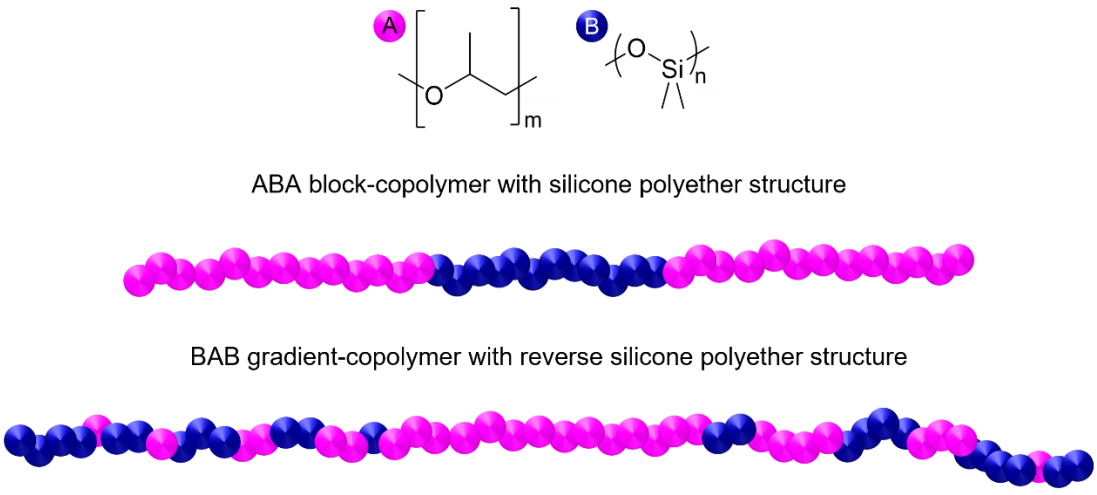

Figure 63: Previously reported ABA block-copolymer structure and new BAB gradient-copolymer structure.

4.2.1 Polypropylene oxide-polydimethylsiloxane copolymers

Polypropylene oxide-polydimethylsiloxane copolymers (Figure 64) were prepared by addition of different amounts of D_3 to the standard polymerization reaction of PO as described in detail in experimental (appendix, chapter A-1.4.5). **DMC2**, CTA and the comonomer D_3 were heated

to 120 °C and propylene oxide was continuously dosed into the reactor. To make the process as applicable to industrial production as possible, neither a glove-box, nor any other inert atmosphere techniques were used to transfer the reactants to the reactor. So no strict exclusion of air or moisture was implemented, in contrast to previous reports of a PO/D_3 copolymerization to produce AB gradient copolymers using a DMC catalyst.[129]

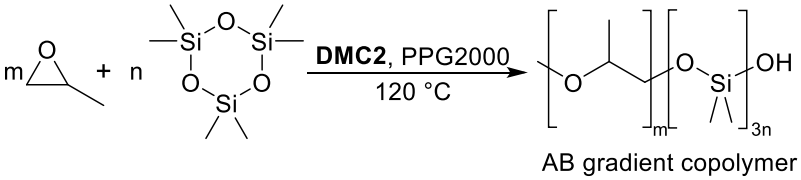

Figure 64: Copolymerization of PO and D3 using **DMC2** catalyst.

The different variations of reaction conditions and corresponding reaction values as well as product properties are presented in Table 7. Over the reaction course of **CP1** (copolymer 1) it was observed that the induction time (t_{ind}) of the polymerization was longer than in a homopolymerization reaction, and that the reactor pressure dropped below the initial gauge pressure ($p_{0,120°C}$) of 0 bar. This shows that the added D_3 has an effect on the reaction course. To assess an influence of the reaction pressure on the product quality, the pressure was varied between **CP2**, **CP3** and **CP7**. It was shown that the argon pressure inside the vessel has no effect on the reaction and therefore $p_{0,120°C}$ was set to 4.8 bar to avoid vacuum and ensure ideal working conditions for the used dosing equipment.

The set of experiments conducted (Table 7) shows that D_3 conversion is limited, unless a minimal amount of 8.3 g of initial PO is added to the reaction and a post-reaction time of several hours at 120 °C is awaited. 94 % conversion of D_3 were achieved under a stirring time ($t_{stirring}$) of 4 h and 99 % conversion under a stirring time of 17 h after full addition of PO. In summary, a D_3 conversion of up to 99 % was achieved, accompanied by a PO conversion of 100 % at a calculated D_3 content of 30-40 %wt.

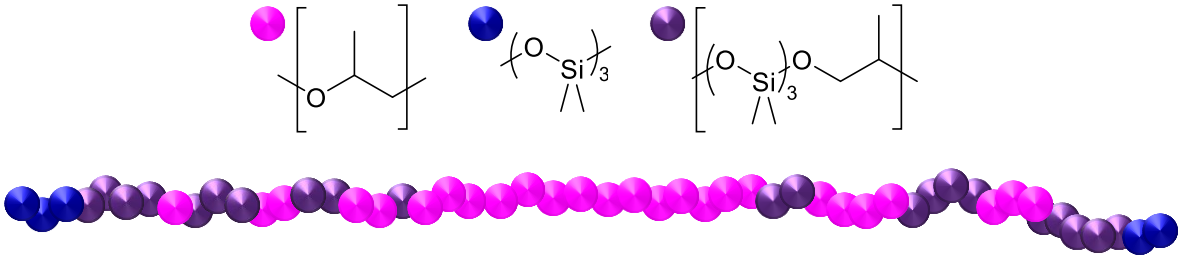

Figure 65: Schematic depiction of the monomer distribution along the PPO-PDMS copolymer chain.

Due to the observation of a fast initial pressure drop and a slow consecutive decrease in pressure (see pressure course throughout the reaction in appendix, Figure A 19) it is assumed that a polypropylene glycol core of the polymer is created with low amounts of D_3 incorporated. Towards the end of the polymer chain a gradual change in composition from mostly PO

monomer to D_3 (schematically in Figure 65) is expected. The presence of Si-OH end-groups was proven by ^{29}Si NMR (see appendix, chapter A-3).

The products of the copolymerization were obtained in form of an opaque liquid of low viscosity. All of them showed a narrow monomodal molecular weight distribution as presented exemplarily for **CP5** in Figure 66. A small shoulder is observable, which can be explained by the formation of higher molecular weight homopolymer side product or by insufficient mobility of the chain transfer agent PPG 2000 (g/mol) and therefore slow chain transfer.

All samples show one clear T_G, varying between -72.1 °C and -73.7 °C in differential scanning calorimetry, indicating only one type of polymer being present (exemplary thermogram in Figure 67). Hence, there is no phase separation between the copolymer segments.

Table 7: Experiments conducted to perform PO/D3 copolymerization using **DMC2**.

	reaction conditions					Results					
CP	initiation PO addition mode	propagation PO addition mode	$t_{stirring}$ [h]	t_{total} [h]	$p_{0,\ 120°C}$ [bar]	t_{ind} [min]	D3 conv.[a] [%]	Mn[b] [g/mol]	PDI[b]	η[c] [mPas]	T_g [°C]
1	discrete (4.15 g)	-	24	24	0	25	15	3113	1.33	419	-
2	discrete (8.3 g)	discrete (2 x 4.15 g)	19	22	1	14	97	12970	1.38	1223	-81.6
3	continuous (4.15 g, 4.17 g/min)	continuous (12.45 g, 0.167 g/min)	19	24	4.8	12	86	10344	1.28	819	-81.9
4	discrete (8.3 g)	discrete (2 x 4.15 g)	20	22.5	4.8	10	97	9939	1.45	1274	-81.6
5	continuous (8.3 g, 4.17 g/min)	continuous (8.3 g, 0.167 g/min)	17	19.5	4.8	12	99	9406	1.38	765	-81.1
6	discrete (8.3 g)	continuous (8.3 g, 0.167 g/min)	18	19.5	4.5	12	98	9309	1.41	1158	-81.1
7	discrete (8.3 g)	continuous (8.3 g, 0.167 g/min)	4	6.5	5.2	15	94	8659	1.33	873	-81.5
8	continuous (8.3 g, 4.17 g/min)	continuous (8.3 g, 0.417 g/min)	22	23	4.8	12	99	8455	1.42	864	-81.7
9	continuous (8.3 g, 4.17 g/min)	continuous (18.66 g, 0.417 g/min)	16	18	4.8	6	98	9679	1.47	2381	-78.6

All experiments were carried out using 10.08 g of PPG2000, 16.02 g of D3 and 300 ppm (mass) of catalyst. | CP: Copolymer | [a]: calculated from 29-Si (IG) NMR. | [b]: determined using GPC with THF eluent and polystyrene standard | [c]: determined on Haake RheoStress one with cone-plate method in CR mode.

The observed T_G listed in Table 7 are lowered in comparison to those reported for PPG 2000 to 4000 (g/mol), which are ranging from -73.8 °C to -69.4 °C.[201] This indicates the introduction of PDMS blocks in the copolymer, since the T_G shifts towards the lower temperatures generally observed for PDMS homopolymers (approx. -125 °C[202]). PPG 2000 is used as chain transfer agent and the PDMS content of the products is 30 – 40 %wt, which explains the observed behavior. It must be evaluated whether a higher PDMS content leads to lowering of the glass transition temperature.

If the resulting polymer products are true copolymers, they contain Si-O-C bonds (purple units in Figure 65) which are known to be hydrolysable.[203] Hence, the products of the copolymerizations were exposed to hydrochloric acid (1 M) for 5 h at 50 °C, which led to a

decreased turbidity and phase separation of the samples, indicating hydrolytic degradation. GPC analysis before and after the experiment show a new molecular mass of approximately one third of the original sample (see appendix, Figure A 33 and Figure A 62). ^{29}Si and ^{13}C NMR spectra of the hydrolyzed samples reveal that both PDMS and PPG bonds are still present after the hydrolysis as well as newly formed D_4 (octamethyltetracyclosiloxane), which is not formed when homopolymeric PDMS lacking OH end-groups is exposed to hydrolysis conditions.

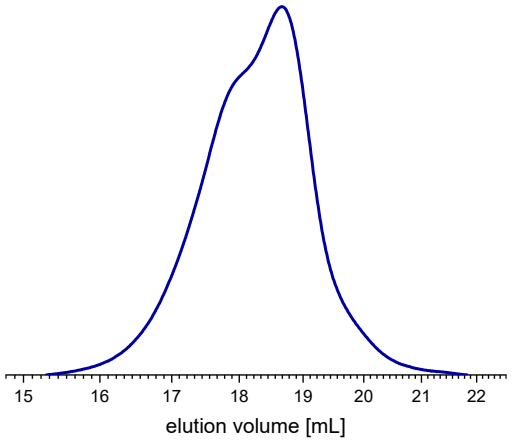

Figure 66: GPC diagram of PPO-PDMS copolymer **CP5** (using polystyrene standard and THF eluent).

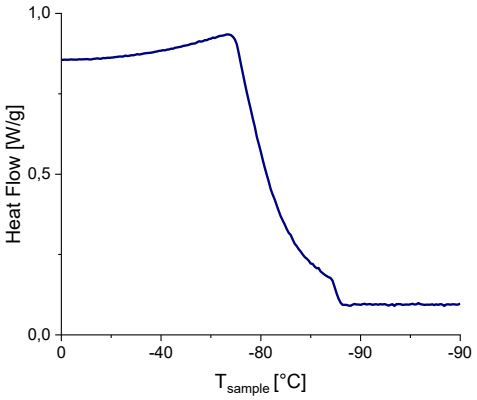

Figure 67: DSC Thermogram of PPO-PDMS copolymer **CP5** (-5 K/min).

Next to this, signals in the ^{29}Si-IG NMR spectrum at δ(ppm)=13.6 (**Si**$(CH_3)_2$-O-C) and the ^{13}C NMR spectrum at δ(ppm)= 1.2, -1.6, -2.0, -2.1 (Si(**C**$H_3)_2$-O-C) disappeared and were therefore attributed to the hydrolysis sensitive Si-O-C bond (see appendix, chapter A-3 for NMR spectra). This degradation of the polymer, which is regarded as a proof of copolymerization, leads to the separation of PPG and PDMS blocks yielding blended homopolymers. The PDMS blocks are expected to be short in comparison the PPG blocks (*vide supra*) and are partially depolymerized under these conditions, as attested by the formation of D_4. Whether the separated homopolymers are really of one third of their original molecular mass cannot be confirmed, because the different elution behavior of the homopolymeric and copolymeric samples makes their obtained molecular weights by GPC not comparable.

The co-existence of PO and D_3 moieties within the same polymer chain was additionally proven by a ^{1}H^{1}H NOESY NMR experiment showing the correlation between the methyl groups at the different copolymer units (protons **a** and **b**, Figure 68) and a DOSY ^{1}H NMR spectrum in which the same diffusion coefficient for both PPG and PDMS signals can be observed (Figure 69). The DOSY spectrum shows broad, distributed signals due to the polydispersity of the sample as well as signals for homopolymeric PDMS next to the copolymer signal.

Based on this observation, centrifugation experiments were conducted (45 min, 10000 rpm) to test if a phase separation of the product appears. All copolymers listed in Table 7 show phase

separation upon centrifugation except for **CP9**, which was prepared using previously dried PPG 2000 and resublimed D_3 in a previously dried reactor.

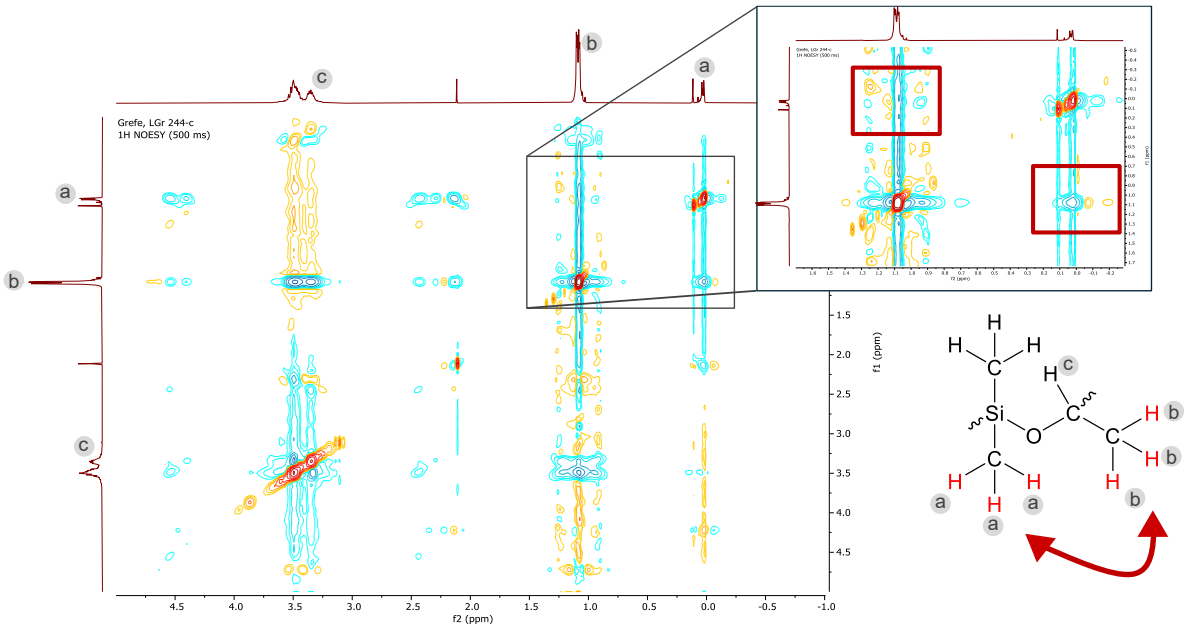

Figure 68: $^1H^1H$ NOESY NMR spectrum of **CP1** ($CDCl_3$, 297.5 K, 300 MHz), cross peaks in red boxes suggest NOE between the protons **a** and **b**.

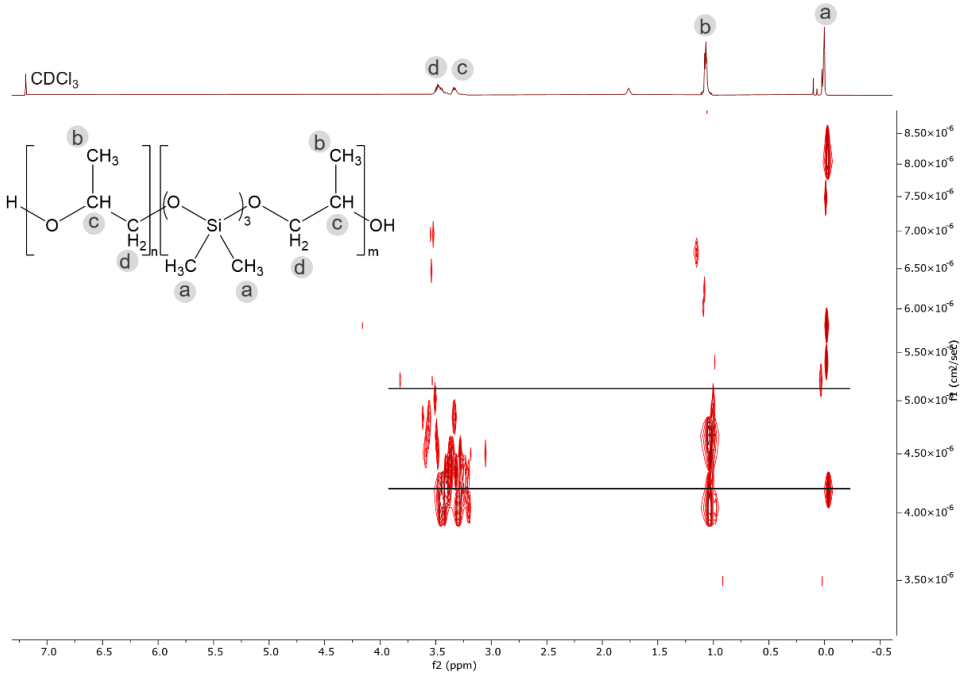

Figure 69: DOSY ^1H NMR spectrum ($CDCl_3$, 298 K, 500 MHz) of **CP2** (horizontal lines show polymer signals with the same diffusion coefficient which are copolymer signals).

^1H NMR analysis of the separated phases (Figure 70) shows a higher relative PDMS content in the lower density phase, supporting the observations from the ^1H DOSY NMR experiment. It was concluded that the high reactivity of the D_3 cyclic molecule allows for a ring-opening reaction with residual water in the reactor. The high ring-strain however seems to be necessary for the reaction to proceed since less ring-strained D_4 does not show any conversion under the

same reaction conditions. Thus, impurities that can react with the monomer must be excluded from the reaction.

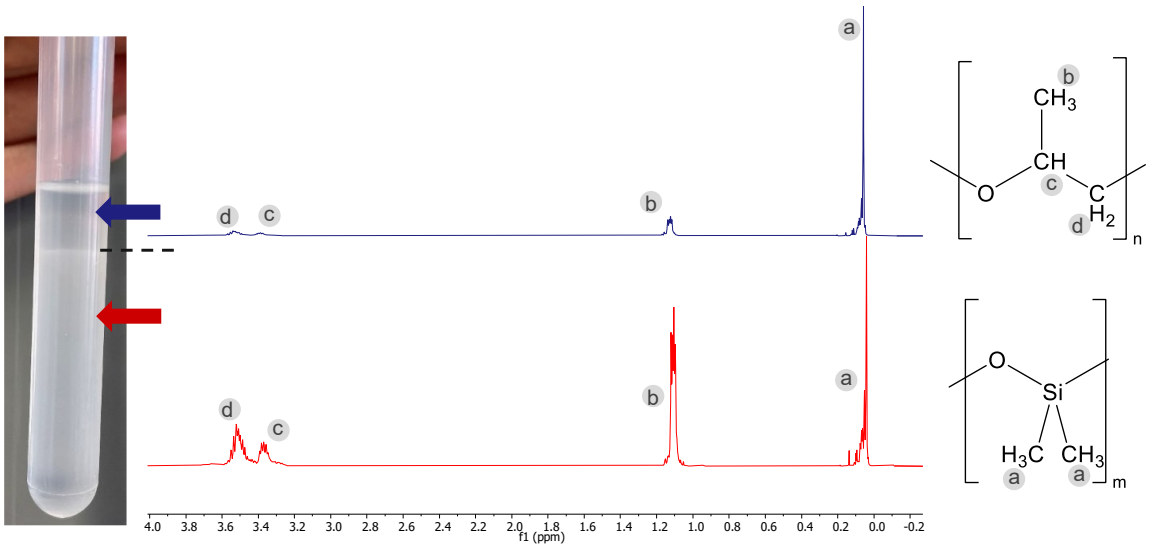

Figure 70: ^{1}H NMR spectra of a phase separated sample (CP2 | CDCl3, 400 MHz, 297.0 K | intensity adjusted to signal **a**).

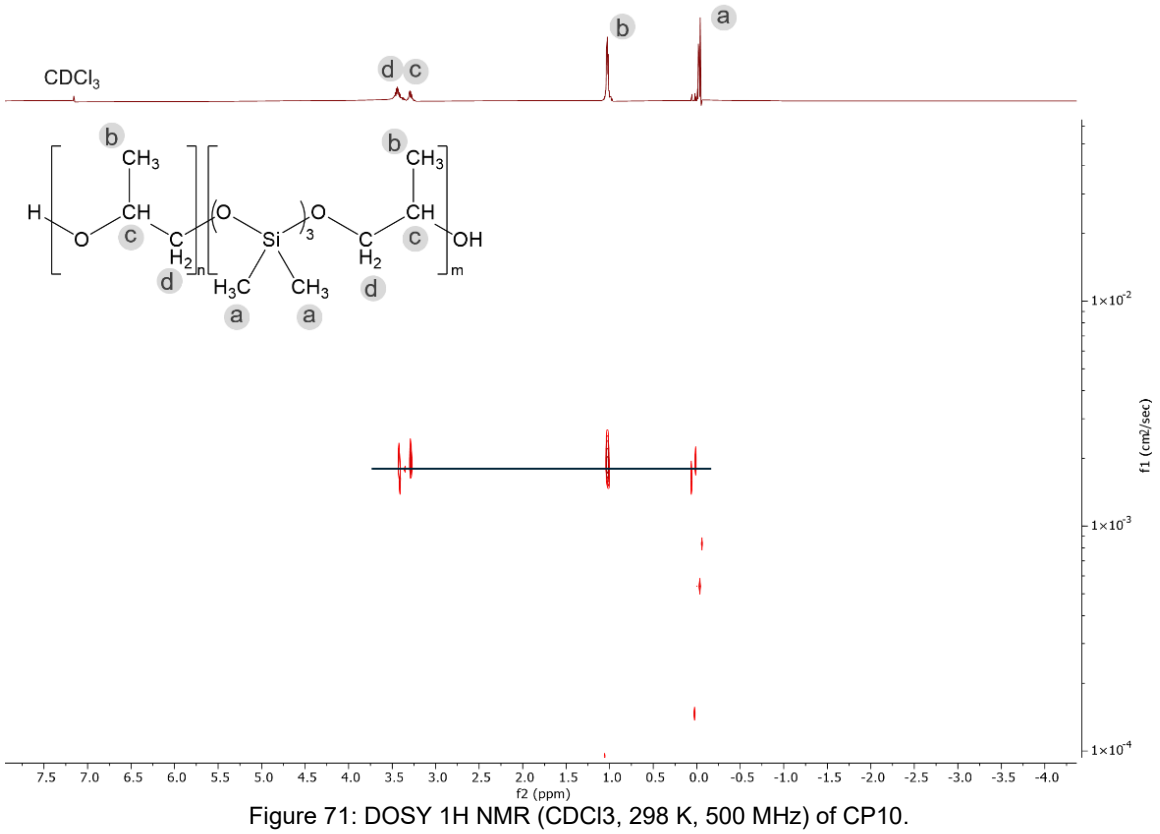

Figure 71: DOSY 1H NMR (CDCl3, 298 K, 500 MHz) of CP10.

To further test in which time of the reaction the homopolymerization side reaction takes place - during PO dosing or D_3 consumption period - the amount of propylene oxide was increased with a constant PO/D_3 ratio to extend the dosage phase. To achieve this goal the reaction was scaled up to 250 g in a 1 L stainless steel reactor (**CP10**). The ^{1}H DOSY NMR spectrum (Figure

71) shows mostly copolymer, and no phase separation of the product was observed after centrifugation. This indicates that the homopolymerization takes place during the D_3 consumption phase and can be prevented by increasing PO dosage without the need of drying the reactants. An ideal PO dosing time can be determined by process optimization and variation of PO mass flow to minimize homopolymerization side products.

4.2.2 Copolymers of epoxides with cyclic esters

A classical pathway for the bipolymerization of cyclic esters and epoxides is using polyethers as macroinitiators in the ROP of cyclic esters yielding block-copolymers.[204-205] Statistic copolymers however, can be obtained by the direct bipolymerization of propylene oxide with *rac*-lactide or lactones using 2-benzyloxy-ethanol as initiator. The obtained products are monofunctional.[133,137,177,206-208] Bifunctional products are reported to be prepared using N-heterocyclic carbenes as catalysts with diethylene glycol as initiator[209], Vandenberg catalyst[178], cationic indium complexes,[179] and a dual 1,8-diazabicyclo[5.4.0]undec-7-ene / Cr(salen) catalyst system.[210]

The terpolymerization of cyclic esters, epoxides and CO_2 to yield block-copolymers can be achieved using switchable catalysts like macrocyclic dizinc complexes,[187] and Zn β-diimine chelates.[184] Statistical copolymers are obtained using heterogeneous zinc glutarate,[174] or zinc adipate,[181-182] and catalyst combinations of Co^{III}(salen), zinc glutarate and PPNCl.[189] Next to this, various types of homogeneous catalysts with different metals and accompanying ligands can be used.[175,180,183,188]

DMC catalysts have as well been reported to perform the terpolymerization of epoxides, cyclic esters and CO_2. However, the used DMC catalysts require a cocatalyst,[132-133,211] yield monofunctional products[133] or need quenching after the reaction is finished.[176,186]

The use of DMC catalyst **DMC2** enables the above mentioned bipolymerization and terpolymerization of epoxides, CO_2 and *rac*-lactide/ε-caprolactone (Figure 72) without the need of initiators, cocatalysts or quenching.

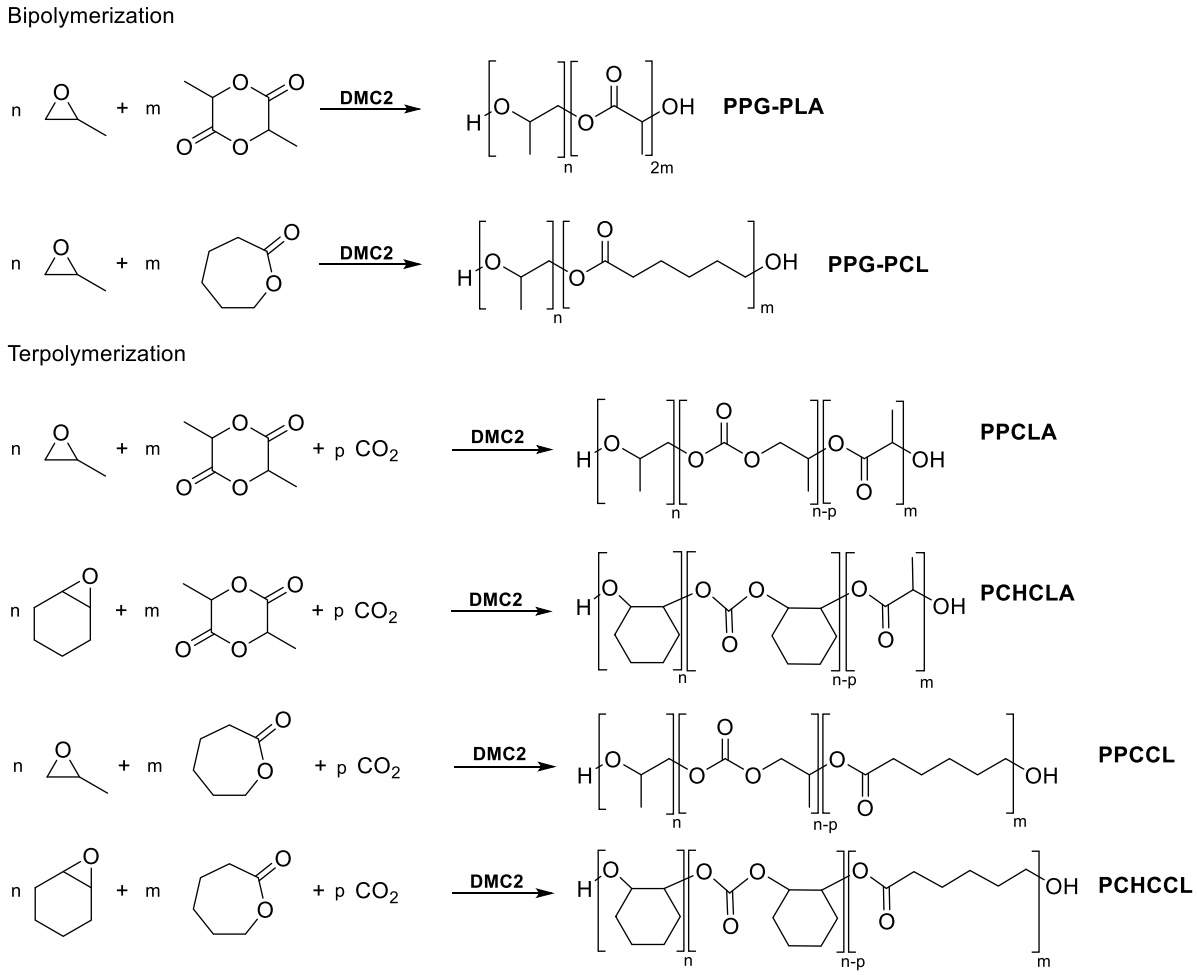

Figure 72: Bi- and terpolymerizations conducted using **DMC2** with cyclic esters as comonomers.

Bipolymerization

The successful bipolymerization of PO and *rac*-lactide can be seen in the ^{1}H NMR of the product **PPG-PLA.2** (Figure 73). The characteristic shift of the methine proton in propylene oxide confirms copolymerization due to de-shielding of the bond in the vicinity of an ester group (δ=4.62 ppm).[177,179] The GPC chromatogram of **PPG-PLA.2** (Figure 74) depicts a monomodal distribution and an unprecedented high molecular weight M_n of 11086 g/mol with a polydispersity index of 2.70. This PDI is similar to known copolymers of PO and *rac*-lactide ranging from 1.2 to 6.5 reaching a maximum M_n of 2760 g/mol.[177-178] In an attempt to narrow the PDI, the copolymerization was additionally conducted implementing tripropylene glycol as chain transfer agent (**PPG-PLA.1**). The resulting copolymer however shows a broadened PDI.

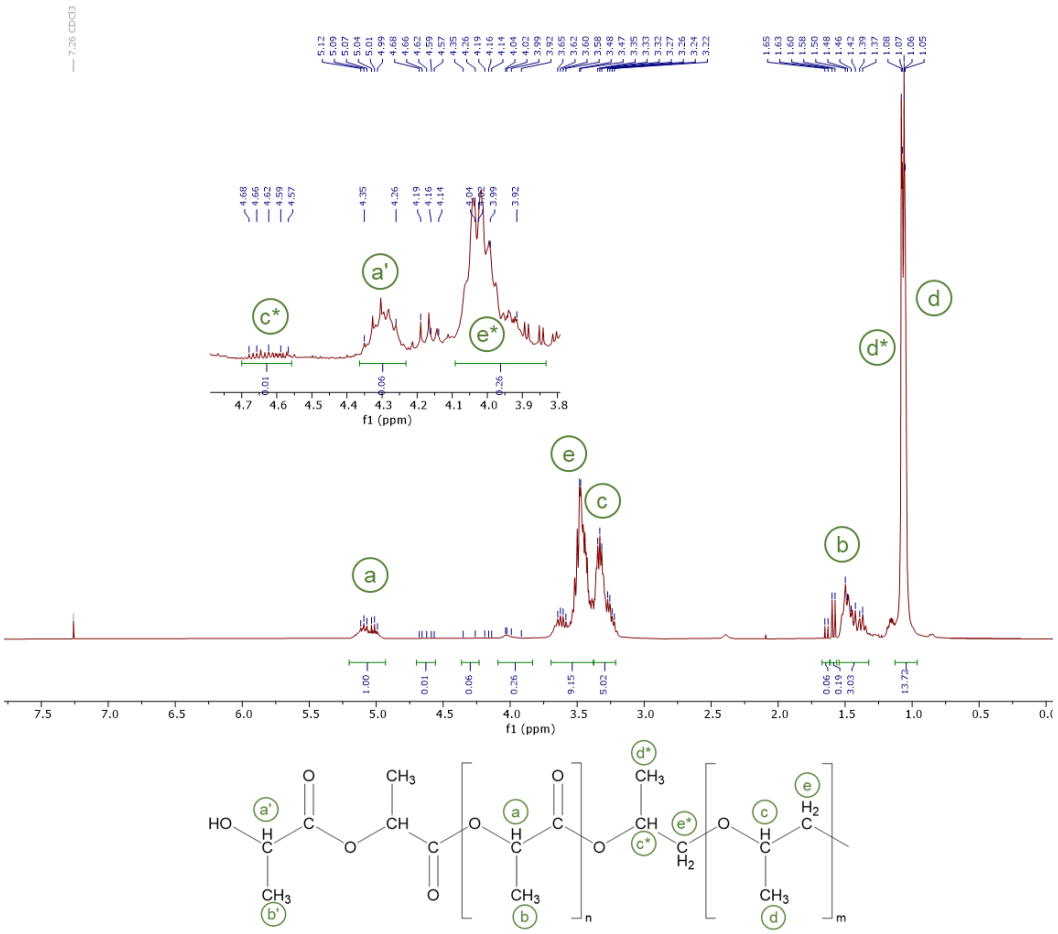

Figure 73: ^{1}H NMR spectrum of **PPG-PLA.2** ($CDCl_3$, 297.5 K, 300 MHz).

This contrasts with the observations in the homopolymerization of PO (*vide supra*) and leads to the conclusion that chain transfer within the copolymerization reaction is hindered by addition of *rac*-lactide. To elucidate whether a CTA can be implemented, more experiments using different amounts and types of CTAs must be conducted. **DMC2** was also found to be active in the homopolymerization of *rac*-lactide (see appendix, chapter A-3.11).

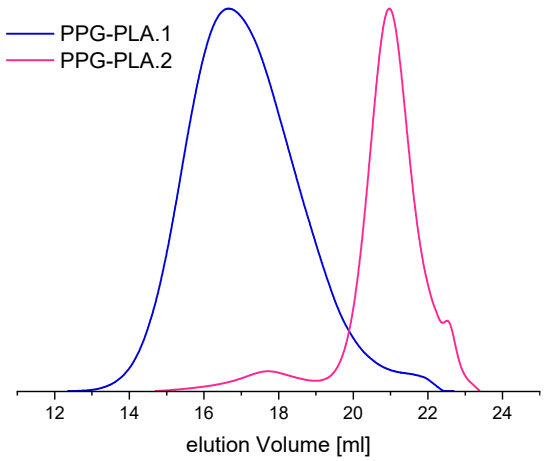

Figure 74: GPC diagram of PPG-PLA.1 and PPG-PLA.2 (eluent: THF, standard: polystyrene).

Terpolymerization

Next to this, **DMC2** was tested for activity in the terpolymerization of epoxides, cyclic esters, and CO_2. As mentioned above, incorporation of CO_2 into polymers introduces biodegradable carbonyl groups and depicts a way to incorporate anthropogenic carbon emissions from exhaust flows into a widely applicable polymer product.[16]

Table 8: Terpolymerization trials with CO_2 conducted using **DMC2**.

Polymer	Comonomer 1	Comonomer 2	Conv. 1 [mol%]	Conv. 2[b] [mol%]	M_n [g/mol]	PDI
PPCLA	PO	rac-lactide	100	95	9116	1.36
PPCCL	PO	ε-caprolacton	100	61	3822	1.49
PCHCLA	CHO	rac-lactide	73	93	4853	1.63
PCHCCL	CHO	ε-caprolacton	100	51	2564	1.48

a: calculated from ^{1}H NMR before polymer workup from the methyl signals of polymer (δ=1.11 ppm for PPC; δ=4.6-4.8 for PCHC) and monomer (δ=1.31 ppm for PO; δ=3.1 ppm for CHO) conv = $I_{polymer}/(I_{polymer}+I_{monomer})$ | b: calculated from ^{1}H NMR before polymer workup from the methine/methylene signals of polymer (δ=5.16 ppm for PLA; δ=2.25 ppm for ε-CL) and monomer (δ=5.03 ppm for lactide; δ=2.61 ppm for ε-CL) conv = $I_{polymer}/(I_{polymer}+I_{monomer})$.

The characteristics of the monophasic terpolymers of epoxide / cyclic ester / CO_2 are presented in Table 8. All measured GPC curves were monomodal (Figure 75) and copolymerization was proven for all four terpolymers by ^{1}H NMR. Lactide-containing terpolymers were additionally investigated using 2D ^{1}H^{1}H-COSY and ^{1}H^{13}C-HMBC NMR spectroscopy. As it is exemplarily shown for PCHCLA in Figure 76, signals for all three types of possible bonds – polyester bonds from PLA as well as polycarbonate bonds and polyether bonds – can be found, suggesting a block-copolymer. Signals at 5.16 ppm (methine proton in the lactide unit) and 1.53 ppm (methyl protons in the lactide unit) indicate the incorporation of polylactic acid blocks into the copolymer.[174-175] Next to this, polyether blocks are found (signals at 3.37 ppm) and cyclohexene oxide carbonate blocks can be seen by the methine protons adjacent to the carbonate's carbonyl group at δ=4.65 ppm. The ^{1}H^{1}H-COSY spectrum of PCHCLA shows that the blocks of the terpolymer are connected by a bond between the polycarbonate unit and the PLA unit (δ=4.34 ppm) as it is shown in Figure 77. For PPCLA the ^{1}H^{1}H-COSY spectrum (see appendix, Figure A 72) shows a correlation between the methine proton of the PPC unit (δ=4.34 ppm) and the methyl protons of the PLA unit (1.44-1.57 ppm), confirming copolymerization.

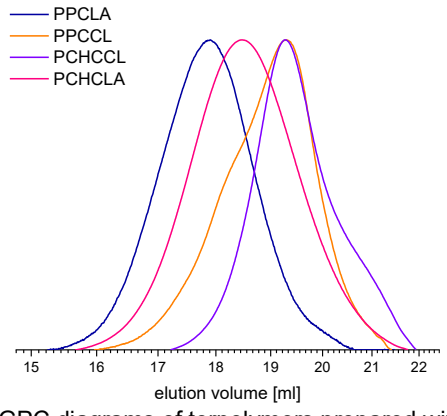

Figure 75: GPC diagrams of terpolymers prepared with **DMC2.**

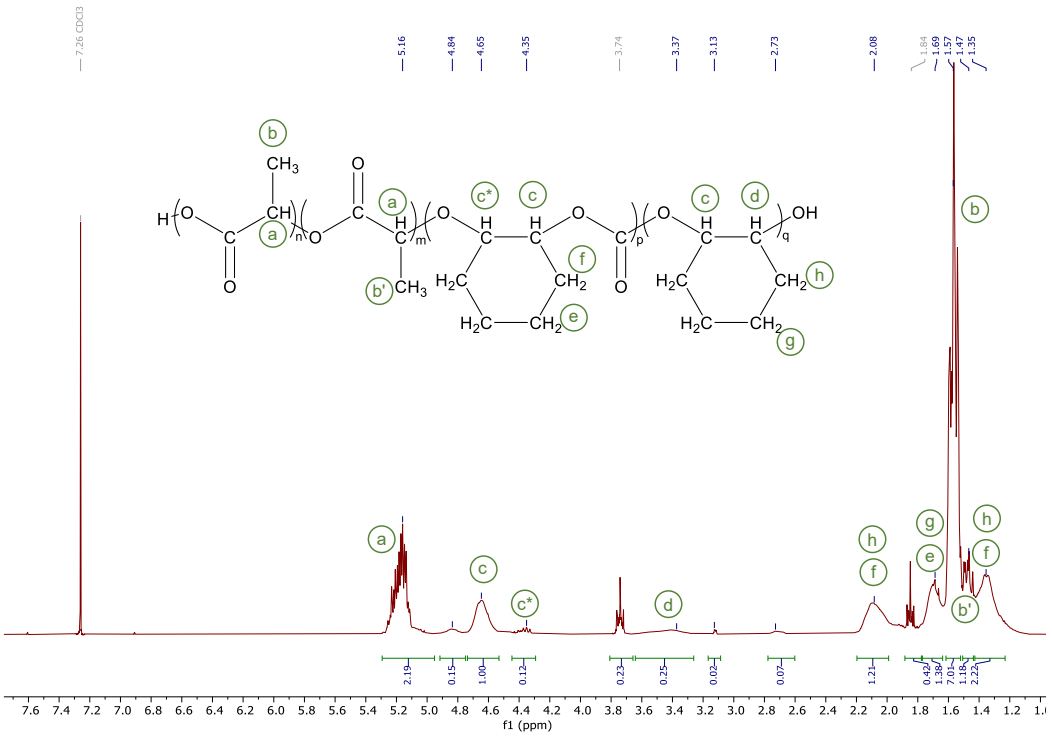

Figure 76: ^{1}H NMR spectra of **PCHCLA** ($CDCl_3$, 297.0 K, 400 MHz).

Additionally, the correlation of the lactide carbonyl carbon (δ=175 ppm) and the methine proton of the PPC unit (δ=4.34 ppm) can be observed in the $^{1}H^{13}C$-HMBC NMR spectrum (see appendix, Figure A 73). Next to the PPC and the PLA units also ether units can be observed, which leads to the conclusion that both PPCLA and PCHCLA copolymerize in a random manner. Monomodal GPC curves with a PDI below 1.65 (Figure 75) further show the formation of only one block-copolymer each.

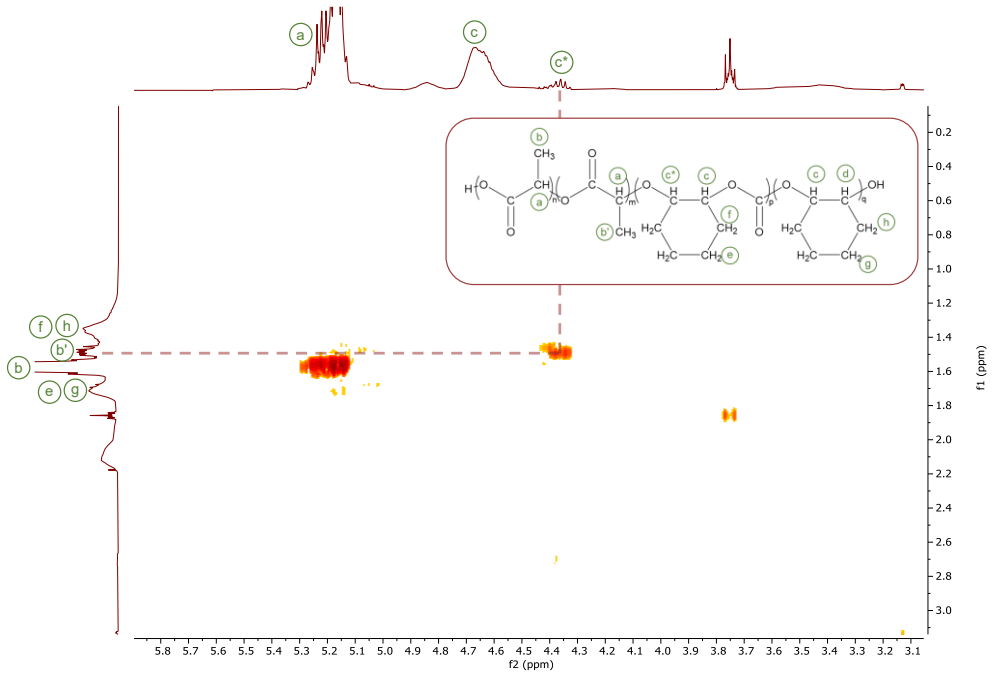

Figure 77: Cut-out of the $^{1}H^{1}H$-COSY NMR spectrum of **PCHCLA** ($CDCl_3$, 400 MHz, 297 K).

4.2.3 Conclusion: DMC-catalyzed copolymerization reactions

DMC2 catalyst was used for the first time to prepare hydroxyl-endcapped PO/D_3 diol-copolymers without the use of an initiator, which is uncommon in cyclosiloxane ROP. The obtained polymers were proven to be copolymers by ^{1}H DOSY and ^{1}H^{1}H NOESY NMR analysis as well as hydrolysis experiments. They are expected to be of a gradient-type structure due to the process control established. High molecular weight copolymers (up to M_n of 12970 g/mol) with narrow PDI (1.28-1.47) were produced in a process easily applicable in industrial-scale production. This comprises a vast improvement in comparison to known PO/D_3 copolymers.[129,212]

Additionally, this work shows that **DMC2** is an active catalyst for the ROCOP of PO and *rac*-lactide as well as the homopolymerization of *rac*-lactide yielding narrow PDI products of a high molecular weight. Moreover, **DMC2** was found to show activity in the terpolymerization of epoxides, CO_2 and cyclic esters yielding monophasic products with a narrow monomodal PDI ranging from 1.36 to 1.63. The terpolymerization of PO/CHO with CO_2 and *rac*-lactide was proven by 2D ^{1}H^{1}H-COSY and ^{1}H^{13}C HMBC NMR whilst the terpolymerization of PO/CHO with CO_2 and ε-caprolactone was proven by ^{1}H NMR. In a next step, the properties of these terpolymers need to be further investigated.

4.3 DMC-inspired molecular catalysts

Inspired by the findings described in chapter 4.1 and 4.2, molecular multinuclear zinc complexes were prepared, characterized, and assessed for catalytic activity in the ROCOP of the epoxide PO or CHO and CO_2.

Due to their ability to chelate multiple metal centers, 2,6-dipicolinoylbis(N,N-diethylthiourea) (Figure 78) and 2,6-bis(acetobenzoyl)-pyridine (Figure 79) were chosen as promising ligand candidates in catalysts for epoxide/CO_2 ROCOP. It is known that these ligands self-assemble with transition metals and lanthanides into well-defined trinuclear complexes.[213-216] Reported 2,6-dipicolinoylbis(N,N-diethylthiourea)-complexes combining two zinc and one lanthanide center show zinc-zinc distances of approx. 7.2 Å[215], which is a similar distance to the Zn-Zn distance within the simulated model of the DMC catalyst (see chapter 4.1.3.1) of 7.632 Å - 7.662 Å. Therefore, we hypothesized that these complexes can be active in epoxide/CO_2 copolymerization like DMC catalysts. Next to this, the complexes coordinate acetate ligands which are known to lead to high catalytic activity in other epoxide/CO_2 ROCOP catalysts, e.g., β-diiminate complexes by Coates *et al.*[217-218] or catalysts with macrocyclic ligands by Williams *et al*.[219-220]

To elucidate the influence of the lanthanide atom on the reaction, two new homotrinuclear complexes containing solely zinc centers were prepared, characterized, and tested for their catalytic activity in the ROCOP reaction. Furthermore, the ring-opening homopolymerization (ROP) activity towards the monomer lactide is explored to evaluate further similarities to the catalyst **DMC2**.

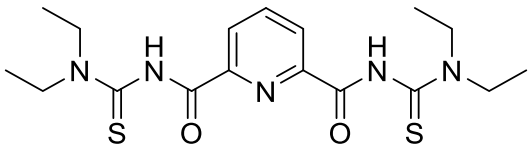

Figure 78: 2,6-dipicolinoylbis(N,N-diethylthiourea)

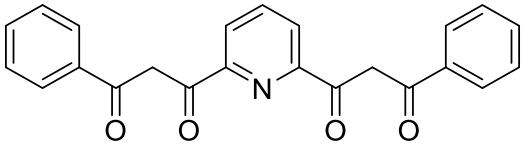

Figure 79: 2,6-bis(acetobenzoyl)pyridine

4.3.1 Synthesis and structural characterization of the multinuclear zinc complexes

The 2,6-dipicolinoylbis(N,N-diethylthiourea) ligand (**L_{NN}1**) was prepared from N,N-diethylthiourea (preparation procedure by Yokoyama *et al.*[221]) following a previously reported procedure by Pham *et al.*[214]

The 2,6-bis(acetobenzoyl)pyridine ligand (**L_{NN}2**) as well as $Zn^{II}Ln^{III}Zn^{II}$-L_{NN}1$(OAc)_3$ complexes (Ln = Ce, Nd, Sm, Er) were kindly provided by the group of Hung Huy Nguyen at VNU University of Science (Hanoi, Vietnam). For further experiments $Zn^{II}Sm^{III}Zn^{II}$-L_{NN}1$(OAc)_3$ complex (**3**) was synthesized following a procedure by Pham *et al.*[215]

Complex **1** ($Zn^{II}{}_3L_{NN}1_2(OAc)_2$) and **2** ($Zn^{II}{}_3L_{NN}2_2(OAc)_2$) were prepared in yields > 85 % from reaction of one equivalent of the corresponding ligand with two equivalents of zinc chloride ($ZnCl_2$) in methanol under addition of triethylamine and subsequent exchange of the chloride ligand with acetate (see experimental, appendix chapter A-1.5.1). Complex **1** was characterized by EA, ATR IR, ^{1}H-NMR, single crystal XRD and ESI-MS whilst complex **2** was only characterized by ATR IR and EA due to limitations in solubility. Analysis of the ^{1}H NMR spectra of **1** (appendix, Figure A 87) shows vanishing of NH signals as well as a split of the -CH_2 and -CH_3 resonances compared to the free ligand, which indicates successful coordination of metals. The formation of a complex in which the two ligands are coordinated to the zinc atoms in different ways is expected. This is confirmed by the single crystal X-ray diffraction structure of complex **1** (Figure 80, only one of the two molecules in the asymmetric cell shown; full cell, crystallographic information and information on data collection are shown in the appendix, chapter A-4.2). Whilst one ligand coordinates the three zinc atoms via the sulfur and oxygen atoms, the other ligand binds the zinc center via nitrogen and sulfur atoms. Selected bond lengths are listed in Table 9. In comparison to the previously reported lanthanide-zinc complexes by Pham *et al.*[215] it can be observed that within the homotrinuclear complex **1** bond

lengths between the central metal and the adjacent nitrogen and oxygen atoms are shorter. This might be explained by the smaller atomic radius of zinc.[222] The difference in bond lengths can possibly lead to a difference in catalytic activity. ESI-MS shows that **1** exists as mono-, di- and tetranuclear complex in solution (see appendix, Figure A 88), which can lead to a lower concentration of active species within the reaction mixture.

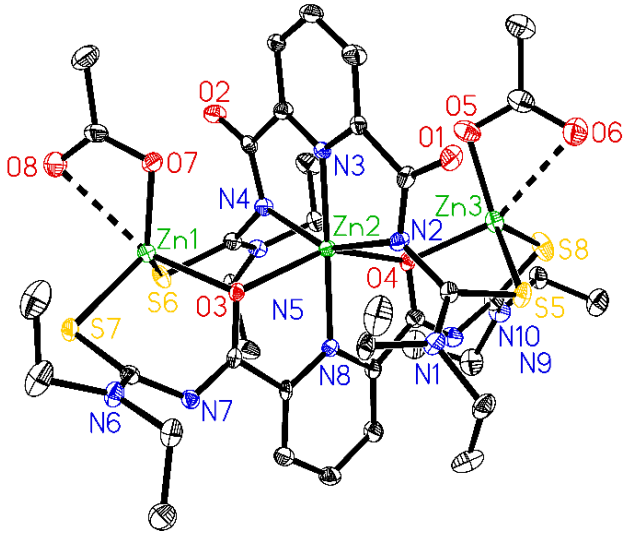

Figure 80: Molecular structure of **1**. The second molecule of the asymmetric unit and co-crystallized solvent (methanol) are not shown. Displacement ellipsoids correspond to 30% probability. Hydrogen atoms are omitted for clarity.

Table 9: Selected bond lengths [Å] and angles [°] for **1** (values for the second molecule of the asymmetric unit are given in square brackets).

	Zn1-O3	Zn2-O3	Zn2-O4	Zn3-O4	Zn1-S6	Zn1-S7
Bond lengths	2.113(4) [2.115(4)]	2.224(4) [2.223(4)]	2.210(4) [2.245(4)]	2.085(4) [2.052(4)]	2.3236(17) [2.3236(17)]	2.3369(17) [2.3295(17)]
	Zn3-S5	Zn3-S8	Zn2-N3	Zn2-N8	Zn2-N2	Zn2-N4
Bond lengths	2.3168(19) [2.302(2)]	2.229(2) [2.3116(19)]	2.036(5) [2.039(5)]	2.060(5) [2.071(5)]	2.162(5) [2.169(5)]	2.139(5) [2.155(5)]

The homotrinuclear zinc complex **2** using the ligand $\mathbf{L_{NN}2}$ is expected to be of a similar structure to complex **1** with the difference of the absence of nitrogen and sulfur atoms. The difference in ligands leads most probably to a more symmetric complex. The formation of single crystals and therefore the structure analysis using single crystal X-Ray diffraction was, however, not possible. The IR spectrum of the newly formed complex shows a shift of the two ν_{CO} bands towards lower wavenumbers indicating complexation to the zinc atoms (Figure 81). The hereby proposed structure of **2** is shown in Figure 82.

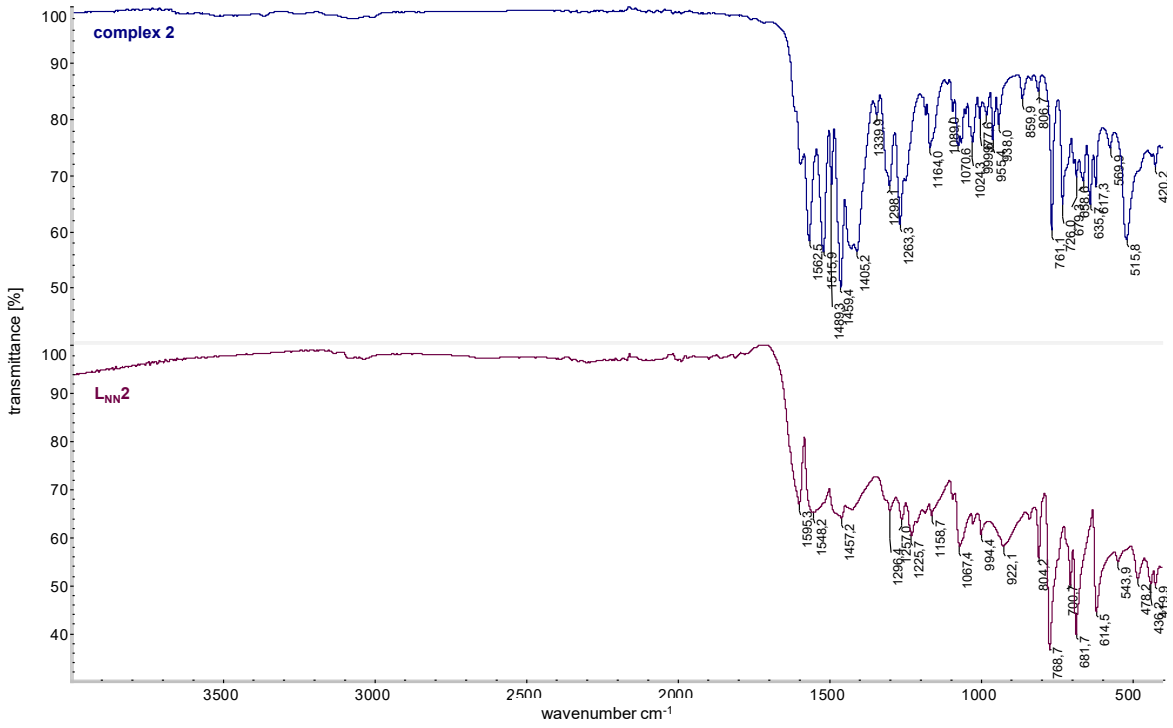

Figure 81: ATR IR of **$L_{NN}2$** and complex **2**.

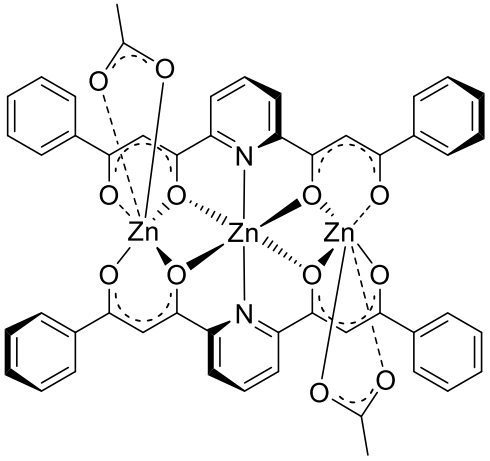

Figure 82: Proposed structure of complex **2**.

4.3.2 Catalytic activity for the copolymerization of epoxides and CO_2

Homonuclear complexes (1 and 2)

The homotrinuclear complexes **1** and **2** were examined for their activity in the ROCOP of CHO/PO and CO_2. The copolymerization was conducted at 80 °C and 20 bar CO_2 for 24 h in CH_2Cl_2 as described in experimental (appendix, chapter A-1.5.2). No activity was observed for the PO/CO_2 copolymerization.

Nevertheless, both complexes were able to perform the CHO/CO_2 copolymerization reaction yielding a polyether carbonate (Table 10). However, the copolymers are not stable and quickly undergo backbiting reactions to yield oligoethers of cyclohexene oxide. This might be caused

by insufficient inactivation of the complexes by quenching (addition of HCl). Because of this no GPC measurements could be conducted on the resulting copolymers.

Table 10: Catalytic activity of complex **1** and **2** in the ROCOP of CO_2 and CHO.

complex	conversion[a] [%]	$F_{carbonate}$[b] [%]
1	13	19
2	11	13

Reactions were carried out in CH_2Cl_2, 5 mol% catalyst loading, 80 °C, 20 bar CO_2, 24 h | a: calculated from NMR before quenching | b: calculated from ^{1}H NMR signals of ether linkages (3.5 ppm) and carbonate linkages (4.6 ppm).

For alternating copolymerization of epoxides and CO_2 a binuclear mechanism is expected,[14] while homopolymerization can be performed via a mononuclear mechanism. The low carbonate content of the obtained polymers and their observed disintegration indicates that the distances of the metal centers within the complexes are not supporting a binuclear mechanism. Therefore, the copolymerization can only be performed if two catalyst molecules come in close proximity to each other. The content of bi- and trinuclear complexes in solution and therefore adjacent zinc centers is assumed to be low (from ESI-MS, Figure A 88, appendix) which is leading to more polyether bonds being formed than polycarbonate bonds. Complex **2** shows both, lower conversion, and lower CO_2 incorporation in comparison to **1**. The more electron withdrawing nitrogen and sulfur atoms in the $\mathbf{L_{NN}1}$ ligand seem to lead to a higher catalytic activity at the same catalyst concentration.

Heteronuclear complexes (3-6)

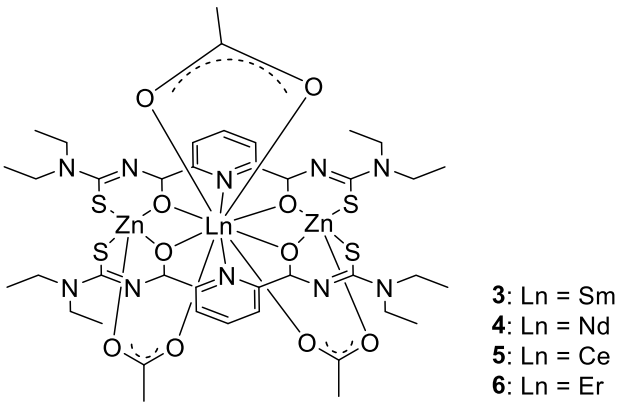

3: Ln = Sm
4: Ln = Nd
5: Ln = Ce
6: Ln = Er

Figure 83: Heteronuclear complexes.[216]

Complexes **3-6** (Figure 83) were also tested for catalytic activity in a CHO/CO_2 copolymerization reaction. ^{1}H NMR analysis of the resulting crude products reveal that all tested complexes showed activity in ROCOP, except for complex **5** that yielded polyether only (Table 11). The low conversions in comparison to other catalysts can be regarded as a general proof of activity of these complexes, alas with the need of further reaction optimization.

Complex **3** was chosen as the most promising heteronuclear complex for further reaction optimization, because of the comparably high carbonate fraction in the product.

Table 11: Conversion and carbonate fraction in crude product of CHO/CO_2 ROCOP using complex **3-6**.

complex	Ln	conversion[a] [%]	$F_{carbonate}$[b] [%]
3[c]	Sm	9	40
4	Nd	8	30
5	Ce	8	N/S
6	Er	1.5	16

Reactions were carried out in CH_2Cl_2, 1 mol% catalyst loading, 80 °C, 20 bar CO_2, 24 h | a: calculated from NMR before quenching | b: calculated from ^{1}H NMR signals of ether linkages (3.5 ppm) and carbonate linkages (4.6 ppm) | c: Reaction in CH_2Cl_2, 0.1 mol% catalyst loading, 80 °C, 20 bar CO_2, 24 h.

Reaction conditions using complex **3** were varied (Table 12). The highest conversion of 40 % was obtained at 80 °C, 20 bar CO_2 and a catalyst concentration of 5 mol%. This corresponds to a TOF of 0.33 h^{-1}. Which is a very low value in comparison to other known molecular ROCOP catalysts that can reach TOFs of up to 155000 h^{-1}.[223]

It was observed that an increase in catalyst concentration leads to an increase in conversion, but a decrease of the carbonate fraction. Because higher catalyst concentrations lead to polyether formation being favored over polycarbonate formation, the binuclear ROCOP mechanism seems to be performed within one complex molecule. Therefore, the conclusion can be drawn that the distance between two adjacent metal centers in the samarium containing complex is more suitable for CO_2/CHO copolymerization than within the homotrinuclear zinc complexes **1** and **2**. Multinuclear complexes being superior to homonuclear complexes in this kind of reaction has also been observed for other ROCOP catalysts, like catalysts by Williams *et al*. bearing diphenolate tetra(amine) macrocyclic ligands[219,224-226] or as lanthanide containing catalysts by Asaba *et al.*[227] and Nagae *et al*.[228]

Table 12: Copolymerization of CHO & CO_2 at varying reaction conditions.

run	catalyst concentration [mol%]	temperature [°C]	p_{CO2} [bar]	reaction time [h]	conversion[a] [%]	$F_{carbonate}$[b] [%]
1	0.1	80	20	24	9	40
2	1	80	20	24	5	16
3	2	80	20	24	20	8
4	5	80	20	24	40	9
5	1	80	20	1	10	9
6	1	60	20	24	7	0
7	1	80	30	24	5	11

a: calculated from NMR before quenching | b: calculated from 1H NMR signals of ether linkages (3.5 ppm) and carbonate linkages (4.6 ppm).

4.3.3 Catalytic activity for the homopolymerization of (*rac*-)lactide

Since many catalysts that are active for the ROCOP of epoxides and CO_2 (including **DMC2**) are known to be excellent ring-opening polymerization catalysts, the complexes **1**, **2** and **3**

were tested as catalysts in the polymerization of *rac*-lactide. Polylactic acid (PLA) was one of the biobased polyesters with the highest production capacity in the 2010s as it can be used in biodegradable packaging and medical appliances.[229-230] All three investigated complexes showed to be active in this reaction.

Table 13: Conversion and MWD of PLA polymers obtained using complex **1**, **2** and **3**.

Complex	Maximum conversion[a] [%]	reaction time [h]	Mn[c] [g/mol]	PDI[d]
1	98	22	22120	1.72
1[e]	84	19	15740	1.24
2	92	26	37869	2.03
3	92	27	9283	1.31
zinc acetate[e]	91	22	5800	1.64

All reactions were carried out in neat conditions under Ar atmosphere, [catalyst]=5*10-3 mol%, 140 °C. | a: determined from ^{1}H NMR (CH_3 monomer: δ=1.70 ppm, CH_3 polymer δ=1.56 ppm) | b: turnover frequency calculated as mol monomer converted per mol catalyst per hour | c: determined by GPC, standard: polystyrene, eluent: THF, Mark-Houwink-correction factor $M_n^{obs} = 0.58\ M_n$.[231] | d: determined by GPC, standard: polystyrene, eluent: THF | e: [catalyst]=1*10-3 mol%.

In a solvent-free reaction at 140 °C a conversion of 98 %, 92 % and 92 % was achieved in neat conditions for complex **1**, **2** and **3**, respectively (Table 13). As it can be seen in Figure 84, complex **1** performs the reaction the fastest and reaches a conversion of 84 % after only 5 h. Complexes **2** and **3** however show an induction time of 1-2 h before the polymerization starts and only show a conversion of 9 % and 8 % after 5 h, respectively. This may be due to the complexes being transformed into the active form only in the reaction medium by activation or degradation.

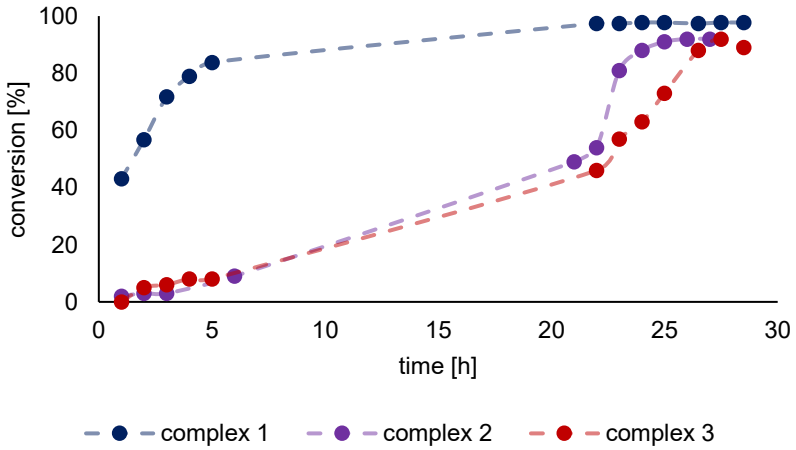

Figure 84: Conversion over time in the *rac*-lactide homopolymerization using complex **1**, **2** and **3**.

One of the degradation products of the complexes is zinc acetate. Using zinc-acetate only (1 mol%), a conversion of 91 % was achieved after 22 h, but only a M_n of 5800 g/mol (PDI: 1.64) could be obtained (Mark-Houwink corrected[231]). Using 1 mol% of complex **1**, a product with a M_n of 15740 g/mol and a PDI of 1.24 was obtained (Table 13). The comparably low molecular mass of the product obtained using **3** (Table 13) can be seen as indicator for this

degradation. However, this cannot be the case for **2** which achieves a Mn of 37869 g/mol and also shows an induction period. Therefore, it is likely that the active form of both complexes, **2** and **3**, is not the degradation product zinc-acetate.

The ^{1}H NMR spectra of PLA prepared using a higher catalyst concentration (3 mol% of **1**) shows -OH, -OMe and -O(CO)Me end groups (Figure 85).[232] The integrals of the methoxy-end group signal (δ=3.73 ppm) and the acetate-end group signal (δ=1.84 ppm) are of the same area whilst the integral for the hydroxy-end group signal is small in comparison. A mechanism can be proposed in which the polymerization is initiated through the nucleophilic attack of an acetate ligand of complex **1** after coordination of the lactic acid molecule to a zinc center. The methoxy- end group is then formed by the quenching of the polymerization by precipitation in methanol. OH-end groups can be caused by traces of water in the methanol. Regarding the activity of the zinc centers in complex **1**, it can be concluded that the central zinc atom of complex **1** is most likely not taking part in the polymerization reaction, because it does not bear an acetate ligand.

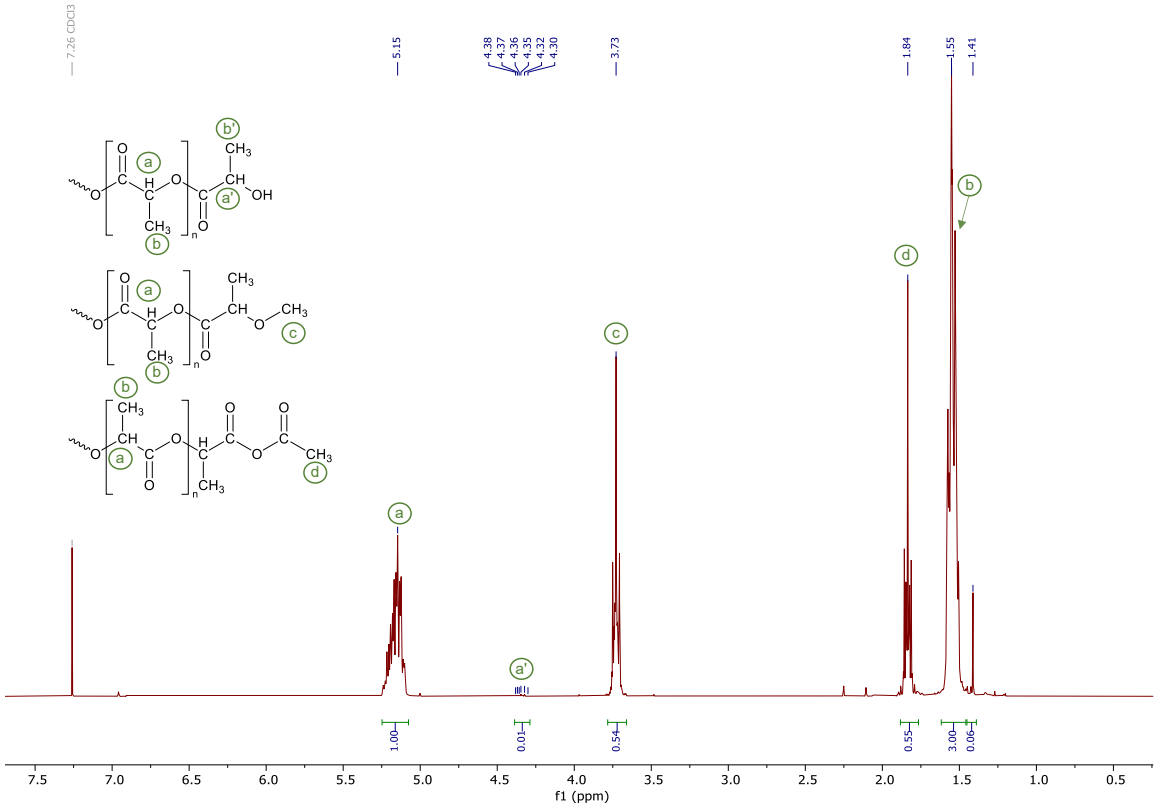

Figure 85: ^{1}H NMR of a PLA prepared using 3 mol% of complex **1** ($CDCl_3$, 300 MHz, 298.0 K).

^{1}H NMR spectra of PLA products using complex **2** and complex **3** do not show acetate end-groups (see appendix, Figure A 100 and Figure A 108). This indicates that the polymerization reaction is not initiated by the acetate ligands. The less electron withdrawing ligand in complex **2** leads to lowered Lewis acidity of the zinc centers which might hamper the monomer coordination. Complex **3** is known to coordinate three $\mathbf{L_{NN}1}$ ligands to the detriment of acetate ligand coordination. This can lead to lesser active zinc sites present in the reaction mixture.[216]

Additionally, the complexation can be hindered by the changed geometry due to the samarium central atom. Since the integrals of the methoxy- and the hyxdroxy-end groups are about the same area in the PLA macromolecules prepared with complex **2** and complex **3**, it can be expected that the lactide monomer is ring-opened by traces of water. Supporting this, the catalytic activity of the complexes based on conversion and obtained molecular mass can be estimated to be of the order **1** > **2** = **3**. To further strengthen these hypothesizes a more detailed end-group analysis of the products must be performed. This can be achieved by MALDI-MS, or by developing a polymerization procedure that yields oligomeric products suitable for ESI-MS analysis.

When assessing the development of the molecular mass and PDI over time (Figure 86), a depolymerization after an equilibrium conversion of around 90 % is reached can be observed for all three complexes. An equilibrium conversion is typically observed in ring-opening polymerization and indicates the existence of an active polymerization chain throughout the whole of the reaction period.[48]

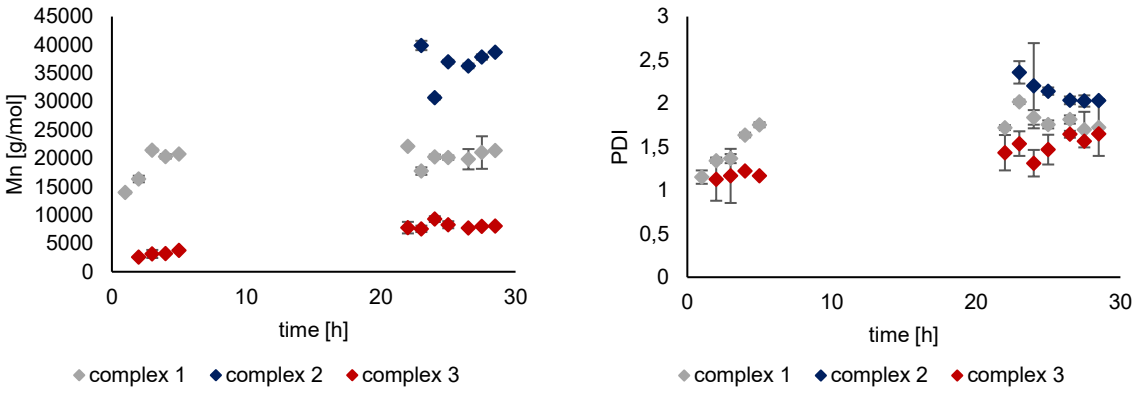

Figure 86: Development of the molecular mass (M_n) and PDI over time using complex **1**, **2** and **3** at 140 °C in neat conditions (determined by GPC with polystytrene standard and THF as eluent; Mn is Mark-Houwink corrected $M_n^{obs} = 0.58\ M_n$.[231])

Based on all the observations above, the initiation mechanisms shown in Figure 87 for complex **1** and for complex **2** / **3** can be proposed. Complex **1** undergoes a coordination insertion mechanism directly (Figure 87**A**), whilst complex **2** and **3** need to undergo an activation step first in which the acetate ligand is exchanged with a hydroxy group stemming from residual water in the reaction mixture (Figure 87**B**).

Overall, a narrow PDI of 1.72 can be obtained using complex **1** which is comparable with other known zinc-containing catalysts for this reaction.[229,233-234]

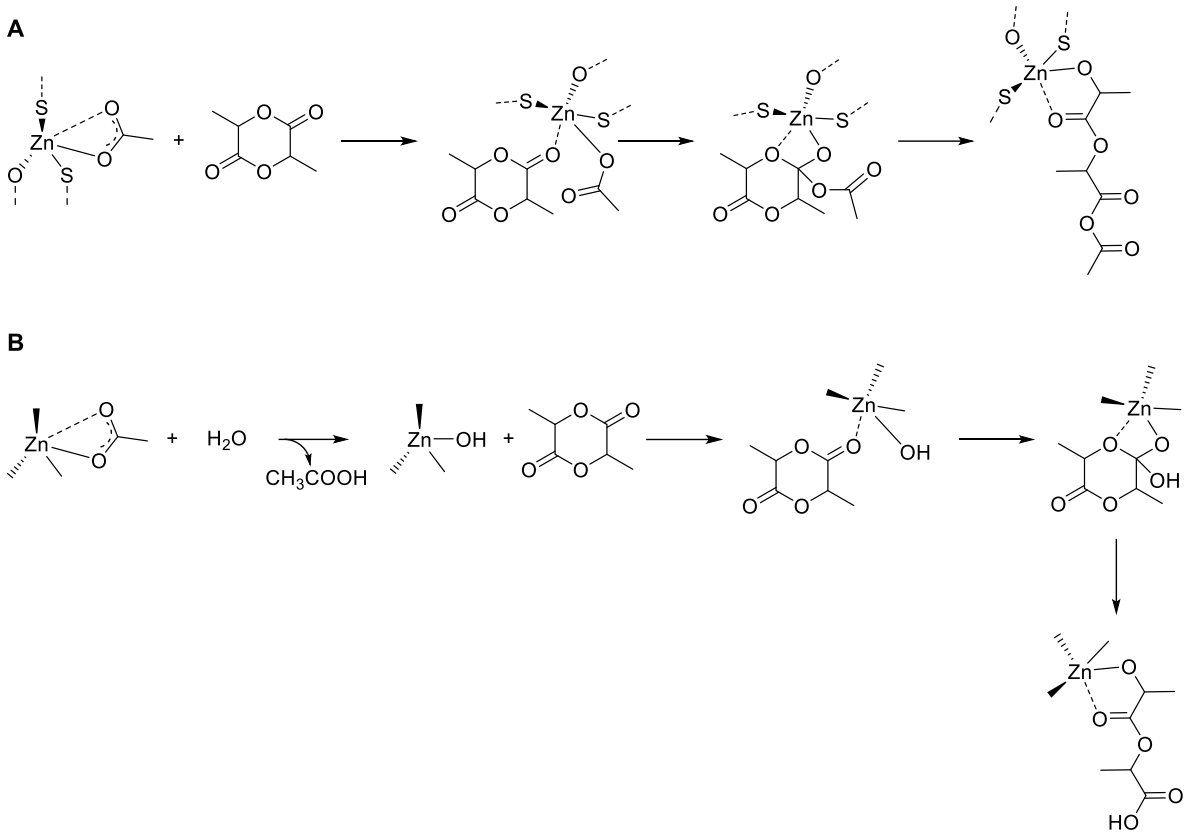

Figure 87: Proposed mechanisms for the initiation by an acetate ligand in complex **1** (**A**) and by water in complex **2** and **3** (**B**).

The necessary reaction time to obtain the product and the controllability of the reaction cannot compete with high activity ROP catalysts, like the industrially used tin(II)octanoate with an alcohol as initiator,[235] dizinc complexes with folded bis(imino)diphenylamido ligands by Thevenon *et al*.[236] or iron(II) hybrid guanidine complexes by Rittinghaus *et al*.[237] This might be due to the lack of an external initiating agent that can be used in ROP of lactide to obtain high activity and good controllability of the reaction.[238-239] Nevertheless, complex **1** yields very high molecular weights compared to many other known catalysts that often yield PLA of a molecular weight below 1000 g/mol within the examined reaction times.[234,236] This can be advantageous depending on the intended application of the polymer product, but still needs optimization to be applicable in industrial processes.

4.3.4 Conclusion: DMC-inspired molecular catalysts

Complex **3** was shown to be catalytically active in the ROP of *rac*-lactide and the ROCOP of CHO and CO_2 yielding a polycyclohexene/carbonate block-copolymer with a carbonate fraction of 9 % at a conversion of 40 %. Additionally, two new catalysts - complexes **1** and **2** - were prepared and characterized. These new complexes showed low activity for the CHO/CO_2 ROCOP but showed high activity for *rac*-lactide homopolymerization. Conversions of over

90 % were obtained yielding products with low PDI of 1.31 - 2.03 and high Mn of up to 37869 g/mol.

5 Perspectives

5.1 Characterization of DMC catalysts

The many insights into the structure and ROP mechanism of the DMC catalyst that have been gained in this thesis are naturally accompanied by a lot of unresolved and new questions concerning its nature. As every project is limited in time, there are many aspects that should be taken up in a future further investigation of the heterogeneous polymerization catalysts.
Because the ROP was found to take place on the particle's surface exclusively, the differences between the bulk and the surface structure should be further elucidated by DNP-SENS measurements. For this, a method must be developed to overcome the radical-scavenging properties of the DMC catalyst. These measurements can give additional insight into the exact nature of the catalytical centers located on the particle's surface. Since it was found that the active sites are most likely part of its amorphous phase, the percentages of crystalline features of the DMC catalysts should be determined using wide angle X-ray diffraction. Next to this, a specific analytical method to analyze non-crystalline solids, the pair distribution function analysis (or total scattering) can give further structural information on the amorphous phase. Of particular interest here is the chlorine content and the coordination sphere of cobalt within the disordered material, as it stood out in XPS, IR and EDX measurements as deviating from previous assumptions. The aim should be to find out whether the involvement of cobalt in the catalytic reaction exceeds its previously assumed structural role.
The two coordination-types found of the complexing agent *tert*-butanol when used in combination with 2-octyl-1-dodecanol should be investigated further regarding cobalt atoms in addition to the zinc centers. Moreover, it is necessary to analyze whether these effects appear only with 2-octyl-1-dodecanol or with all co-complexing agents. Therefore, additional MAS NMR measurements with a broader sample set can be conducted. It would also be of great interest to follow the polymerization by performing solid state NMR analysis while exposing the sample to gaseous propylene oxide to gain further insight into the activation of the catalyst.

Over the course of this thesis, mainly the atomic structure of the DMC catalyst was analyzed. Kinetic measurements indicated an influence of the particles' morphology on the catalytic activity. The question on how the nature of the (co-)CA influences the surface area, the pore size and subsequently the fragmentation of the catalysts, remains unanswered. The exploration of the fragmentation behavior of Ziegler-Natta-catalysts can be used as a blueprint to understand the reaction behavior further.

Regarding the polymerization mechanism of the investigated DMC catalyst, the fast chain transfer reaction necessary for a high-quality polymer product opens up potential for further reaction optimization. Clarification on how to overcome limitations and on how to enhance chain transfer can help with developing an improved catalytic reaction.

5.2 DMC-catalyzed copolymerization reactions

Over the course of this thesis, the potential of a Zn/Co DMC catalysts to be used in the production of a range of copolymers was shown. However, further improvements are necessary for an industrial-scale application of the reactions.

In the copolymerization of PO and D_3 further process optimization needs to be done with regards to the ideal duration of the PO dosing period to minimize the formation of side products. Depending on the desired application of the resulting copolymers, the PDMS content of the polymers can be varied. With this, the effect of the PDMS content on the glass transition temperature of the polymer needs to be investigated in greater detail to obtain more insight in its effects on the product's properties. The hydrolytic stability of the polymers must be tested in the subsequent reactions to form an applicable product and in the desired final product formulation.

To improve the copolymerization of epoxides with cyclic esters, the possibility of adding a chain transfer agent to the reaction needs to be investigated further. A CTA could enable the production of copolymers with narrower molecular weight distributions. For the obtained terpolymers of epoxides, cyclic esters, and CO_2, a suitable application field still needs to be validated. Additionally, the biodegradability and the degradation products of the terpolymers needs to be investigated since this is of high interest when using them in "green" products.

5.3 DMC-inspired molecular catalysis

The molecular catalysts that were investigated based on the knowledge gained on the DMC catalysts were not able to compete with the latter in the ROCOP of epoxides and CO_2. Additionally, the exact structure of complex **2** remains unknown. Hence, future investigations should focus on enabling single crystal XRD measurements of **2** by testing more complex solvent systems or trying to grow single crystals using slow diffusion methodologies. Next to this, the obtained copolymers of CHO and CO_2 need to be stabilized for further characterization. Therefore, the development of a suitable quenching procedure is needed.

Even though these complexes were not able to match the catalytic activity of other catalysts in the ROCOP of epoxides and CO_2, they showed high activity in the ROP of *rac*-lactide.

Additional mechanistic insights on this catalytic reaction can be obtained by, *inter alia*, MALDI-MS, or through the preparation of oligomeric products for end group analysis by ESI-MS.

6 Summary

6.1 Characterization of DMC catalysts

Over the course of this thesis many insights into the structural features of DMC catalysts were obtained:

- The currently accepted sum formula of the DMC catalyst ($M_a^I[M^{II}(CN)_b] \times wM^IX_c \times xL^I \times yL^{II} \times zH_2O$) is, as it was previously suspected, not correct.
- $M_a^I[M^{II}(CN)_b]X_c \times \left[M_a^IL_e^IL_f^{II}X_g\right] \times yL^{II} \times zH_2O$ was ascertained to represent more accurately the structure of DMC catalysts.
- The catalysts consist of a crystalline ($M_a^I[M^{II}(CN)_b]X_c$) and an amorphous ($\left[M_a^IL_e^IL_f^{II}X_g\right] \times yL^{II} \times zH_2O$) phase.
- The crystalline parts of the bulk structure of a Zn/Co DMC catalyst were confirmed to correspond to the formula $Zn_4[Co(CN)_6]_2Cl_2$, as previously proposed by the group of Wojdeł *et. al.*[90]
- The amorphous phase of the catalysts was found to be located mainly on their surface and therefore suspected to contain the catalytically active structures.
- The complexing agents that introduce catalytic activity to the DMC catalysts were also found to be only located only on the surface of the particles.
- Under the addition of the activity enhancing co-complexing agent, the complexing agent is found to exist in two states: a strongly and a loosely coordinated form. The strongly coordinated form might lead to the discovered smaller crystallite size and hence, higher activity.
- The structure of the dormant active sites was elucidated.
- The coordination of the complexing agent to the zinc atoms on the catalyst's surface was confirmed. A chlorine atom needs to be in close proximity.
- The electronic state of cobalt was found to play a crucial role in the introduction of catalytic activity to the structures which needs to be further investigated. A coordination of the CAs to cobalt cannot be excluded.

Next to the structure of the DMC catalysts, also the catalytic mechanism of a Zn/Co DMC catalyst was explored:

- The catalyst is activated by monomer coordination and subsequent insertion into the Zn-CA bond, which is also the reason for the observed induction time.
- Once the catalyst is activated, a coordination insertion mechanism competes with an activated chain end mechanism during the propagation stage.
- A high hydroxyl-group concentration pushes the reaction towards the coordination insertion mechanism leading to the low amount of side reactions found under addition of CTA and continuous addition of monomer.
- The particles were known to undergo fragmentation which leads to the DMC catalyst mimicking a living behavior in the activation phase. Under further addition of monomer, it becomes apparent that activation is not consistently faster than chain elongation.
- The polymerization reaction is accompanied by a fast chain transfer leading to a monomodal and narrow PDI. Nevertheless, limitations in mass transport and therefore chain transfer were observed. This opens further potential for optimization of the reaction.

6.2 DMC-catalyzed copolymerization reactions

Polypropylene glycol – polydimethylsiloxane copolymers

- **DMC2** catalyst was used for the first time to prepare hydroxyl-endcapped PO/D_3 diol-copolymers.
- The reaction was found to proceed without the need of an initiator or solvent.
- The copolymerization was confirmed using ^{1}H DOSY, ^{1}H^{1}H NOESY NMR and hydrolysis experiments.
- The copolymers are expected to be of a gradient-type structure.
- High molecular weight copolymers (up to M_n of 12970 g/mol) with narrow PDI (1.28-1.47) were obtained in a process easily applicable in industrial-scale production.

Copolymers of epoxides, cyclic esters and CO_2

- **DMC2** was shown to be an active catalyst for the ROCOP of PO and *rac*-lactide as well as for the homopolymerization of *rac*-lactide.
- Products of high molecular weight and narrow PDI were obtained.
- **DMC2** was shown to be active for the terpolymerization of CHO, CO_2 and cyclic esters as well as PO, CO_2 and cyclic esters without the need of initiators, cocatalysts or quenching for the first time.
- Monophasic products with narrow monomodal PDI were obtained.
- The terpolymerization was proven using 2D ^{1}H^{1}H-COSY, ^{1}H^{13}C HMBC and 1D ^{1}H NMR.

6.3 DMC-inspired molecular catalysis

- Two new trinuclear zinc complexes (complex **1** and **2**) were prepared, characterized, and used for the catalysis of a CHO/CO_2 ROCOP and the ROP of *rac*-lactide.
- Despite the low catalytic activity of **1** and **2** in the ROCOP, they were shown to be of high activity in the ROP of *rac*-lactide with conversions of over 90 %, yielding products with low PDI of 1.31 - 2.03 and high Mn of up to 37869 g/mol.
- A previously reported heteronuclear complex (**3**),[215] was shown to be catalytically active in the ROP of *rac*-lactide and the ROCOP of CHO and CO_2.
- The obtained polycyclohexene carbonate block-copolymer using complex **3** had a carbonate fraction of 9 % at a conversion of 40 %.

7 References

[1] F. E. Golling, R. Pires, A. Hecking *et al.*, *Polym. Int.* **2019**, *68*, 848-855.
[2] B. Love in *Biomaterials*, **2017**, S. 205-238.
[3] R. Klein, F. R. Wurm, *Macromol. Rapid Commun.* **2015**, *36*, 1147-1165.
[4] X. Jin, J. Dong, X. Guo *et al.*, *Polym. Int.* **2022**, *71*, 1384-1392.
[5] R. J. Herold, US3278459, The General Tire & Rubber Company, **1966**.
[6] J. Milgrom, US3278457, The General Tire & Rubber Company, **1966**.
[7] R. J. Belner, US3278458, The General Tire & Rubber Company, **1966**.
[8] W. J. Kruper, D. J. Swart, US4500704, The Dow Chemical Company, **1985**.
[9] S. Chen, L. Chen, *Colloid Polym. Sci.* **2004**, *282*, 1033-1038.
[10] J. Herzberger, K. Niederer, H. Pohlit *et al.*, *Chem. Rev. (Washington, DC, U. S.)* **2016**, *116*, 2170-2243.
[11] A. Chruściel, W. Hreczuch, J. Janik *et al.*, *Ind. Eng. Chem. Res.* **2014**, *53*, 6636-6646.
[12] Y. J. Huang, G. R. Qi, L. S. Chen, *Appl. Catal., A* **2003**, *240*, 263-271.
[13] N. P. Korotkova, A. A. Mishchenko, E. A. Antipova, V. S. Lebedev, *Polym. Sci., Ser. D* **2013**, *6*, 41-43.
[14] L. Grefe, E. Mejía, *Tetrahedron* **2021**, *98*, 132433.
[15] J. Langanke, A. Wolf, J. Hofmann *et al.*, *Green Chem.* **2014**, *16*, 1865-1870.
[16] N. von der Assen, A. Bardow, *Green Chem.* **2014**, *16*, 3272-3280.
[17] J. Sebastian, D. Srinivas, *Appl. Catal., A* **2014**, *482*, 300-308.
[18] J. Sebastian, D. Srinivas, *Appl. Catal., A* **2013**, *464-465*, 51-60.
[19] J. Sebastian, S. Darbha, *J. Chem. Sci. (Bangalore, India)* **2014**, *126*, 499-509.
[20] I. Kim, J.-T. Ahn, C. S. Ha *et al.*, *Polymer* **2003**, *44*, 3417-3428.
[21] Y.-J. Huang, X.-H. Zhang, Z.-J. Hua *et al.*, *Macromol. Chem. Phys.* **2010**, *211*, 1229-1237.
[22] C. H. Tran, L. T. T. Pham, H. B. Jang *et al.*, *Catal. Today* **2021**, *375*, 429-440.
[23] S.-F. Stahl, G. A. Luinstra, *Catalysts* **2020**, *10*, 1066.
[24] A. Doricchi, C. M. Platnich, A. Gimpel *et al.*, *ACS Nano* **2022**, *16*, 17552-17571.
[25] H.-G. Elias in *Macromolecules*, **2008**, S. 1-5.
[26] Y. Hao, Q. Li, C. Fan, F. Wang, *Small Structures* **2021**, *2*, 2000046.
[27] L. L. Böhm, *Angew. Chem., Int. Ed.* **2003**, *42*, 5010-5030.
[28] C. A. Wurtz, *Ann. Chim. Phys.* **1863**, *69*, 317-354.
[29] H. Staudinger, O. Schweitzer, *Ber. Dtsch. Chem. Ges.* **1929**, *62*, 2395-2405.
[30] K. E. S. Marple, Edward C.; Evans, Theodore W., US2327053, Shell Development Company, **1939**.
[31] M. E. J. Pruitt, L.; Baggett, J. M.; Bloomfield, R. J.; Templeton, J. H., US2706182, The Dow Chemical Company, **1952**.
[32] H.-G. Elias in *Macromolecules*, **2006**, S. 309-364.
[33] M. D. Lechner, K. Gehrke, E. H. Nordmeier, *Makromolekulare Chemie : ein Lehrbuch für Chemiker, Physiker, Materialwissenschaftler und Verfahrenstechniker*, 5, **2014**.
[34] M. H. Chisholm, D. Navarro-Llobet, *Macromolecules* **2002**, *35*, 2389-2392.
[35] B. M. Lipinski, L. S. Morris, M. N. Silberstein, G. W. Coates, *J. Am. Chem. Soc.* **2020**, *142*, 6800-6806.
[36] M. I. Childers, J. M. Longo, N. J. Van Zee *et al.*, *Chem. Rev. (Washington, DC, U. S.)* **2014**, *114*, 8129-8152.
[37] H.-G. Elias in *Macromolecules*, **2005**, S. 23-64.
[38] H.-G. Elias in *Macromolecules*, **2005**, S. 153-191.
[39] A. Basterretxea, E. Gabirondo, C. Jehanno *et al.*, *ACS Sustainable Chem. Eng.* **2019**, *7*, 4103-4111.
[40] S. Kobayashi, H. Tadokoro, Y. Chatani, *Makromol. Chem.* **1968**, *112*, 225-241.
[41] T. Endo in *Handbook of Ring-Opening Polymerization*, **2009**, S. 53-63.
[42] R. Quirk in *Handbook of Polymer Synthesis, Characterization, and Processing*, **2013**, S. 127-162.
[43] H.-G. Elias in *Macromolecules*, **2005**, S. 221-268.

[44] A. Deffieux, S. Carlotti, A. Barrère in *Polymer Science: A Comprehensive Reference*, **2012**, S. 117-140.
[45] M. Szwarc, *Nature* **1956**, *178*, 1168-1169.
[46] M. Szwarc, M. Levy, R. Milkovich, *J. Am. Chem. Soc.* **1956**, *78*, 2656-2657.
[47] S. Penczek, J. Pretula, P. Lewiński, *Polymers* **2017**, *9*, 646.
[48] A. Duda, A. Kowalski in *Handbook of Ring-Opening Polymerization*, **2009**, S. 1-51.
[49] O. Nuyken, S. D. Pask, *Polymers* **2013**, *5*, 361-403.
[50] Y. Sarazin, J.-F. Carpentier, *Chem. Rev. (Washington, DC, U. S.)* **2015**, *115*, 3564-3614.
[51] P. Kubisa, S. Penczek, *Prog. Polym. Sci.* **1999**, *24*, 1409-1437.
[52] P. Kubisa, *Makromol. Chem., Macromol. Symp.* **1988**, *13-14*, 203-210.
[53] S. Penczek, M. Cypryk, A. Duda *et al.*, *Prog. Polym. Sci.* **2007**, *32*, 247-282.
[54] H.-G. Elias, *Macromolecules Chemical structures and syntheses, Vol. 1*, **2005**.
[55] H.-G. Elias in *Macromolecules*, **2005**, S. 269-308.
[56] T. Aida, S. Inoue, *Macromolecules* **1981**, *14*, 1166-1169.
[57] T. Aida, S. Inoue, *Macromolecules* **1981**, *14*, 1162-1166.
[58] T. Aida, R. Mizuta, Y. Yoshida, S. Inoue, *Makromol. Chem.* **1981**, *182*, 1073-1079.
[59] H. Sugimoto, C. Kawamura, M. Kuroki *et al.*, *Macromolecules* **1994**, *27*, 2013-2018.
[60] C. Billouard, S. Carlotti, P. Desbois, A. Deffieux, *Macromolecules* **2004**, *37*, 4038-4043.
[61] A. Labbé, S. Carlotti, C. Billouard *et al.*, *Macromolecules* **2007**, *40*, 7842-7847.
[62] S. Carlotti, C. Billouard, E. Gautriaud *et al.*, *Macromol. Symp.* **2005**, *226*, 61-68.
[63] S. Carlotti, P. Desbois, C. Billouard, A. Deffieux, *Polym. Int.* **2006**, *55*, 1126-1131.
[64] in *Compendium of Polymer Terminology and Nomenclature: IUPAC Recommendations 2008*, **2009**, S. 3-21.
[65] J.-E. Damke, J. Klein, M. Marquardt *et al.*, WO2019243067, Henkel AG & Co. KGaA, **2019**.
[66] J.-E. Damke, J. Klein, L. Zander *et al.*, WO 201213665, Henkel AG & Co. KGaA, **2012**.
[67] B. Le-Khac, EP700949, ARCO Chemical Technology, **1999**.
[68] E. M. Dexheimer, J. Wildeson, W. Hinz, US6921737, BASF Corporation, **2005**.
[69] P. Ooms, J. Hofmann, P. Gupta, W. Schaefer, EP1100617, Bayer MaterialScience AG, **1999**.
[70] J.-P. Masy, C. M. Villa, D. A. Babb *et al.*, EP3317322, Covestro LLC, **2016**.
[71] L. Zander, C. Kunze, J. Klein *et al.*, EP2694210, Henkel AG & Co KGaA, **2014**.
[72] W. J. Kruper, D. J. Swart, US4500704, The Dow Chemical Company, **1985**.
[73] M. D. Blanco Gonzàlez, M. Garcia Ruiz, J. P. Gonzàles Rivero, EP2837648A1, Repsol, **2015**.
[74] L. Qiang, G. Zhifang, P. Lisha, X. Xue, *Catal. Commun.* **2015**, *64*, 114-118.
[75] N. J. Robertson, Z. Qin, G. C. Dallinger *et al.*, *Dalton Trans.* **2006**, 5390-5395.
[76] S. J. Yu, Y. Liu, S. J. Byeon *et al.*, *Catal. Today* **2014**, *232*, 75-81.
[77] J. Tharun, M. M. Dharman, Y. Hwang *et al.*, *Appl. Catal., A* **2012**, *419-420*, 178-184.
[78] J. H. Yoon, I. K. Lee, H. Y. Choi *et al.*, *Green Chem.* **2011**, *13*, 631-639.
[79] S. S. Kaye, J. R. Long, *J. Am. Chem. Soc.* **2005**, *127*, 6506-6507.
[80] L.-J. Krystyna, C. Arkadiusz, *J. Phys.: Conf. Ser.* **2016**, *712*, 012062.
[81] X.-H. Zhang, Z.-J. Hua, S. Chen *et al.*, *Appl. Catal., A* **2007**, *325*, 91-98.
[82] S. Chen, G. R. Qi, Z. J. Hua, H. Q. Yan, *J. Polym. Sci., Part A: Polym. Chem.* **2004**, *42*, 5284-5291.
[83] C. Marquez, M. Rivera-Torrente, P. P. Paalanen *et al.*, *J. Catal.* **2017**, *354*, 92-99.
[84] Y. Gu, X. Dong, *Des. Monomers Polym.* **2013**, *16*, 72-78.
[85] V. Šutinská, M. Pajtášová, D. Ondrušová *et al.*, *J. Therm. Anal. Calorim.* **2011**, *104*, 923-927.
[86] I. Kim, S. H. Byun, C.-S. Ha, *J. Polym. Sci., Part A: Polym. Chem.* **2005**, *43*, 4393-4404.
[87] D. J. Darensbourg, M. J. Adams, J. C. Yarbrough, A. L. Phelps, *Inorg. Chem.* **2003**, *42*, 7809-7818.
[88] D. J. Darensbourg, M. J. Adams, J. C. Yarbrough, *Inorg. Chem.* **2001**, *40*, 6543-6544.
[89] D. J. Darensbourg, A. L. Phelps, *Inorg. Chim. Acta* **2004**, *357*, 1603-1607.

[90] J. C. Wojdeł, S. T. Bromley, F. Illas, J. C. Jansen, *J. Mol. Model.* **2007**, *13*, 751-756.
[91] N. Almora-Barrios, S. Pogodin, L. Bellarosa *et al.*, *ChemCatChem* **2015**, *7*, 928-935.
[92] C. H. Tran, L. T. T. Pham, Y. Lee *et al.*, *J. Catal.* **2019**, *372*, 86-102.
[93] A. Peeters, P. Valvekens, R. Ameloot *et al.*, *ACS Catal.* **2013**, *3*, 597-607.
[94] P. Valvekens, D. De Vos in *New Materials for Catalytic Applications*, **2016**, S. 1-12.
[95] G. Wegener, M. Brandt, L. Duda *et al.*, *Appl. Catal., A* **2001**, *221*, 303-335.
[96] A. Chruściel, W. Hreczuch, K. Czaja, B. Sacher-Majewska, *Thermochim. Acta* **2016**, *630*, 78-89.
[97] S. H. Lee, I. K. Lee, J. Y. Ha *et al.*, *Ind. Eng. Chem. Res.* **2010**, *49*, 4107-4116.
[98] C. H. Tran, S. A. Kim, Y. Moon *et al.*, *Catal. Today* **2020**, *375*, 335-342.
[99] Z. Guo, Q. Lin, *J. Mol. Catal. A: Chem.* **2014**, *390*, 63-68.
[100] Z. Guo, Q. Lin, X. Wang *et al.*, *Mater. Lett.* **2014**, *124*, 184-187.
[101] J. Shi, Z. Shi, H. Yan *et al.*, *RSC Adv.* **2018**, *8*, 6565-6571.
[102] W. Zhang, L. Lu, Y. Cheng *et al.*, *Green Chem.* **2011**, *13*, 2701-2703.
[103] Y. Zhou, Z. Tang, M. He, Q. Xu, *J. Chem. Pharm. Res.* **2017**, *9*, 22-32.
[104] I. K. Lee, J. Y. Ha, C. Cao *et al.*, *Catal. Today* **2009**, *148*, 389-397.
[105] M. Pinilla-de Dios, C. Andrés-Iglesias, A. Fernández *et al.*, *Eur. Polym. J.* **2017**, *88*, 280-291.
[106] J. Sebastian, D. Srinivas, *Appl. Catal., A* **2015**, *506*, 163-172.
[107] J. Sebastian, S. Darbha, *RSC Adv.* **2015**, *5*, 18196-18203.
[108] X. H. Zhang, S. Chen, X. M. Wu *et al.*, *Chin. Chem. Lett.* **2007**, *18*, 887-890.
[109] I. Kim, M. J. Yi, K. J. Lee *et al.*, *Catal. Today* **2006**, *111*, 292-296.
[110] K. Varghese Jobi, S. Park Dong, Y. Jeon Jong, Y. Lee Bun, *J. Polym. Sci., Part A: Polym. Chem.* **2013**, *51*, 4811-4818.
[111] Y.-J. Huang, G.-R. Qi, Y.-H. Wang, *J. Polym. Sci., Part A: Polym. Chem.* **2002**, *40*, 1142-1150.
[112] L.-C. Wu, A.-F. Yu, M. Zhang *et al.*, *J. Appl. Polym. Sci.* **2004**, *92*, 1302-1309.
[113] I. Kim, J.-T. Ahn, S.-H. Lee *et al.*, *Catal. Today* **2004**, *93-95*, 511-516.
[114] S. H. Lee, C.-S. Ha, I. Kim, *Macromol. Res.* **2007**, *15*, 202-204.
[115] X.-K. Sun, X.-H. Zhang, R.-J. Wei *et al.*, *J. Polym. Sci., Part A: Polym. Chem.* **2012**, *50*, 2924-2934.
[116] M. M. Dharman, J.-Y. Ahn, M.-K. Lee *et al.*, *Green Chem.* **2008**, *10*, 678-684.
[117] S. Chen, Z. Hua, Z. Fang, G. Qi, *Polymer* **2004**, *45*, 6519-6524.
[118] T. Zhou, Z. Zou, J. Gan *et al.*, *J. Polym. Res.* **2011**, *18*, 2071-2076.
[119] Z. Li, Y. Qin, X. Zhao *et al.*, *Eur. Polym. J.* **2011**, *47*, 2152-2157.
[120] X.-H. Zhang, R.-J. Wei, X.-K. Sun *et al.*, *Polymer* **2011**, *52*, 5494-5502.
[121] K. Ma, Q. Bai, L. Zhang, B. Liu, *RSC Adv.* **2016**, *6*, 48405-48410.
[122] S. Inoue, *J. Polym. Sci., Part A: Polym. Chem.* **2000**, *38*, 2861-2871.
[123] Y. Gao, Y. Qin, X. Zhao *et al.*, *J. Polym. Res.* **2012**, *19*, 9878.
[124] Y. J. Huang, X. H. Zhang, Z. J. Hua, G. R. Qi, *Chin. Chem. Lett.* **2010**, *21*, 897-901.
[125] S. Lee, S. T. Baek, K. Anas *et al.*, *Polymer* **2007**, *48*, 4361-4367.
[126] I. Kim, K. Anas, S. Lee *et al.*, *Catal. Today* **2008**, *131*, 541-547.
[127] A. Raghuraman, D. Babb, M. Miller *et al.*, *Macromolecules* **2016**, *49*, 6790-6798.
[128] M. A. Subhani, C. Gürtler, W. Leitner, T. E. Müller, *Eur. J. Inorg. Chem.* **2016**, *13-14*, 1944-1949.
[129] R. Mohr, M. Wagner, S. Zarbakhsh, H. Frey, *Macromol. Rapid Commun.* **2021**, *42*, 2000542.
[130] X.-K. Sun, X.-H. Zhang, S. Chen *et al.*, *Polymer* **2010**, *51*, 5719-5725.
[131] L.-F. Hu, C.-J. Zhang, D.-J. Chen *et al.*, *ACS Appl. Polym. Mater.* **2020**, *2*, 5817-5823.
[132] N. Liu, C. Gu, M. Chen *et al.*, *ChemistrySelect* **2020**, *5*, 2388-2394.
[133] Y. Li, J. Hong, R. Wei *et al.*, *Chem. Sci.* **2015**, *6*, 1530-1536.
[134] L. Luo, W.-Z. Wang, L. Wang *et al.*, *e-Polymers* **2021**, *21*, 854-868.
[135] H. S. Suh, J. Y. Ha, J. H. Yoon *et al.*, *React. Funct. Polym.* **2010**, *70*, 288-293.
[136] Z. Hua, G. Qi, S. Chen, *J. Appl. Polym. Sci.* **2004**, *93*, 1788-1792.
[137] S. D. Harper, US5032671, Arco Chemical Technology, Inc., **1991**.
[138] X. Kang, X. Sun, Q. Zhu *et al.*, *Green Chem.* **2016**, *18*, 1869-1873.

[139] M. Rani, U. Shanker, *Environ. Sci. Pollut. Res.* **2018**, *25*, 23764-23779.
[140] K. Lawniczak-Jablonska, E. Dynowska, W. Lisowski *et al.*, *X-Ray Spectrom.* **2015**, *44*, 330-338.
[141] D. C. Apperley, R. K. Harris, P. Hodgkinson, *Solid-State NMR : Basic Principles and Practice*, **2012**.
[142] A. S. Lilly Thankamony, J. J. Wittmann, M. Kaushik, B. Corzilius, *Prog. Nucl. Magn. Reson. Spectrosc.* **2017**, *102-103*, 120-195.
[143] R. G. Griffin, *Nature* **2010**, *468*, 381-382.
[144] C. P. Krap, B. Zamora, L. Reguera, E. Reguera, *Microporous Mesoporous Mater.* **2009**, *120*, 414-420.
[145] J. P. Perdew, Y. Wang, *Phys. Rev. B* **1992**, *45*, 13244-13249.
[146] G. E. Yu, A. J. Masters, F. Heatley *et al.*, *Macromol. Chem. Phys.* **1994**, *195*, 1517-1538.
[147] J. Ding, F. Heatley, C. Price, C. Booth, *Eur. Polym. J.* **1991**, *27*, 895-899.
[148] Y. Doi, T. Keii, *Chromatography/Foams/Copolymers*, **1986**, Berlin, Heidelberg, 201-248.
[149] P. F. Yang, J. Y. Li, T. D. Li, *Adv. Mater. Res.* **2011**, *160-162*, 60-64.
[150] M. C. Tobin, *Spectrochim. Acta* **1960**, *16*, 1108-1110.
[151] D. G. Blackmond, *Angew. Chem., Int. Ed.* **2005**, *44*, 4302-4320.
[152] D. G. Blackmond, *Angew. Chem., Int. Ed.* **2009**, *48*, 386-390.
[153] A. I. Hanopolskyi, V. A. Smaliak, A. I. Novichkov, S. N. Semenov, *ChemSystemsChem* **2021**, *3*, e2000026.
[154] R. Plasson, A. Brandenburg, L. Jullien, H. Bersini, *J. Phys. Chem. A* **2011**, *115*, 8073-8085.
[155] T. F. L. McKenna, A. Di Martino, G. Weickert, J. B. P. Soares, *Macromol. React. Eng.* **2010**, *4*, 40-64.
[156] A. Alizadeh, T. F. L. McKenna, *Macromol. React. Eng.* **2018**, *12*, 1700027.
[157] F. Kapteijn, J. A. Moulijn, G. Emig *et al.* in *Handbook of Heterogeneous Catalysis*, **1997**, S. 1189-1261.
[158] D. G. Truhlar, A. Kohen, *Proc. Natl. Acad. Sci., India* **2001**, *98*, 848.
[159] M. A. Vannice in *Kinetics of Catalytic Reactions*, **2005**, S. 38-86.
[160] A. Fick, *Ann. Phys.* **1855**, *170*, 59-86.
[161] J. Burés, *Angew. Chem., Int. Ed.* **2016**, *55*, 16084-16087.
[162] J. Burés, *Angew. Chem., Int. Ed.* **2016**, *55*, 2028-2031.
[163] F. C. Schilling, A. E. Tonelli, *Macromolecules* **1986**, *19*, 1337-1343.
[164] N. Oguni, K. Lee, H. Tani, *Macromolecules* **1972**, *5*, 819-820.
[165] M. Regitz, E. Hillen-Maske, *Römpp-Chemie-Lexikon*, 9., erweiterte und neubearbeitete Auflage, **1989**.
[166] P. Alexandridis, T. Alan Hatton, *Colloids Surf., A* **1995**, *96*, 1-46.
[167] M. Bachmann, A. Kätelhön, B. Winter *et al.*, *Faraday Discuss.* **2021**, *230*, 227-246.
[168] C. Liu, J. Xin, J. Tan *et al.*, *ACS Omega* **2018**, *3*, 8718-8723.
[169] Z. Yu, L. Xu, Y. Wei *et al.*, *Chem. Commun. (Cambridge, U. K.)* **2009**, 3934-3936.
[170] M. A. Abdel-Rahman, Y. Tashiro, K. Sonomoto, *Biotechnol. Adv.* **2013**, *31*, 877-902.
[171] V. Thaore, D. Chadwick, N. Shah, *Chem. Eng. Res. Des.* **2018**, *135*, 140-152.
[172] B. M. Stadler, C. Wulf, T. Werner *et al.*, *ACS Catal.* **2019**, *9*, 8012-8067.
[173] J. G. de Vries in *Adv. Heterocycl. Chem., Vol. 121*, **2017**, S. 247-293.
[174] P. Song, H. Xu, X. Mao *et al.*, *Polym. Adv. Technol.* **2017**, *28*, 736-741.
[175] L. Gu, Y. Qin, Y. Gao *et al.*, *Chin. J. Chem.* **2012**, *30*, 2121-2125.
[176] S. Liu, H. Xiao, K. Huang *et al.*, *Polym. Bull. (Berlin)* **2006**, *56*, 53-62.
[177] R. Lindner, M. L. Lejkowski, S. Lavy *et al.*, *ChemCatChem* **2014**, *6*, 618-625.
[178] M. Chwatko, N. A. Lynd, *Macromolecules* **2017**, *50*, 2714-2723.
[179] C. Diaz, T. Tomković, C. Goonesinghe *et al.*, *Macromolecules* **2020**, *53*, 8819-8828.
[180] D. Xie, Z. Yang, L. Wu *et al.*, *Polym. Int.* **2018**, *67*, 883-893.
[181] Z. N. Nysenko, E. E. Said-Galiev, M. I. Buzin *et al.*, *Mendeleev Commun.* **2014**, *24*, 236-238.

[182] Z. N. Nysenko, E. E. Said-Galiev, M. M. Ilyin *et al.*, *Russ. Chem. Bull.* **2015**, *64*, 2914-2918.
[183] X. Li, C.-y. Hu, R.-l. Duan *et al.*, *Polym. Chem.* **2021**, *12*, 3124-3131.
[184] S. Kernbichl, M. Reiter, F. Adams *et al.*, *J. Am. Chem. Soc.* **2017**, *139*, 6787-6790.
[185] S. Kernbichl, M. Reiter, J. Mock, B. Rieger, *Macromolecules* **2019**, *52*, 8476-8483.
[186] S. Liu, J. Wang, K. Huang *et al.*, *Polym. Bull. (Berlin)* **2011**, *66*, 327-340.
[187] T. T. D. Chen, Y. Zhu, C. K. Williams, *Macromolecules* **2018**, *51*, 5346-5351.
[188] Y. Chen, W. Wang, D. Xie *et al.*, *J. Polym. Sci.* **2021**, *59*, 1528-1539.
[189] X. Li, R.-l. Duan, C.-y. Hu *et al.*, *Polym. Chem.* **2021**, *12*, 1700-1706.
[190] L. Tang, W. Luo, M. Xiao *et al.*, *J. Polym. Sci., Part A: Polym. Chem.* **2015**, *53*, 1734-1741.
[191] H.-H. Moretto, M. Schulze, G. Wagner in *Ullmann's Encyclopedia of Industrial Chemistry*.
[192] Q. An, G. Yang, Q. Wang, L. Huang, *J. Appl. Polym. Sci.* **2008**, *110*, 2595-2600.
[193] H. Bai, *Ind. Eng. Chem. Res.* **2014**, *53*, 1588-1597.
[194] Z. Dai, K. Yang, Q. Dong, *J. Appl. Polym. Sci.* **2015**, *132*, 42521.
[195] M. Woźnicka, U. Kragl, *Synthesis and properties of telechelic polysiloxane and polyether homo- and co-polymers*, **2017**.
[196] M. Woznicka, S. Ghosh, M. Marquardt *et al.*, WO2019206739A1, Henkel AG & Co. KGaA, **2019**.
[197] K. W. Haider, J. Y. Chung, J. F. Dormish *et al.*, US20080171829, Bayer MaterialScience LLC, **2007**.
[198] J.-F. Lutz, T. Pakula, K. Matyjaszewski in *Advances in Controlled/Living Radical Polymerization, Vol. 854*, **2003**, S. 268-282.
[199] D. J. Lohse, N. Hadjichristidis, *Curr. Opin. Colloid Interface Sci.* **1997**, *2*, 171-176.
[200] U. Beginn, *Colloid Polym. Sci.* **2008**, *286*, 1465-1474.
[201] H. P. Diogo, J. J. Moura Ramos, *Polym. Eng. Sci.* **2021**, *61*, 1638-1649.
[202] M. Varma-Nair, J. P. Wesson, B. Wunderlich, *J. Therm. Anal.* **1989**, *35*, 1913-1939.
[203] W. Noll, *Chemie und Technologie der Silicone*, **1960**.
[204] C. Diaz, P. Mehrkhodavandi, *Polym. Chem.* **2021**
[205] D. Yang, Q. Lu, Z. Fan *et al.*, *J. Appl. Polym. Sci.* **2010**, *118*, 2304-2313.
[206] M. Vaughn, EP0826012, Dow Chemical Company, **1995**.
[207] F. E. Bailey, H. G. France, US3312753, Union Carbide Corporation, **1964**.
[208] P. Deglmann, S. Zarbakhsh, A. Löffler, K. Wiss, EP2765151, BASF, **2010**.
[209] P. Deglmann, S. Zarbakhsh, A. Löffler, K. Wiss, WO2011141492A1, BASF, **2011**.
[210] N. E. Clayman, L. S. Morris, A. M. LaPointe *et al.*, *Chem. Commun. (Cambridge, U. K.)* **2019**, *55*, 6914-6917.
[211] N. Liu, C. Gu, Q. Wang *et al.*, *RSC Adv.* **2021**, *11*, 8782-8792.
[212] P. Deglmann, S. Zarbakhsh, A. Löffler, K. Wiss, BASF, **2011**.
[213] T. N. Trieu, M. H. Nguyen, U. Abram, H. H. Nguyen, *Z. Anorg. Allg. Chem.* **2015**, *641*, 863-870.
[214] C. T. Pham, H. H. Nguyen, A. Hagenbach, U. Abram, *Inorg. Chem.* **2017**, *56*, 11406-11416.
[215] C. T. Pham, T. H. Nguyen, T. N. Trieu *et al.*, *Z. Anorg. Allg. Chem.* **2019**, *645*, 1072-1078.
[216] J. J. Jesudas, C. T. Pham, A. Hagenbach *et al.*, *Inorg. Chem.* **2020**, *59*, 386-395.
[217] S. D. Allen, D. R. Moore, E. B. Lobkovsky, G. W. Coates, *J. Am. Chem. Soc.* **2002**, *124*, 14284-14285.
[218] S. D. Allen, D. R. Moore, E. B. Lobkovsky, G. W. Coates, *J. Organomet. Chem.* **2003**, *683*, 137-148.
[219] R. Kember Michael , D. Knight Paul , T. R. Reung Palarp , K. Williams Charlotte *Angew. Chem., Int. Ed.* **2009**, *48*, 931-933.
[220] M. R. Kember, A. J. P. White, C. K. Williams, *Inorg. Chem.* **2009**, *48*, 9535-9542.
[221] M. Yokoyama, T. Ikuma, N. Obara, H. Togo, *J. Chem. Soc., Perkin Trans. 1* **1990**, 3243-3247.
[222] J. C. Slater, *J. Chem. Phys.* **1964**, *41*, 3199-3204.

[223] S. Kissling, M. W. Lehenmeier, P. T. Altenbuchner *et al.*, *Chem. Commun. (Cambridge, U. K.)* **2015**, *51*, 4579-4582.
[224] J. A. Garden, A. J. P. White, C. K. Williams, *Dalton Trans.* **2017**, *46*, 2532-2541.
[225] A. C. Deacy, E. Moreby, A. Phanopoulos, C. K. Williams, *J. Am. Chem. Soc.* **2020**, *142*, 19150-19160.
[226] A. C. Deacy, C. B. Durr, J. A. Garden *et al.*, *Inorg. Chem.* **2018**, *57*, 15575-15583.
[227] H. Asaba, T. Iwasaki, M. Hatazawa *et al.*, *Inorg. Chem.* **2020**, *59*, 7928-7933.
[228] H. Nagae, R. Aoki, S.-n. Akutagawa *et al.*, *Angew. Chem., Int. Ed.* **2018**, *57*, 2492-2496.
[229] E. Fazekas, R. D. McIntosh in *Organometallic Chemistry, Vol. 43*, **2021**, S. 63-82.
[230] M. Gumienna, B. Górna, *Molecules* **2021**, *26*, 3735.
[231] S. Ghosh, A. Spannenberg, E. Mejía, *Helv. Chim. Acta* **2017**, *100*, e1700176.
[232] P. Horeglad, G. Szczepaniak, M. Dranka, J. Zachara, *Chem. Commun. (Cambridge, U. K.)* **2012**, *48*, 1171-1173.
[233] A. Otero, J. Fernández-Baeza, L. F. Sánchez-Barba *et al.*, *Organometallics* **2012**, *31*, 4191-4202.
[234] E. Bukhaltsev, L. Frish, Y. Cohen, A. Vigalok, *Org. Lett.* **2005**, *7*, 5123-5126.
[235] P. Degée, P. Dubois, R. Jérôme *et al.*, *Macromol. Symp.* **1999**, *144*, 289-302.
[236] A. Thevenon, C. Romain, M. S. Bennington *et al.*, *Angew. Chem., Int. Ed.* **2016**, *55*, 8680-8685.
[237] R. D. Rittinghaus, P. M. Schäfer, P. Albrecht *et al.*, *ChemSusChem* **2019**, *12*, 2161-2165.
[238] H. R. Kricheldorf, S. M. Weidner, F. Scheliga, *Macromol. Chem. Phys.* **2022**, *223*, 2100464.
[239] O. Dechy-Cabaret, B. Martin-Vaca, D. Bourissou in *Handbook of Ring-Opening Polymerization*, **2009**, S. 255-286.

Appendix

Table of contents

A-1 Experimental

A-1.1 Calculations

A-1.1.1 Calculation of DMC catalyst concentration in mol% for online FTIR analysis

The catalyst concentration ($mol\%_{DMC(Zn)}$) with regards to the moles of propylene oxide used (n_{PO}) was calculated by the contained amount of zinc determined by elemental analysis (w%) as described in **Eq. A 1**.

$$mol\%_{DMC(Zn)} = \frac{m_{DMC} * w\%}{M_{Zn} * n_{PO}} \qquad \textbf{Eq. A 1}$$

A-1.1.2 Calculation of D3 conversion from ^{29}Si-IG NMR

D3 conversion was determined using the ^{29}Si-IG (inverse gated) NMR spectrum of a sample before removing excess monomer from the reaction mixture by **Eq. A 2**, in which I_{D3} is the integral of the D3 signal at 8.3 ppm and I_{total} is the sum of all integrals in the ^{29}Si-IG spectrum.

$$conversion_{D3} = 100\% - \frac{\mathrm{I_{D3}}}{\mathrm{I_{total}}} \qquad \textbf{Eq. A 2}$$

A-1.1.3 Calculation of the carbonate fraction from ^{1}H-NMR

The carbonate fraction F_{CO2} of a CO_2 containing copolymer was determined using the ^{1}H NMR spectrum of a sample before quenching and workup by, in which I_{CO2} is the integral of the carbonate bond signal at 4.6 ppm and I_{ether} is the Integral of the ether bonds at 3.5 ppm (**Eq. A 3**).

$$\mathrm{F_{CO2}} = \frac{\mathrm{I_{CO2}}}{(\mathrm{I_{CO2}} + \mathrm{I_{ether}})} * 100\% \qquad \textbf{Eq. A 3}$$

A-1.1.4 Calculation of the *rac*-lactide conversion from ^{1}H-NMR

The *rac*-lactide conversion was determined using the ^{1}H NMR spectrum of a sample before quenching and workup using **Eq. A 4**. The integral of the methyl proton's signal of the polymer

at 1.56 ppm (I_{PLA}) and the integral of the monomer's methyl proton signal at 1.69 ppm ($I_{lactide}$) were considered for this calculation. Both integrals depict six protons, either in the monomer or in the repeating unit of the polymer.

$$\text{conversion}_{\text{lactide}} = 100\% - \frac{\text{I}_{\text{lactide}}}{\text{I}_{\text{lactide}} + \text{I}_{\text{PLA}}}\% \qquad \textbf{Eq. A 4}$$

A-1.2 Pressure Reactor

Pressure Reactions were carried out in an electronically monitored 100 ml Parr stainless steel reactor equipped with a mechanical stirrer, heat jacket and a computer-controlled dosing system. The reactor setup additionally gives the additional option to add liquids to the reaction manually. The structure of the autoclave system is shown in Figure A 1. The vessel of the reactor can be exchanged to a vessel with a fit for the ReactIR15 IR probe head.

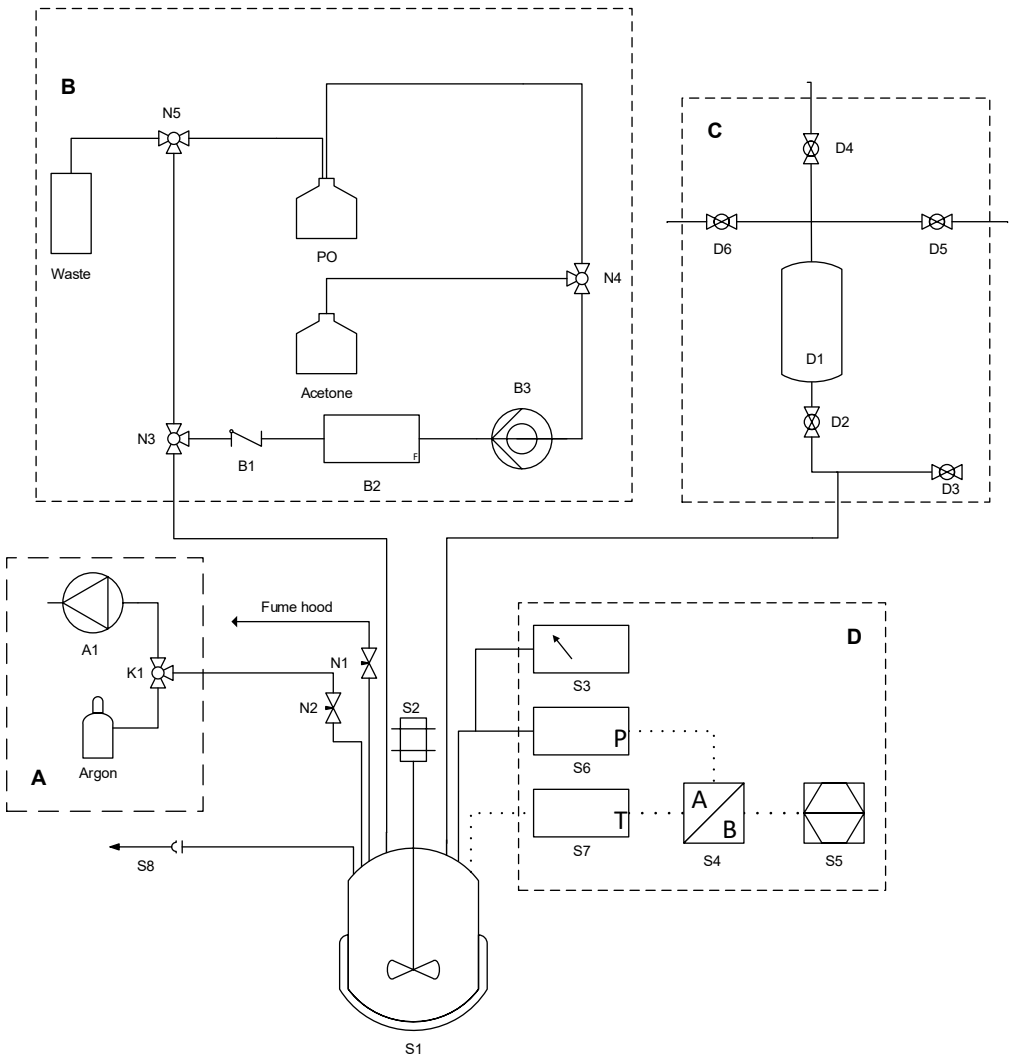

Figure A 1: Structure of the 100 ml Parr stainless steel pressure reactor system.

Rudimentary and control system (System D)	
S1	Reactor vessel 4560 with stirrer
S2	Agitator motor
S3	Manometer
S4	PARR-Controller 4848
S5	Computer
S6	Pressure sensor
S7	Temperature sensor
S8	Rupture disc (3500 psi/ 240 bar)
N1	Needle valve to SCHLENK line
N2	Needle valve for venting

System A: Venting and Aerating	
A1	Vacuum pump
K1	SCHLENK Line

System B: Manual Dosing System	
D1	Pressure vessel
D2	Ball valve for the connection of both system
D3	Ball valve for addition to the reactor
D4	Ball valve for addition to the pressure vessel
D5	Ball valve to the fume hood
D6	Ball valve to the fume hood

System C: Automated Dosing System	
B1	Check-valve
B2	Mini Cori Flow M13 (Bronkhorst)
B3	Annular gear pump (HNP microsystems)
N3	Three-way valve to waist and PO/acetone
N4	Three-way valve to PO and acetone
N5	Three-way valve for circulation mode

A-1.3 Analytical procedures

Liquid-state NMR: Three spectrometers were used for ^{1}H, ^{13}C and ^{29}SI-IG NMR analysis (model specifications shown in Table A 1). Spectra shifts are reported as δ-values in ppm with reference to the shift of the deuterated solvent used. The used solvents are d_1-chloroform (^{1}H = 7.26 ppm, ^{13}C = 77.16 ppm), d_2-methylene chloride (1H = 5.32, ^{13}C = 53.84 ppm) and d_6-benzene (^{1}H = 7.160, ^{13}C = 128.06 ppm). ^{29}Si-IG spectra were used without referencing for calculations from integration only.

The abbreviations used to describe the multiplicity of the spectra peaks are: s (singlet), d (doublet), t (triplet), q (quadruplet) and m (multiplet), etc. Coupling constant *J* is reported in Hertz (Hz).

Table A 1: NMR spectrometers.

spectrometer	purchased in	magnetic flux	proton resonance frequency
Bruker AV300	2005	9.4 Tesla	300 MHz
Bruker AV400	2005	7.0 Tesla	400 MHz
Bruker Fourier300	2012	7.0 Tesla	300 MHz

Solid-state NMR: All catalyst samples were measured with a Bruker Ascend 400 MHz DNP magnet which is connected to a Bruker Avance III console. Experiments were performed with a Bruker MAS3 pneumatic system using a 4 mm triple-resonance probe. Each measurement was performed at 14 kHz MAS frequency and at 297 K. The carrier frequencies were set to 80 ppm (^{13}C) and 3 ppm (^{1}H) and the radio frequency of the hard pulses were set to 50 kHz (^{13}C) and 83.33 kHz (^{1}H).

The 1D ^{13}C direct polarization experiments which consisted of one 90° ^{13}C pulse followed by acquisition and ^{1}H decoupling were conducted with a repetition delay between 10 and 60 s and a SPINAL-64[1] proton decoupling scheme during acquisition for 50 ms. Thereby, either 4096 or 4994 points were sampled per scan with a total number of scans between 1024 and 32768 scans.
The 1D ^{13}C cross polarization experiments consisted of a 90° pulse on protons followed by the cross polarization contact pulses and acquisition with proton decoupling. They were performed with a repetition delay of 5 s. During acquisition, either 4096 or 4994 points were sampled, and a SPINAL-64 proton decoupling scheme was applied for 50 ms. Time average of each experiment was performed with a total number of scans between 1024 and 32768 scans. A CP contact time of 5 ms was applied at the above mentioned radio frequencies.
Each experiment was processed with zero filling to 16384 points and apodization was performed with an exponential window function using a broadening factor (LB) of 10 Hz before applying the Fourier transformation. Linear prediction calculation comprising 4096 points was applied to increase the FID if the FID was cut off due to decoupling length limits.[1]

XPS: The XPS (X-ray Photoelectron Spectroscopy) measurements were performed on an ESCALAB 220iXL (Thermo Fisher Scientific) with monochromated Al Kα radiation (E = 1486.6 eV). Samples are prepared on a stainless-steel holder with conductive double-sided adhesive carbon tape. The electron binding energies were obtained with charge compensation using a flood electron source and referenced to the N 1s core level of nitrogen at 399.1 eV (C≡N bonds). For quantitative analysis the peaks were deconvoluted with Gaussian-Lorentzian curves using the software Unifit 2020. The peak areas were normalized by the transmission function of the spectrometer and the element specific sensitivity factor of Scofield.[2]

GPC: Gel permeation chromatography was carried out using HP1090 II Chromatography with DAD detector (HEWLETT PACKARD) at 40 °C. Tetrahydrofuran (THF) was used as an eluent. THF was passed through three PSS SDV gel columns with molecular weight ranges of 102, 103 and 104 g·mol-1 with a flow rate of 1 ml·min-1. The calibration of the device was carried out using polystyrene standards.

DSC: Glass transition temperatures were determined with a differential scanning calorimetry DSC 1 STARe System (400 W) from Mettler Toledo equipped with an A FRS5 sensor and the dynamic temperature system IntraCooler TC100 RC by HUBER. Al-crucibles 40 µL with pin and lid were filled with 10–20 mg sample and an empty sample pan was used as a reference. Crucible lids were penetrated with a needle and the lids were closed by cold welding. All measurements were carried out at atmospheric pressure and under inert conditions. The used

method employs a constant heating and cooling rate of 5 $K \cdot min^{-1}$ within a temperature range from -90 °C to 50 °C. The temperature at the inversion point was defined as glass transition temperature.

Mass Spectrometry: Liquid Chromatography Mass Spectrometry (LC MS) was carried out using an Agilent 1200/6210 device. The ionization method of choice was electrospray ionization. A time-of-flight measurement was used which enables a high resolution recording with a mass accuracy of < 3 ppm. MALDI (matrix assisted laser desorption/ionization) TOF MS was conducted on a Bruker autoflex speed in reflection mode. The used matrix is 1,8-Dihydroxy-10H-anthracen-9-on + LiCl.

Elemental Analysis: The elements C, H, N and S were determined via combustion analysis using a Leco TruSpec Micro CHNS elemental analyzer. Zn, Co, Fe, K and Na were determined using flame atom-absorption spectroscopy with a Perkin-Elmer Analyst 300. Halogens and water content were titrated potentiometrically using Radiometer Analytical titration station TIM 580 and TIM 870.

Rheology: Viscosity was determined on a Haake RheoStress 1 rheometer by the company Thermo Scientific using cone/plate method with a C35/1° titanium cone geometry in constant shear rate mode. At a temperature of 25 °C a linear stepwise increase of the shear rate from 1.000 s^{-1} to 100.0 s^{-1} is performed within 10 measurements to determine the dynamic viscosity.

ATR-IR Spectroscopy: ATR (attenuated total reflection)-IR spectra were recorded on a Bruker Alpha FT-IR-Spectrometer with a spectral range of 7500-375 cm^{-1} (wavelength range 1,3-27 mm).

Online IR Spectroscopy: Reaction monitoring with online FTIR was done using a Mettler Toledo ReactIR 15 with a 9.5 mm diameter silver halide fiber conduit and a liquid nitrogen cooled MCT (mercuric cadmium telluride) detector. The used equipment has a diamond composite sensor with an optical window of 2500 – 2250 cm^{-1} and 2000 – 650 cm^{-1}.The device is able to collect a sample every 15 s with a number of 16 scans and a maximum resolution of 4 cm^{-1}. The software iCIR was used to evaluate the obtained spectral data. Background correction was performed and the second derivate of the spectrum was used.

TEM and EDX: The nanostructure of the DMC samples was investigated in an analytical, probe aberration corrected scanning transmission electron microscope (STEM) JOEL JEM-ARM200F NEOARM equipped with a cold field emission gun operated at 200 kV acceleration

voltage. Images were acquired by a high-angle annular dark field detector (HAADF) and an annular bright field detector (ABF). The chemical composition of relevant features was analyzed by a JEOL energy-dispersive X-ray (EDS) detector with an area of 100 mm^2.

SEM: Scanning electron microscopy was performed on a Field Emission Scanning Electron Microscope SUPRA 25 by the company Zeiss.

XAS: X-Ray absorption spectroscopy (XAS) was performed on the CLAESS beamline at the ALBA synchrotron in Barcelona.

SR-PXRD: Synchrotron radiation powder X-ray diffraction spectroscopy was performed on the MSPD beamline at the ALBA synchrotron in Barcelona.

Determination of CA content in DMC catalysts: The catalyst sample is extracted with a 2:1 $CHCl_2/CH_3OH$ mixture in the microwave (40 °C, 400 W, 10 min). The solvent phase is separated, left to cool down to room temperature and subsequently evaporated under argon to dryness. The residue is then added to ultrapure water. This solution is submitted to Ion-Exchange-Chromatography using a KNAUER HPLC box Model-96, equipped with an RI detector. The column by the company THERMO SCIENTIFIC is packed with Hyper Rez XP Carbohydrate. Sulfuric acid is used as the eluent at a temperature of 20 °C and a flow rate of 1.2 ml/min.

Determination of 2-octyldodecan-1-ol in DMC catalysts: The catalyst sample is extracted with a 2:1 $CHCl_2/CH_3OH$ mixture in the microwave (40 °C, 400 W, 10 min). The solvent phase is separated, left to cool down to room temperature and subsequently evaporated under argon to dryness. The residue is then dissolved in ethyl acetate. The obtained solution is submitted to gas chromatography coupled with mass spectrometry using a Trace GC Ultra with a TG 5 SIL MS 30x0,25x0,25 column coupled with a ITQ 1100 MS, both manufactured by THERMO SCIENTIFIC.

A-1.4 Preparation Procedures

A-1.4.1 Preparation of DMC0

For **DMC0** two solutions were prepared. For solution 1 $K_3Co(CN)_6$ (3.0 g, 9.0 mmol) was dissolved in 100 ml of deionized H_2O. Solution 2 consisted of $ZnCl_2$ (20 g, 146.75 mmol) dissolved in 100 ml of deionized H_2O. To prepare **DMC0** solution 1 and 2 were mixed using a homogenizer for 20 min. Subsequently, the resulting precipitate was separated from the solvent using a centrifuge (10 min, 10000 rpm). Following the centrifugation, the precipitate was reslurried in 100 ml of deionized H_2O for 20 min. Afterwards, the precipitate was again separated from the supernatant using a centrifuge (10 min, 10000 rpm). This was step was conducted three times in total. The final complex was separated from the solution by centrifugation (10 min, 10000 rpm) and dried at 50 °C and 20 mbar for 24 h (yield: m = 3.4263 g).

A-1.4.2 Preparation of DMC catalysts

DMC catalysts are prepared according to a procedure developed in our group.[3] In a first solution, the cyanide salt (1 Eq.), complexing agent (CA, 11 Eq.) and co-complexing agent (co-CA, 0.03 Eq.) are dissolved in deionized H_2O (615 Eq.). In a second solution, $ZnCl_2$ (16 Eq.) and the CA (21 Eq.) are also dissolved in deionized H_2O (615 Eq.). Both solutions are combined and stirred vigorously for 20 min. Subsequently, the mixture is centrifuged for 10 min at 10000. The supernatant is decanted from the precipitate followed by a washing of the precipitate with a solution consisting of deionized water (309 Eq.), CA (59 Eq.) and co-CA (0.03 Eq.) under stirring. The procedure of centrifuging and washing is repeated two times with two different washing solutions. The second washing solution consists of deionized water (154 Eq.), CA (89 Eq.) and co-CA (0.03 Eq.). The third washing solution contains CA (118.4 Eq.) and co-CA (0.017 Eq.). The resulting precipitate is decanted from the solution and is dried for 18 h in vacuo at 50 °C.

Table A 2: DMC catalysts prepared.

catalyst	salt 1	salt 2	CA	co-CA
DMC0	$ZnCl_2$	$K_3[Co(CN)_6]$	-	-
DMC1	$ZnCl_2$	$K_3[Co(CN)_6]$	*tert*-butanol	-
DMC2	$ZnCl_2$	$K_3[Co(CN)_6]$	*tert*-butanol	2-octyl-1-dodecanol
DMC3	$ZnCl_2$	$K_3[Co(CN)_6]$	*tert*-butanol	PPG4000
DMC4	$ZnCl_2$	$K_3[Co(CN)_6]$	dimethoxyethane	-
DMC5	$ZnCl_2$	$K_3[Co(CN)_6]$	tripropylene-glycol	-
DMC6	$ZnCl_2$	$K_3[Co(CN)_6]$	*tert*-butanol	PEG380-420
DMC7	$ZnCl_2$	$K_4[Fe(CN)_6]$	*tert*-butanol	-
DMC8	$ZnCl_2$	$K_4[Fe(CN)_6]$	*tert*-butanol	2-octyl-1-dodecanol

A-1.4.3 PO Polymerization procedure using a DMC catalyst

The following polymerization procedure was routinely used in the homopolymerization of PO during activity testing and investigations on kinetics. Catalyst and the corresponding amount of chain transfer agent are dried under vacuum at 105 °C for 45 min in a 100 ml pressure reactor. Subsequently, the reactor is heated to 120 °C and propylene oxide is added in one portion. The end of the induction time is marked by a rapid increase in temperature and pressure and the end of the reaction is reached when the pressure drops to the reaction pressure before the PO addition. This is followed by addition of another portion of monomer or continuous addition of monomer. After venting the reactor, possible propylene oxide residue is removed under vacuum to obtain pure polymer product.

A-1.4.4 Homopolymerization of *rac*-lactide using DMC2:

0.77 mg (500 ppm) of **DMC2** are placed in a vial with of PO. The vial is placed in a stainless steel pressure reactor which is quenched with argon three times and then heated to 120 °C. After a reaction time of 24 h excess monomer and solvent are removed in vacuum at 80 °C. The product is obtained as colorless solid (0.8879 g, 76 %). **^{1}H NMR** ($CDCl_3$, 400 MHz, 297.0 K, ppm): δ 5.26-5.16 (1H, C**H**), 1.59-1.53 (3H, C**H$_3$**).

A-1.4.5 Polypropylene oxide-polydimethylsiloxane copolymers

PO/D3 Copolymerization CP1: DMC2 Catalyst (10.6 mg) and polypropylene glycol with a molar mass of 2000 g/mol (19.5 g, 9.72 mmol) are charged into the vessel of a 100 ml Parr Mini Benchtop reactor. Moisture and oxygen are removed from the mixture by heating to 105 °C and < 1 mbar for 45 min. Subsequently, the reaction is cooled to 50 °C and the vessel is opened to atmosphere to introduce hexamethylcyclotrisiloxane (16.02 g, 72 mmol) to the mixture. After closing the vessel, the reactor is quenched with Argon three times and heated to 120 °C at a stirring speed of approx. 400 rpm. Once the desired reaction temperature is reached, propylene oxide (4.176 g, 72 mmol) is added through an opening of the reactor head. The reaction mixture is then stirred at 120 °C for 24 h. After cooling down the reaction to room temperature, the mixture is transferred into a flask which is followed by removing excess monomer in vacuo to isolate the product in form of an opaque liquid (yield: 34.9627 g, 88 %). ^{1}H NMR ($CDCl_3$, 400 MHz, 298.0 K, ppm) δ = 5.88 (m, traces, CH_2=C**H**CH_2O-), 5.20 (m, traces, C**H$_2$**=$CHCH_2$O-), 4.00 (m, traces, CH_2=$CHCH_2$O-), 3.91 (m, 0.05 H, HOC**H**(CH_3)CH_2-), 3.54 (m, 2H, -OCH(CH_3)C**H$_2$**-), 3.38 (m, 1H, -OC**H**(CH_3)CH_2-), 3.14 (t, 0.05H, HOCH(CH_3)C**H$_2$**-one of two non-equivalent), 1.12 (m, 3H, -OCH(C**H$_3$**)CH_2-), 0.15 (s, 0.09H, D3(Si-(C**H$_3$**)$_2$), 0.07 (m, 0.5H, -Si(C**H$_3$**)$_2$-). ^{13}C NMR ($CDCl_3$, 100 MHz, 298.0 K, ppm) δ = 75.56 - 75.17

(-O**C**H(CH_3)CH_2-), 73.87 - 72.90 (-OCH(CH_3)**C**H_2-), 67.31 - 65.57 (HO**C**H-), 18.52 - 17.02 (-OCH(**C**H_3)CH_2-), 1.09 - 0.45 (Si(**C**H_3)$_2$-O-C-), -0.16, -0.49, -1.09 (Si(CH_3)$_2$-O-**C**-). ^{29}Si NMR($CDCl_3$, 79.5 MHz, 298.0 K) δ = -8.3 (D3) , -21.89 (PDMS). GPC (eluent: THF, standard: polystyrene): M_n = 3113 g/mol, PDI = 1.33.

PO/D3 Copolymerization CP2-8: DMC2 Catalyst (14.1 mg), polypropylene glycol with a molar mass of 2000 g/mol (10.1 g, 5.04 mmol) and hexamethylcyclotrisiloxane (16.02 g, 72.00 mmol) are charged into the vessel of a 100 ml Parr Mini Benchtop stainless steel reactor. Moisture and oxygen are removed from the mixture by quenching with Argon three times and subsequently the reactor is heated to 120 °C at a stirring speed of approx. 400 rpm. Once the desired reaction temperature is reached, Argon pressure is adjusted to 4.3 bar and the desired amount of initiating propylene oxide is added through an opening of the reactor head or by continuous dosing. After a rapid pressure drop indicates the activation of the catalyst a second amount of propylene oxide is added. After stirring at 120 °C, the reaction is stopped by removing excess monomer in vacuo. The isolated product is obtained in form of an opaque liquid. CP2: ^{1}H NMR ($CDCl_3$, 400 MHz, 298.0 K, ppm) δ = 5.87 (m, traces, CH_2=C**H**CH_2O-), 5.21 (m, traces, C**H₂**=$CHCH_2$O-), 4.24 (m, traces, CH_2=CHC**H₂**O-), 3.94 (m, 0.07 H, HOC**H**(CH_3)CH_2-), 3.50 (m, 2H, -OCH(CH_3)C**H₂**-), 3.38 (m, 1H, -OC**H**(CH_3)CH_2-), 3.13 (t, 0.01H, HOCH(CH_3)C**H**$_2$- one of two non-equivalent), 1.11 (m, 3H, -OCH(C**H₃**)CH_2-), 0.14 (s, 0.03H, D3(Si-(C**H₃**)$_2$), 0.06 (m, 2.53H, -Si(C**H₃**)$_2$-). ^{13}C NMR ($CDCl_3$, 100 MHz, 298.0 K, ppm) δ = 75.62 - 75.22 (-O**C**H(CH_3)CH_2-), 73.97 - 72.95 (-OCH(CH_3)C**H₂**-), 69.30 - 67.39 (HO**C**H-), 18.87 - 17.46 (-OCH(**C**H_3)CH_2-), 1.13 (Si(**C**H_3)$_2$-O-C-), -0.12, -0.46, -1.05 (Si(CH_3)$_2$-O-**C**-). ^{29}Si NMR($CDCl_3$, 79.5 MHz, 298.0 K) δ = -8.18 (D3) , -13.59 (Si-O-C), -21,04, -21.96 (PDMS). GPC (eluent: THF, standard: polystyrene): M_n = 12970 g/mol, PDI = 1.38.

PO/D3 Copolymerization CP9: DMC2 Catalyst (14.1 mg), polypropylene glycol with a molar mass of 2000 g/mol (10.1 g, 5.04 mmol) and hexamethylcyclotrisiloxane (16.02 g, 72.00 mmol) are charged into the vessel of a 100 ml Parr Mini Benchtop stainless steel reactor. Moisture and oxygen are removed from the mixture by quenching with Argon three times and subsequently the reactor is heated to 120 °C at a stirring speed of approx. 400 rpm. Once the desired reaction temperature is reached, Argon pressure is adjusted to 4.3 bar and propylene oxide (10 ml, 8.352 g, 144 mmol) is added through an opening of the reactor head. After a rapid pressure drop indicates the activation of the catalyst a second amount of propylene oxide is added in two consecutive 5 ml (4.176 g, 72 mmol) portions. After 17 h of stirring at 120 °C a fourth 5 ml (4.176 g, 72 mmol) portion of propylene oxide is added. Immediately after the pressure reaches the value it showed before the last PO addition, the reaction is stopped by removing all volatiles in vacuo. The isolated product is obtained in form of an opaque liquid.

^{1}H NMR ($CDCl_3$, 400 MHz, 298.0 K, ppm) δ = 5.88 (m, traces, CH_2=C**H**CH_2O-), 5.23 (m, traces, C**H$_2$**=$CHCH_2$O-), 4.24 (m, traces, CH_2=CHC**H$_2$**O-), 3.95 (m, 0.05 H, HOC**H**(CH_3)CH_2-), 3.53 (m, 2H, -OCH(CH_3)C**H$_2$**-), 3.38 (m, 1H, -OC**H**(CH_3)CH_2-), 3.14 (t, 0.03H, HOCH(CH_3)C**H**$_2$- one of two non-equivalent), 1.12 (m, 3H, -OCH(C**H$_3$**)CH_2-), 0.15 (s, 0.03H, D3(Si-(C**H$_3$**)$_2$), 0.07 (m, 2.33H, -Si(C**H$_3$**)$_2$-). ^{13}C NMR ($CDCl_3$, 100 MHz, 298.0 K, ppm) δ = 75.64 - 75.23 (-O**C**H(CH_3)CH_2-), 73.95 - 72.96 (-OCH(CH_3)C**H$_2$**-), 67.40 – 65.82 (HO**C**H-), 18.38 - 17.48 (-OCH(**C**H_3)CH_2-), 1.14 (Si(**C**H_3)$_2$-O-C-), -0.10, -0.45, -0.89 (Si(CH_3)$_2$-O-**C**-). ^{29}Si NMR($CDCl_3$, 79.5 MHz, 298.0 K) δ = -8.29 (D3) , -13.54 (Si-O-C), -21.95 (PDMS). GPC (eluent: THF, standard: polystyrene): M_n = 6261 g/mol, PDI = 1.54.

PO/D3 Copolymerization in 250 g scale, 9.83 mol% CP10: In a 1 L stainless steel reactor, 41.7 g (20.85 mmol) of previously dried polypropylene glycol with a molar mass of 2000 g/mol, resublimed hexamethylcyclotrisiloxane (73.86 g, 332.00 mmol) and 75.11 mg of **DMC2** catalyst are pressurized with Argon three times to 3.0 bar to remove moisture and air and subsequently heated to 120 °C. Once the reaction temperature is reached, the Argon pressure is adjusted to 2.0 bar. With a mass flow of 4.17 g/min, 20.75 g (357.75 mmol) of propylene oxide are dosed into the reactor. After a significant pressure drop is observed the catalyst is activated and 94.0 g (1620.69 mmol) of propylene oxide are continuously dosed into the reactor at a mass flow of 0.417 g/min. Following the completion of dosing, the reaction is stirred at 120 °C over night to allow the full reaction of hexamethylcyclotrisiloxane. Subsequently, additional 20.0 g (344.83 mmol) of propylene oxide are does to the reactor at a mass flow of 0.417 g/min. Once the PO-dosage is completed, the reaction is allowed to stir at 120 °C for 1 h followed by removal of volatiles in vacuo at 80 °C. The product is obtained in form of an opaque liquid. ^{1}H NMR ($CDCl_3$, 400 MHz, 298.0 K, ppm) δ = 3.96 (m, 0.08 H, HOC**H**(CH_3)CH_2-), 3.54 (m, 2H, -OCH(CH_3)C**H$_2$**-), 3.38 (m, 1H, -OC**H**(CH_3)CH_2-), 3.14 (t, 0.02H, HOCH(CH_3)C**H**$_2$- one of two non-equivalent), 1.12 (m, 3H, -OCH(C**H$_3$**)CH_2-), 0.15 (s, 0.09H, D3(Si-(C**H$_3$**)$_2$), 0.08 (m, 2.00H, -Si(C**H$_3$**)$_2$-). ^{13}C NMR ($CDCl_3$, 100 MHz, 298.0 K, ppm) δ = 75.65 - 75.24 (-O**C**H(CH_3)CH_2-), 73.50 – 73.05 (-OCH(CH_3)C**H$_2$**-), 68.78 - 67.23 (HO**C**H-), 18.38 - 17.48 (-OCH(**C**H_3)CH_2-), 1.15 (Si(**C**H_3)$_2$-O-C-), -0.09, -0.43, -0.93 (Si(CH_3)$_2$-O-**C**-). ^{29}Si NMR($CDCl_3$, 79.5 MHz, 298.0 K) δ = -8.30 (D3) , -13.64 (Si-O-C), -19.01 (D4), -21.94 (PDMS). GPC (eluent: THF, standard: polystyrene): M_n = 8074 g/mol, PDI = 1.72.

Hydrolysis experiments on PPG/PDMS Copolymers: Approx. 2 g of copolymer, 0.5 ml of water and a drop of concentrated HCl are mixed in a round bottom flask that is open to atmosphere. The mixture is heated to 50 °C for 5 h and subsequently analyzed using ^{1}H, ^{13}C and ^{29}Si-NMR.

A-1.4.6 Copolymers of epoxides with cyclic esters

PPG-PLA.1: 1.5 mg of **DMC2** catalyst and 1.874 g (13 mmol) of *rac*-lactide are dried in vacuo for 1 h at 50 °C in a 100 ml stainless steel pressure reactor. Subsequently, the reactor is vented with argon and heated to 120 °C. Once the reaction temperature is reached, 7.550 g (130 mmol) of propylene oxide are dosed continuously to the reaction with a mass flow of 0.417 g/min. After the reaction is finished, indicated by a sharp temperature increase and pressure decrease, the mixture is allowed to stir at 120 °C for 1 h. Residual monomer is then removed in vacuo. (yield: 8.57 g, 91 %). ^{1}H NMR ($CDCl_3$, 300 MHz, 297.5 K, ppm) δ = 5.12-4.99 (m, 1H ,PLA C**H**), 4.68-4.57 (m, 0.01H, PPG-PLA -OCOC**H**(CH_3)CH_2-), 4.33-4.26 (m, 0.06H, PLA HOC**H**CH_3-) 4.04-3.99 (m, 0.26H, PPG-PLA -OCOCH(CH_3)C**H₂**-) 3.65-3.47 (m, 9.15H, -OCH(CH_3)C**H₂**-), 3.35-3.22 (m, 5.02H, -OCH(CH_3)C**H₂**-), 1.50-1.37 (m, 3H, PLA CH_3), 1.08-1.05 (m, 13.72H, -OCH(C**H₃**)CH_2-). ^{13}C NMR ($CDCl_3$, 75 MHz, 299.3 K, ppm) δ = 169.20, 167.27 (PLA **C**=O), 75.84-75.10 (-O**C**H(CH_3)CH_2-), 73.81-72.40 (-OCH(CH_3)C**H₂**-), 68.97 (PLA **C**H), 18.52-17.22 (-OCH(**C**H_3)CH_2-), 16.69, 15.74 (PLA, **C**H_3).

PPG-PLA.2: 1.71 mg of **DMC2** catalyst, 0.385 g (2.00 mmol) of tripropylene glycol, 1.874 g (13 mmol) of *rac*-lactide and 1.162 g (20 mmol) of propylene oxide are placed in a 5 ml reaction vial equipped with a magnetic stirrer. Subsequently, the vial is placed in a stainless steel pressure reactor, which is vented with argon and heated to 120 °C. After 15 h the reactor is cooled down in an ice bath. Residual monomer is afterwards removed in vacuo. (yield: 2.05 g, 60 %). ^{1}H NMR ($CDCl_3$, 300 MHz, 298.0 K, ppm) δ = 5.21- 4.98 (m, 1H ,PLA C**H**), 4.70-4.59 (m, 0.01H, PPG-PLA -OCOC**H**(CH_3)CH_2-), 4.37-4.17 (m, 0.31H, PLA HOC**H**CH_3-) 4.13-3.95 (m, 0.41H, PPG-PLA -OCOCH(CH_3)C**H₂**-) 3.79-3.44 (m, 1.45H, -OCH(CH_3)C**H₂**-), 3.40-3.18 (m, 1.20H, -OCH(CH_3)C**H₂**-), 1.56-1.34 (m, 3H, PLA CH_3), 1.20-1.07 (m, 2.79H, -OCH(C**H₃**)CH_2-). ^{13}C NMR ($CDCl_3$, 75 MHz, 298.6 K, ppm) δ = 174.97, 170.07, 169.22 (PLA **C**=O), 75.48-74.80 (-O**C**H(CH_3)CH_2-), 73.75-72.65 (-OCH(CH_3)C**H₂**-), 68.99, 66.45 (PLA **C**H), 20.41-17.27 (-OCH(**C**H_3)CH_2-), 16.72, 16.45 (PLA, **C**H_3).

PPCLA: For the terpolymerization of 0.581 g (10 mmol) of propylene oxide and 1.874 g (13 mmol) of *rac*-lactide are dissolved in 2 ml of THF in a 5 ml reaction vial equipped with a magnetic stirrer. Subsequently, 1.227 mg (500 ppm mass) of **DMC2** catalyst are added to the mixture, the vial is placed in a pressure reactor and the reactor is quenched three times with CO_2 to remove moisture and air. Afterwards, the reactor is pressurized to 20 bar CO_2 and heated to 120 °C. The reaction is stirred at 120 °C for 18 h, followed by cooling the reactor to 0 °C in an ice bath. The reactor is slowly depressurized, and volatiles are removed from the reaction mixture in vacuo in a separate flask. For purification, the sample was then dissolved in a minimal amount of $CHCl_3$, precipitated in the tenfold amount of cold methanol and dried in

vacuo. The product is obtained in form of a highly viscous clear liquid (yield: 2.22 g; 90 %). **^{1}H NMR** ($CDCl_3$, 400 MHz, 297.0 K, ppm) δ = 5.26-5.12 (m, 1H, PLA-C**H**) 4.91-4.85 (m, 0.04H. PPC-PLA -OCOC**H**(CH_3)CH_2-), 4.40-4.33 (m, 0.12H, cyclic propylene carbonate), 4.26-4.04 (m, 0.11 H, PPC-PLA -OCOCH(CH_3)C**H$_2$**-), 3.68- 3.50 (m, -OCH(CH_3)C**H$_2$**-), 3.41-3.39 (m, -OC**H**(CH_3)CH_2), 1.76-1.44 (m, 3H, PLA-C**H$_3$**), 1.33-1.12 (m, -OCH(C**H$_3$**)CH_2-).

PPCCL: For the terpolymerization 0.581 g (10 mmol) of propylene oxide and 1.484 g (13 mmol) of ε-caprolactone are dissolved in 2 ml of THF in a 5 ml reaction vial equipped with a magnetic stirrer. Subsequently, 1.0323 mg (500 ppm mass) of **DMC2** catalyst are added to the mixture, the vial is placed in a pressure reactor and the reactor is quenched three times with CO_2 to remove moisture and air. Afterwards, the reactor is pressurized to 20 bar CO_2 and heated to 120 °C. The reaction is stirred at 120 °C for 18 h, followed by cooling the reactor to 0 °C in an ice bath. The reactor is slowly depressurized, and volatiles are removed from the reaction mixture in vacuo in a separate flask. For purification, the sample was then dissolved in a minimal amount of $CHCl_3$, precipitated in the tenfold amount of cold methanol and dried in vacuo. The product is obtained in form of a highly viscous yellow liquid (yield: 0.119 g; 6 %). ^{1}H NMR ($CDCl_3$, 400 MHz, 297.0 K, ppm) δ = 5.04-4.84 (m, 0.2H, PPC-PCL -OCOC**H**(CH_3)CH_2-), 4.33-4.30 (m, 0.02H, cyclic propylene carbonate), 4.24-4.21 (m, 0.26 H, C**H$_2$**O, ε-caprolactone monomer), 4.07-4.04 (m, 1.32H, PCL -C**H$_2$**OCO-), 3.66-3.55 (m, 2H, -OCH(CH_3)C**H$_2$**-), 3.41 (m, 1H, -OC**H**(CH_3)CH_2), 2.65- 2.62 (m, 0.24H, C**H$_2$**CO, ε-caprolactone monomer), 2.32-2.28 (m, 1.44H, PCL -C**H$_2$**COO-), 1.92-1.87 (m, 0.94H, ε-caprolactone monomer), 1.77-1.76, 1.69-1.60 (m, 3.27H, PCL -$COCH_2C$**H$_2$**CH_2C**H$_2$**CH_2O-), 1.42-1.36 (m, 1.5H PCL -$COCH_2CH_2C$**H$_2$**CH_2CH_2O-), 1.28-1.13 (m, 3.13H, -OCH(C**H$_3$**)CH_2-). ^{13}C NMR ($CDCl_3$, 100 MHz, 297.2 K, ppm) δ = 173.72 (PCL **C**=O), 75.46 (-O**C**H(CH_3)CH_2-), 73.91 (-OCH(CH_3)C**H$_2$**-), 69.85 (HO**C**H-), 64.30 (-$COCH_2CH_2CH_2CH_2C$**H**$_2$O-), 34.72, 34.26 (-**C**$OCH_2CH_2CH_2CH_2CH_2O$-), 29.44, 29.17, 28.49 (-$COCH_2CH_2CH_2C$**H**$_2CH_2O$-), 25.67 (-$COCH_2CH_2C$**H**$_2CH_2CH_2O$-), 24.27 (-$COCH_2C$**H**$_2CH_2CH_2CH_2O$-), 23.08, 17.60 (-OCH(**C**H_3)CH_2-).

PCHCLA: 0.982 g (10 mmol) of cyclohexene oxide and 1.874 g (13 mmol) of *rac*-lactide are dissolved in 2 ml of THF in a 5 ml reaction vial equipped with a magnetic stirrer. Subsequently, 1.4276 mg (500 ppm mass) of **DMC2** catalyst are added to the mixture, the reaction is conducted similar to the preparation of PPCLA. ^{1}H NMR ($CDCl_3$, 300 MHz, 299.5 K, ppm) δ = 5.25-5.16 (m, 1H, PLA-C**H**), 4.90-4.60 (m, PCHC-PLA -OCOC**H**(CH_3)CH_2-), 4.35 (m, cyclic cyclohexene carbonate), 3.37 (PCHC -C**H**OC**H**- ether bond), 2.08, 1.69 (m, cyclohexene ring C**H$_2$**), 1.57 (m, 3H, PLA-C**H$_3$**), 1.47, 1.35 (m, cyclohexene ring C**H$_2$**).

PCHCCL: 0.982 g (10 mmol) of cyclohexene oxide and 1.484 g (13 mmol) of ε-caprolactone are dissolved in 2 ml of THF in a 5 ml reaction vial equipped with a magnetic stirrer. Subsequently, 1.2326 mg (500 ppm mass) of **DMC2** catalyst are added to the mixture, the reaction is conducted similar to the preparation of PPCCL. **^{1}H NMR** ($CDCl_3$, 300 MHz, 299.5 K, ppm) δ = 4.79, 4.65 (m, 1.03H, PCHC-PCL -OCOC**H**(CH_3)CH_2-), 4.23- 4.21 (m, 0.26 H, C**H$_2$**O, ε-caprolactone monomer), 4.07-4.04 (m, 2H, PCL -C**H$_2$**OCO-), 3.56- 3.38 (m, 0.49H, PCHC -C**H**OC**H**- ether bond), 2.65-2.62 (m, 0.24H, C**H$_2$**CO, ε-caprolactone monomer), 2.32-2.28 (m, 2H, PCL -C**H$_2$**COO-), 2.10-2.03 (m, 1.84H, cyclohexene ring C**H$_2$**), 1.87 (m, 0.54H, ε-caprolactone monomer), 1.66-1.60 (m, 6H, PCL -$COCH_2$C**H$_2$**C**H$_2$**C**H$_2$**CH_2O-), 1.41-1.33 (m, 4.5H, cyclohexene ring C**H$_2$**). **^{13}C NMR** ($CDCl_3$, 100 MHz, 297.3 K, ppm) δ = 182.30 (PCHC **C**=O), 173.70 (PCL **C**=O), 69.45 (HO**C**H-), 64.29 (-$COCH_2CH_2CH_2CH_2$**C**H_2O-), 34.72, 34.26 (-**C**$OCH_2CH_2CH_2CH_2CH_2O$-), 32.49 (-$COCH_2CH_2CH_2$**C**H_2CH_2O-), 29.44, 29.14, 28.48 (-$COCH_2CH_2CH_2$**C**H_2CH_2O-), 25.67, 25.43 (-$COCH_2CH_2$**C**$H_2CH_2CH_2O$-), 24.71 (-$COCH_2$**C**$H_2CH_2CH_2CH_2O$-), 23.07(-OCH(**C**H_3)CH_2-).

A-1.5 DMC-inspired molecular catalysis

A-1.5.1 Complexes

L_{NN}1:

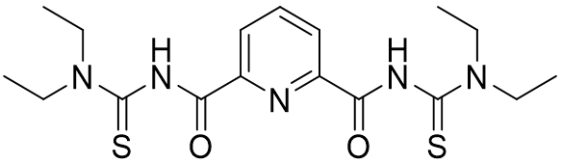

The Ligand LNN1 was prepared following a procedure by Pham *et al.*[4] Vacuum-dried pyridine-2,6-dicarboxylic acid (1.18 g, 25.0 mmol) is added to 8.5 ml thionyl chloride (13.67 g, 114.97 mmol) in a flame dried round bottomed flask and stirred under reflux for 8 h. Subsequently, the mixture is cooled to room temperature and evaporated to dryness in vacuum. 4.95 g (24.24 mmol) of the resulting pyridine-2,6-dicarboxylic acid chloride are dissolved in 65 ml of dry THF and added dropwise to 6.517 g (49.27 mmol) of N,N-diethylthiourea (prepared as described by Yokoyama *et al.*[5]) in 65 ml of dry THF at 0 °C. After the two solutions are combined, the reaction mixture is stirred for 1 h at 40 °C. After cooling to room temperature, the mixture is filtrated followed by the filtrate being evaporated to dryness to yield L_{NN}1. The product is then recrystallized from a CH_2Cl_2/EtOH (2:1) mixture at 50 °C. **Elemental Analysis** (%w, found (calc. for $C_{17}H_{25}N_5O_2S_2$)): C, 51.63 (51.62); H, 6.37 (6.37); N, 17.11 (17.71); S, 16.56 (16.21). **^{1}H NMR** (CD_2Cl_2, 300 MHz, 298.0 K, ppm): δ 9.85 (2H, s, NH), 8.40 (2H, d, Py), 8.13 (1H, t, Py), 4.02 (4H, m, C**H$_2$**CH_3), 3.68 (4H, m, C**H$_2$**CH_3), 1.34 (12H, m, CH_2C**H$_3$**). **IR** (ATR, cm^{-1}): 3262 (m), 2973 (w), 2932 (w), 1672 (s), 1513 (s), 1414 (vs), 1274 (m), 1222 (s), 1099 (m), 752 (m).

Complex **1:**

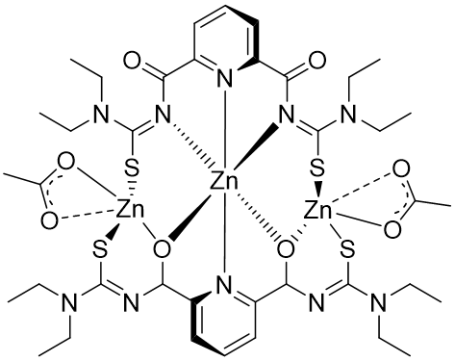

A solution of 263.41 mg (1.20 mmol) of zinc acetate in 5 ml of methanol is added to 237.32 mg (0.60 mmol) of LNN1 suspended in 5 ml of methanol at room temperature. After mixing for 5 min, three drops of triethylamine are added to the mixture, which is subsequently heated to reflux temperature for 60 min. The resulting reaction mixture is cooled to room temperature and concentrated by rotary evaporation. The concentrated solution is left unstirred for the product to precipitate. The precipitate is washed with methanol and dried in vacuum (0.1519 g, 0.14 mmol, 35 %). Elemental Analysis (%w, found (calc. for C17H25N5O2S2)): C, 41.34 (41.22); H, 4.84 (5.28); N, 12.05 (12.03); S, 13.07 (11.58); Zn, 16.76 (17.71). 1H NMR (CD2Cl2, 300 MHz, 298.0 K, ppm): δ 8.59 (2H, s, Py), 8.34 - 8.24 (4H, m, Py), 3.91 (8H, m, CH2CH3) 3.39 (8H, m, CH2CH3), 1.87 - 0.68 (30H, m, CH3). IR (ATR, cm-1): 3267 (w), 2975 (w), 1673 (m), 1588 (m), 1516 (m), 1393 (vs), 666 (s). MS (ESI, m/z (M calculated: 1108.11)): 1095.02 [M+Na+ (-OAc ligands exchanged with -COO)]; 1027.04 [(Zn2LNN12)+Na+ (-OAc ligands exchanged with -COO)], 941.10 [(Zn1LNN12)+Na+].

Complex **2**:

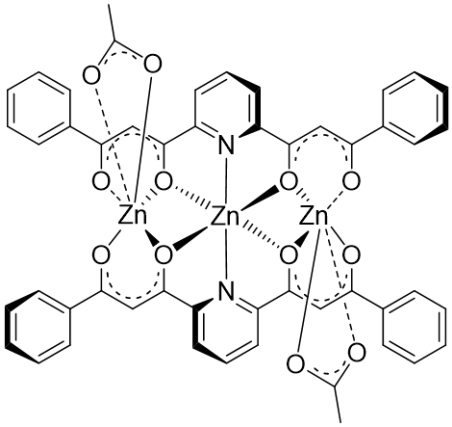

To a suspension of 0.1026 g (0.26 mmol) of $\mathbf{L_{NN}2}$ ligand in 10 ml of methanol a solution of 0.1084 g (0.52 mmol) of $ZnCl_2$ in 10 ml of methanol is added at room temperature whilst stirring. After the mixture stirred for 5 min, three drops of triethylamine are added to the solution and the solvation of all components followed by the precipitation of the chlorinated complex can be observed. Subsequently, the chlorine is exchanged with acetate groups by addition of acetic acid to the solution. The resulting solid is washed with methanol three times and dried in vacuo (0.141 g, 0.134 mmol, 77 %). (ATR, cm^{-1}): 1563 (s), 1516 (s) 1459 (vs), 1298 (m), 1263 (s), 761 (s), 516 (s). EA (%w, found (calc. for $C_{50}H_{42}N_2O_{12}Zn_3$): C, 47.47 (56.71); H, 2.95 (4.00); N, 0.55 (2.65); Zn, 19.06 (18.52).

Complex **3**:

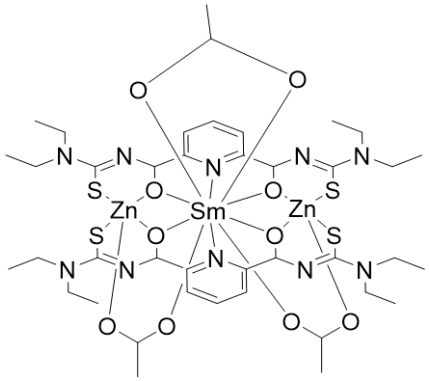

In a round bottom flask, 0.1883 g (0.48 mmol) of $\mathbf{L_{NN}1}$ are added to a solution of 0.1045 g (0.476 mmol) of zinc acetate and 0.0886 g (0.238 mmol) of $SmCl_3$ in 15 ml of methanol. After stirring for 5 min at room temperature six drops of triethylamine are added to the solution. After a precipitate has formed the supernatant is removed via filtration and the precipitate is washed three times with 3 ml of methanol. The resulting complex **3** is then dried in vacuum (0.2755 g, 0.22 mmol, 93 %). **Elemental Analysis** (%w, found (calc. for $C_{40}H_{55}N_{10}O_{10}S_4SmZn_2$)): C, 32.41 (38.36); H, 3.42 (4.99); N, 11.63 (11.18); S, 10.93 (10.24); Sm, 10.79 (12.01); Zn, 9.91 (10.44). **^{1}H NMR** (CD_2Cl_2, 300 MHz, 298.0 K, ppm): δ = 8.94 (4H, d, Py), 8.59 (2H, t, Py), 3.76 (16H, m, C**H_2**CH_3), 1.32 (6H, m, OAc), 1.18 (24H, m, CH_2C**H_3**). **IR** (ATR, cm^{-1}): 2972 (w), 2931 (w), 1580 (m), 1541 (m), 1504 (s), 1424 (s), 1388 (s), 1276 (m), 1252 (m), 1150 (m), 1071 (m), 753 (vs), 669 (w). **MS** (ESI, m/z (M calculated: 1252.13)): 1158 [M^+ (-OAc ligands exchanged with -COO]; 1461 [$(SmZn_2L_{NN}1_3)^+$].

A-1.5.2 Polymerizations

General CHO/CO_2 copolymerization procedure: The desired amount of catalyst is suspended in 1-2 ml of CH_2Cl_2 followed by the addition of the respective amount of CHO. The mixture is placed in a stainless-steel pressure reactor with subsequent quenching of the reactor with CO_2. Then the reactor is pressurized to 20 bar CO_2 and heated to 80 °C. After 24 h of magnetic stirring at the desired temperature the reactor is cooled down in an ice bath and vented. The reaction mixture is transferred into a flask and quenched with two drops of concentrated HCl. The resulting polymer is precipitated in tenfold the volume of the reaction mixture of diethyl ether or cold methanol, which is then decanted, and the polymer is dried in vacuum.

Optimized CHO/CO_2 Copolymerization procedure using complex 3: 39.7 mg (0.032 mmol) of complex **3** are suspended in 1 ml of CH_2Cl_2 followed by the addition of 65.4 µL (0.063 g, 0.64 mmol) CHO. The mixture is placed in a stainless-steel pressure reactor with subsequent quenching of the reactor with CO_2. Then the reactor is pressurized to 20 bar CO_2 and heated to 80 °C. After 24 h of magnetic stirring at the desired temperature the reactor is cooled down in an ice bath and vented. The reaction mixture is transferred into a flask and quenched with two drops of concentrated HCl. The resulting polymer is precipitated in 10 ml diethyl ether, which is then decanted, and the polymer is dried in vacuum (0.06 g, 40 %). **^{1}H NMR** before

workup (CD_2Cl_2, 300 MHz, 298.0 K, ppm): δ 5.28 (solvent, CH_2Cl_2), 4.65 (0.13H, m, C**H** carbonate bond), 3.75-3.43 (1.28H, m, C**H** ether bond), 3.09 (2H, s, C**H** CHO monomer), 1.96-1.14 (14.32H, m, C**H_2** CHO monomer & polymer).

General homopolymerization procedure for *rac*-lactide: The desired amount of catalyst and *rac*-lactide are added to a 5 ml flame-dried Schlenk-finger equipped with a magnetic stirrer in an argon stream. The flask is heated to 140 °C and stirred for 24 h or until stirring ceases. Subsequently, the reaction mixture is cooled down and dissolved in the minimal amount of $CHCl_3$ and then precipitated in the tenfold volume of cold methanol. This step has to be repeated if the PLA polymer is still containing impurities. The resulting polymer is dried in vacuum at 100 °C. For monitoring of the reaction process a sample for NMR and GPC analysis was taken every hour under an argon counterflow.

Exemplary Analysis of a PLA polymer (prepared using complex **1**): **^{1}H NMR** ($CDCl_3$, 300 MHz, 298.0 K, ppm): δ = 5.29-5.08 (1H, m, C**H**), 1.58-1.10 (3H, m, C**H_3**). **^{13}C NMR** ($CDCl_3$, 75 MHz, 298.0 K, ppm) δ = 169.48 (**C**=O), 69.53 – 69.11 (**C**H), 16.86, 16.76 (**C**H_3). Mn (GPC, standard: polystyrene, eluent: THF, Mark-Houwink corrected, (PDI)): 15741 g/mol, 1.24.

A-2 Appendix Chapter 4.1

A-2.1 Assessment of catalytic activity of a DMC catalyst

Induction test (A-Test)	Small scale test designed to evaluate if the catalyst shows any activity. Can be used to estimate if the catalyst can produce a high quality product in bigger scale.
Procedure	27.0 g of polypropylene glycol (diol, 2,000 g/mol) and 0.015 g of DMC catalyst are charged in a 100 ml stirred pressure reactor. The mixture is stirred for 1 hour at 105 ° C and reduced pressure (<10 mbar) to remove aqueous contaminants. Subsequently, the reactor is vented with Argon and heated to 120 °C. After reaching this temperature, propylene oxide (0.1 mol, 5.8 g, 7.0 ml) is added in one portion. An increase of temperature and a pressure drop indicate that the catalyst is active.
Test evaluation	The catalyst is most likely of good activity, when $t_{induction} \leq$ 15 min and $\vartheta_{max} \geq$ 150 °C.
Product analysis	GPC (evaluation if all polymer chains changed in length, indicated by no shoulders or tailing of the GPC signal and PDI ≤ 1.5)
12000 g/mol PPG test (Sample)	Big scale test (500 g) with continuous dosage of PO to evaluate if the catalyst can produce high quality products and is active for the whole reaction process.
Procedure	70 g of polypropylene glycol (Diol, 2000 g/mol) and the desired amount of DMC catalyst (0.015 g for DMC 1.0 & 0.030 g for DMC 2.0) are charged in a 1 L stirred pressure reactor. The mixture is stirred for 1 hour at 105 ° C and reduced pressure (<10 mbar) to remove aqueous contaminants. Subsequently, the reactor is vented with Argon and heated to 120 °C. After reaching this temperature and an initial pressure of 0.2 bar, 10 g propylene oxide (PO) are dosed into the reactor at a high mass flow rate of 4.167 g/min. Promptly, the pressure inside the reactor increases. Once the pressure decreases to the initial pressure of 0.2 bar, the induction reaction took place and further propylene oxide can be added (typically after 30-60 min). The remainder of the propylene oxide (420 g) is added continuously at a low mass flow rate over 17 h (0.4167 g/min). After addition of all the propylene oxide and a 1 hour post-reaction period at 120° C, volatile components are removed in vacuo at 90° C.
Test evaluation	The pressure increase over time is followed hourly to ensure that the catalyst is still active. If the pressure increases above 10 bar, the dosage of PO is stopped, and the polymerization test was not successful.
Product analysis	GPC (PDI ≤ 1.5), Unsaturation (NMR)

The results of the activity assessment of the studied DMC catalysts are shown in Table A 3.

Table A 3: Assessment of catalytic activity of the regarded DMC catalysts.

DMC catalyst	Parameter						activity
	32 g scale			500 g scale		in operando FTIR	
	t_{ind} [min]	ϑ_{max} [°C]	PDI []	$M_{n,obs}=M_{n,calc}$	PDI []	k_{prop}	
DMC0	no induction	n.d.	n.d.	n.d.	n.d.	n.d.	**no activity**
DMC1	10	159	1.11	yes	1.27		**medium**
DMC2	6	163	1.09	yes	1.22		**high**
DMC3	9	161	1.16	n.d.	n.d.	-	**medium**
DMC4	9	131	1.18	n.d.	n.d.	-	**medium**
DMC5	18	122	1.22	n.d.	n.d.	-	**low**
DMC6	19	155	1.14	n.d.	n.d.	-	**low**
DMC7	no induction	n.d.	n.d.	n.d.	n.d.	-	**no activity**
DMC8	70	120	n.a.*	n.d.	n.d.		**no activity**
DMC9	3	132	1.18	yes	1.26	-	**high**

*not applicable due to very low PO conversion

classification	medium weighting	high weighting
no activity		
low to medium activity		
high activity		

A-2.2 Elemental Analysis of DMC catalysts

Table A 4: Elemental Analysis and ligand analysis of DMC catalysts.

sample	Elemental Analysis /wt%							tert-butanol /wt%	2-octyldodecan-1-ol /wt%
	C	H	N	K	Cl	Zn	Co		
DMC0	16.05	3.074	19.55	0.232	0.352	24.308	13.815	-	-
DMC1	23.05	2.666	18.53	0.2666	6.354	28.398	12.09	10.65	-
DMC2	25.27	2.745	19.32	0.3077	5.768	27.443	12.483	8.41	0.49
DMC3	24.16	2.706	18.93	0.2872	6.061	27.921	12.287	0.31	-
DMC4	19.07	2.709	15.43	0.3951	6.282	27.075	11.855	-	-
DMC5	53.32	9.087	0.47	0.2437	0.430	2.298	0.420	-	-
DMC6	25.00	2.922	16.71	0.3563	5.181	27.255	11.590	-	-
	C	H	N	K	Cl	Zn	Fe		
DMC7	18.86	2.236	18.03	1.5755	2.113	31.250	16.690	11.94	-
DMC8	17.66	2.070	20.38	0.6945	0.824	31.605	16.555	-	-

A-2.3 SR-PXRD spectra

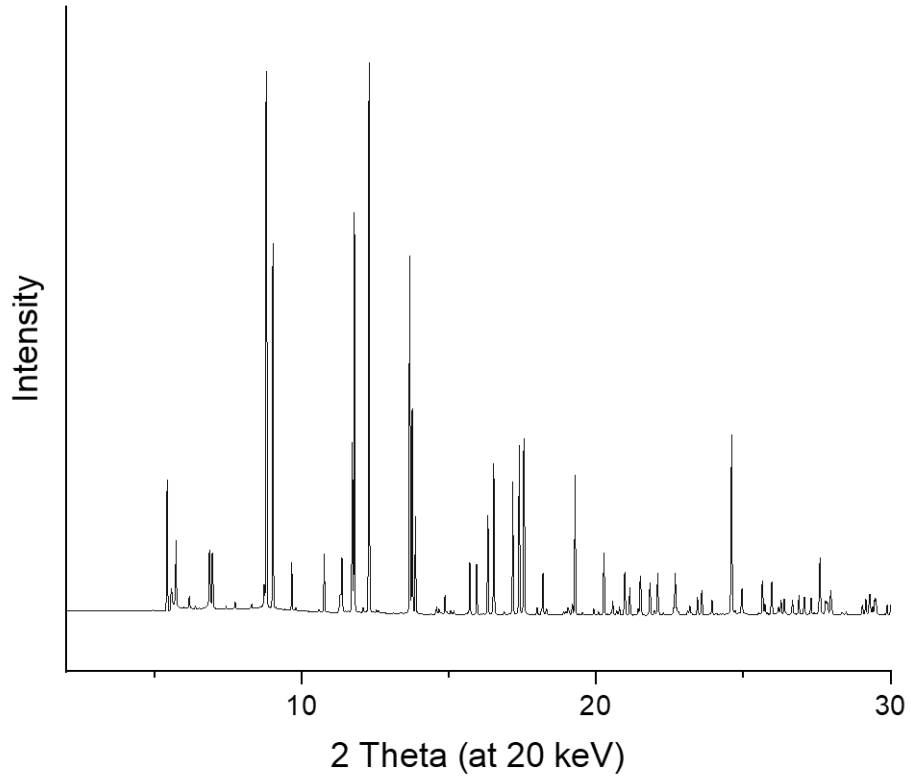

Figure A 2: PXRD spectra of a mixture of $K_3[Co(CN)_6]$ and *tert*-butanol.

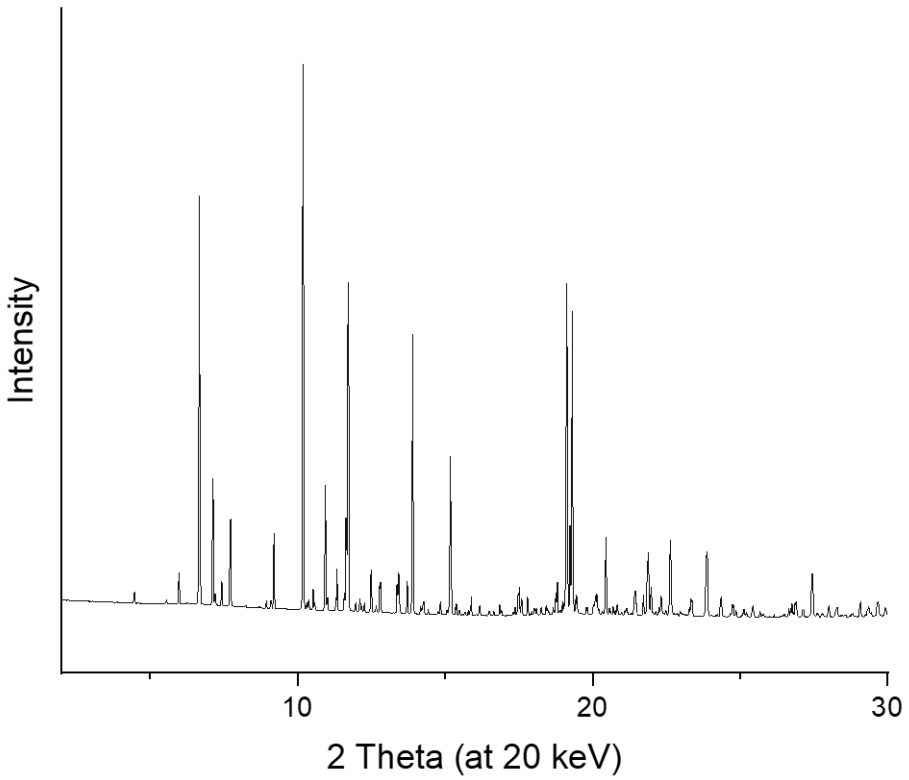

Figure A 3: PXRD spectra of a mixture of $ZnCl_2$ and *tert*-butanol.

A-2.4 EDX spectra

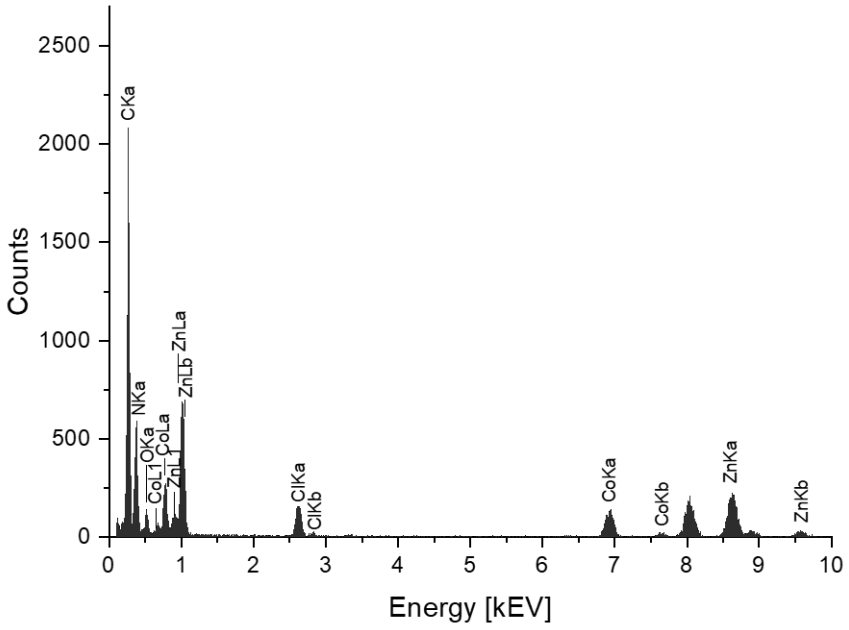

Figure A 4: EDX spectrum of **DMC1**.

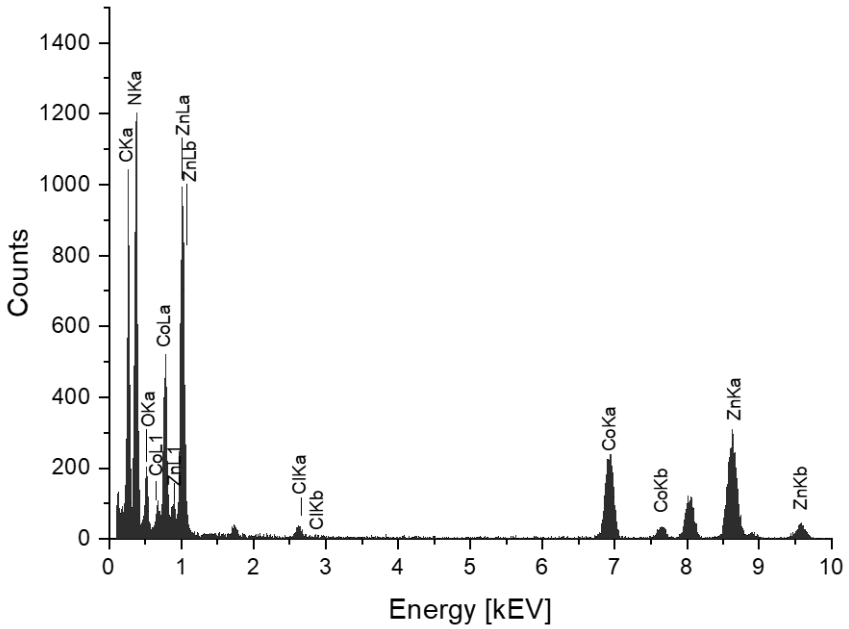

Figure A 5: EDX spectrum of **DMC2**.

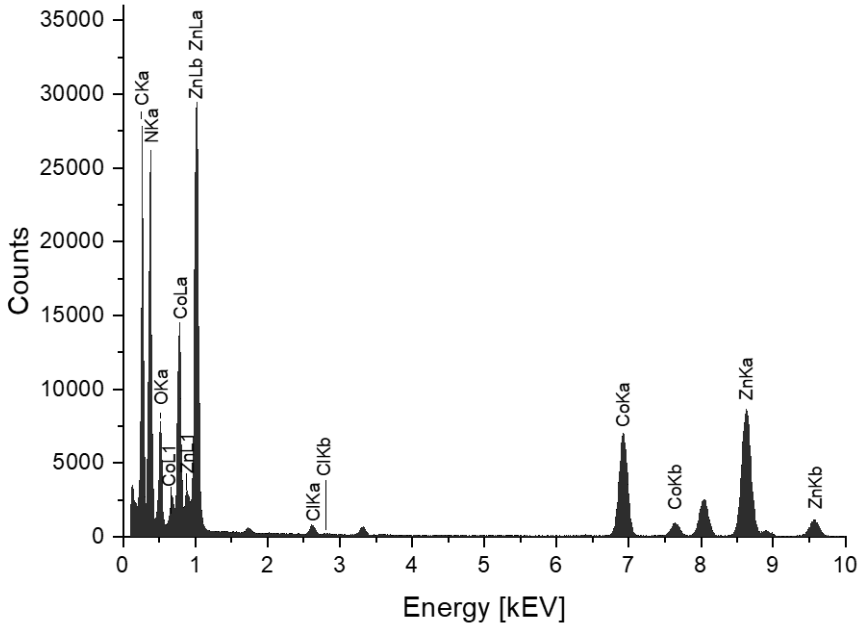

Figure A 6: EDX spectrum of **DMC3**.

A-2.5 XPS spectra

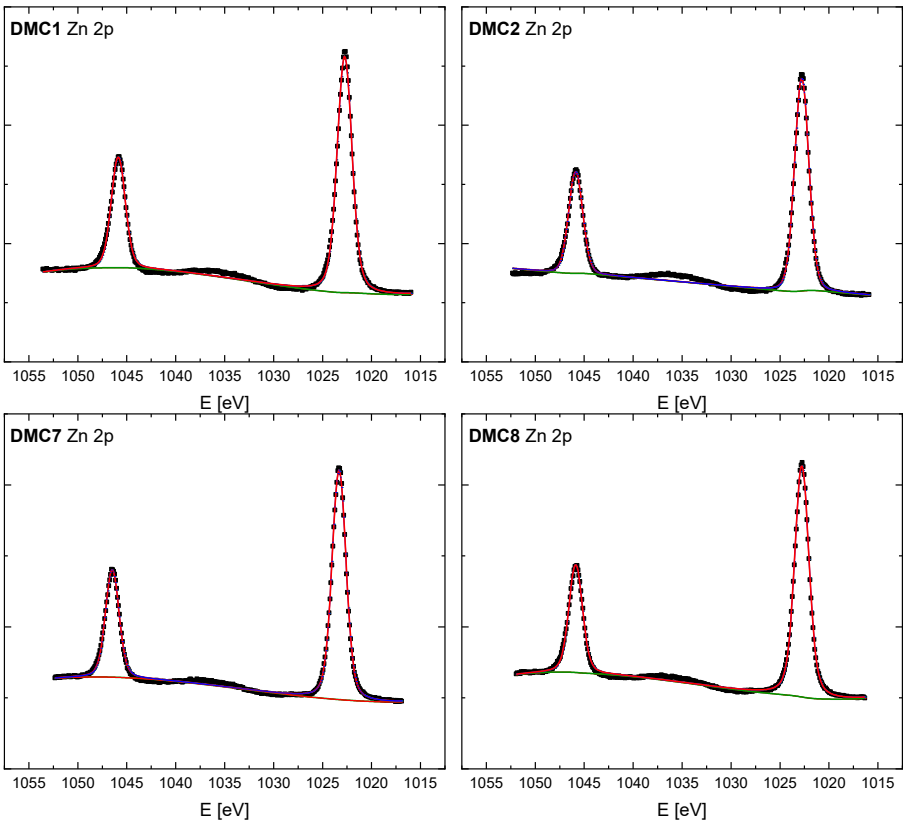

Figure A 7: Deconvoluted Zn 2p XPS spectra recorded on **DMC1**, **DMC2**, **DMC7** and **DMC8** catalyst.

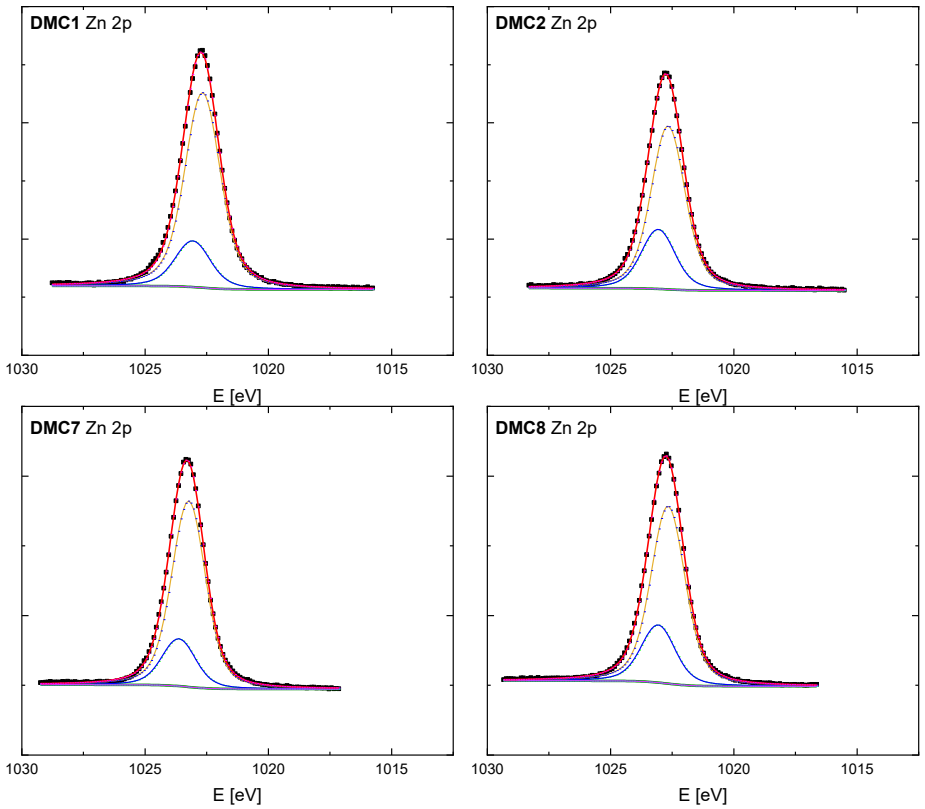

Figure A 8: Deconvoluted Zn 2p XPS spectra (one of the two duplets) recorded on **DMC1**, **DMC2**, **DMC7** and **DMC8** catalyst.

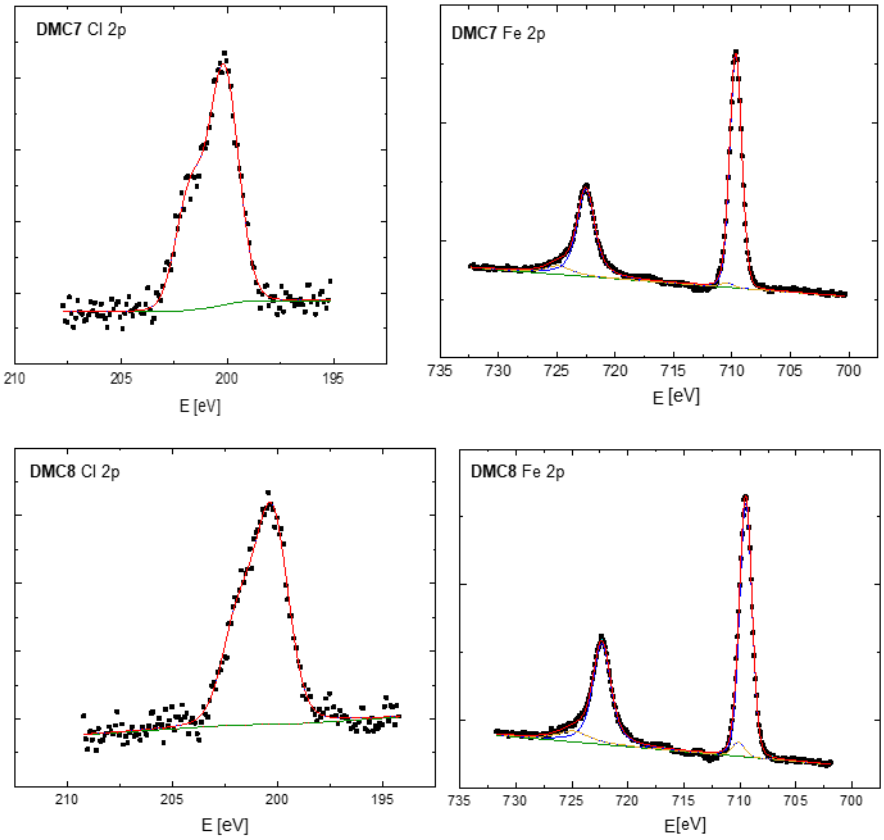

Figure A 9: Deconvoluted Cl 2p and deconvoluted Fe 2p XPS spectra of **DMC7** and **DMC8** catalyst.

A-2.6 Theoretical Calculations

Theoretical calculations were performed using the Adsorption Locator and DMol^3 modules of the Software Materials Studio 2018 by the company Biovia.

The internal atomic coordinates of the DMC catalysts were used as published by Wojdeł *et al.*[6] to construct the unit cell. To refine this unit cell and build a periodic supercell the DMol^3 module was used. Geometric optimization was done with the gradient corrected PW91 functional.[7] The conversion threshold for energy change was set to $1*10^{-5}$ Hartree, the maximum force to 0.002 Ha*Å^{-1} and the maximum displacement to 0.005 Å between the optimization cycles. A maximum number of 50 optimization cycles was chosen at a maximum step size of 0.3 Å. Symmetry information was used in the calculation. The precision in the numerical integration of the Hamiltonian, the threshold used to determine whether an SCF has converged, and the number of integration points used to integrate the wavefunction in reciprocal space was set to “fine”. All electrons were included in the calculation.

This was then followed with forming a slab by cutting the supercell along the [001] surface to obtain an exposed layer of Zn centers with constant distances to a 10 Å vacuum. Two Cl atoms were added to each side of the slab to quench the electrostatic dipole that would otherwise

occur alongside it. The obtained structure is subsequently subjected to another geometry optimization to ensure obtaining a realistic model.

The adsorption of the molecules on the surface was estimated using the Adsorption Locator module to find low energy adsorption sites by carrying out Monte Carlo searches of the configurational space of the substrate-adsorbate system with simultaneous slow decrease of the temperature. In this way the adsorbent-adsorbate combinations were defined that were later refined with the DMol^3 module using the above described parameters.

A-2.7 Ex operando activation of DMC2

290 mg of **DMC2** are placed in a Schlenk-flask and heated to 165 °C under vacuum (p<0.01 mbar) for 5 h. Subsequently, the flask is left to cool to room temperature under vacuum. This is followed by connecting a second Schlenk flask filled with 10 ml (8.3 g; 143 mmol) of dried PO and opening it to vent the DMC-containing flask with gaseous PO. ^{1}H NMR ($CDCl_3$, 400 MHz, 297.0 K, ppm) δ = 1.11 (m, 3H, C**H$_3$**, PPG), 1.29 (d, C**H$_3$**, PO), 2.4 + 2.72 (m, C**H$_2$**, PO), 2.96 (m, C**H**, PO), 3.36 (m, 1H, C**H**, PPG), 3.53 (m, 2H, C**H$_2$**, PPG).

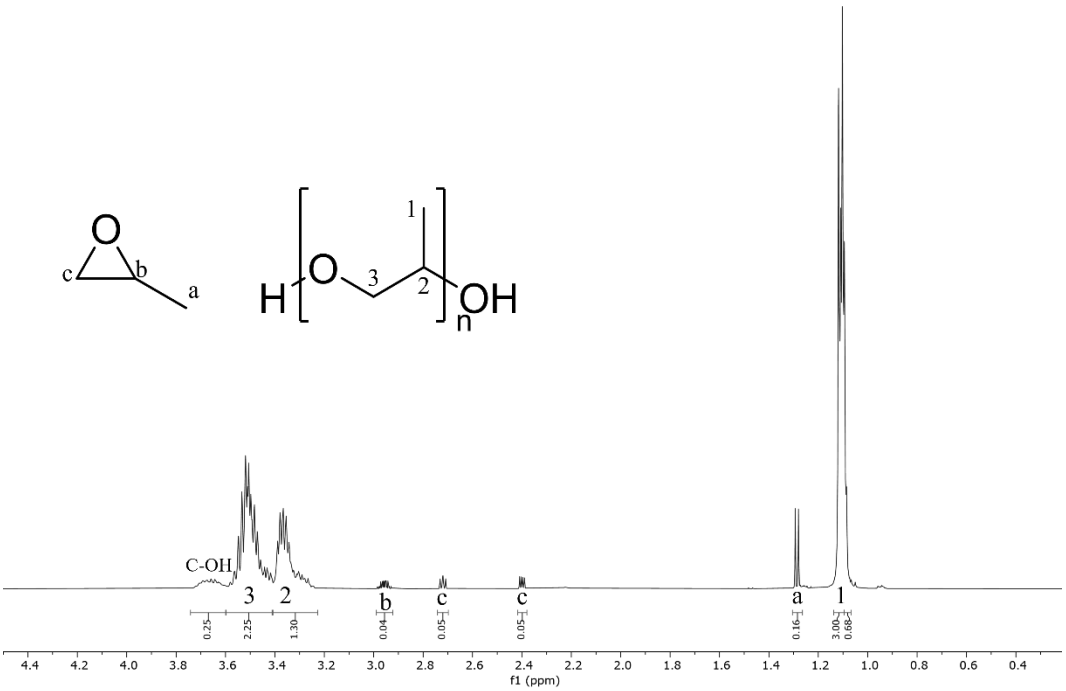

Figure A 10: ^{1}H NMR spectrum of the ex-operando activation product using **DMC2** ($CDCl_3$, 297.0 K, 400 MHz).

A-2.8 MALDI-MS: list of signals

Table A 5: Signals recorded in MALDI-MS of a polypropylene glycol prepared using DMC2.

m/z	Intensity [a.u.]	Polymer	m/z	Intensity [a.u.]	Polymer
371.216	4012		520.993	1962	
373.234	1937		523.242	1910	
414.048	2884		524.011	4119	
416.064	9477		524.995	5374	
429.24	3699	HO-(PPG)-O*t*Bu	525.966	3990	
431.042	3175		526.977	5462	
432.054	17316		530.986	2401	
434.057	2671		538.002	2562	
443.046	2121		540.006	2066	
445.051	1936		543.973	2274	
446.055	2408		545.302	3143	HO-(PPG)-O*t*Bu
447.057	13563		552.638	2120	
448.059	11743		603.346	2740	HO-(PPG)-O*t*Bu
449.048	18156		645.388	2030	HO-(PPG)-$OCH_2CH{=}CH_2$
450.063	77228		661.385	2314	HO-(PPG)-O*t*Bu
451.075	24913		703.427	2946	HO-(PPG)-$OCH_2CH{=}CH_2$
453.063	2429		719.412	2150	HO-(PPG)-O*t*Bu
454.056	2355		720.137	1990	
455.058	4870		721.148	3587	HO-(PPG)-OH
456.064	9866		761.466	4062	HO-(PPG)-$OCH_2CH{=}CH_2$
457.074	10655		777.452	2217	HO-(PPG)-O*t*Bu
459.089	4806		819.505	5585	HO-(PPG)-$OCH_2CH{=}CH_2$
461.058	2557		877.544	6550	HO-(PPG)-$OCH_2CH{=}CH_2$
462.064	4798		935.588	7302	HO-(PPG)-$OCH_2CH{=}CH_2$
463.059	14062		993.626	7123	HO-(PPG)-$OCH_2CH{=}CH_2$
465.102	10879		1051.666	6360	HO-(PPG)-$OCH_2CH{=}CH_2$
468.078	6812		1109.71	5231	HO-(PPG)-$OCH_2CH{=}CH_2$
469.093	10371		1167.749	4347	HO-(PPG)-$OCH_2CH{=}CH_2$
470.099	55705		1225.79	3647	HO-(PPG)-$OCH_2CH{=}CH_2$
471.104	166019		1283.837	2678	HO-(PPG)-$OCH_2CH{=}CH_2$
474.072	3291		1882.261	3650	HO-(PPG)-OH
475.076	2123		1940.304	6186	HO-(PPG)-OH
476.091	4155		1998.347	9772	HO-(PPG)-OH
477.058	15253		2056.389	14300	HO-(PPG)-OH
478.041	7136		2114.434	19420	HO-(PPG)-OH
479.054	4602		2172.478	24174	HO-(PPG)-OH
481.066	1918		2230.522	27893	HO-(PPG)-OH
482.093	5751		2288.565	30649	HO-(PPG)-OH
483.099	13623		2346.609	31740	HO-(PPG)-OH
487.27	3458	HO-(PPG)-O*t*Bu	2404.653	31166	HO-(PPG)-OH
491.033	2227		2462.697	29201	HO-(PPG)-OH
492.023	2076		2520.74	26535	HO-(PPG)-OH
493.036	2868		2578.783	23158	HO-(PPG)-OH
494.039	2020		2636.824	19653	HO-(PPG)-OH
495.039	2718		2694.867	15819	HO-(PPG)-OH
497.023	5202		2752.908	12611	HO-(PPG)-OH
503.988	7868		2810.95	9773	HO-(PPG)-OH

504.975	16655		2868.988	7544	HO-(PPG)-OH
505.982	194875		2927.029	5732	HO-(PPG)-OH
506.993	83369		2985.068	4335	HO-(PPG)-OH
509.019	7343		3043.108	3217	HO-(PPG)-OH
510.989	7370		3101.141	2508	HO-(PPG)-OH
511.986	14995		3159.179	1975	HO-(PPG)-OH
512.993	16772		3217.21	1609	HO-(PPG)-OH
516.996	2164		3275.252	1271	HO-(PPG)-OH
517.994	2616		3333.287	1048	HO-(PPG)-OH
519.003	2500		3391.325	920	HO-(PPG)-OH

A-2.9 ^{13}C NMR PPG microstructure determination

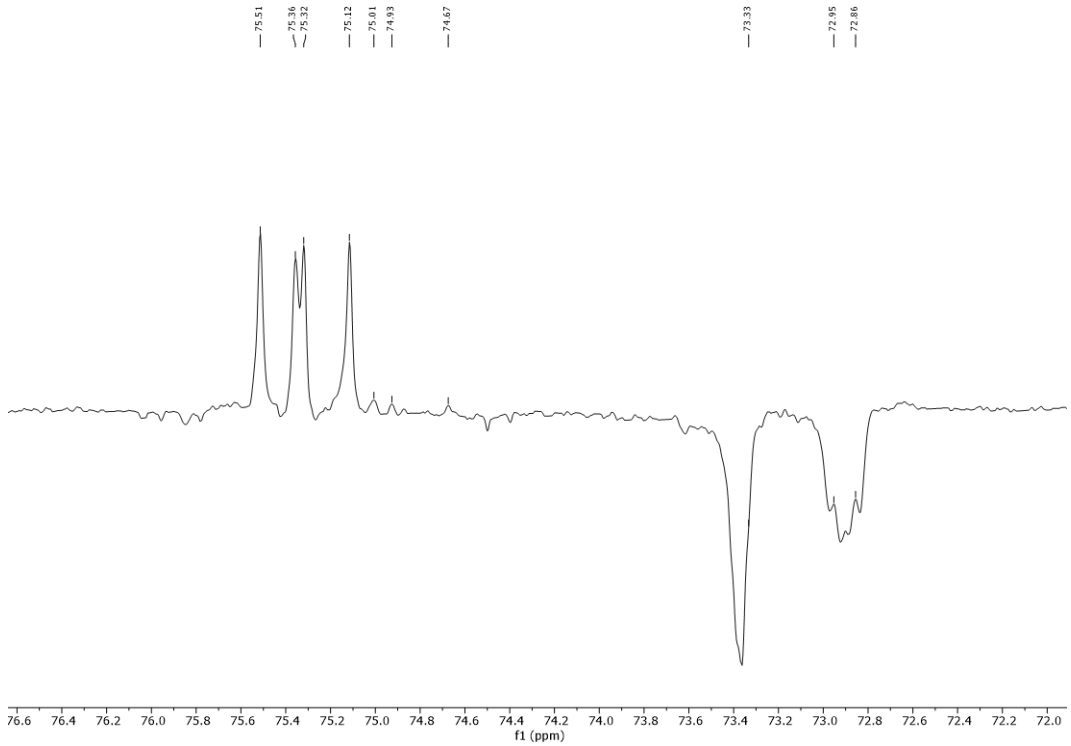

Figure A 11: ^{13}C NMR DEPT spectrum of a 3500 g/mol PPG prepared with 0.05 mol%$_{DMC,Zn}$ ($CDCl_3$, 75.5 MHz, 297.5 K).

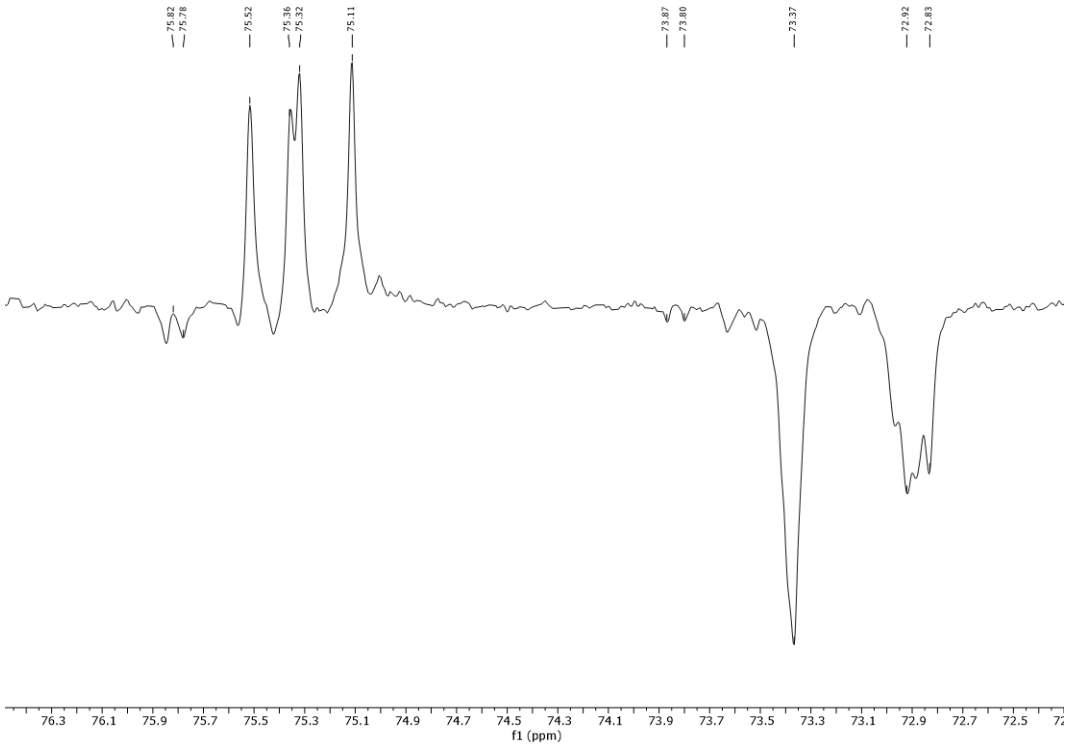

Figure A 12: ^{13}C NMR DEPT spectrum of a 12000 g/mol PPG prepared with 0.0009 mol%$_{DMC,Zn}$ ($CDCl_3$, 75.5 MHz, 297.5 K).

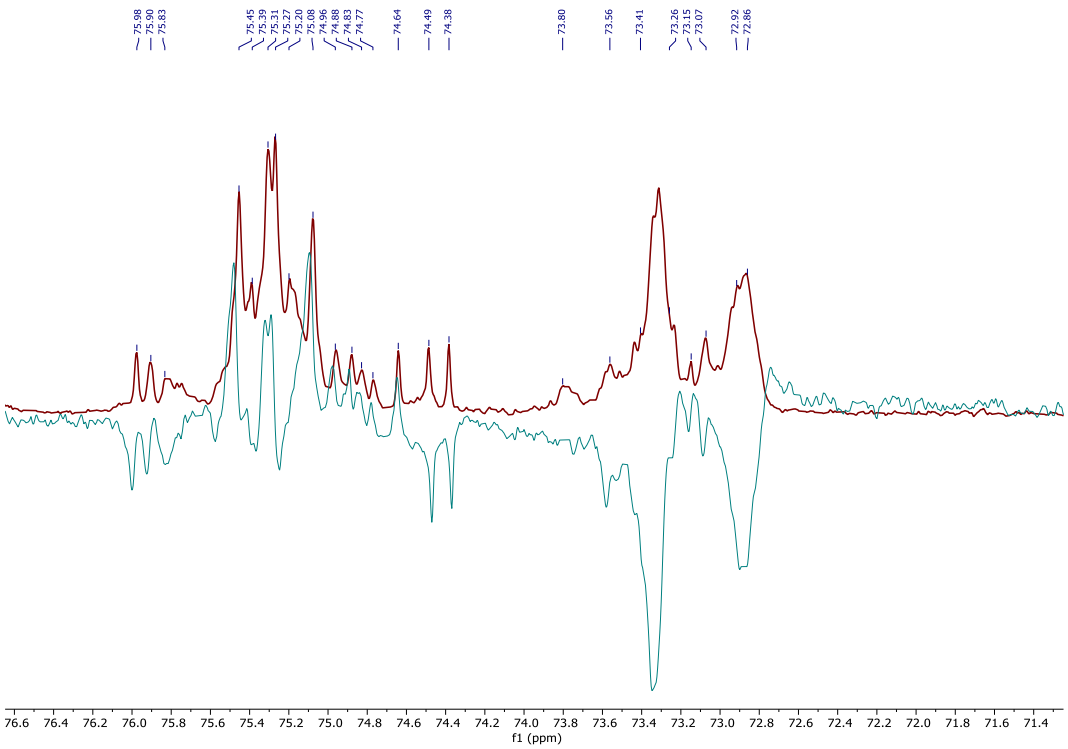

Figure A 13: ^{13}C NMR spectrum (red) and ^{13}C NMR DEPT spectrum (blue) of a 1300 g/mol PPG prepared with 0.13 mol%$_{DMC,Zn}$ ($CDCl_3$, 75.5 MHz, 297.5 K).

A-2.10 In operando FTIR

Calibration:

a)

b)

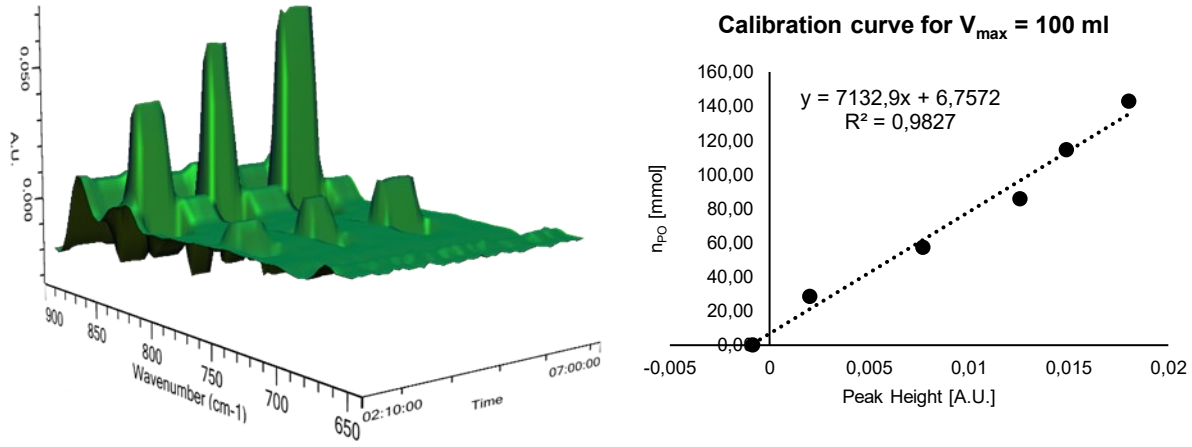

Figure A 14: Calibration spectra (a) and curve (b) of the k = 749 cm^{-1} signal recorded 100 ml reaction vessel.

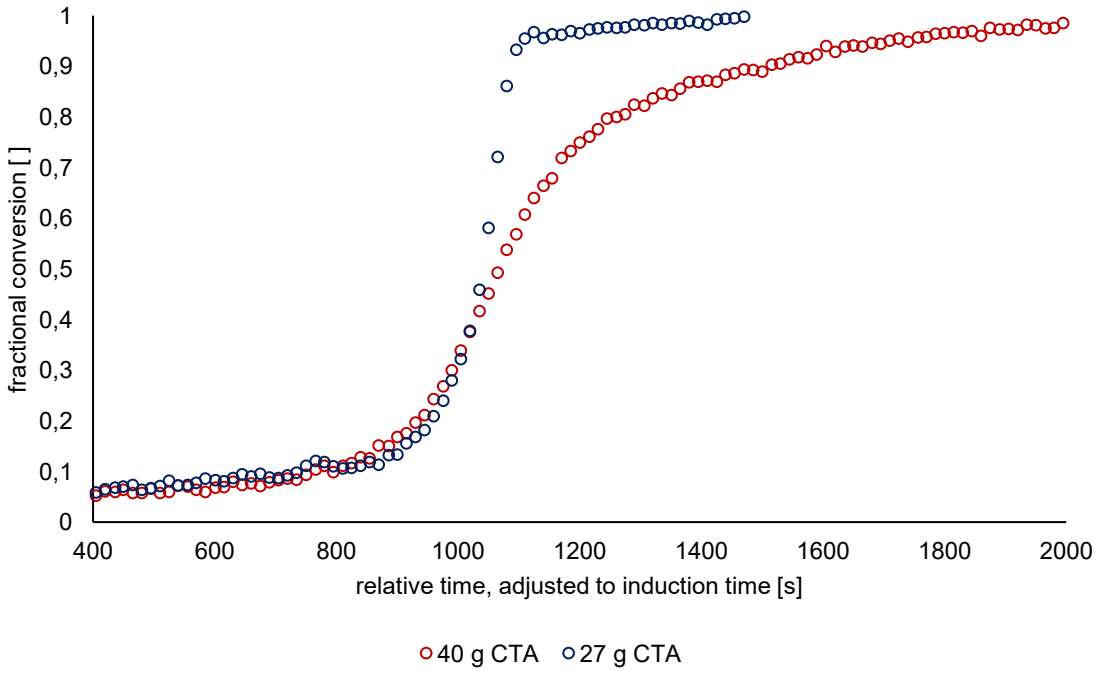

Figure A 15: Comparison of fractional conversion courses under addition of different CTA amounts (0.025 $mol\%_{DMC,Zn}$ of **DMC2**)

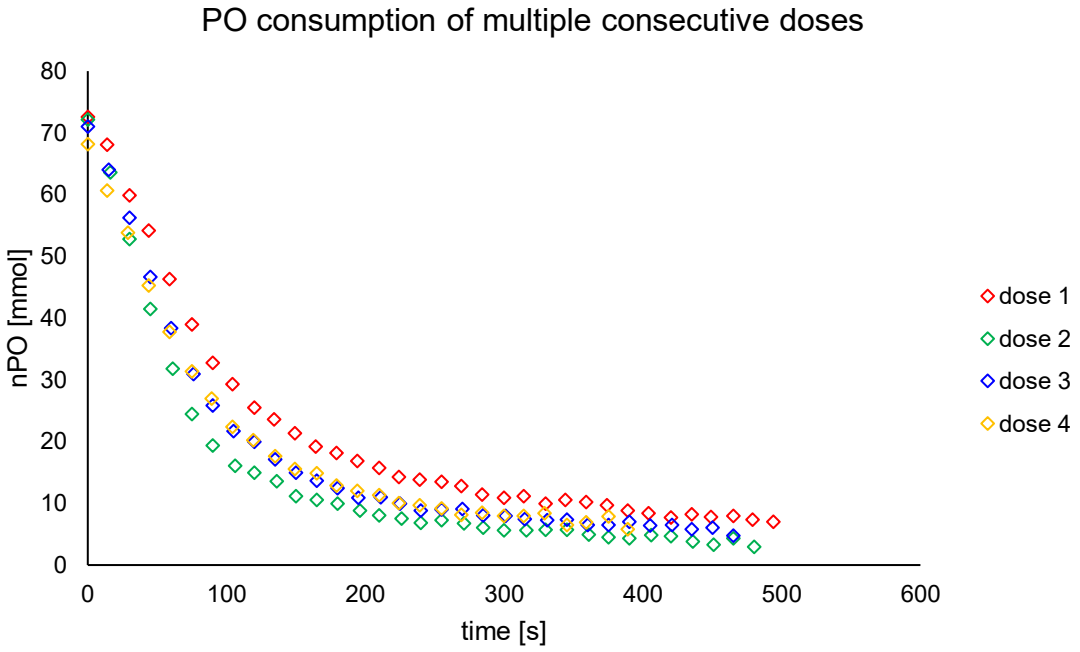

Figure A 16: PO consumption courses for multiple consecutive post-activation additions (0.025 % **DMC2**).

A-2.11 MAS NMR

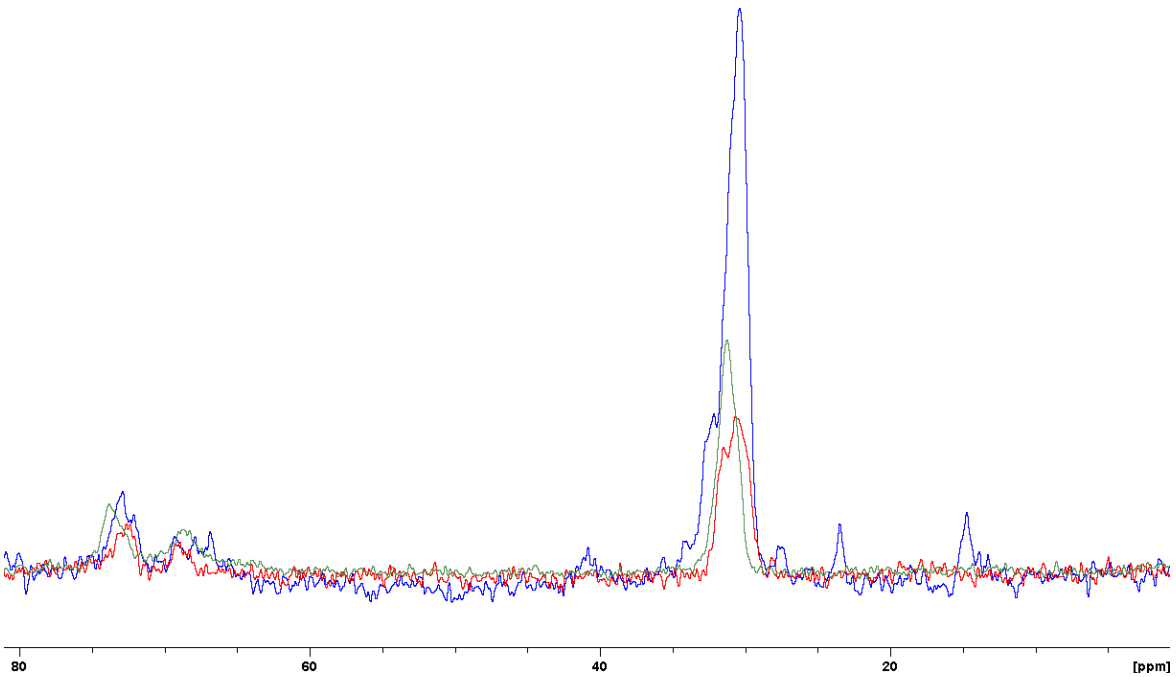

Figure A 17: ^{13}C-DP MAS NMR of ^{2}H-**DMC1** (red), ^{1}H-**DMC1** after immersion in ^{2}H solvent (green) and ^{2}H-**DMC2** (blue), (14 kHz MAS, 297 K).

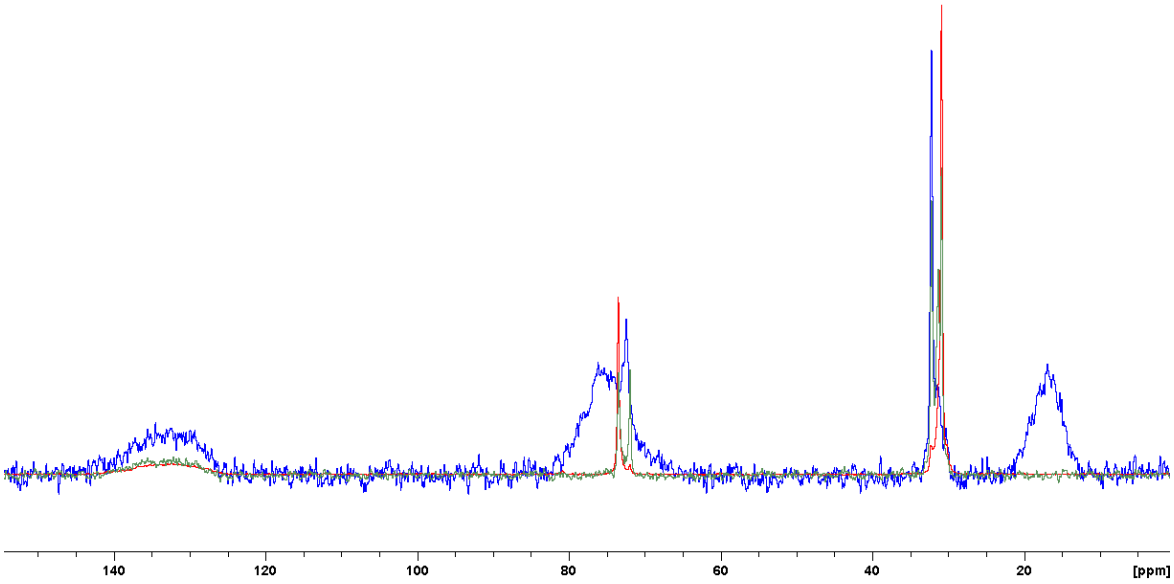

Figure A 18: ^{13}C-CP MAS NMR of ^{1}H-**DMC1** (red), ^{1}H-**DMC2** (green) and ^{1}H-**DMC3** (14 kHz MAS, 297 K).

A-3 Appendix Chapter 4.2

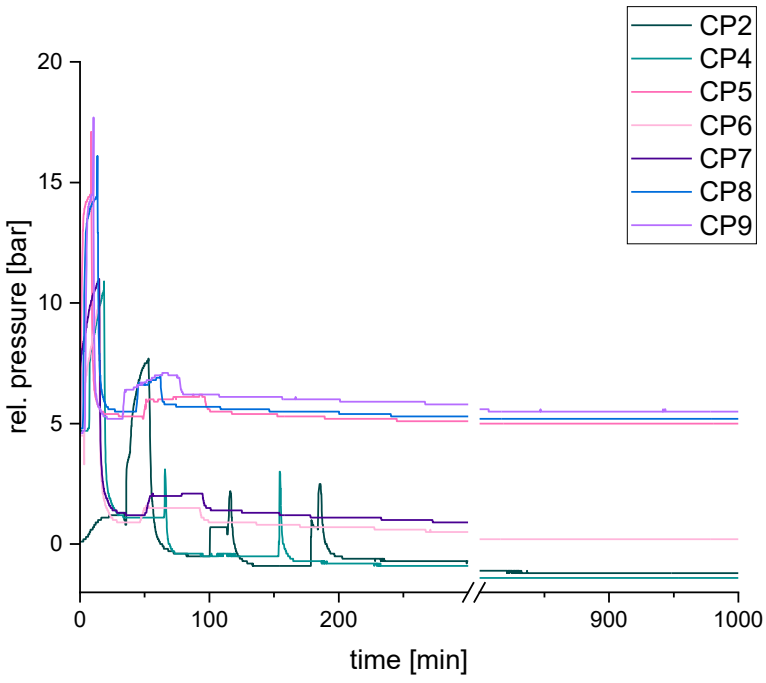

Figure A 19: Pressure course of the polymerization reactions CP2-CP9.

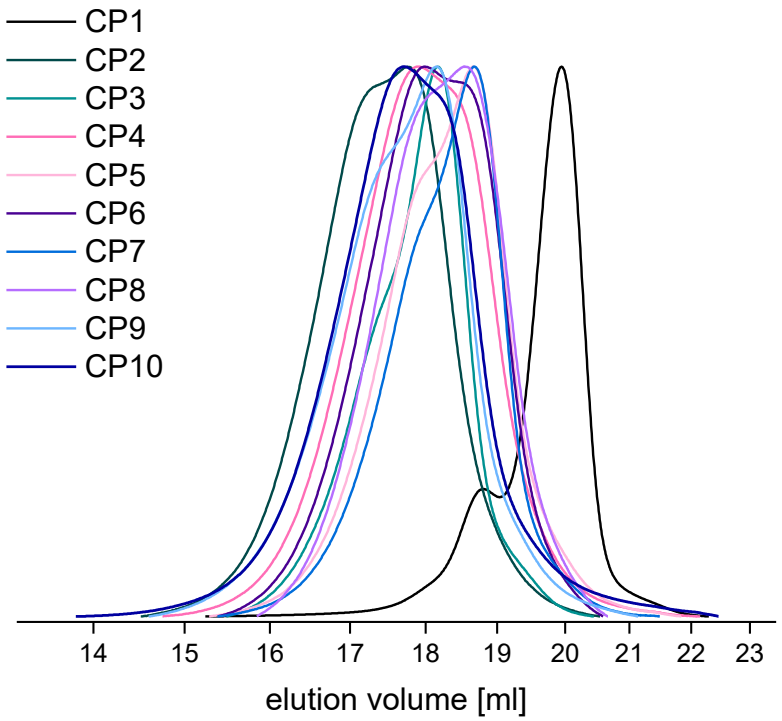

Figure A 20: GPC diagrams of PO/D3 copolymers (eluent: THF; polystyrene standard)

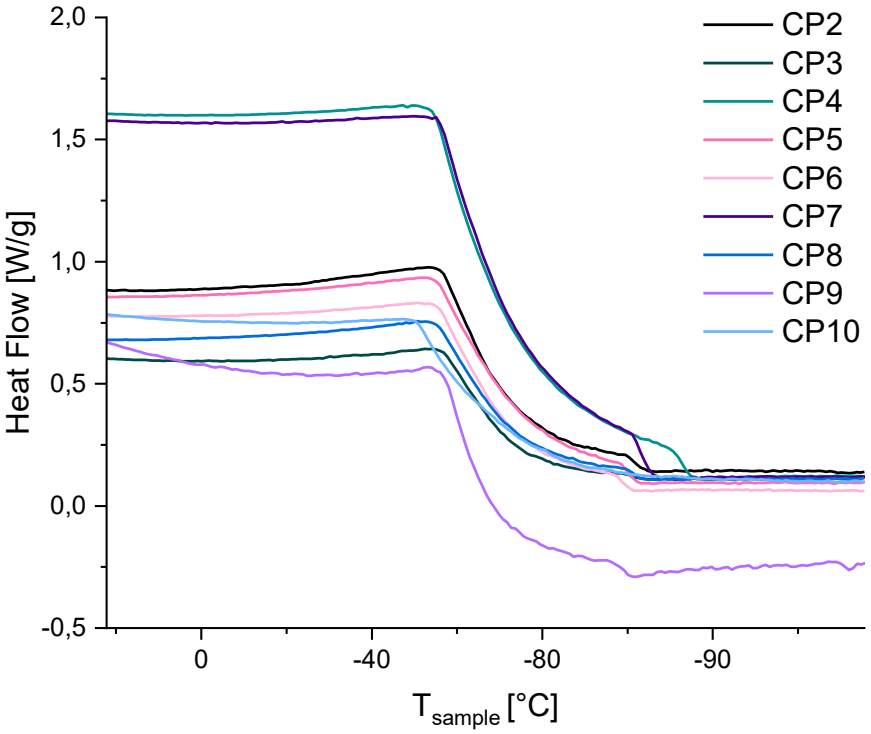

Figure A 21: DSC Thermograms of PO/D3 Copolymers (5 K/min).

A-3.1 CP1

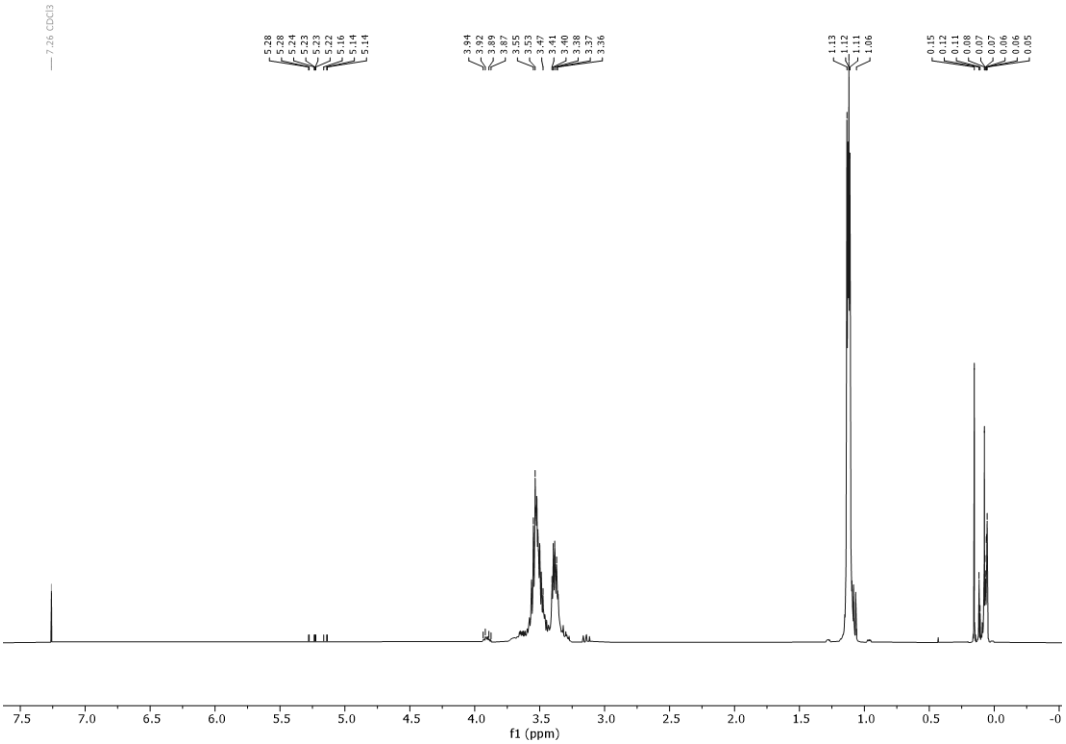

Figure A 22: ^{1}H NMR spectrum of CP1 ($CDCl_3$, 297.0 K, 400 MHz).

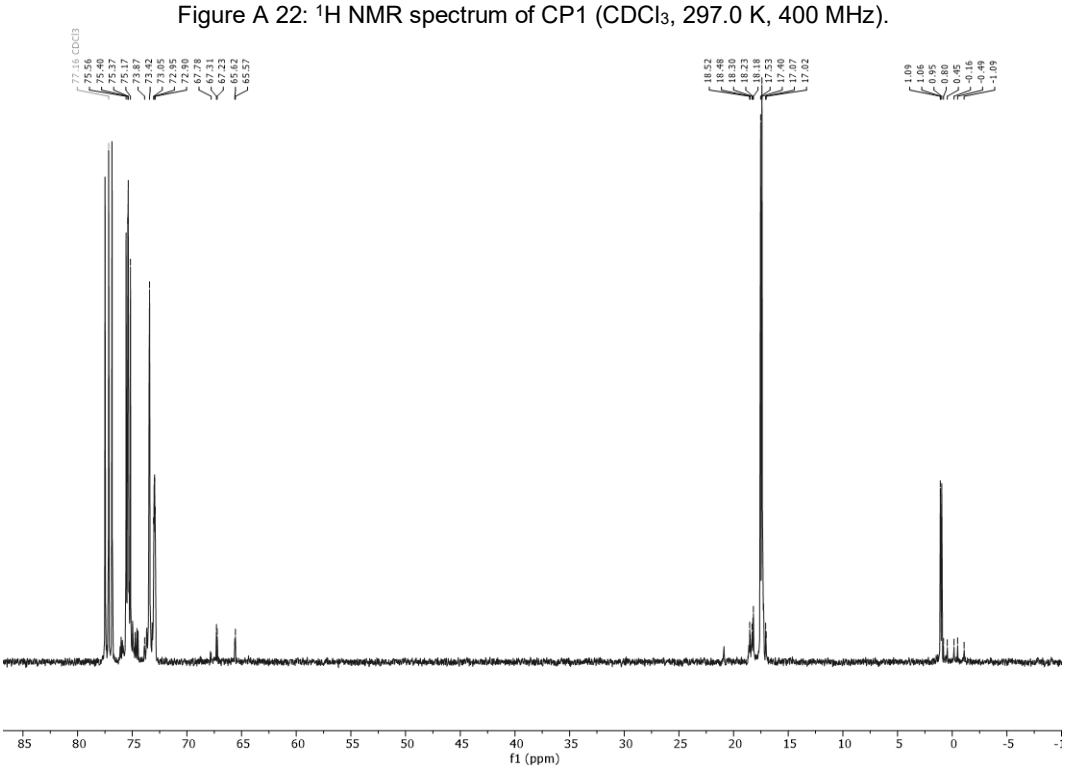

Figure A 23: ^{13}C NMR spectrum of CP1 ($CDCl_3$, 297.0 K, 100 MHz).

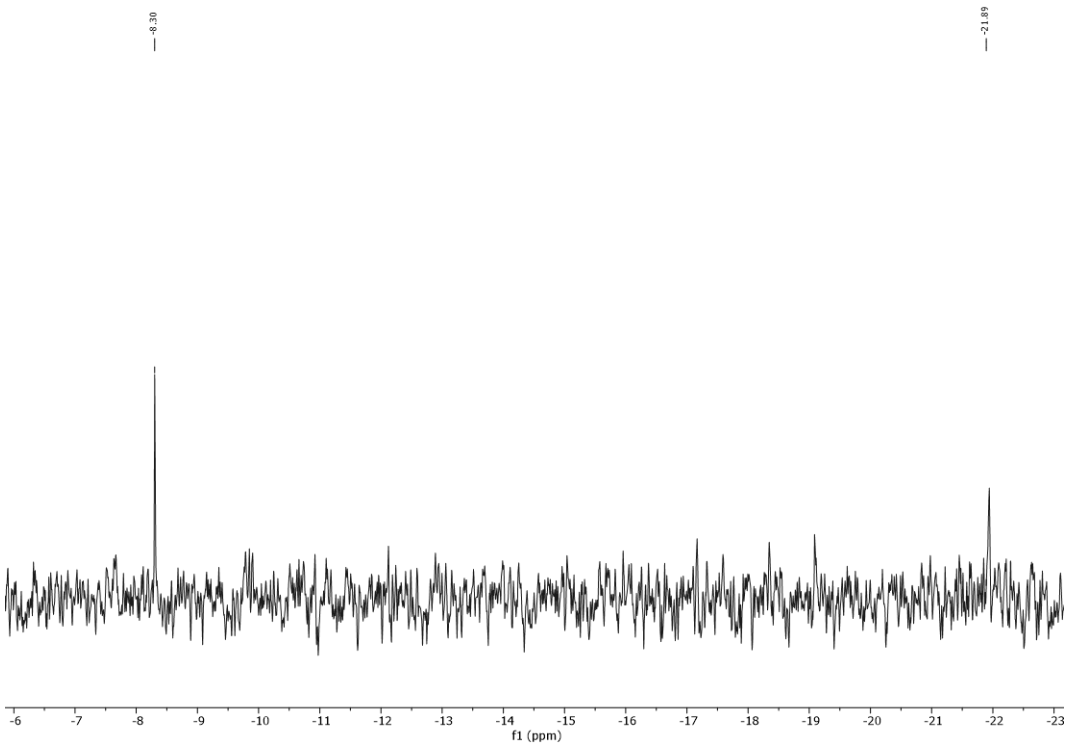

Figure A 24: ^{29}Si NMR spectrum of CP1 ($CDCl_3$, 297.0 K, 79.5 MHz).

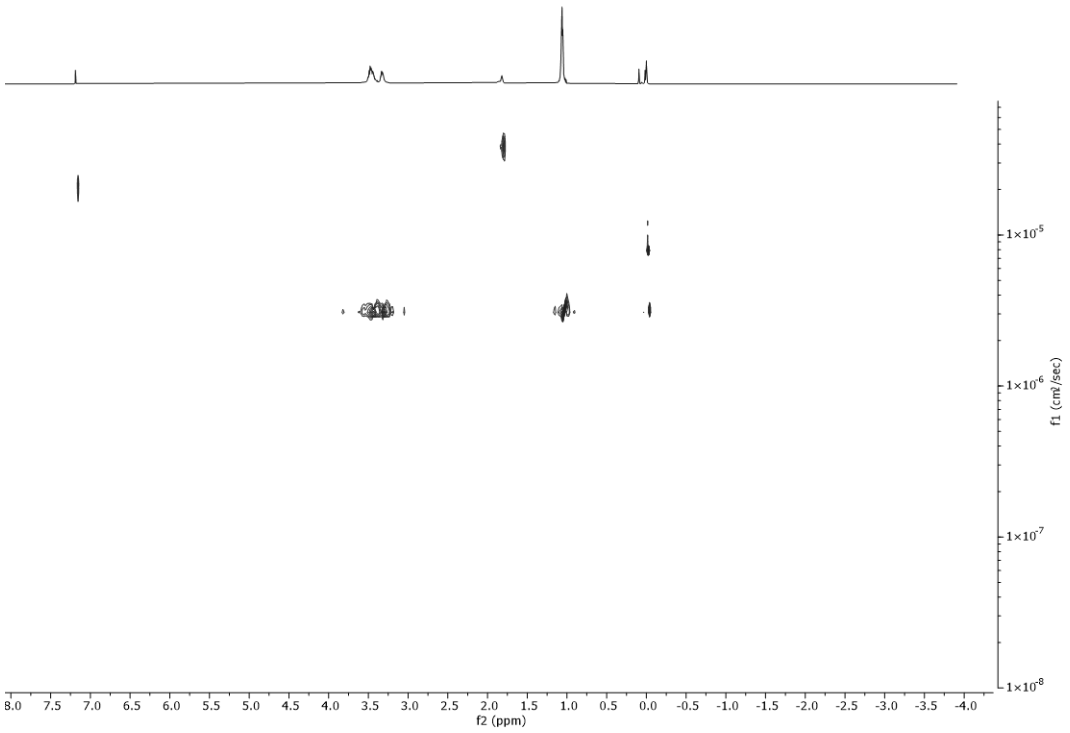

Figure A 25: ^{1}H DOSY NMR spectrum of CP1 ($CDCl_3$, 298.1 K, 500 MHz).

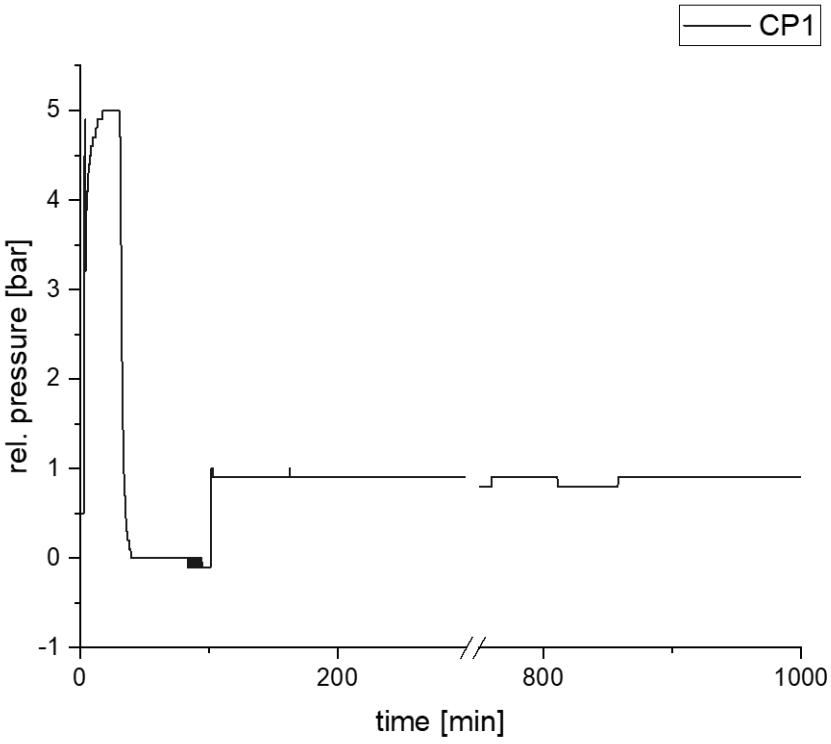

Figure A 26: Pressure course during the polymerization reaction of CP1.

A-3.2 CP2

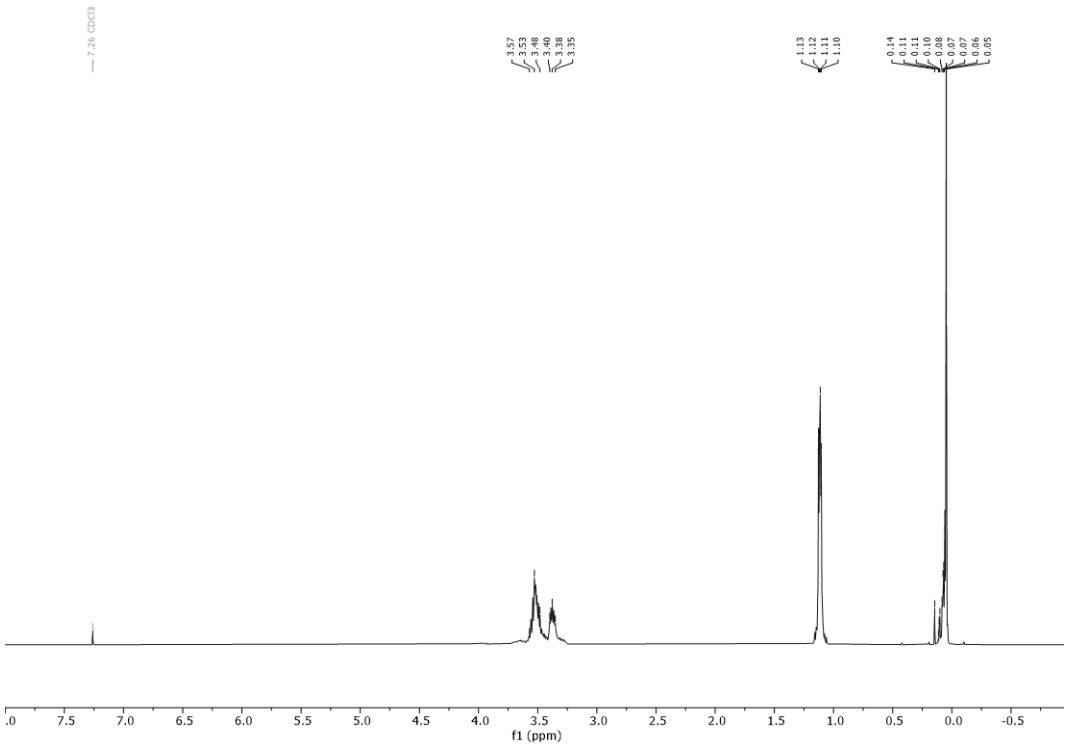

Figure A 27: ^{1}H NMR spectrum of CP2 ($CDCl_3$ 297.0 K, 400 MHz).

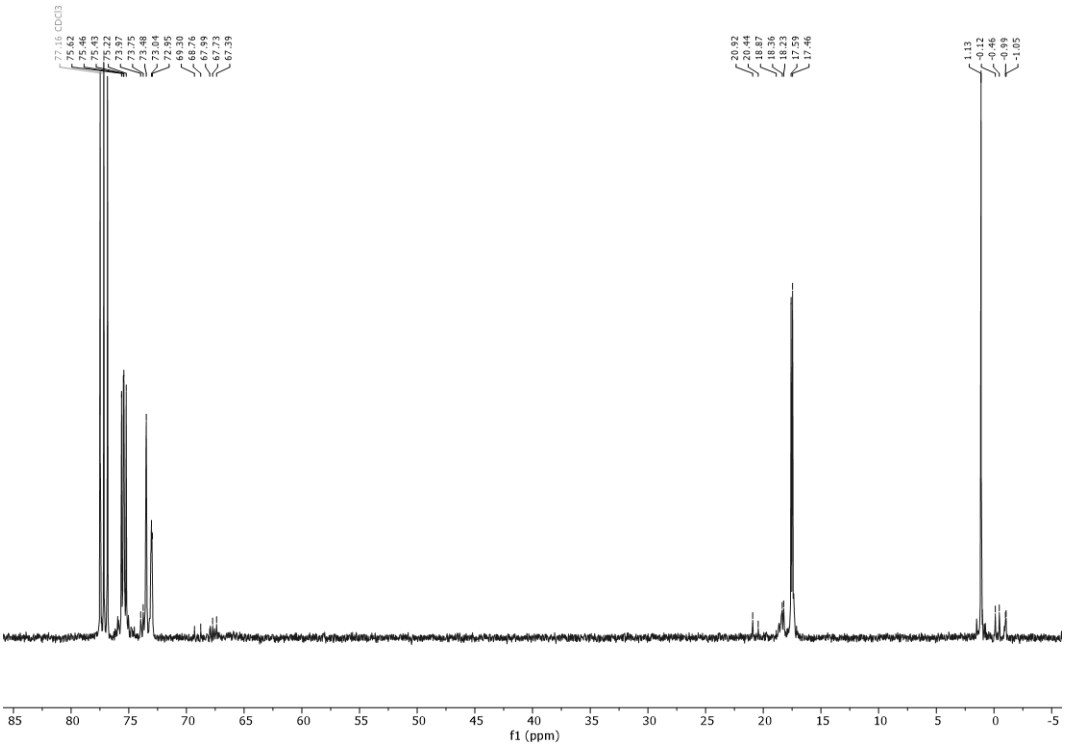

Figure A 28: ^{13}C NMR spectrum of CP2 ($CDCl_3$, 297.0 K, 100 MHz).

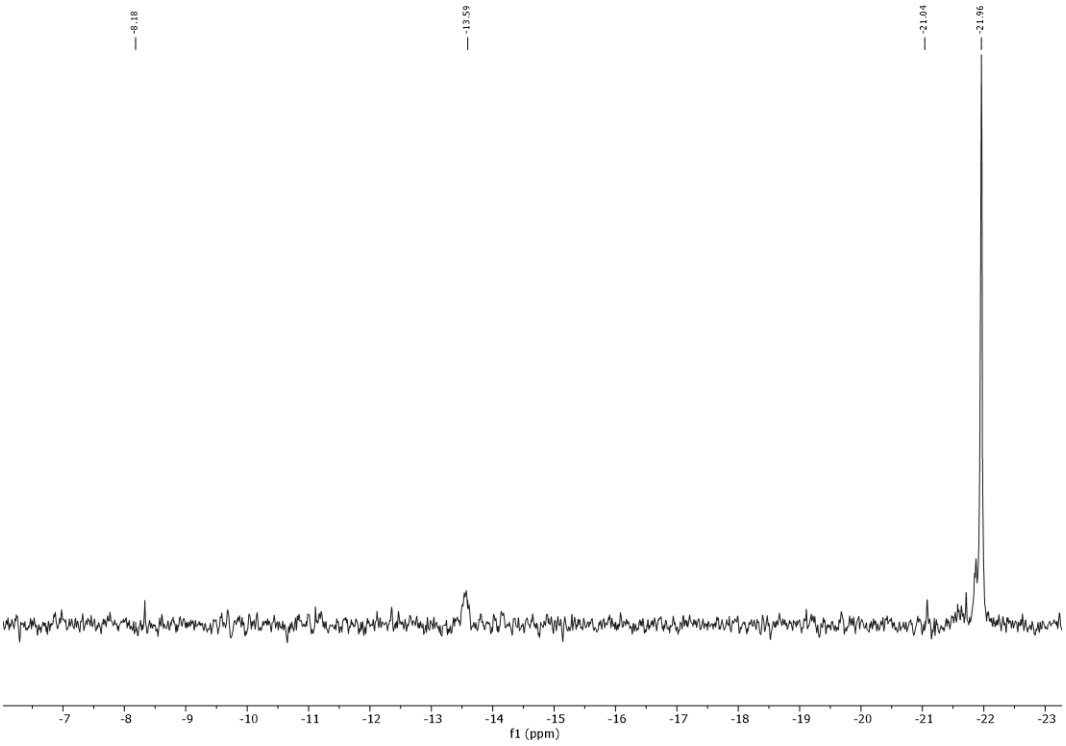

Figure A 29: ^{29}Si-IG NMR spectrum of CP2 ($CDCl_3$, 297.0 K, 79.5 MHz).

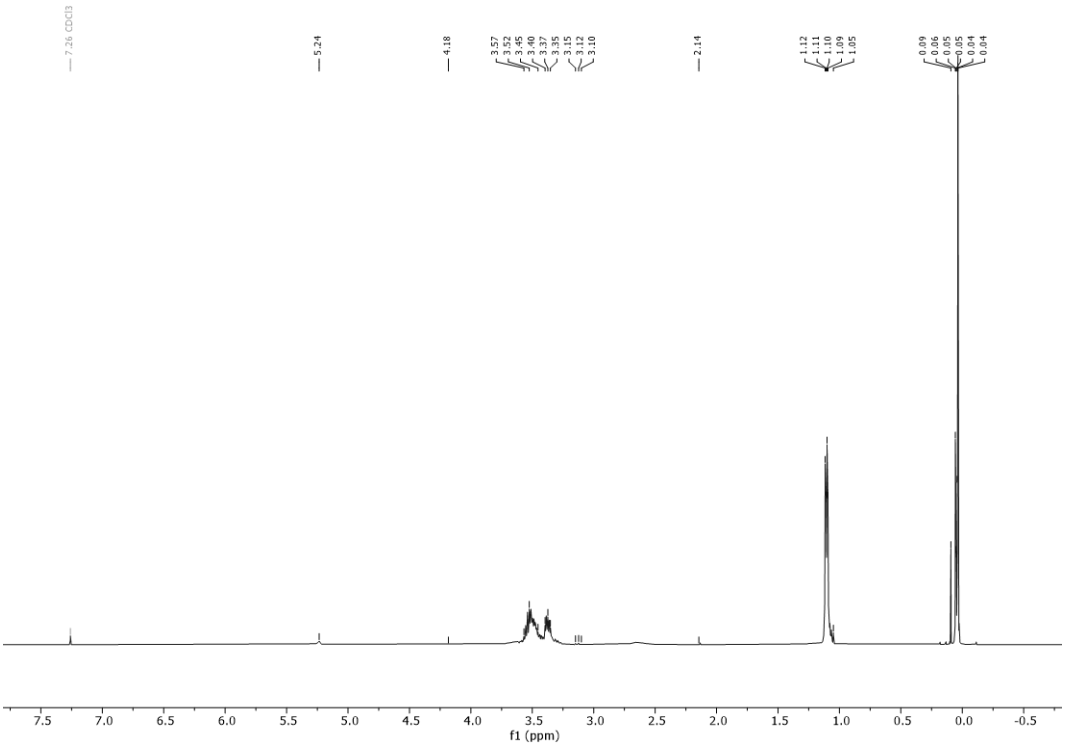

Figure A 30: ^{1}H NMR spectrum of CP2 after hydrolytic degradation ($CDCl_3$, 297.0 K, 400 MHz).

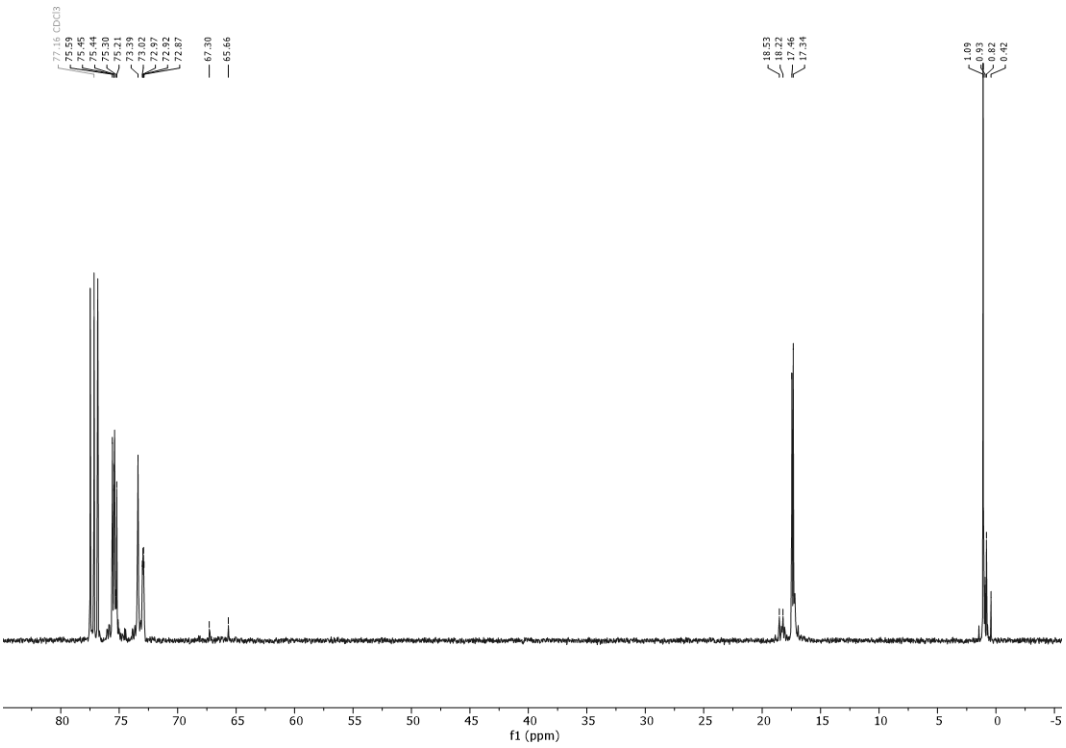

Figure A 31: ^{13}C NMR spectrum of CP2 after hydrolytic degradation ($CDCl_3$, 297.0 K, 100 MHz).

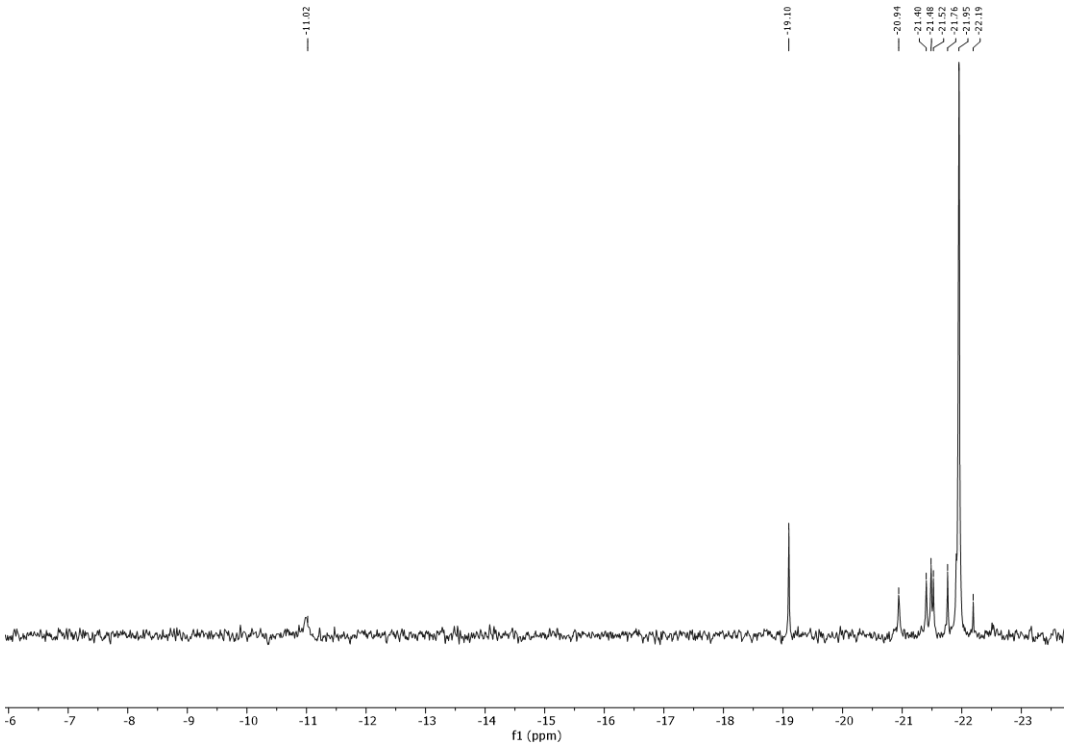

Figure A 32: ^{29}Si-IG NMR spectrum of CP2 after hydrolytic degradation ($CDCl_3$, 297.0 K, 79.5 MHz).

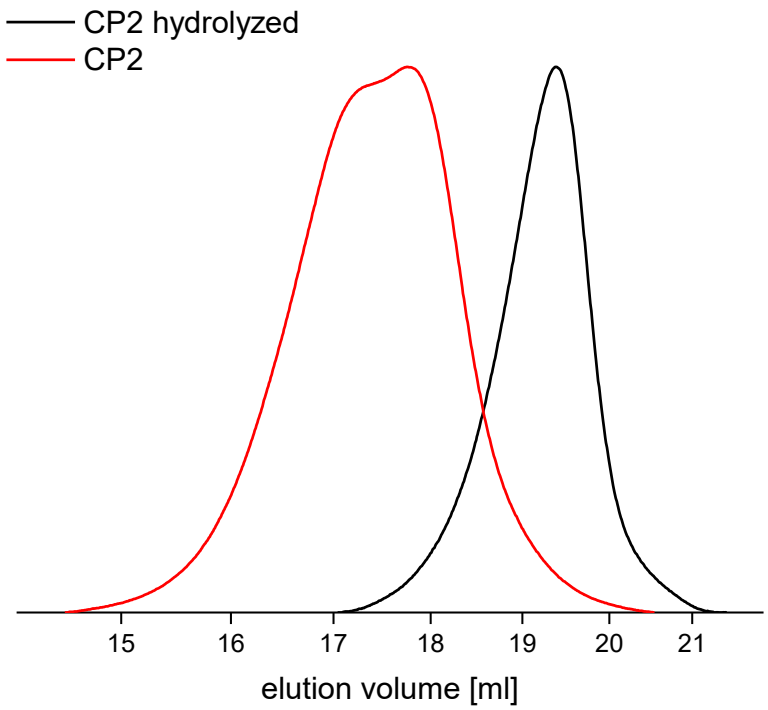

Figure A 33: GPC before and after exposing CP2 diluted HCl (eluent: THF; polystyrene standard).

A-3.3 CP3

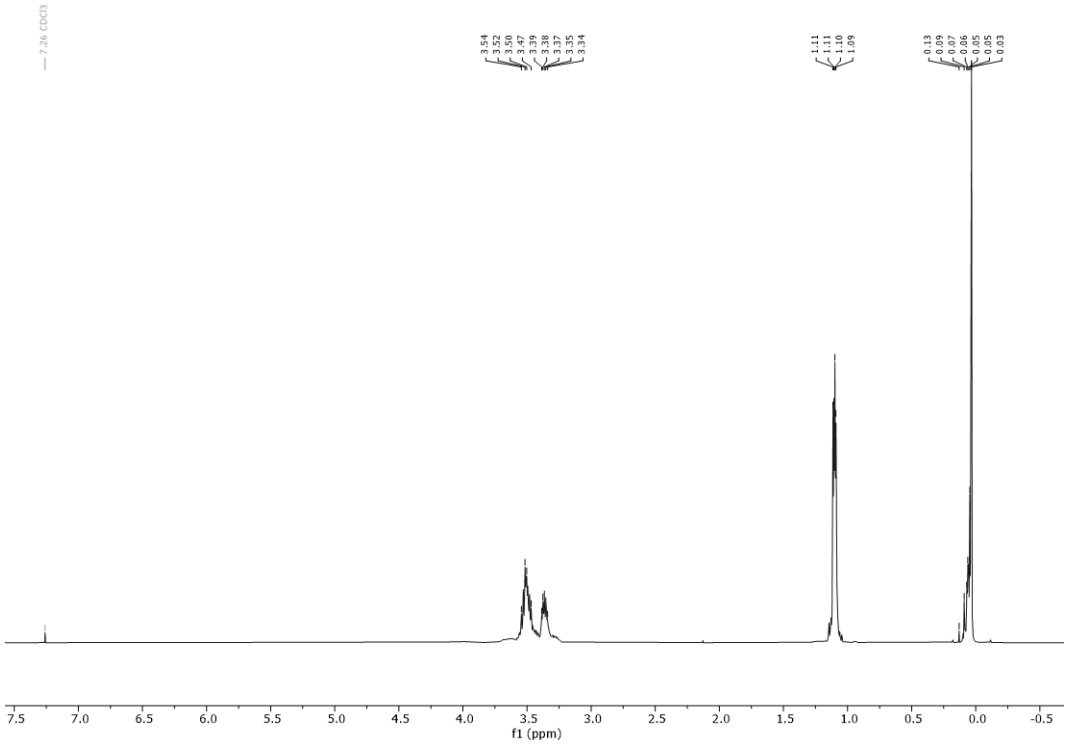

Figure A 34: ^{1}H NMR spectrum of CP3 ($CDCl_3$ 297.0 K, 400 MHz).

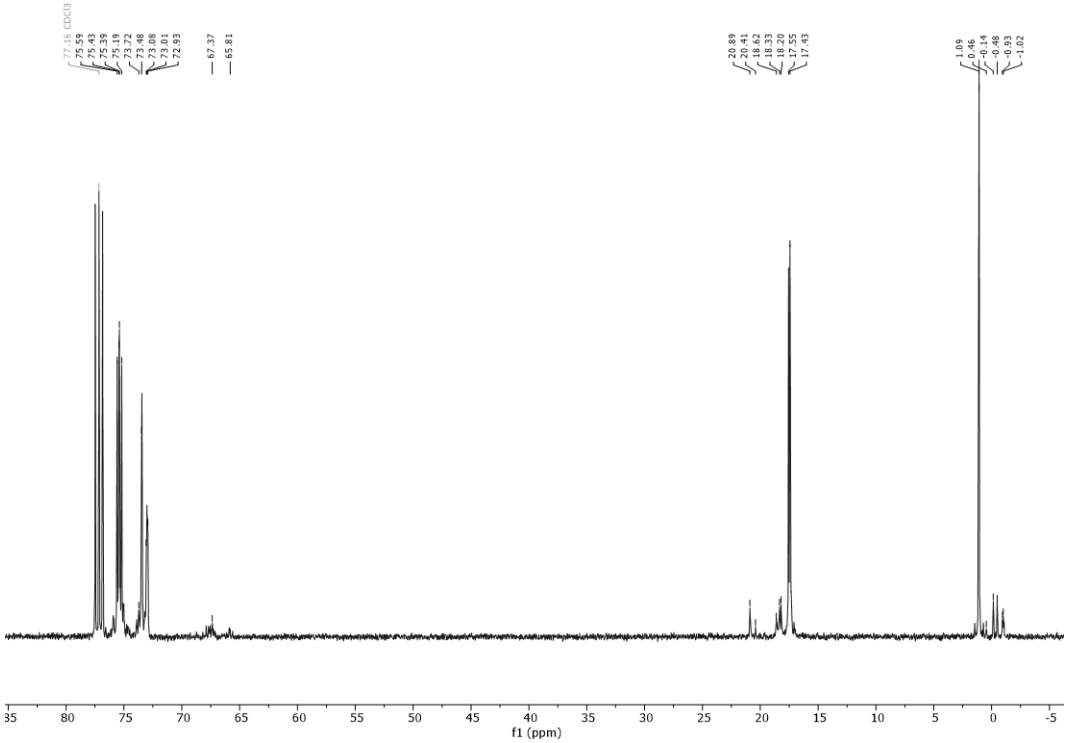

Figure A 35: ^{13}C NMR spectrum of CP3 ($CDCl_3$, 297.0 K, 100 MHz).

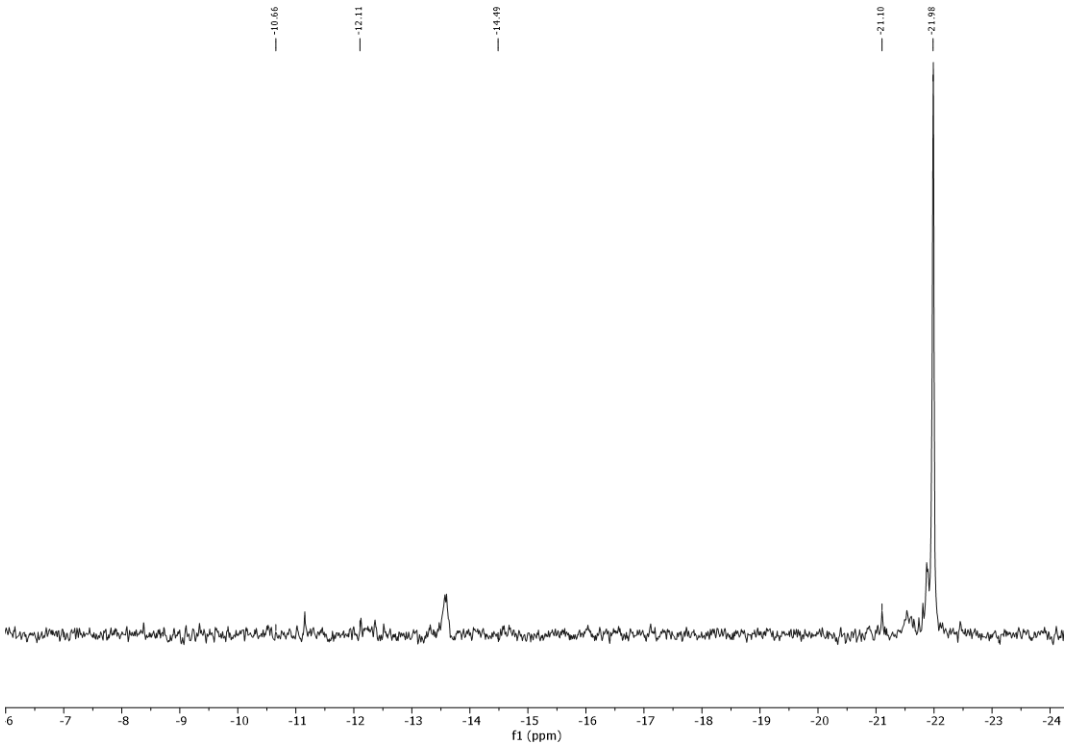

Figure A 36: ^{29}Si-IG NMR spectrum of CP3 ($CDCl_3$, 297.0 K, 79.5 MHz).

A-3.4 CP4

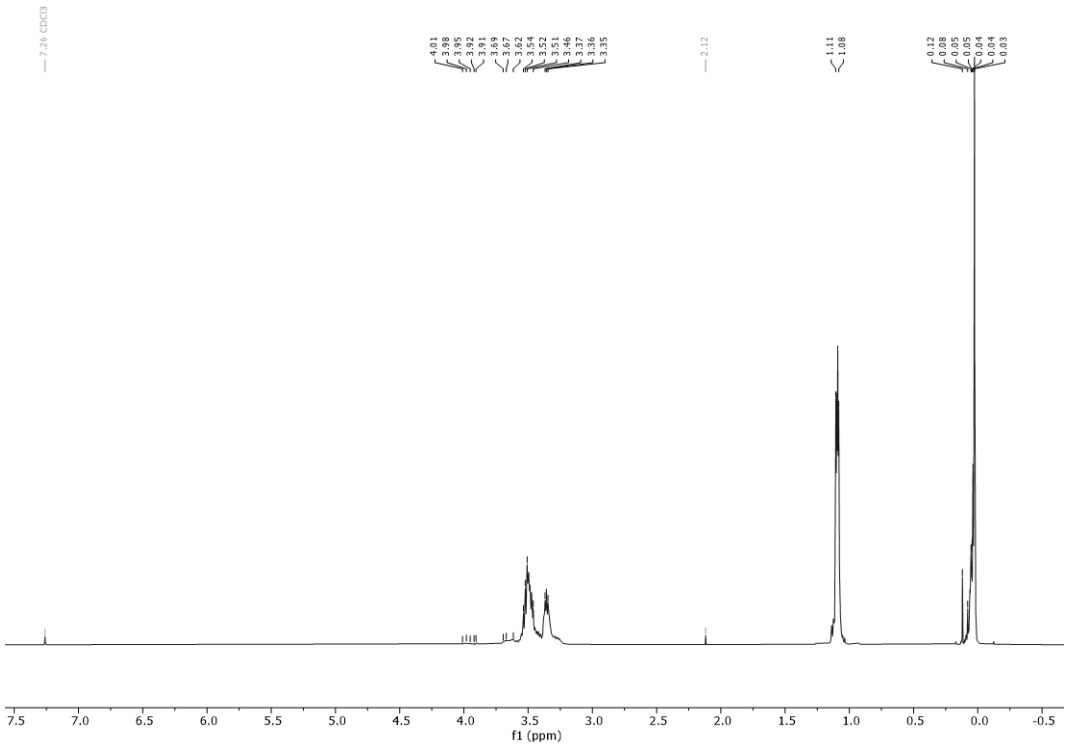

Figure A 37: ^{1}H NMR spectrum of CP4 ($CDCl_3$ 297.0 K, 400 MHz).

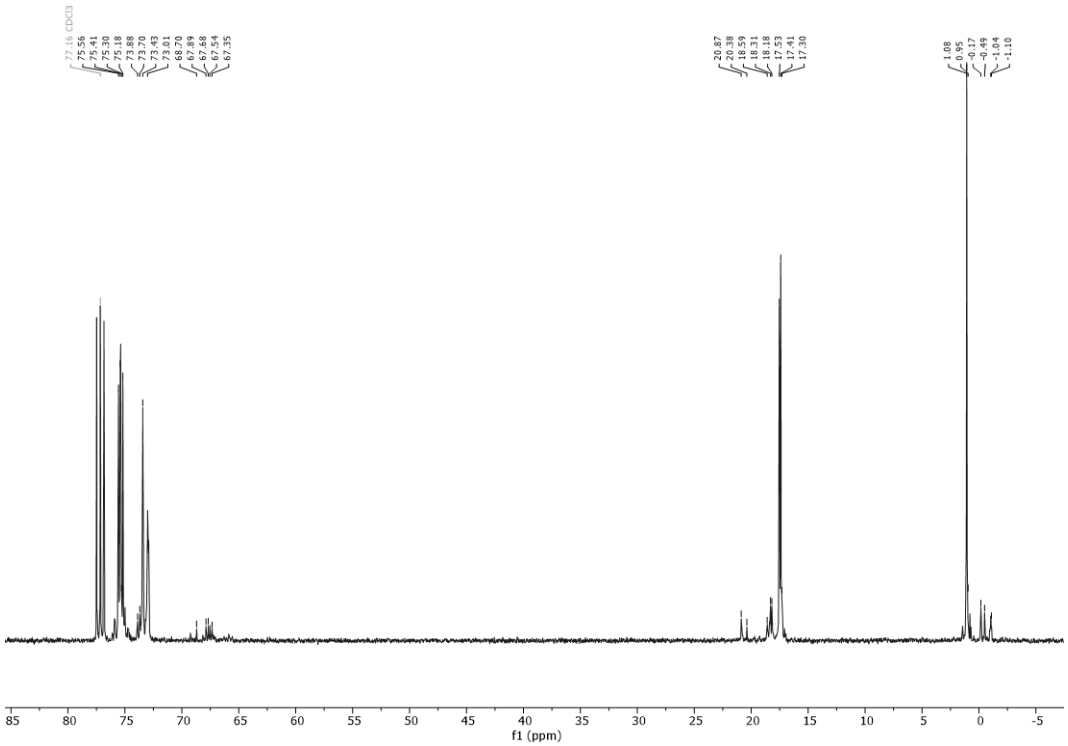

Figure A 38: ^{13}C NMR spectrum of CP4 ($CDCl_3$, 297.0 K, 100 MHz).

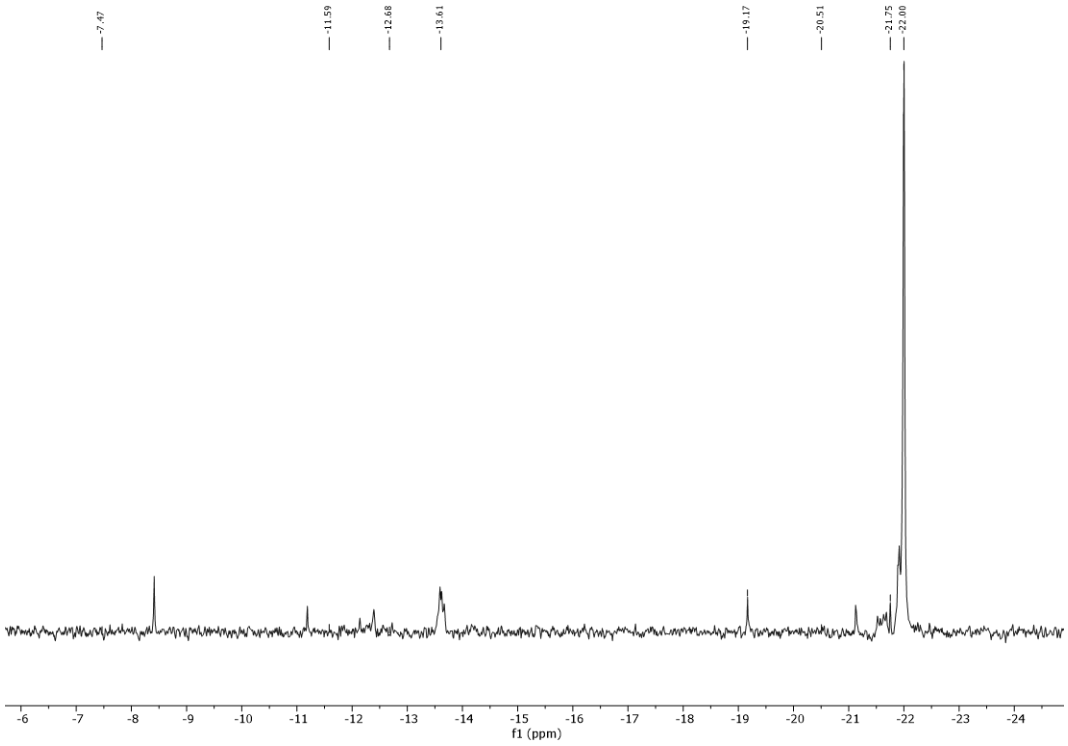

Figure A 39: ^{29}Si-IG NMR spectrum of CP4 ($CDCl_3$, 297.0 K, 79.5 MHz).

A-3.5 CP5

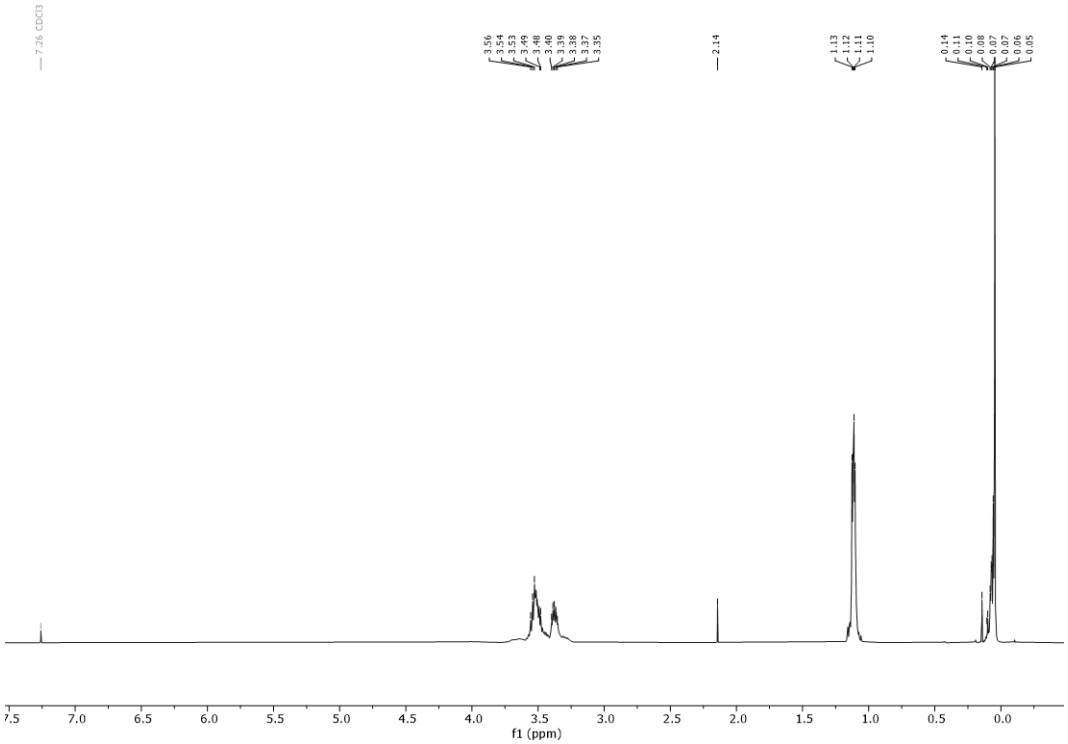

Figure A 40: ^{1}H NMR spectrum of CP5 ($CDCl_3$ 297.0 K, 400 MHz).

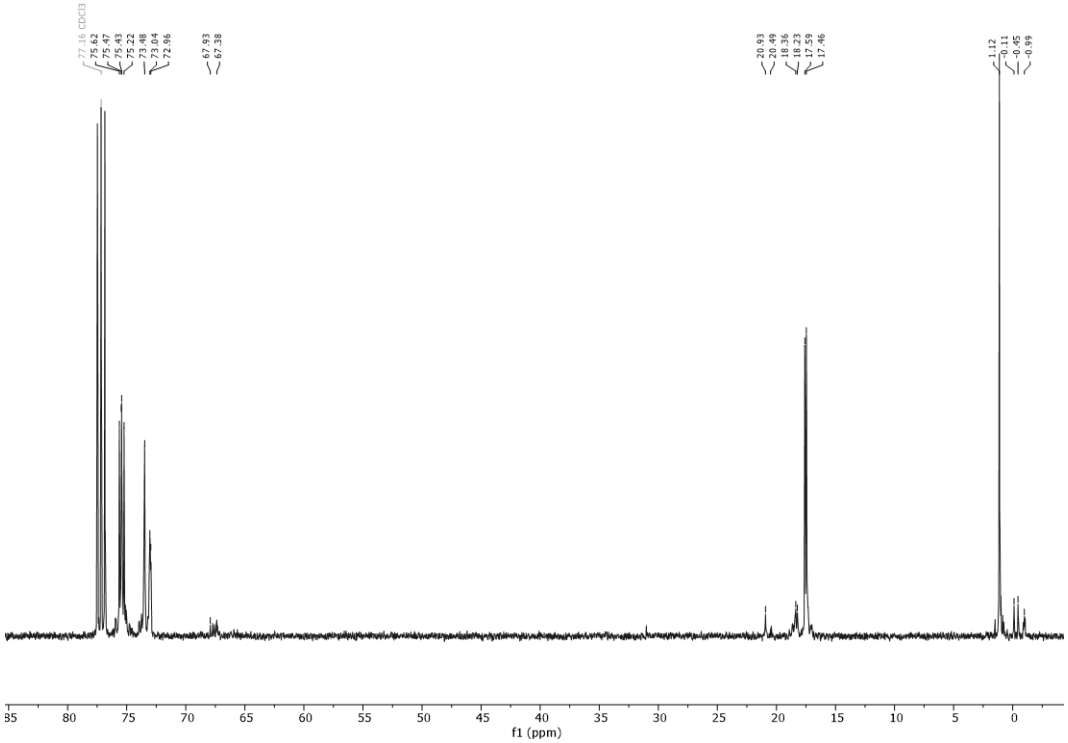

Figure A 41: ^{13}C NMR spectrum of CP5 ($CDCl_3$, 297.0 K, 100 MHz).

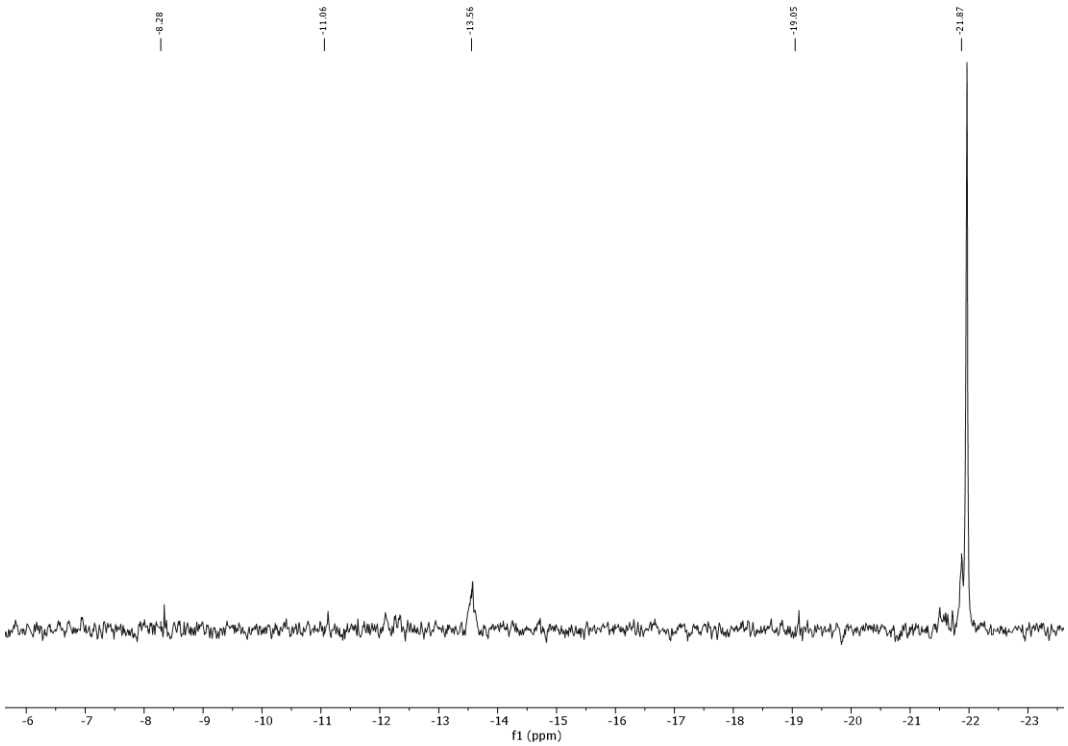

Figure A 42: ^{29}Si-IG NMR spectrum of CP5 ($CDCl_3$, 297.0 K, 79.5 MHz).

A-3.6 CP6

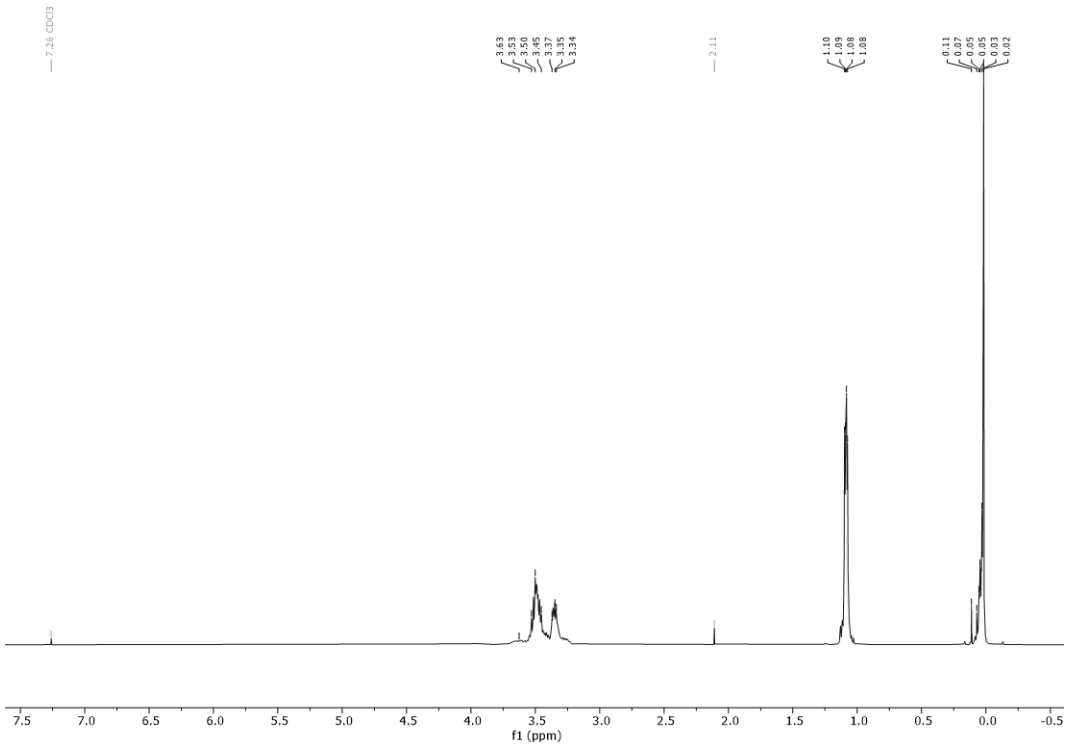

Figure A 43: ^{1}H NMR spectrum of CP6 ($CDCl_3$ 297.0 K, 400 MHz).

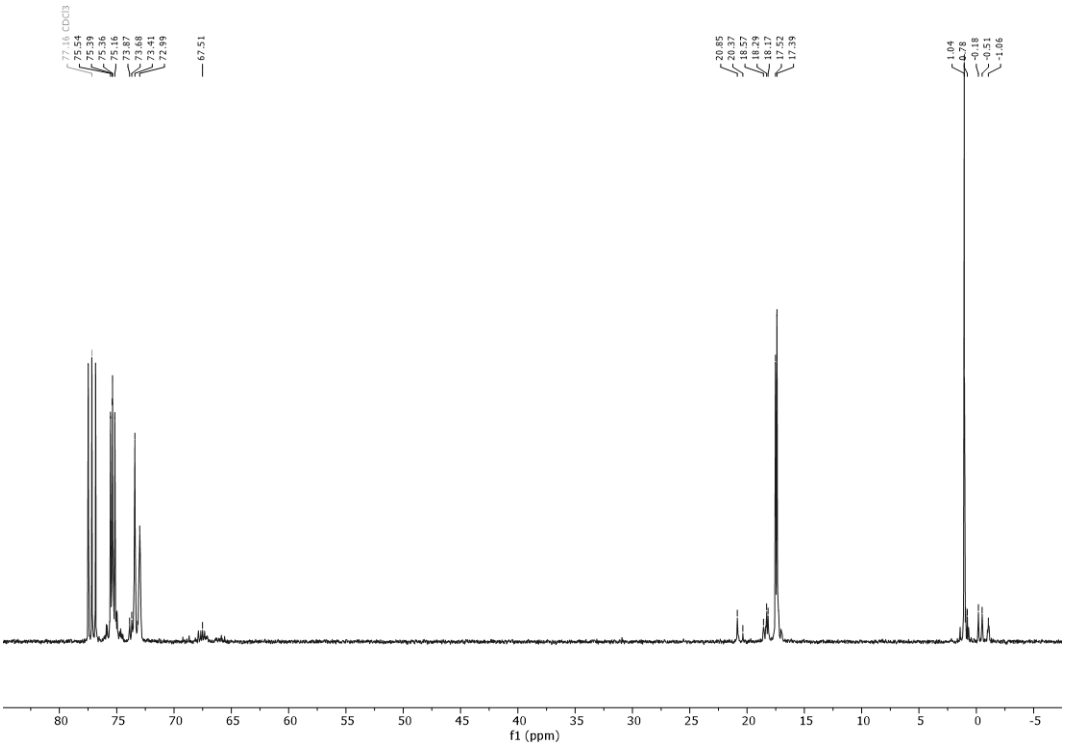

Figure A 44: ^{13}C NMR spectrum of CP6 ($CDCl_3$, 297.0 K, 100 MHz).

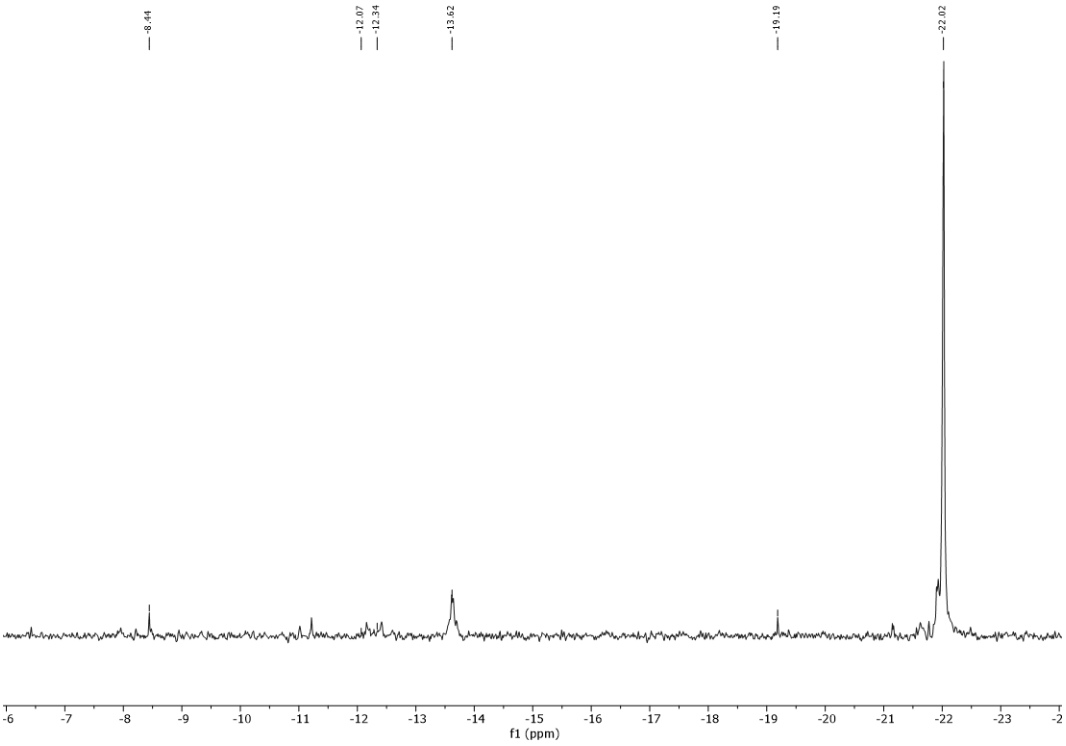

Figure A 45: ^{29}Si-IG NMR spectrum of CP6 ($CDCl_3$, 297.0 K, 79.5 MHz).

A-3.7 CP7

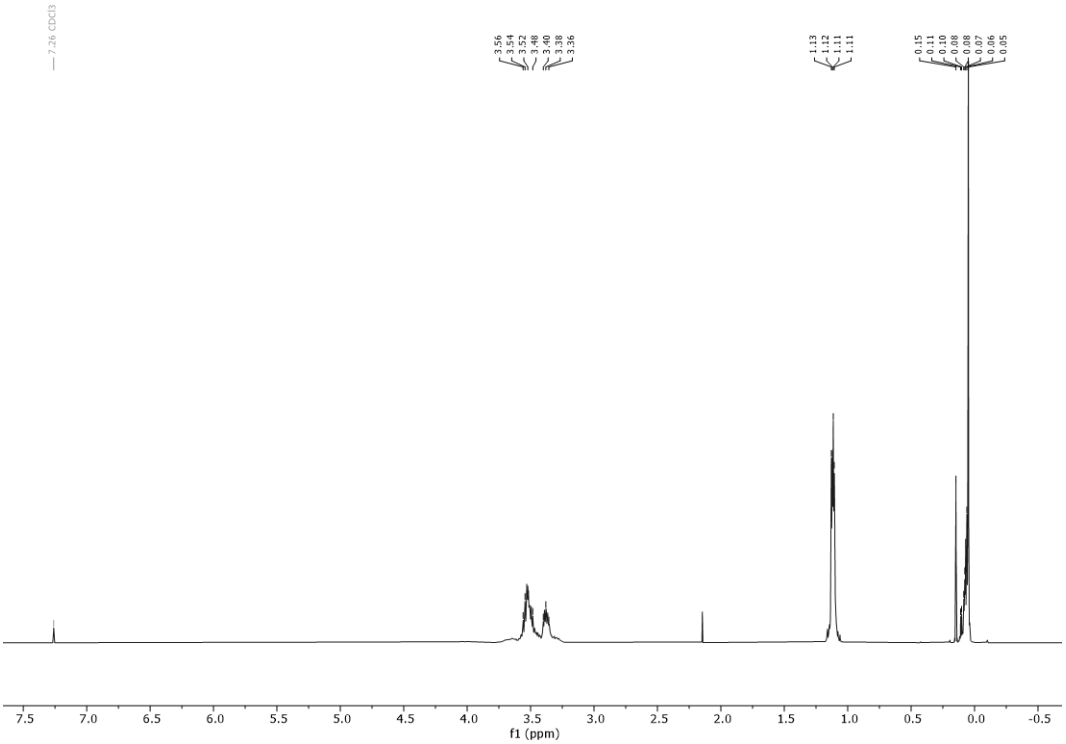

Figure A 46: ^{1}H NMR spectrum of CP7 ($CDCl_3$ 297.0 K, 400 MHz).

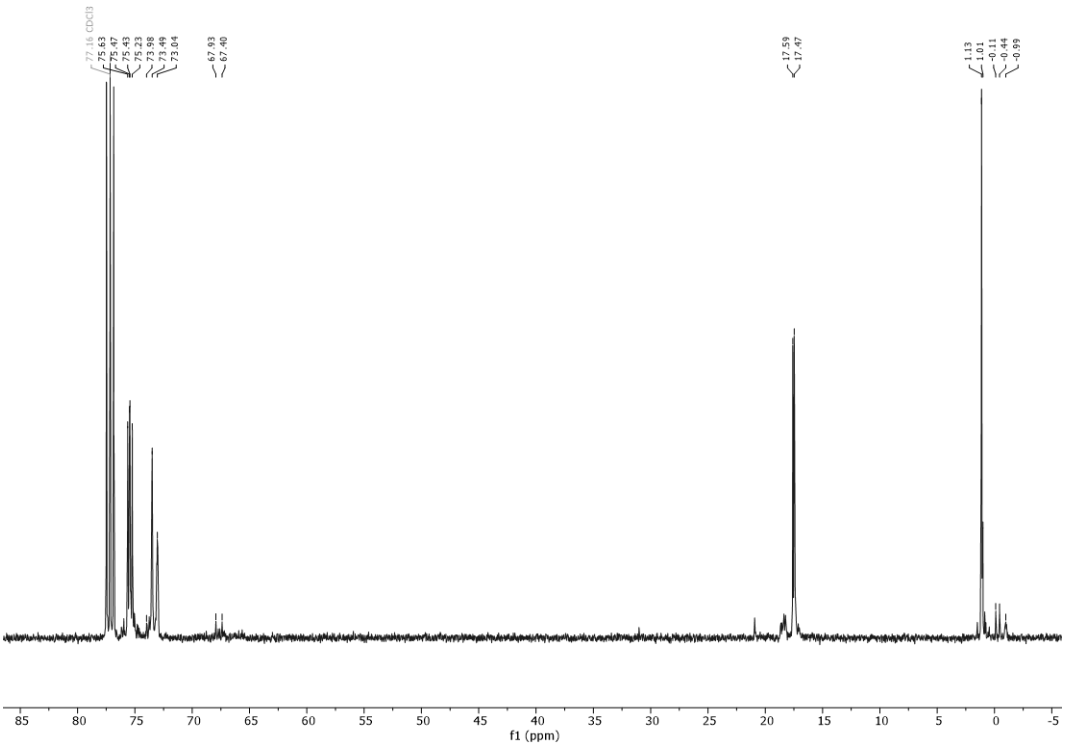

Figure A 47: ^{13}C NMR spectrum of CP7 ($CDCl_3$, 297.0 K, 100 MHz).

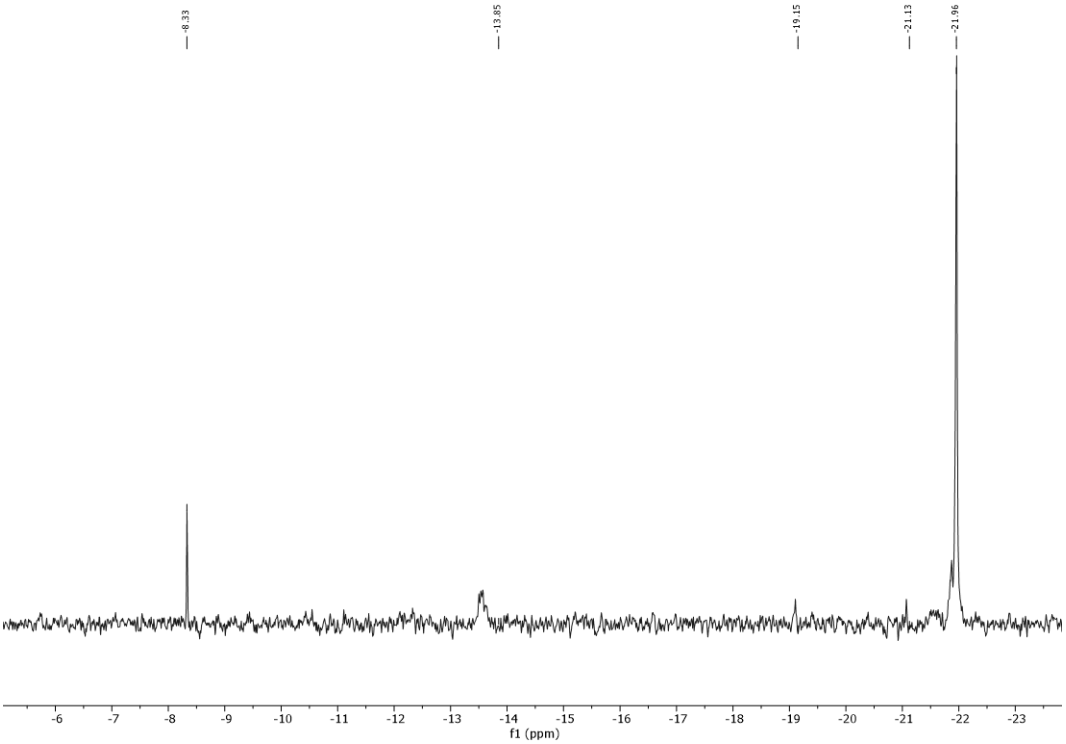

Figure A 48: ^{29}Si-IG NMR spectrum of CP7 ($CDCl_3$, 297.0 K, 79.5 MHz).

A-3.8 CP8

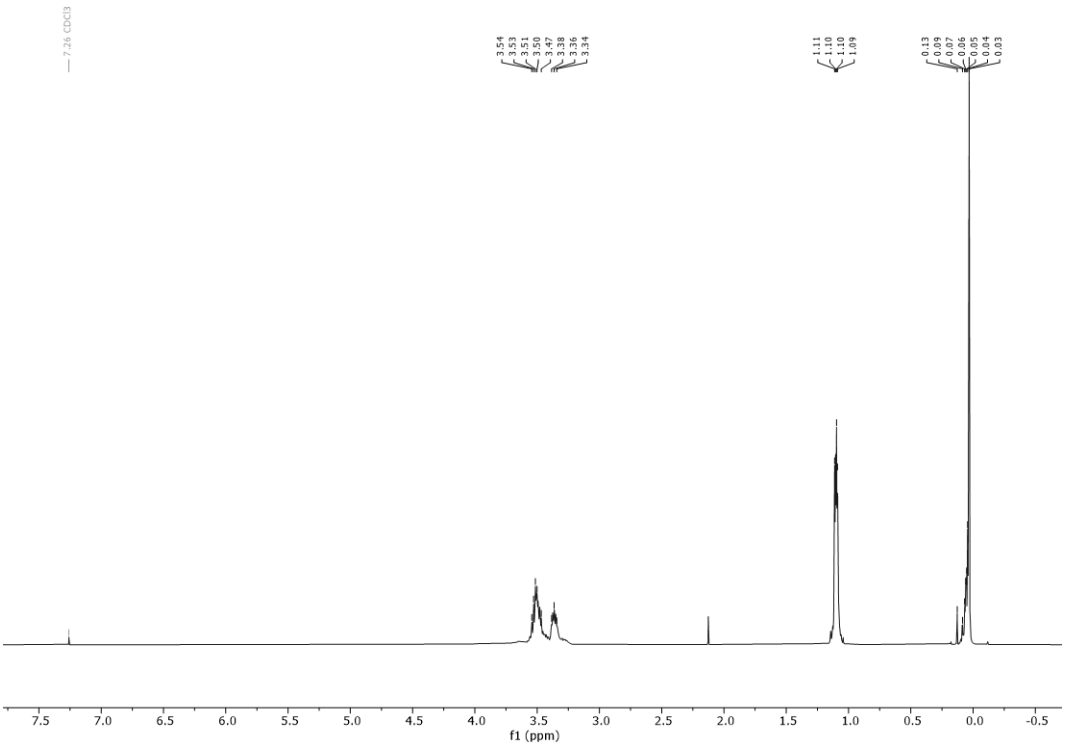

Figure A 49: ^{1}H NMR spectrum of CP8 ($CDCl_3$ 297.0 K, 400 MHz).

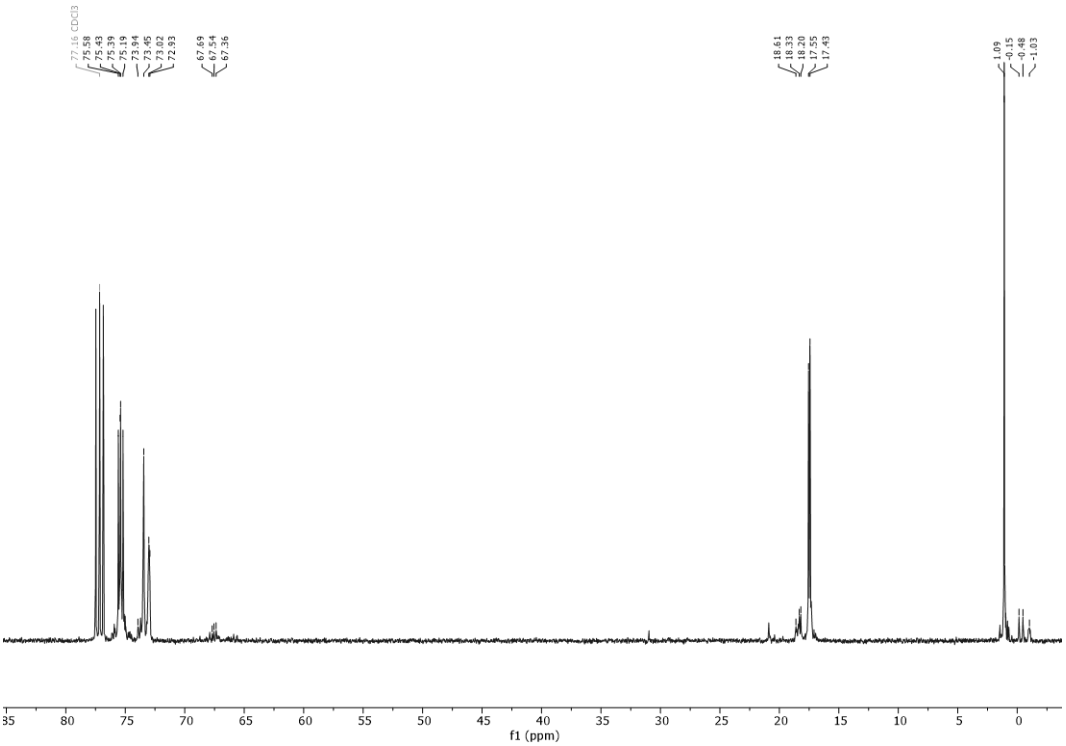

Figure A 50: ^{13}C NMR spectrum of CP8 ($CDCl_3$, 297.0 K, 100 MHz).

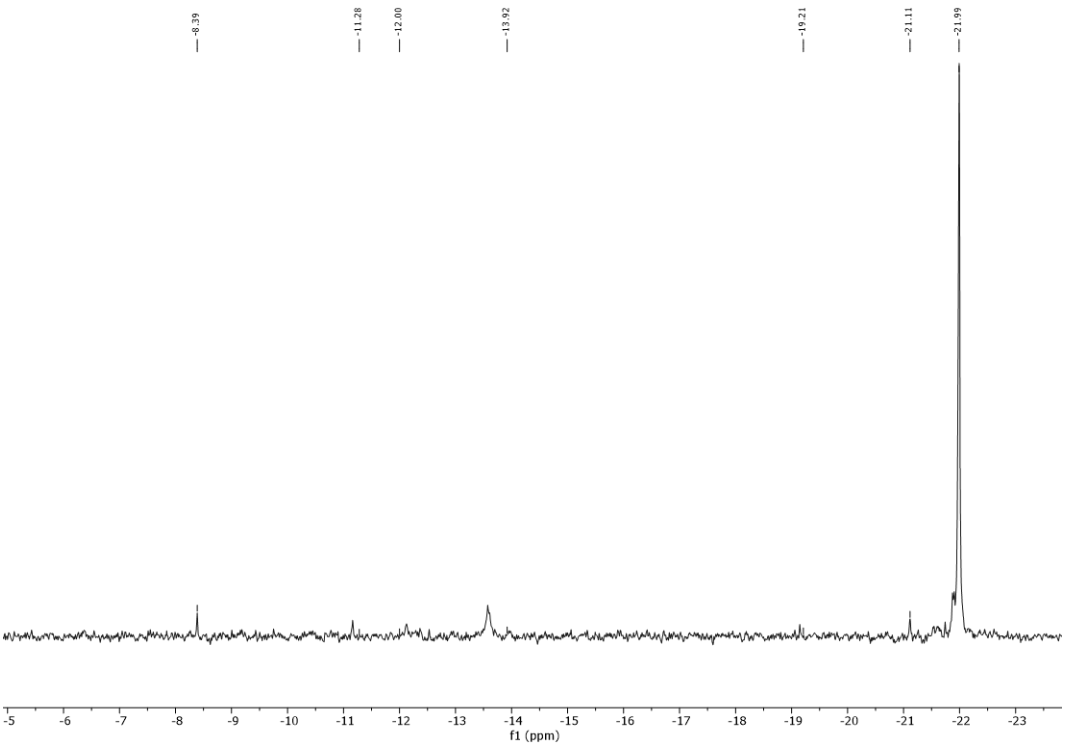

Figure A 51: ^{29}Si-IG NMR spectrum of CP8 ($CDCl_3$, 297.0 K, 79.5 MHz).

A-3.9 CP9

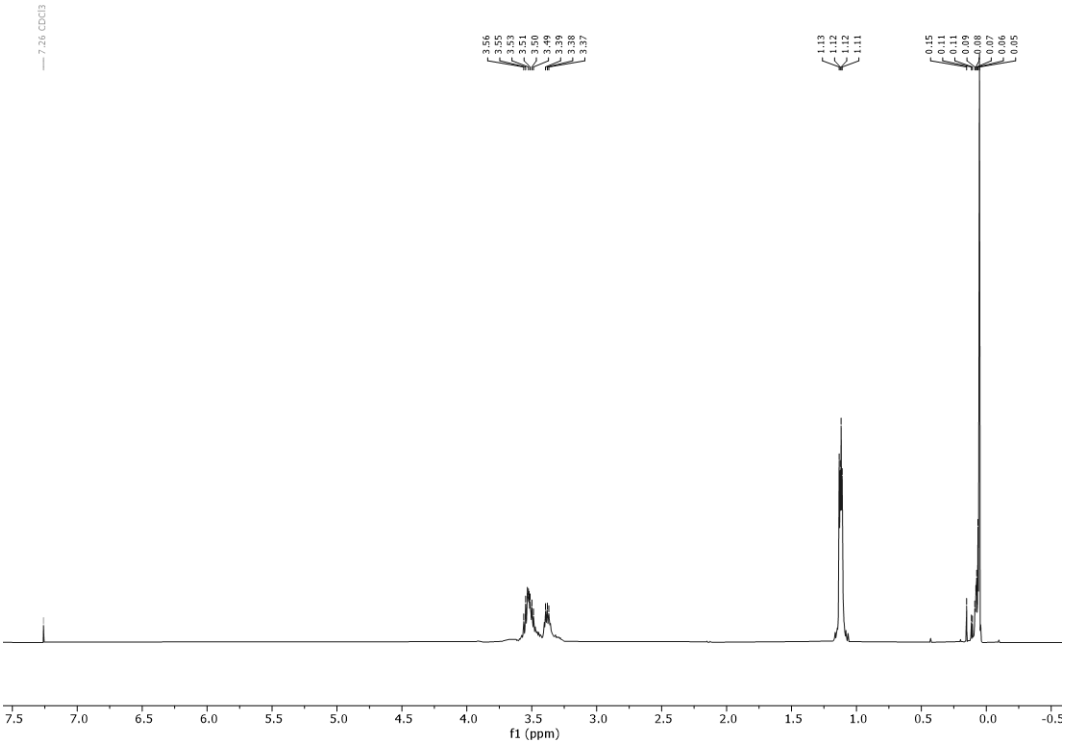

Figure A 52: ^{1}H NMR spectrum of CP9 ($CDCl_3$ 297.0 K, 400 MHz).

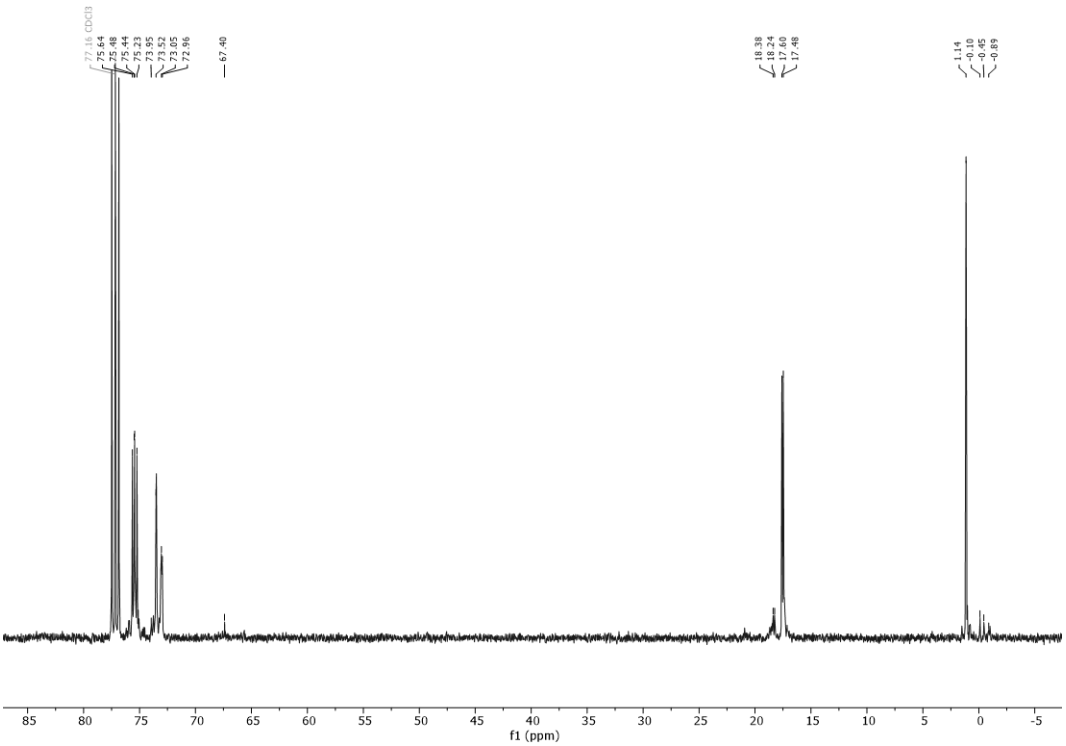

Figure A 53: ^{13}C NMR spectrum of CP9 ($CDCl_3$, 297.0 K, 100 MHz).

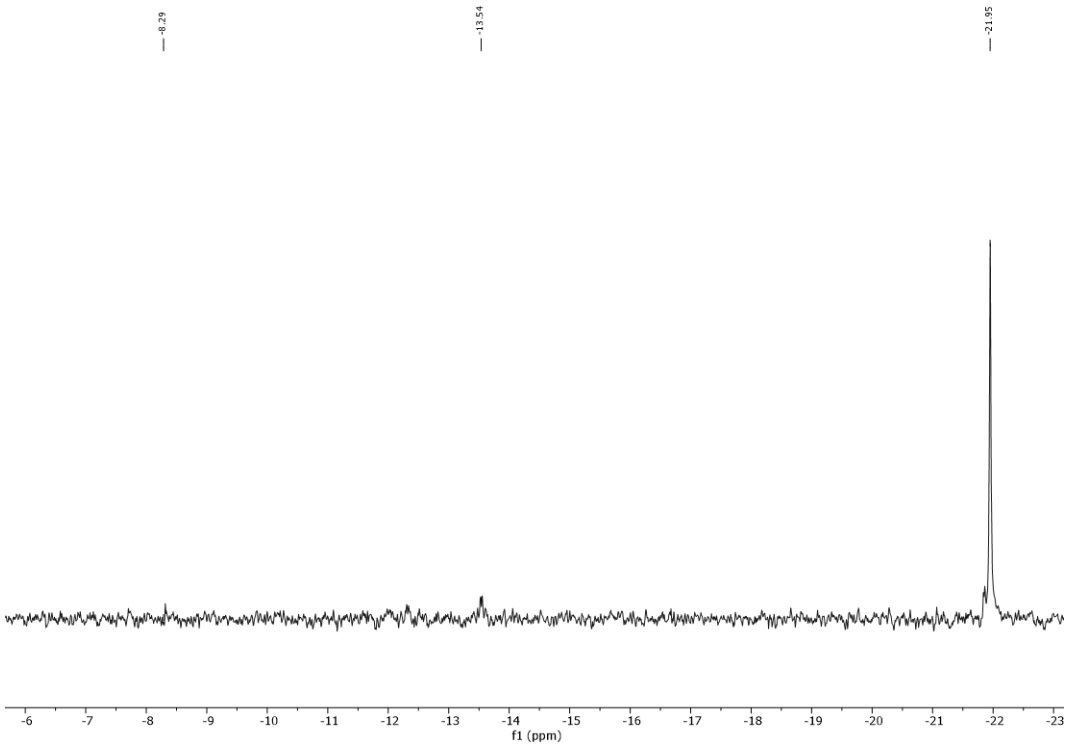

Figure A 54: ^{29}Si-IG NMR spectrum of CP9 ($CDCl_3$, 297.0 K, 79.5 MHz).

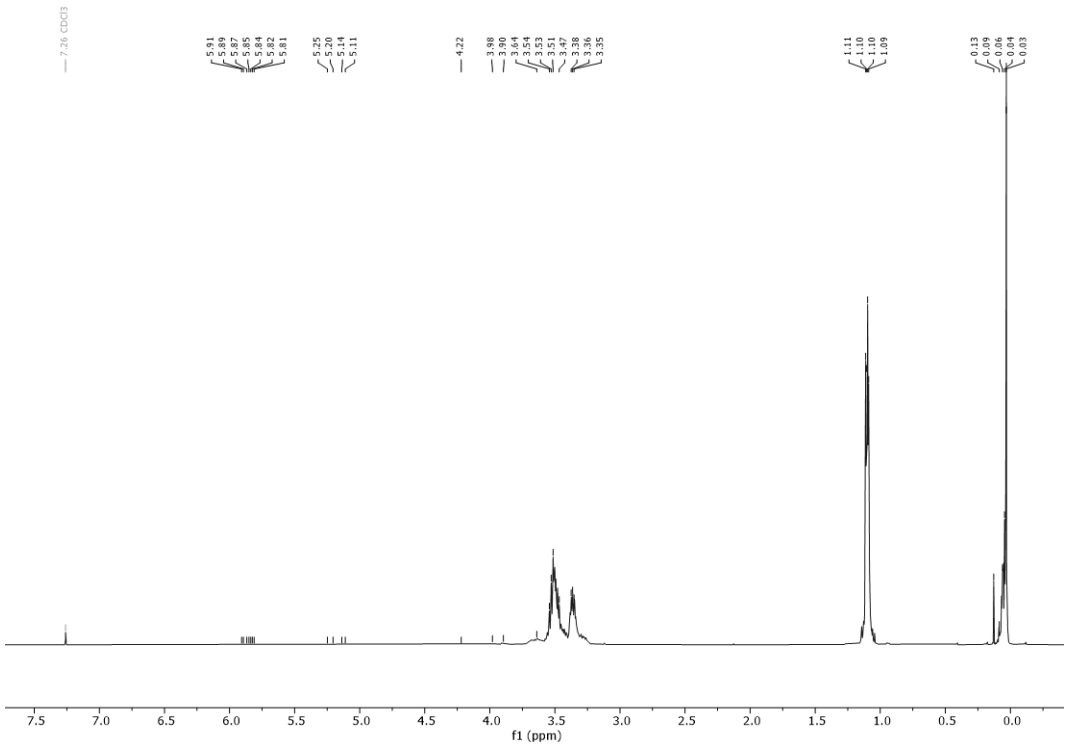

Figure A 55: ^{1}H NMR spectrum of CP9 ($CDCl_3$ 297.0 K, 400 MHz).

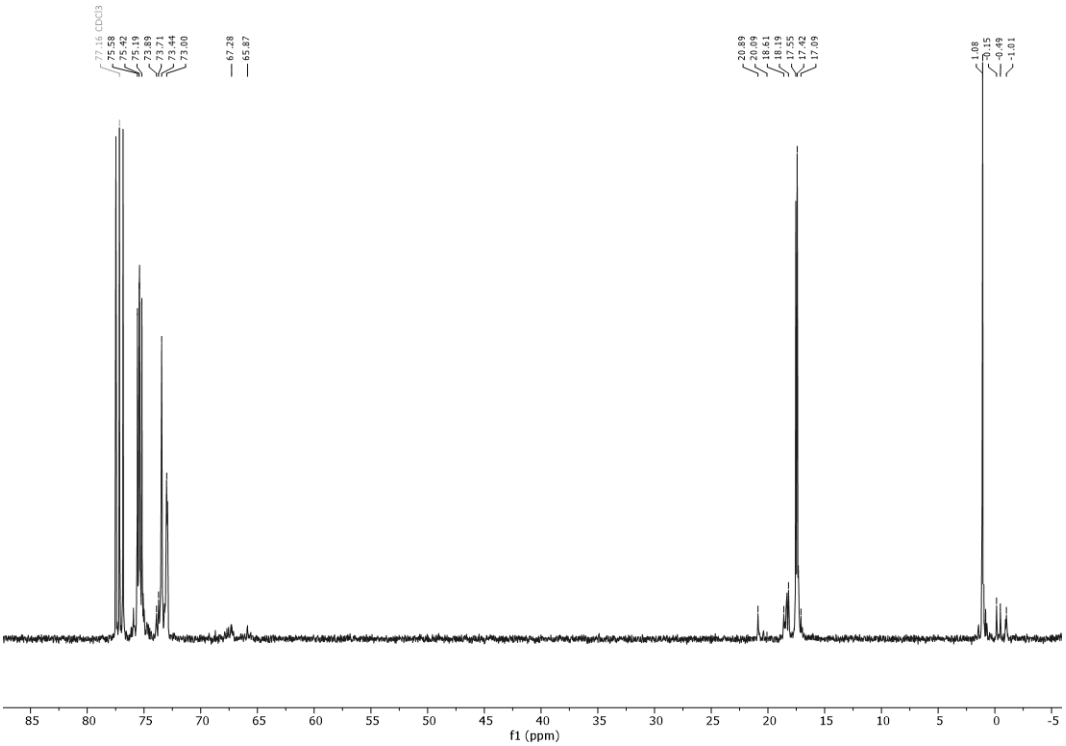

Figure A 56: ^{13}C NMR spectrum of CP9 ($CDCl_3$, 297.0 K, 100 MHz).

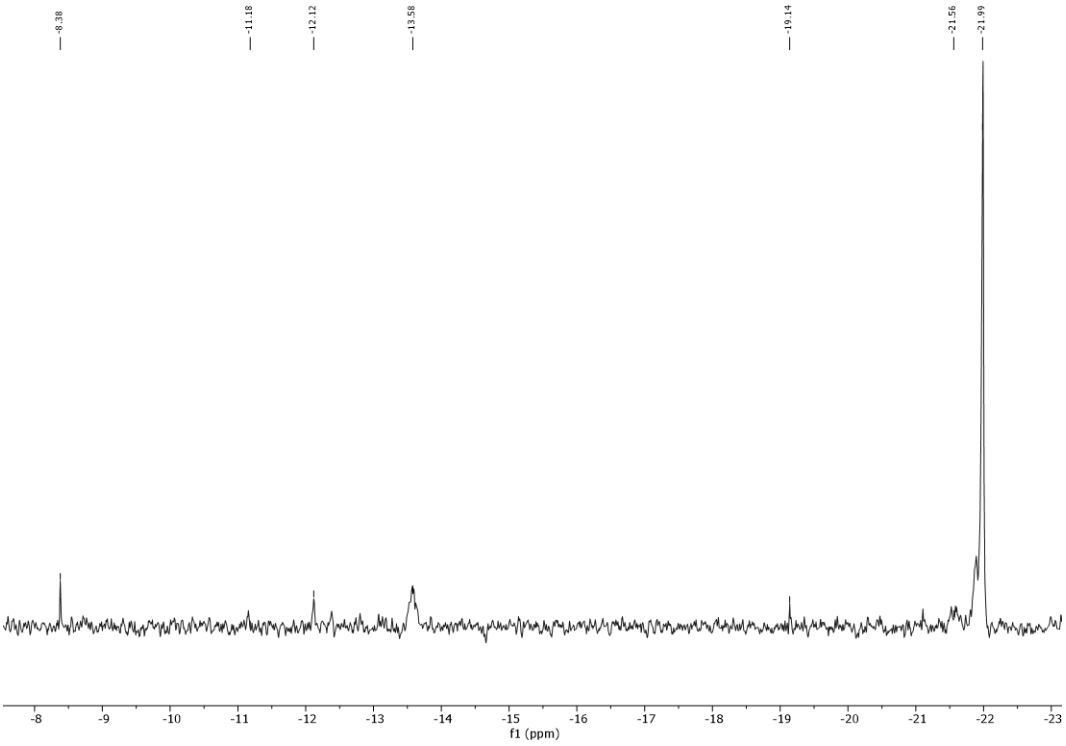

Figure A 57: ^{29}Si-IG NMR spectrum of CP9 ($CDCl_3$, 297.0 K, 79.5 MHz).

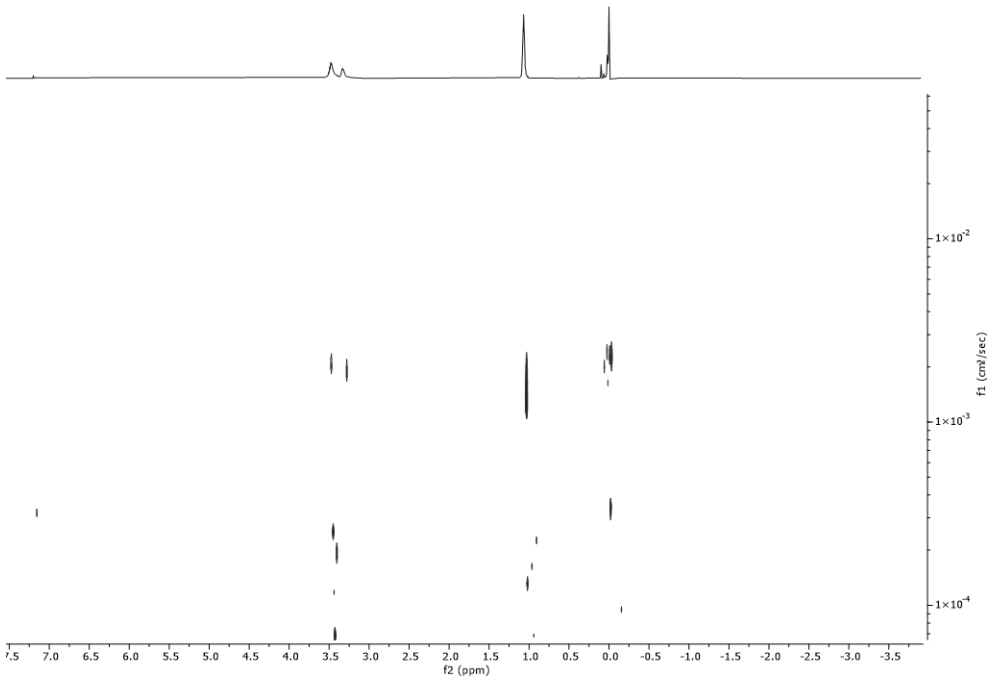

Figure A 58: ^{1}H DOSY NMR spectrum of CP9 ($CDCl_3$, 298 K, 500 MHz)

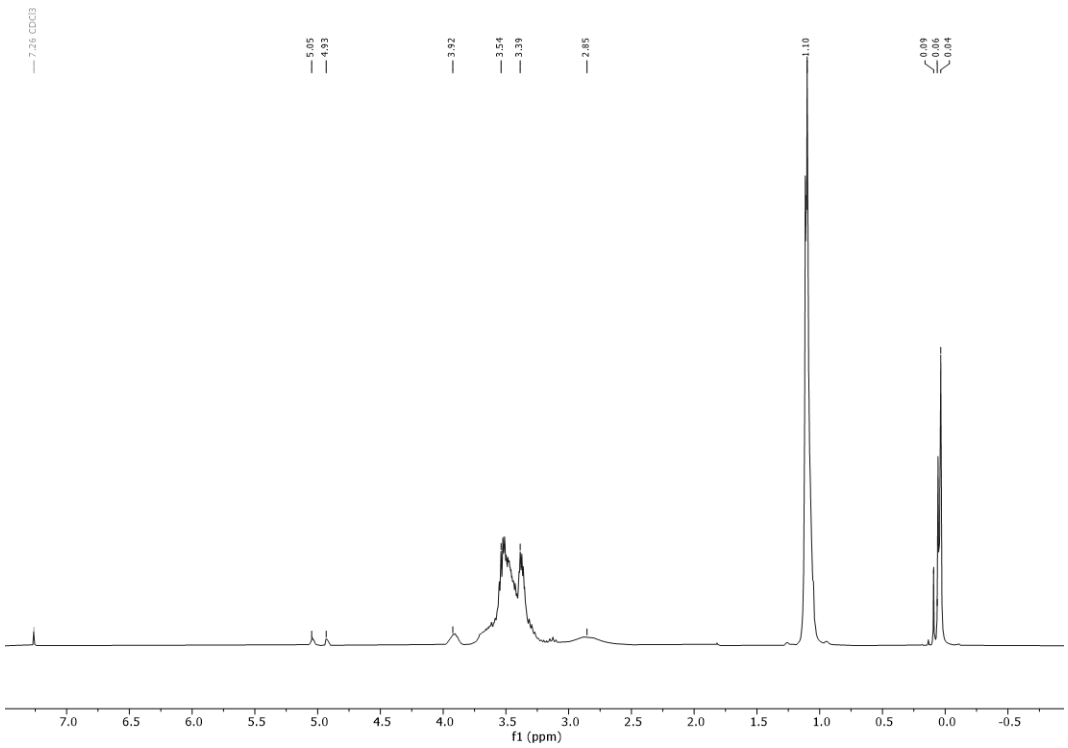

Figure A 59: ^{1}H NMR spectrum of CP9 after hydrolytic degradation ($CDCl_3$, 297.0 K, 400 MHz).

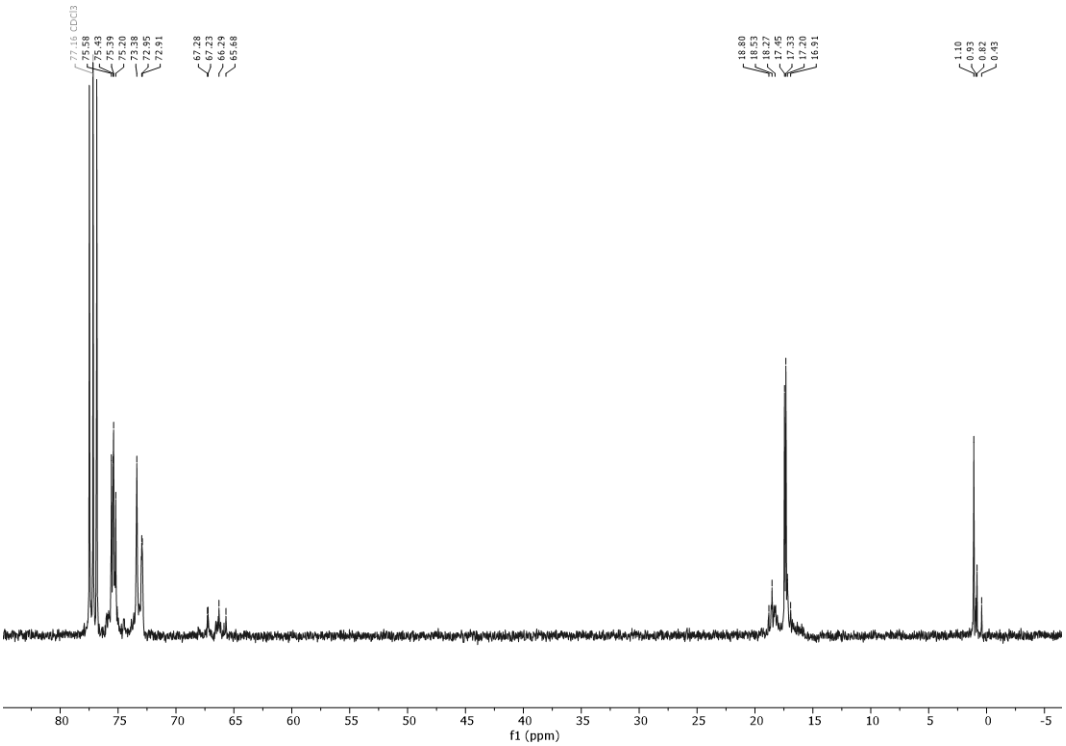

Figure A 60: ^{13}C NMR spectrum of CP9 after hydrolytic degradation ($CDCl_3$, 297.0 K, 100 MHz).

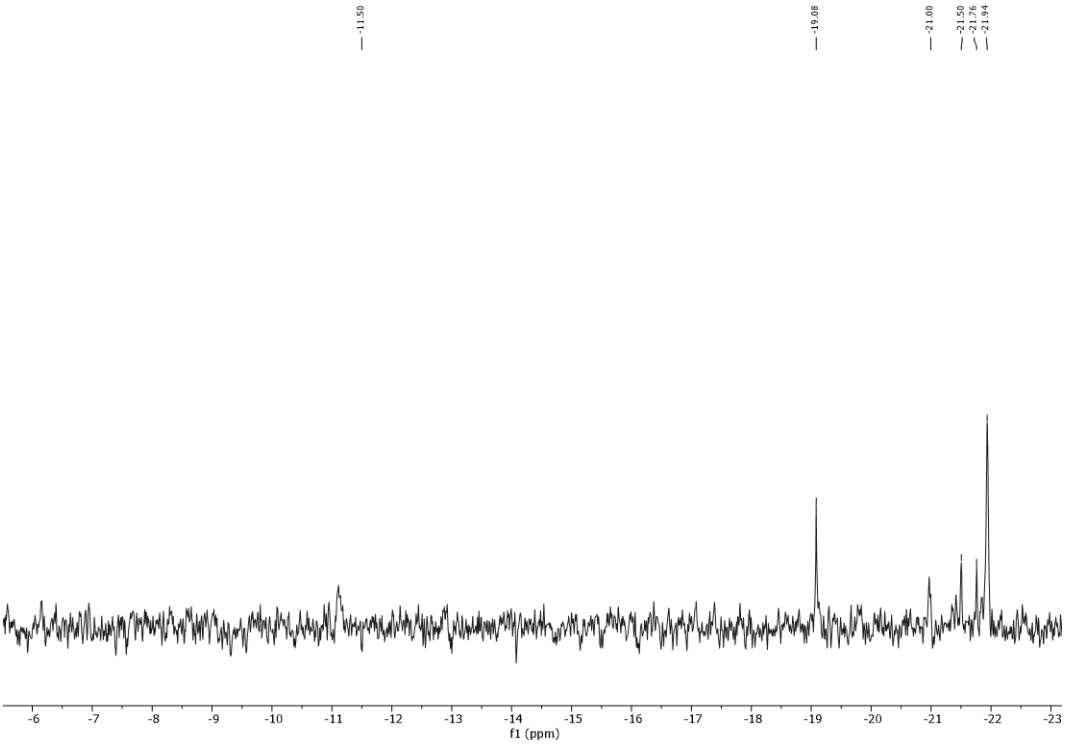

Figure A 61: ^{29}Si-IG NMR spectrum of CP9 after hydrolytic degradation ($CDCl_3$, 297.0 K, 79.5 MHz).

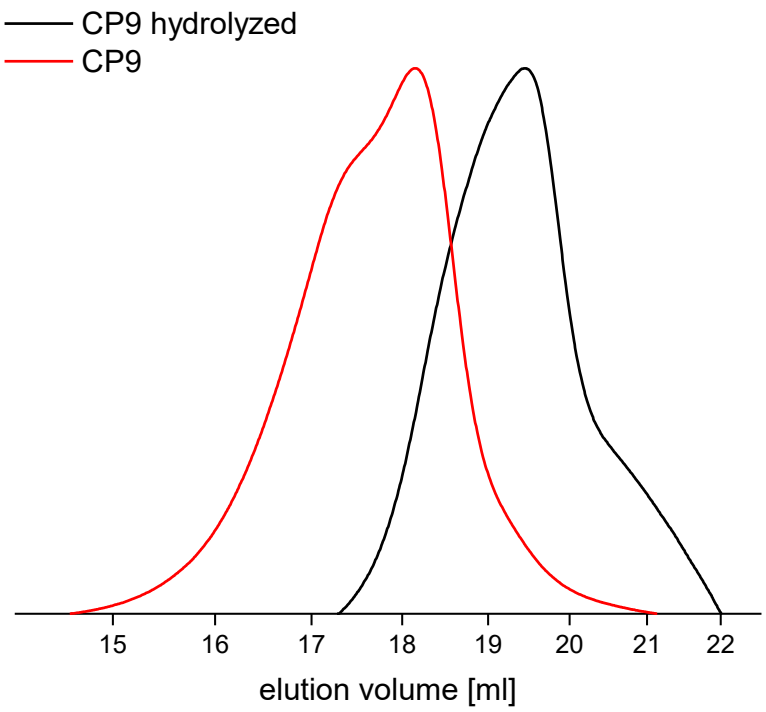

Figure A 62: GPC before and after exposing CP9 to diluted HCl (eluent: THF; polystyrene standard).

A-3.10 CP10

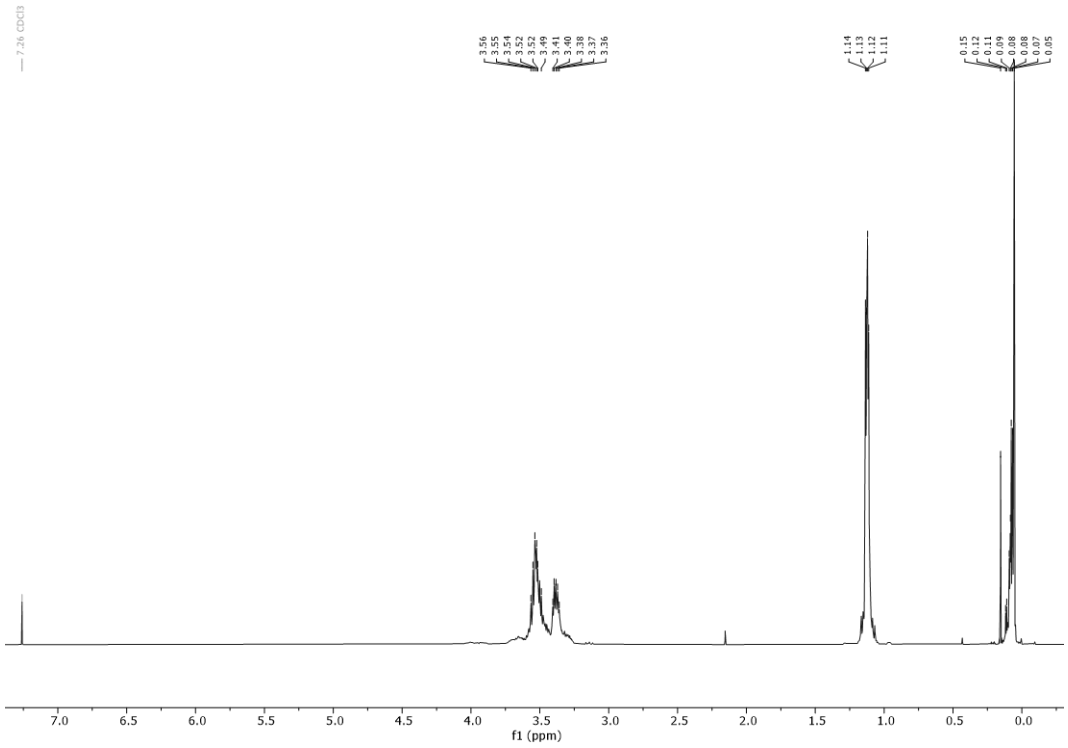

Figure A 63: ^{1}H NMR spectrum of CP10 ($CDCl_3$ 297.0 K, 400 MHz).

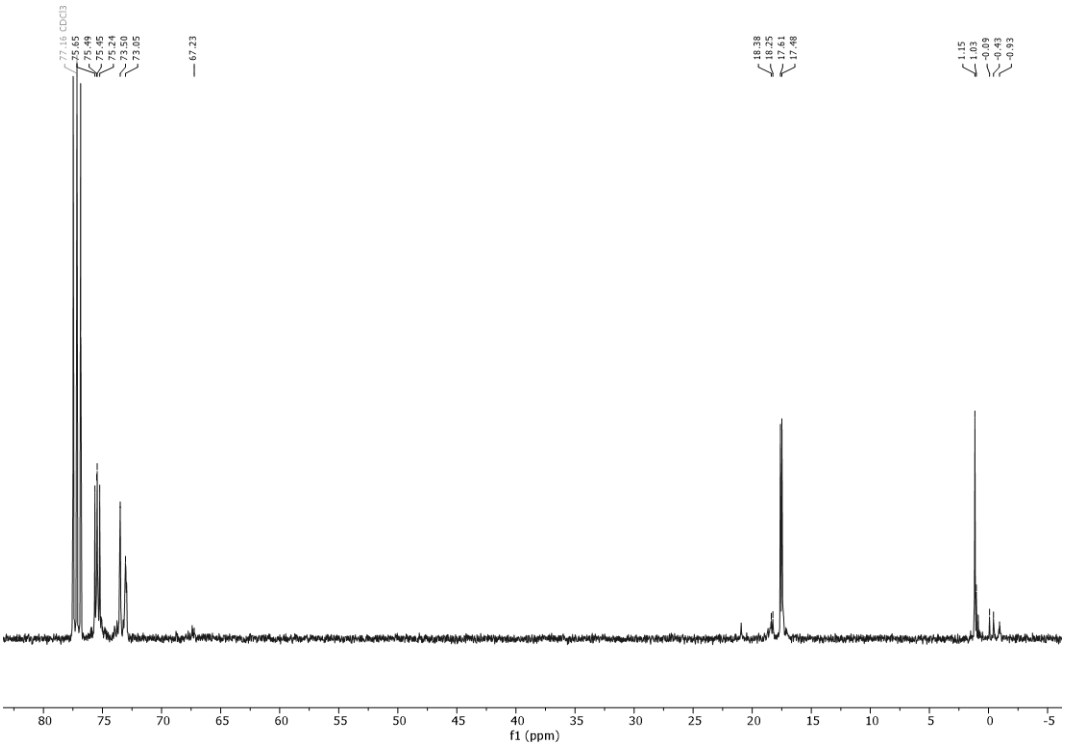

Figure A 64: ^{13}C NMR spectrum of CP10 ($CDCl_3$, 297.0 K, 100 MHz).

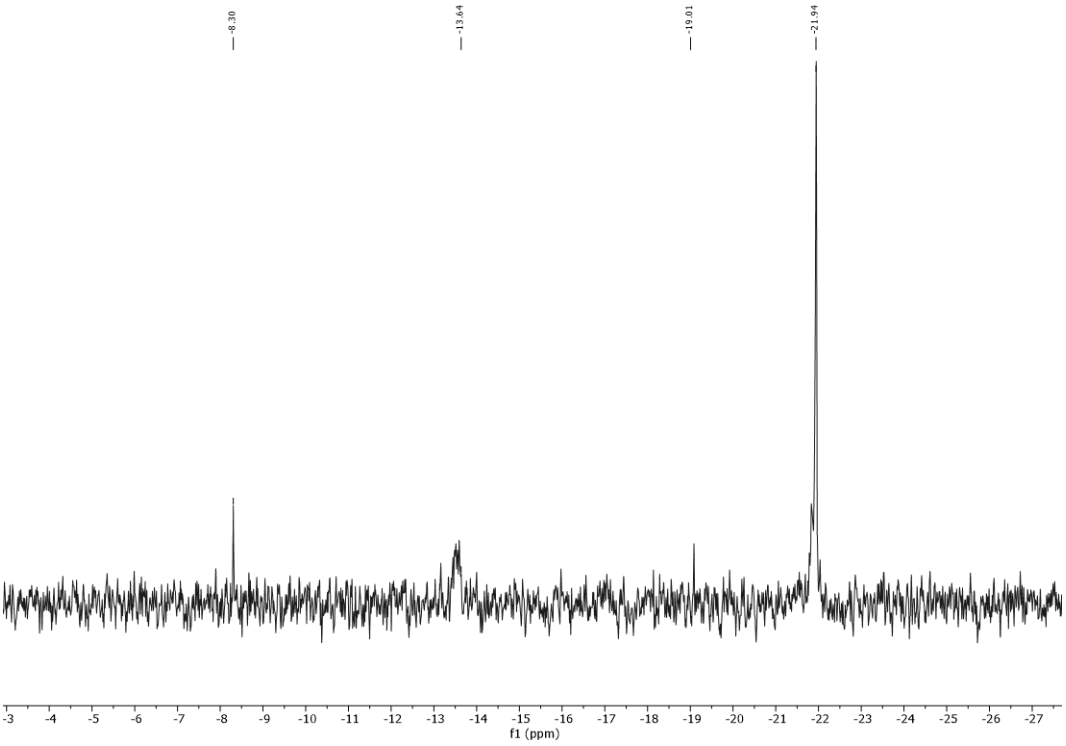

Figure A 65: ^{29}Si-IG NMR spectrum of CP10 ($CDCl_3$, 297.0 K, 79.5 MHz).

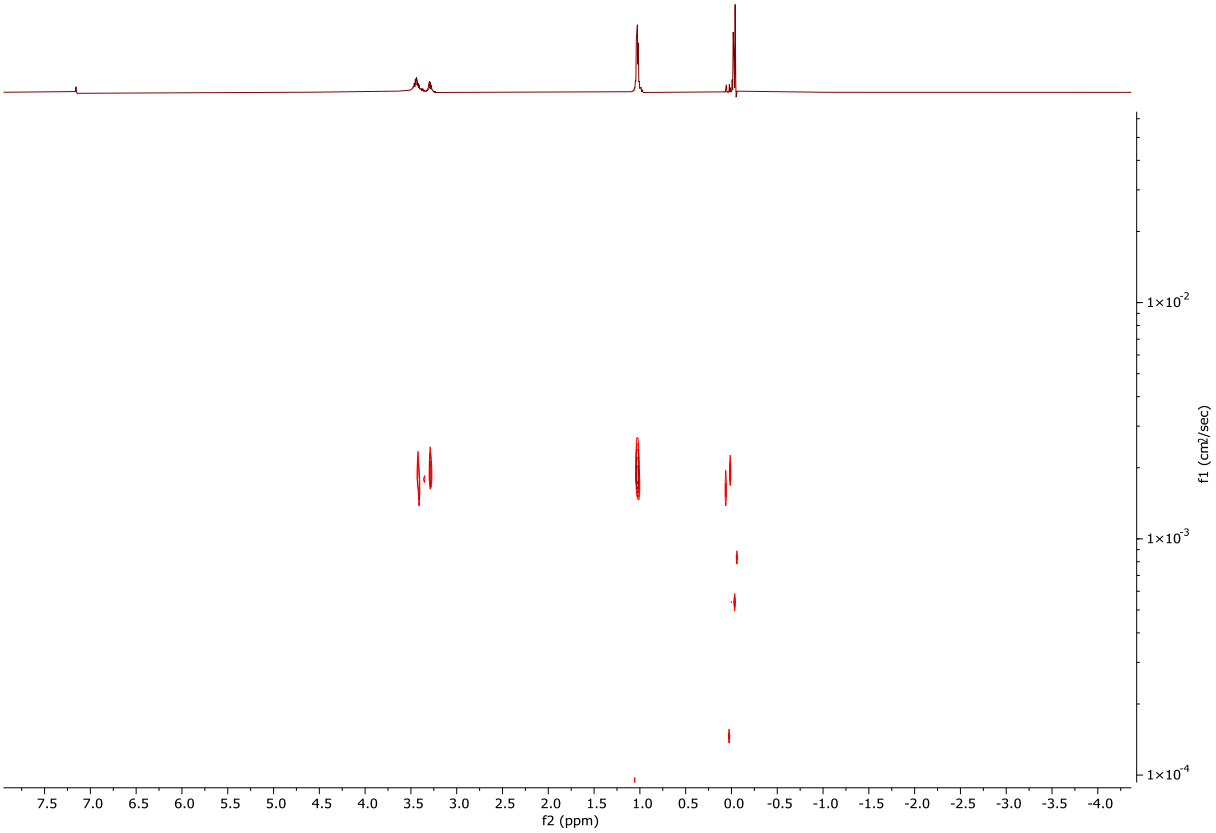

Figure A 66: DOSY 1H NMR (CDCl3, 298 K, 500 MHz) of CP10.

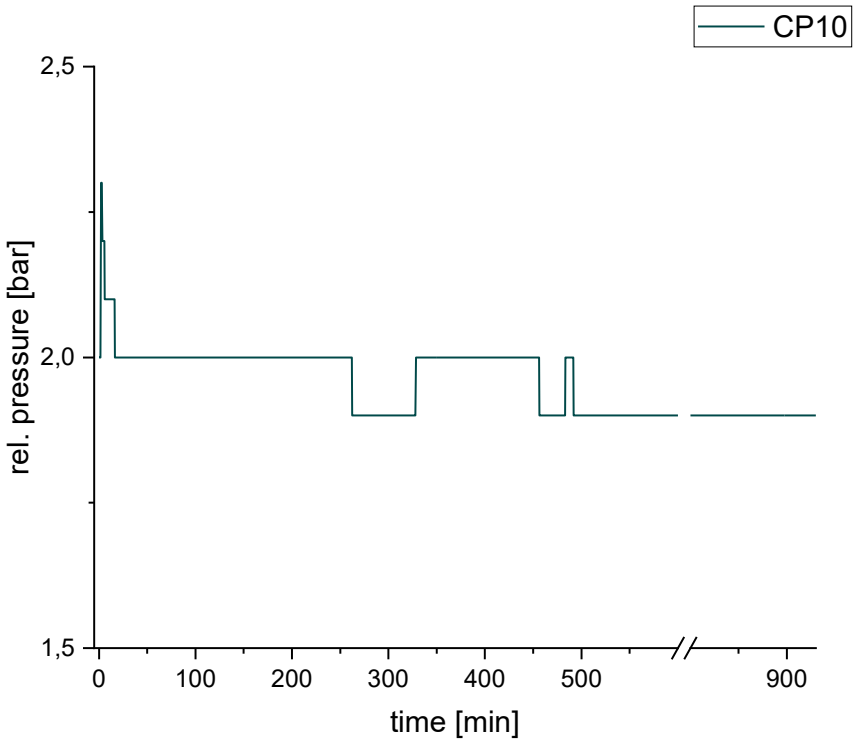

Figure A 67: Pressure course of the polymerization reaction of CP10 in a 1 L reactor.

A-3.11 PLA prepared using DMC2

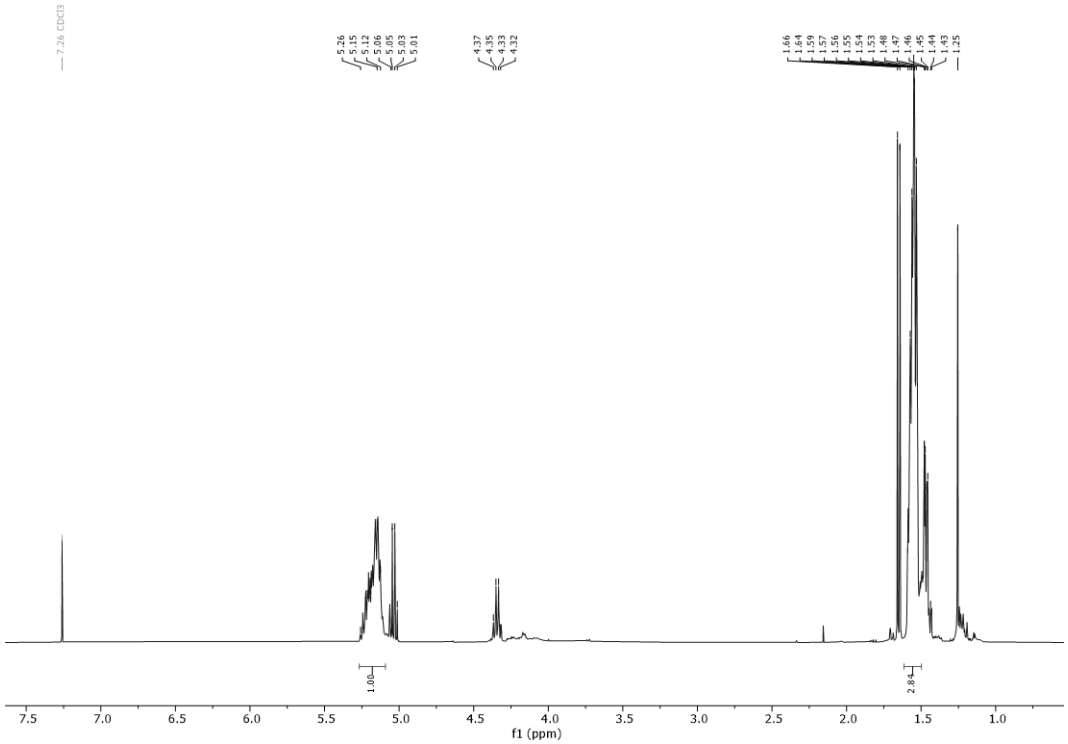

Figure A 68: ^{1}H NMR spectrum of PLA polymerized using **DMC2** as catalyst ($CDCl_3$, 400 MHz, 297.0 K).

A-3.12 PPCLA

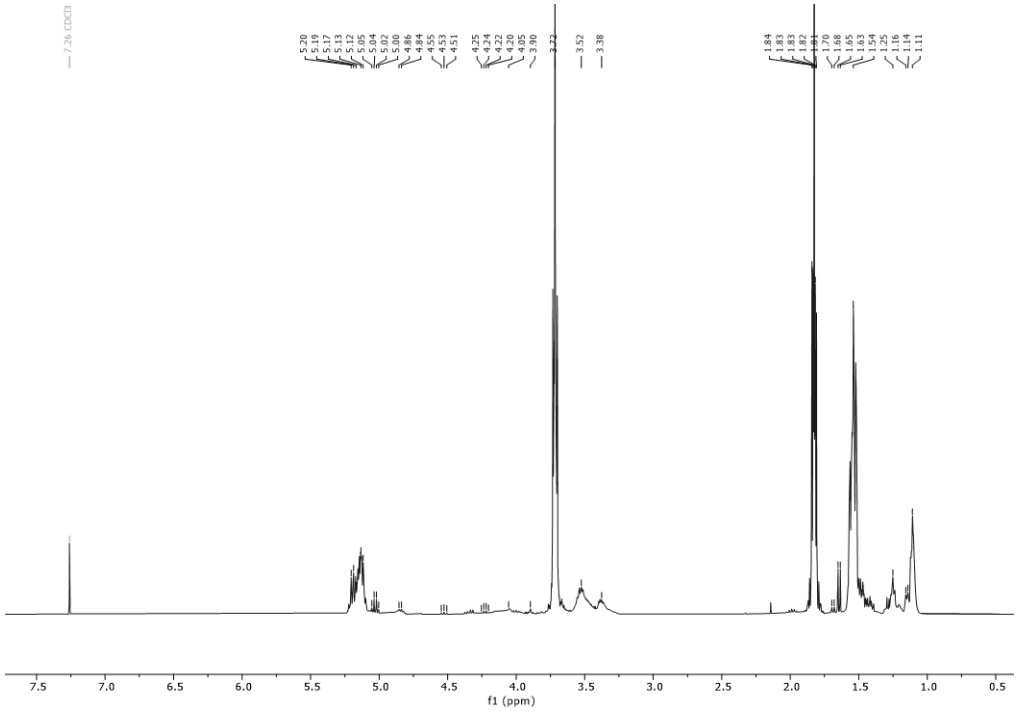

Figure A 69: ^{1}H NMR spectrum of PPCLA before workup ($CDCl_3$ 297.0 K, 400 MHz).

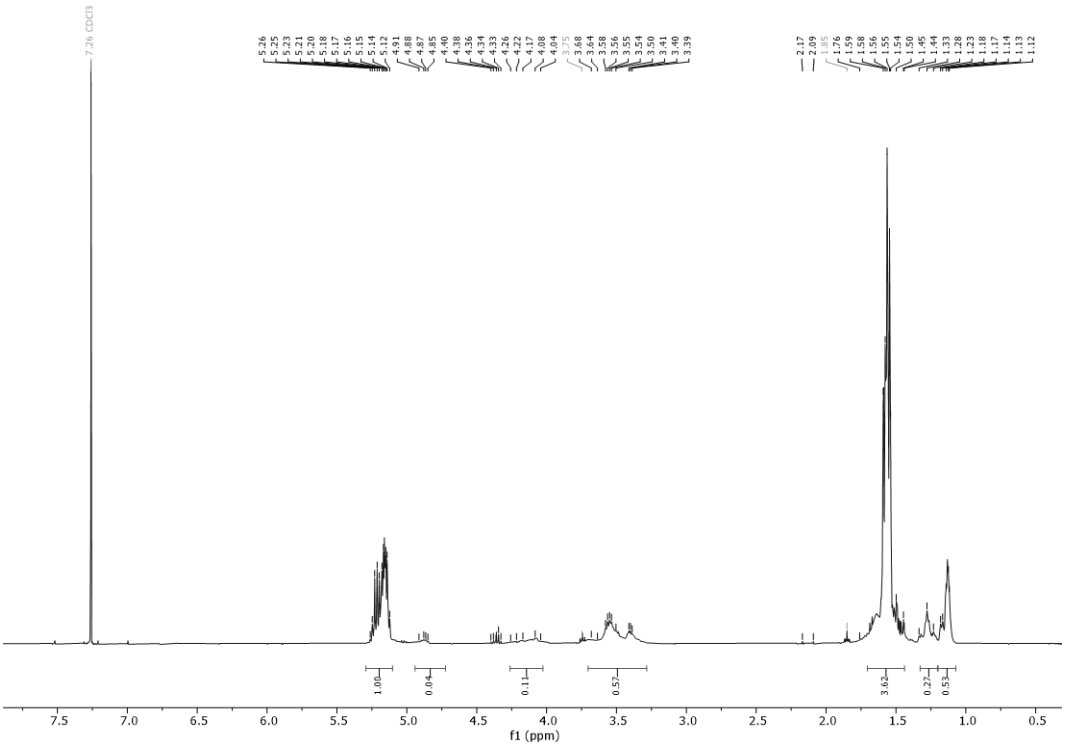

Figure A 70: ^{1}H NMR spectrum of PPCLA ($CDCl_3$ 297.0 K, 400 MHz).

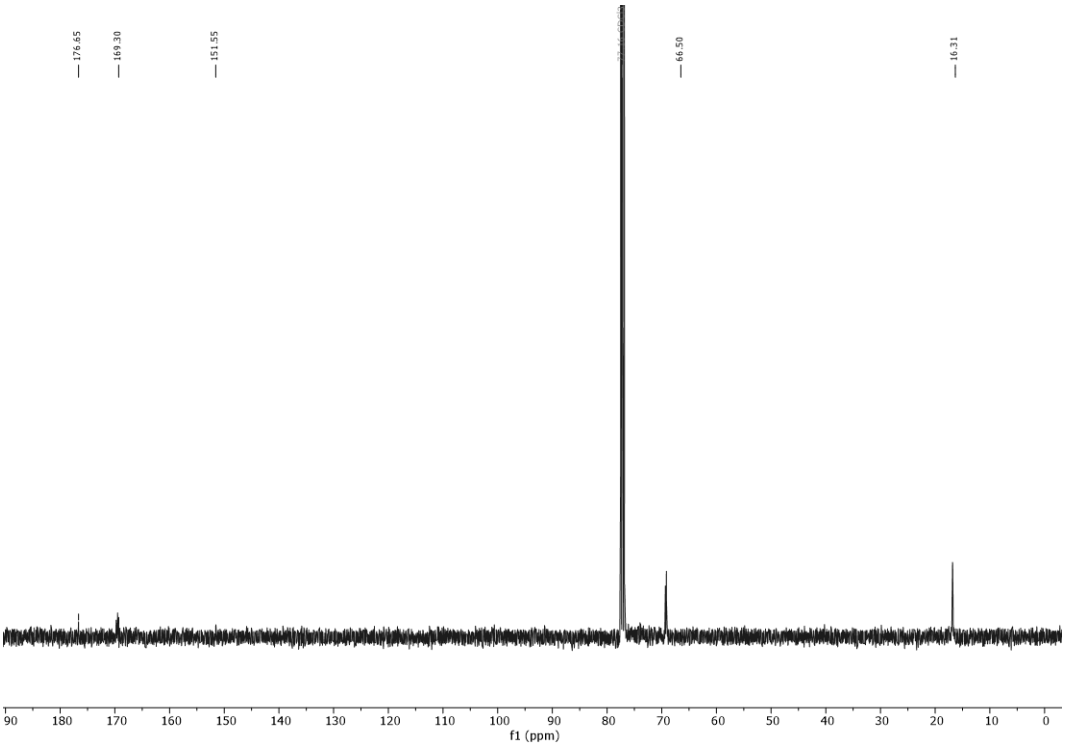

Figure A 71: ^{13}C NMR spectrum of PCCLA ($CDCl_3$, 297.3 K, 100 MHz)

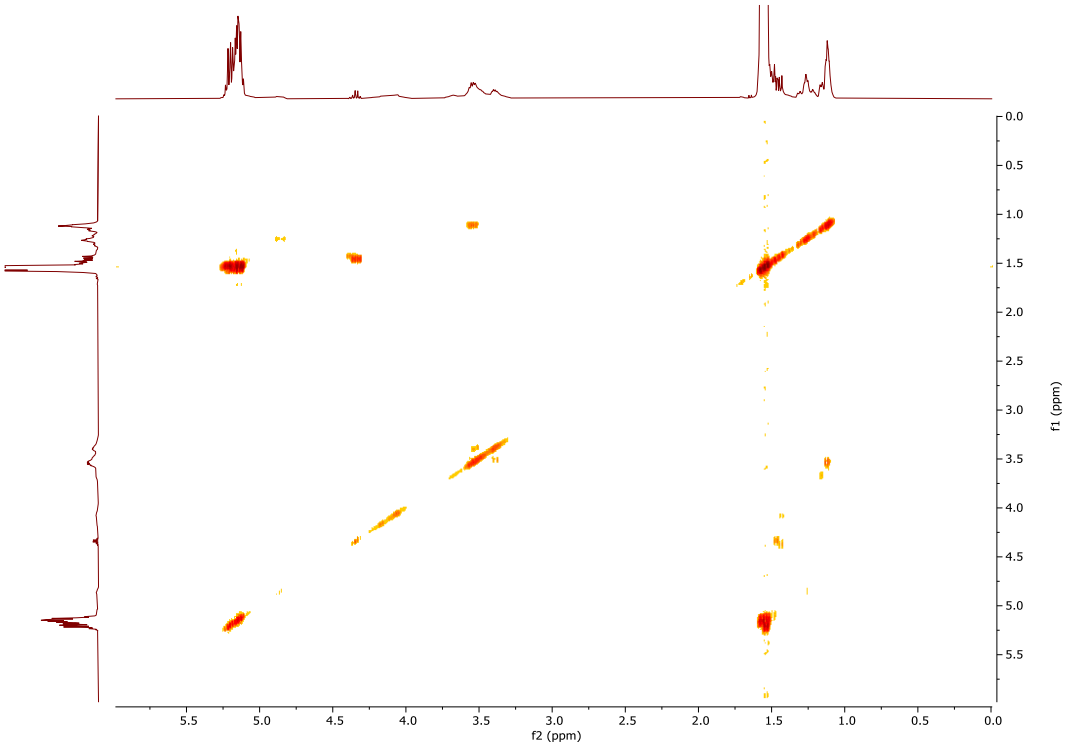

Figure A 72: $^{1}H^{1}H$-COSY spectrum of PPCLA ($CDCl_3$, 400 MHz, 297 K).

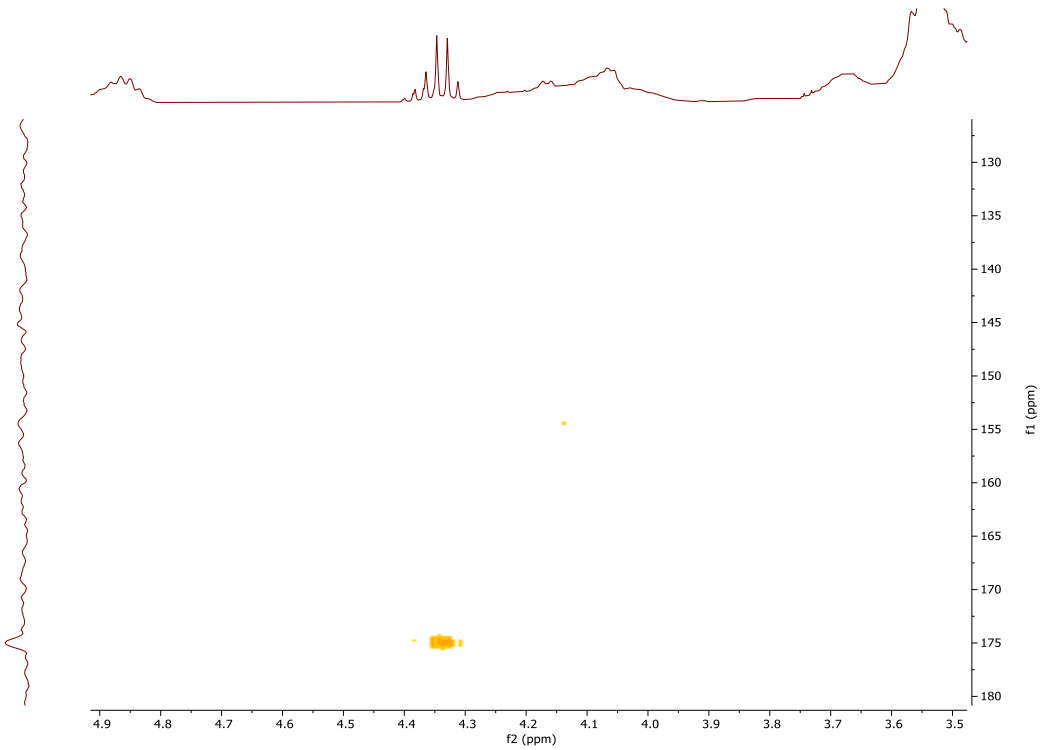

Figure A 73: $^{1}H^{13}C$-HMBC spectrum of PPCLA ($CDCl_3$, 400 MHz, 297 K).

A-3.13 PPCCL

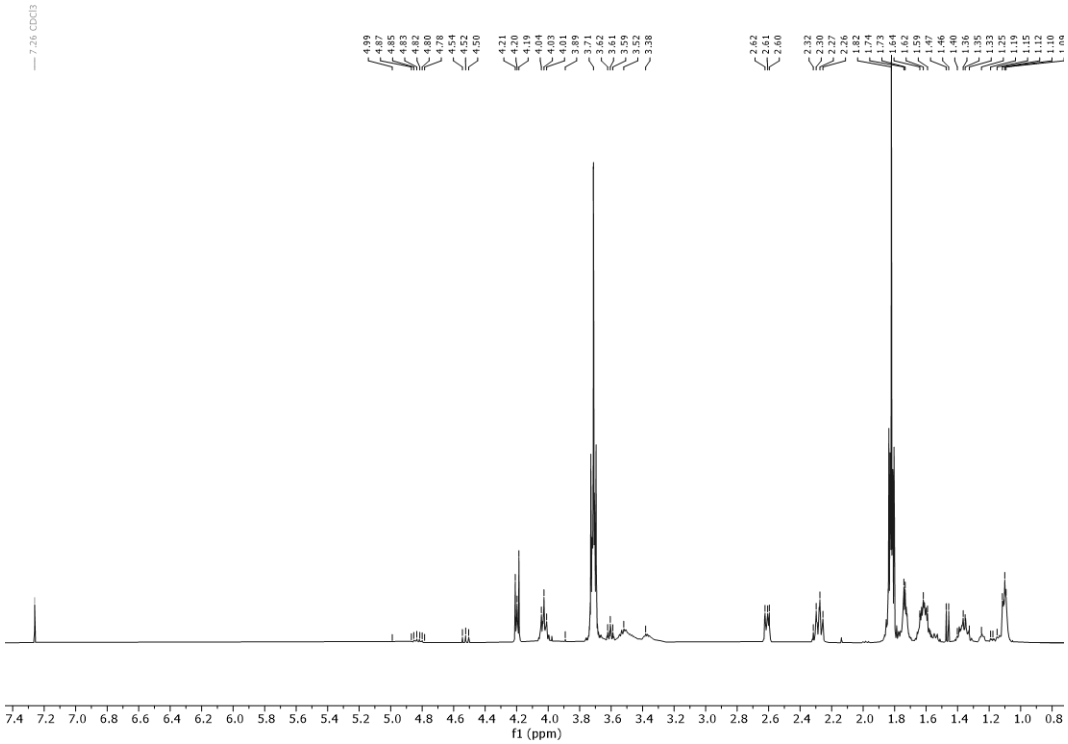

Figure A 74: ^{1}H NMR spectrum of PPCCL before workup ($CDCl_3$ 297.0 K, 400 MHz).

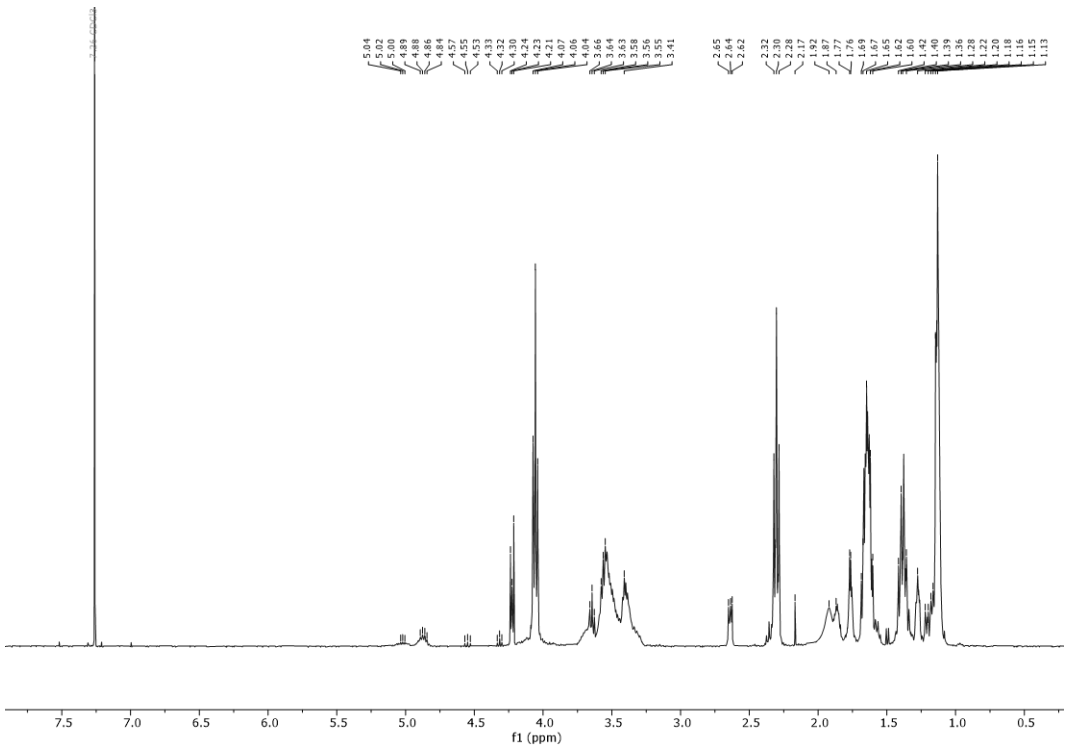

Figure A 75: ^{1}H NMR spectrum of PPCCL ($CDCl_3$ 297.0 K, 300 MHz).

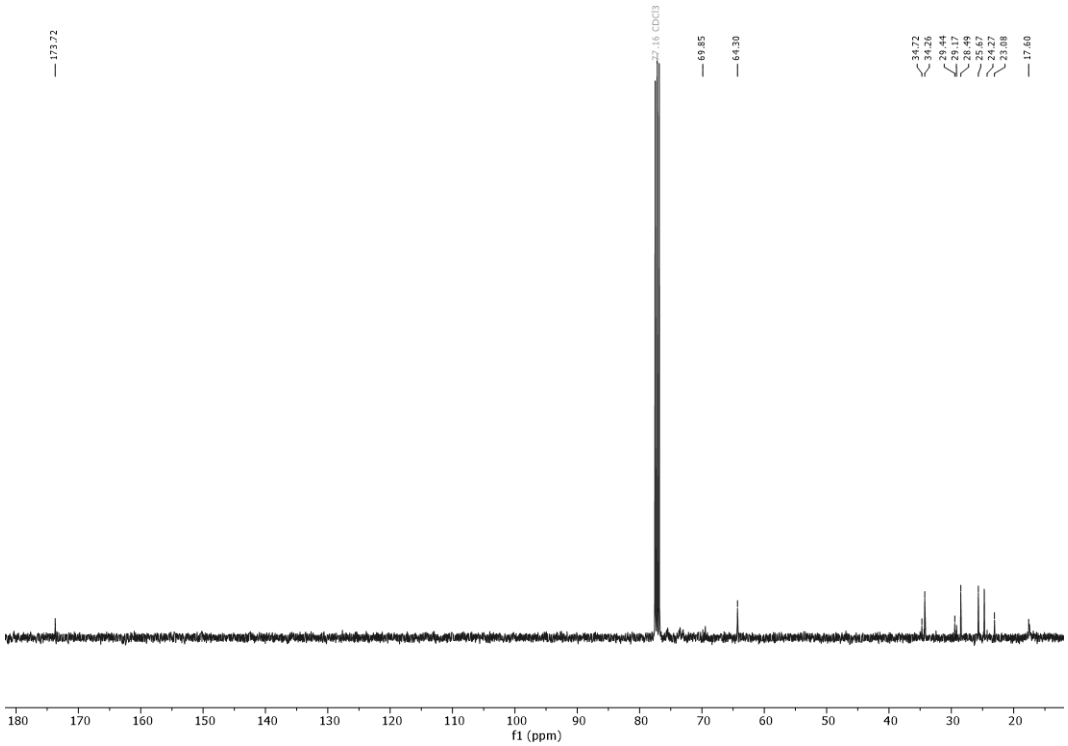

Figure A 76: ^{13}C NMR spectrum of PPCCL ($CDCl_3$ 297.0 K, 100 MHz).

A-3.14 PCHCLA

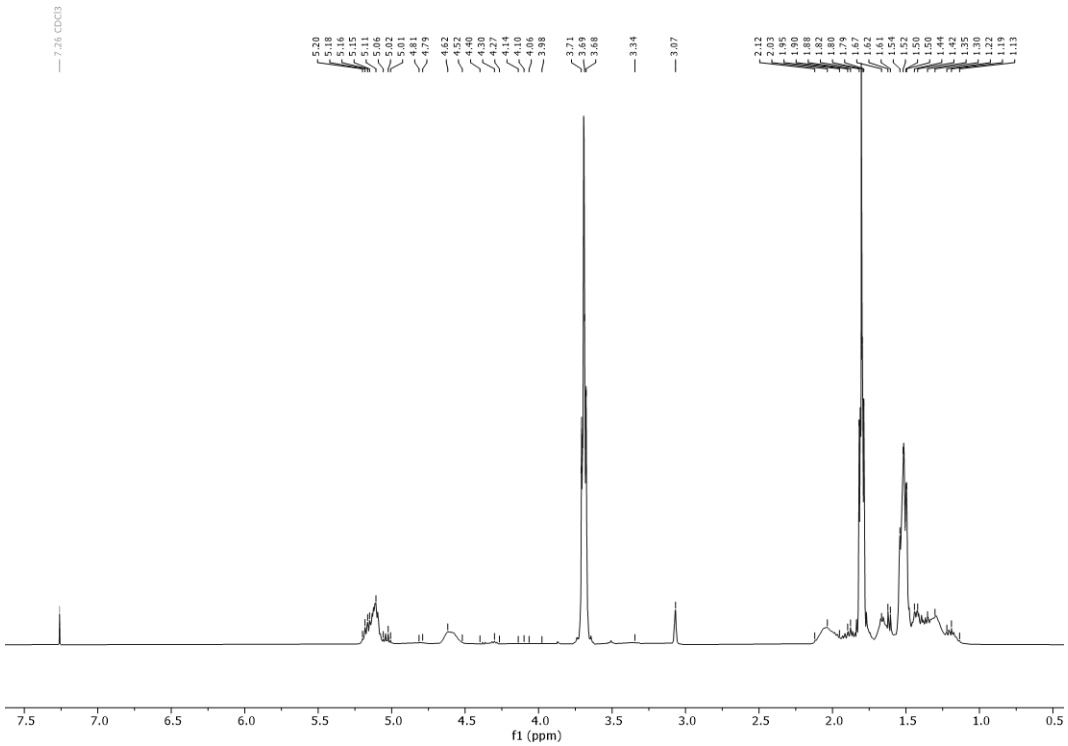

Figure A 77: ^{1}H NMR spectrum of PCHCLA before workup ($CDCl_3$ 297.0 K, 400 MHz).

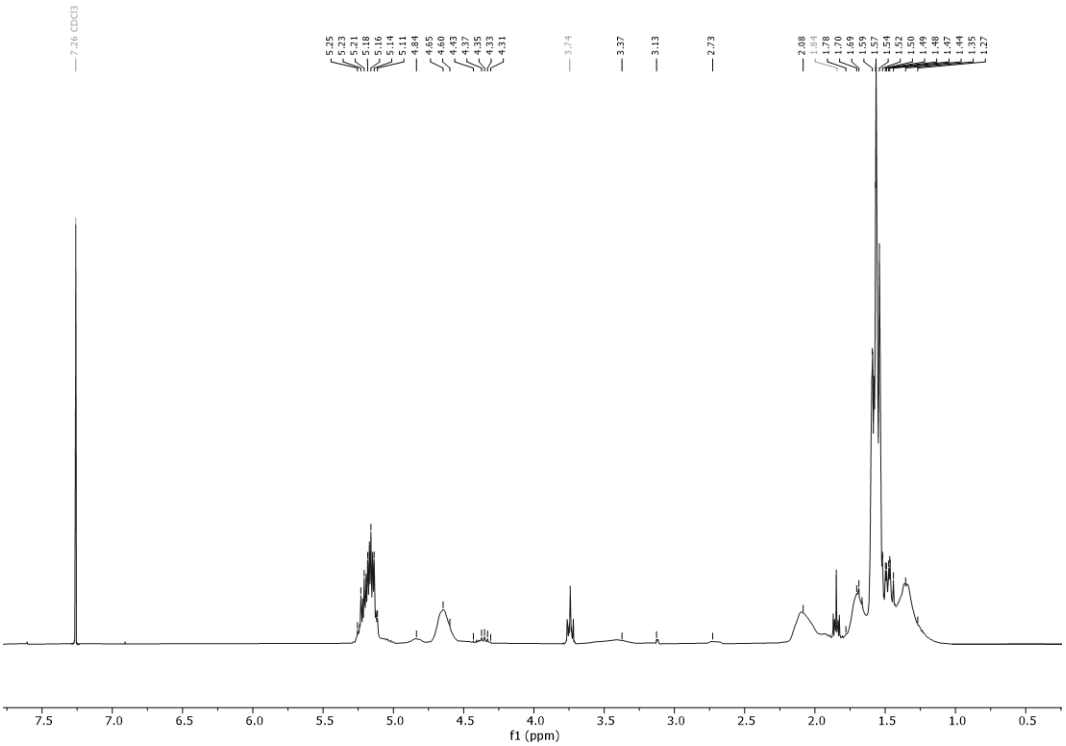

Figure A 78: ^{1}H NMR spectrum of PCHCLA ($CDCl_3$ 297.0 K, 400 MHz).

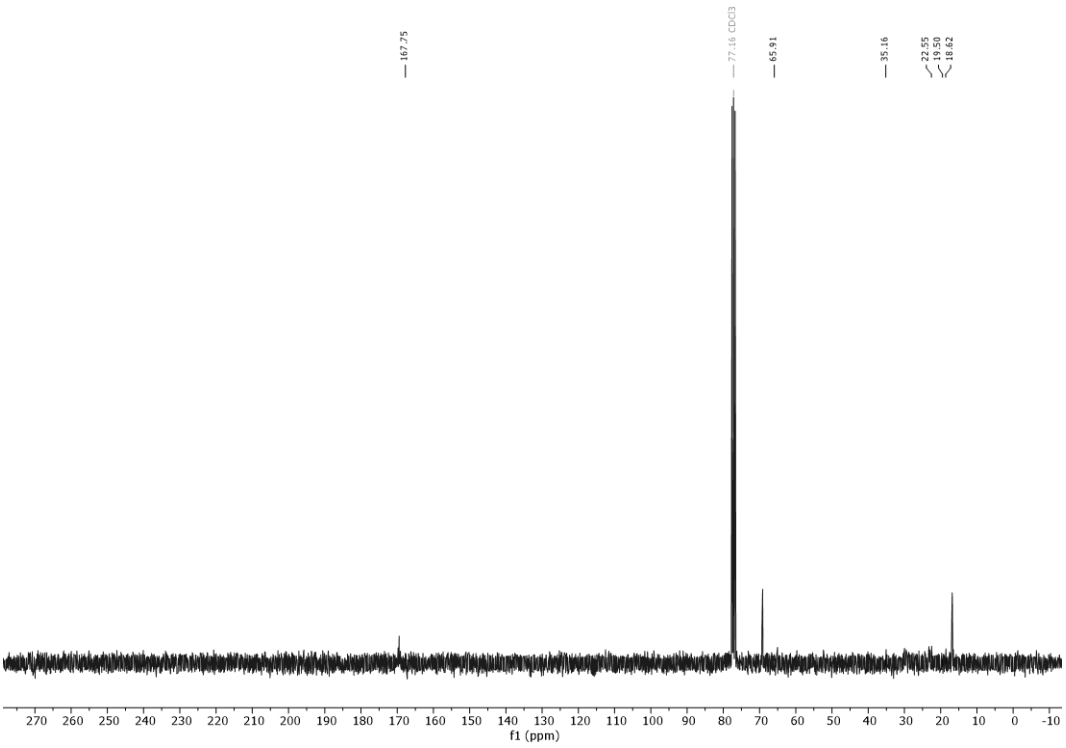

Figure A 79: ^{13}C NMR spectrum of PCHCLA (CDCl3, 299.3 K, 75.5 MHz).

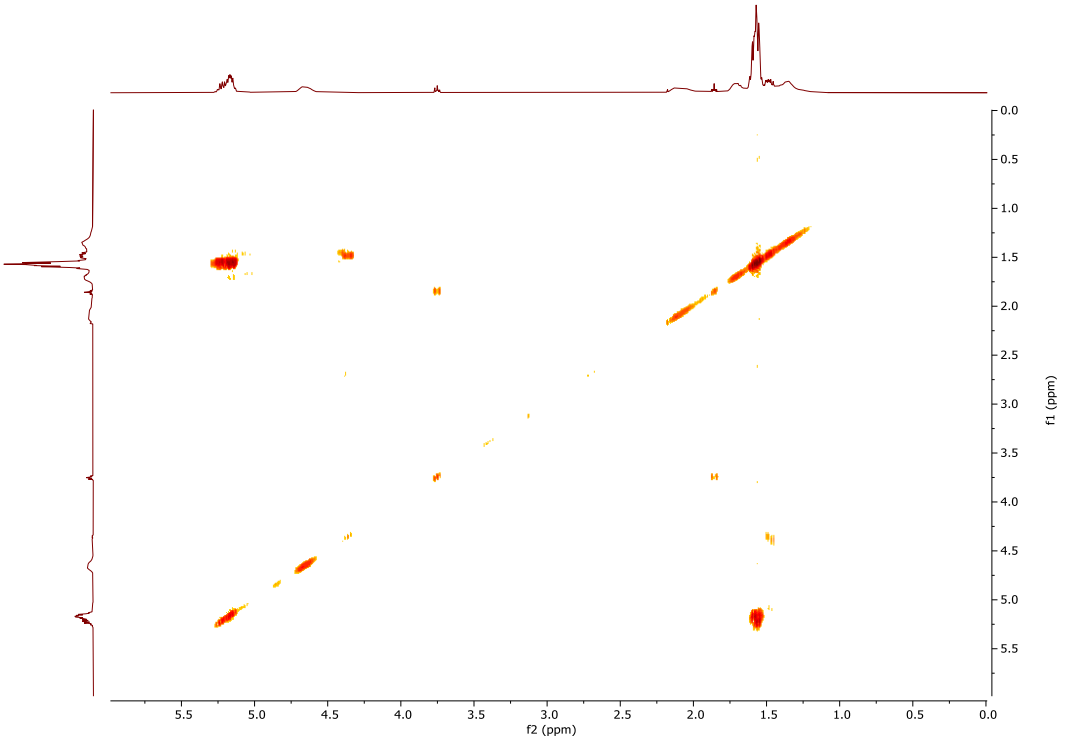

Figure A 80: $^{1}H^{1}H$ COSY NMR spectrum of PCHCLA ($CDCl_3$, 297.0 K, 400 MHz).

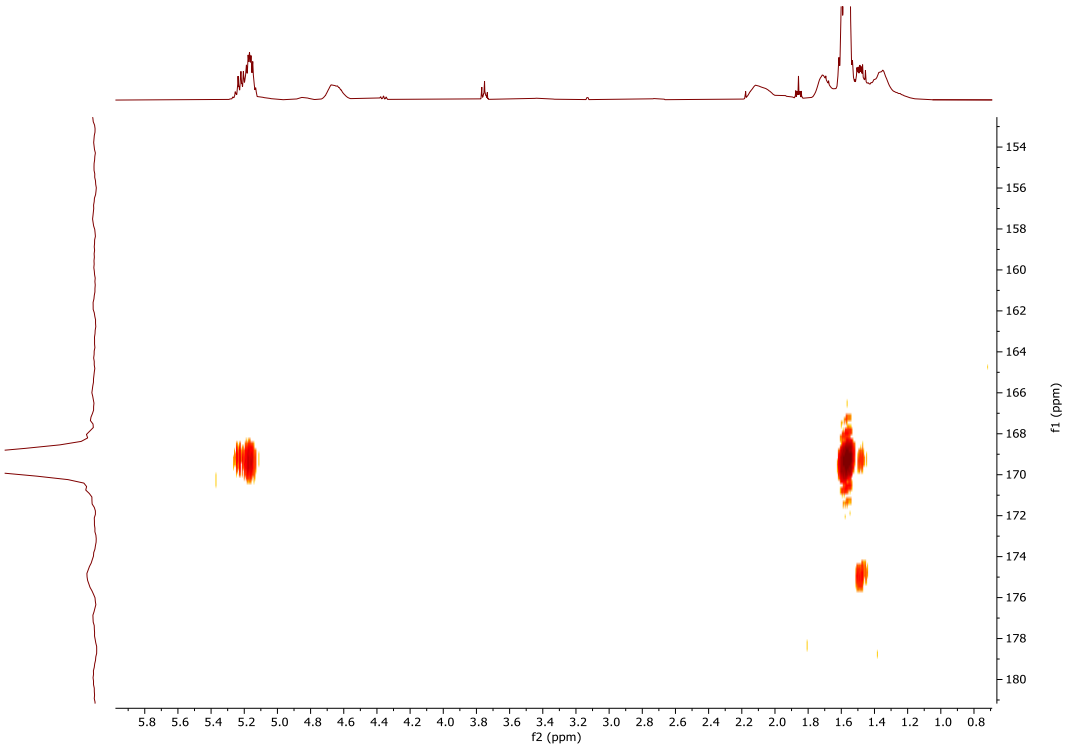

Figure A 81: $^{1}H^{13}C$-HMBC NMR of PCHCLA ($CDCl_3$, 297.0 K, 400 MHz).

A-3.15 PCHCCL

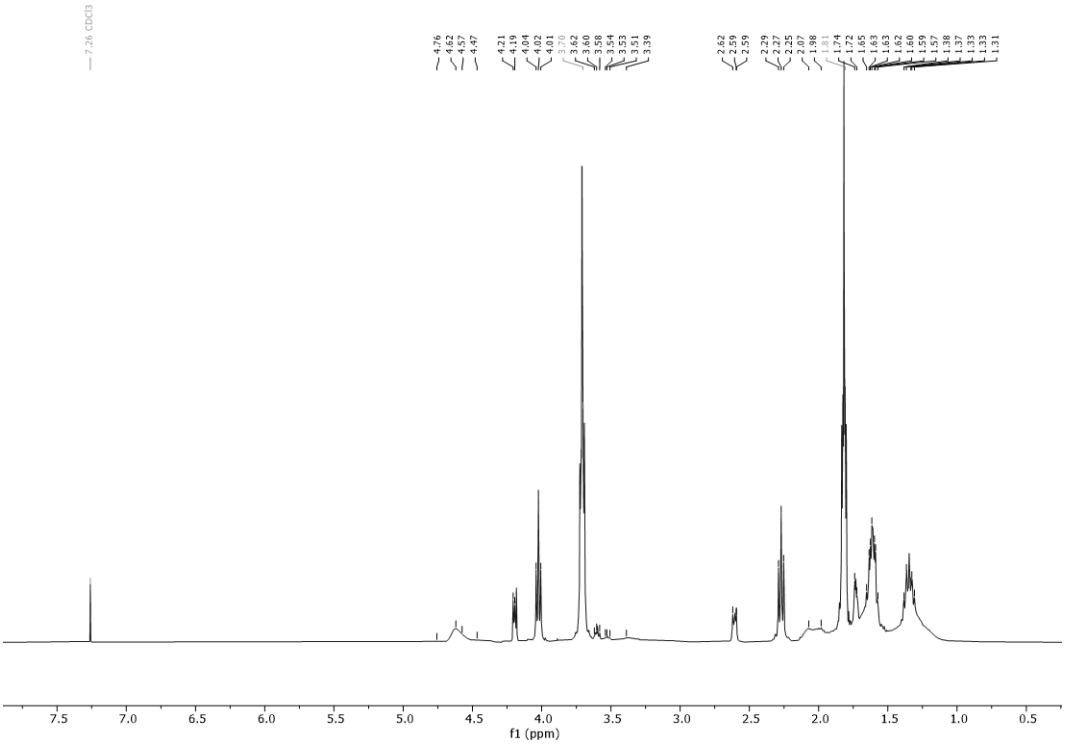

Figure A 82: ^{1}H NMR spectrum of PCHCCL before workup ($CDCl_3$ 297.0 K, 400 MHz).

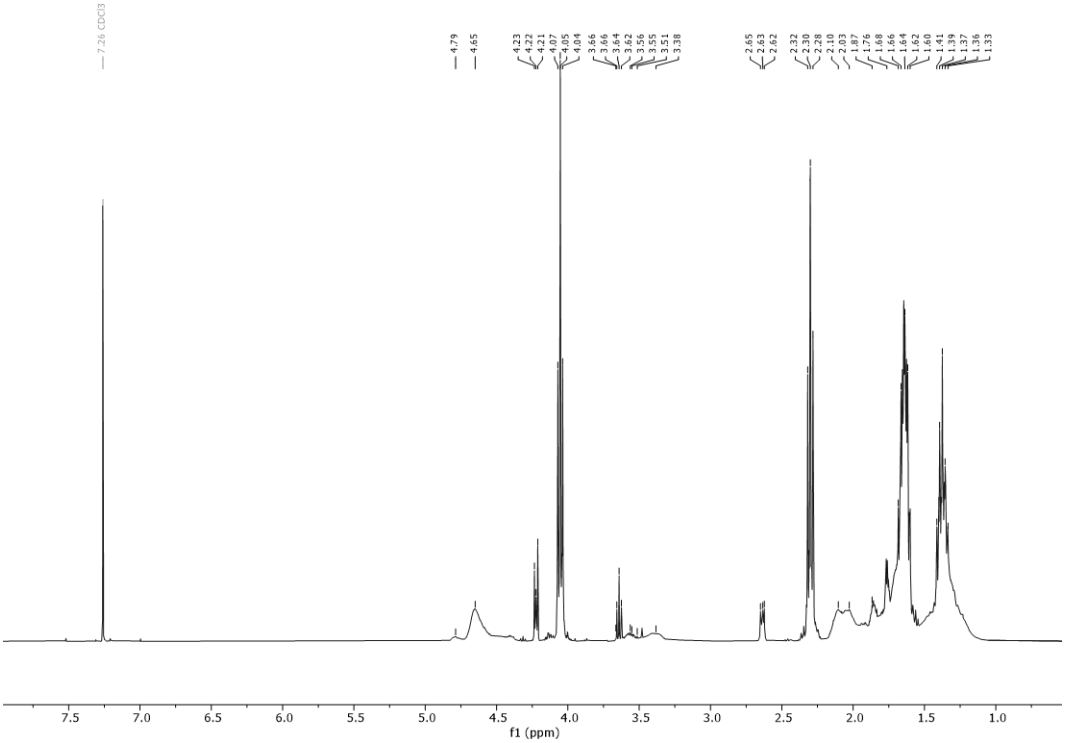

Figure A 83: ^{1}H NMR spectrum of PCHCCL ($CDCl_3$ 299.5 K, 300 MHz).

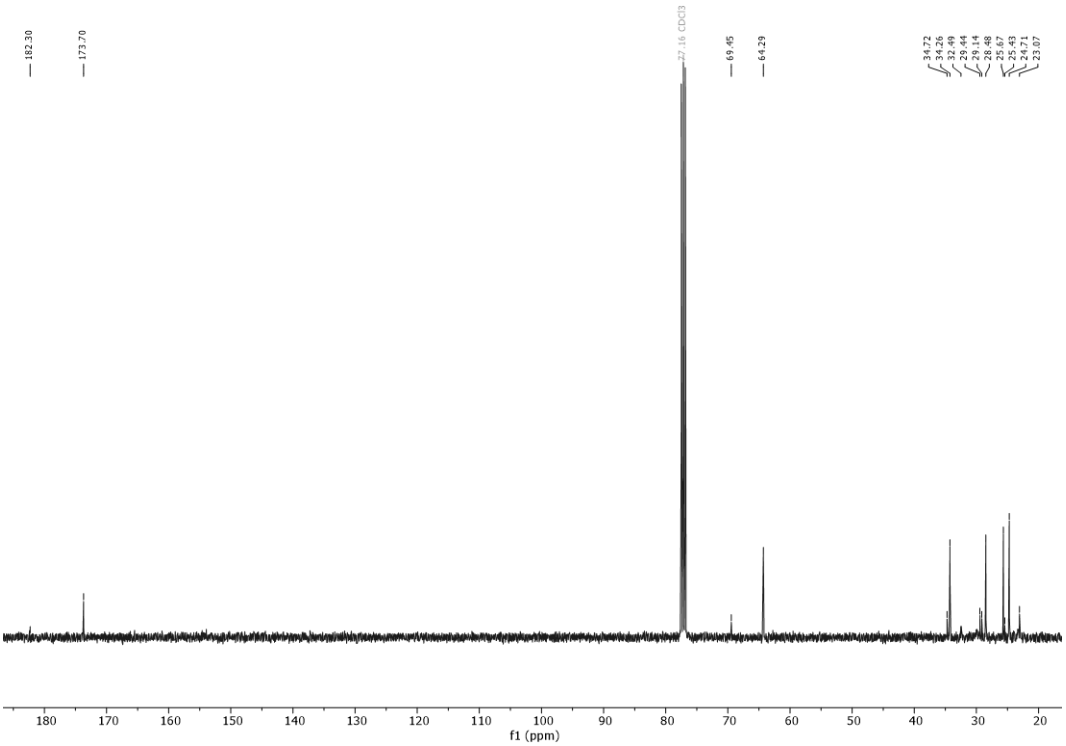

Figure A 84: ^{13}C NMR spectrum of PCHCCL ($CDCl_3$ 299.2 K, 75 MHz).

A-4 Appendix Chapter 4.3

A-4.1 $L_{NN}1$

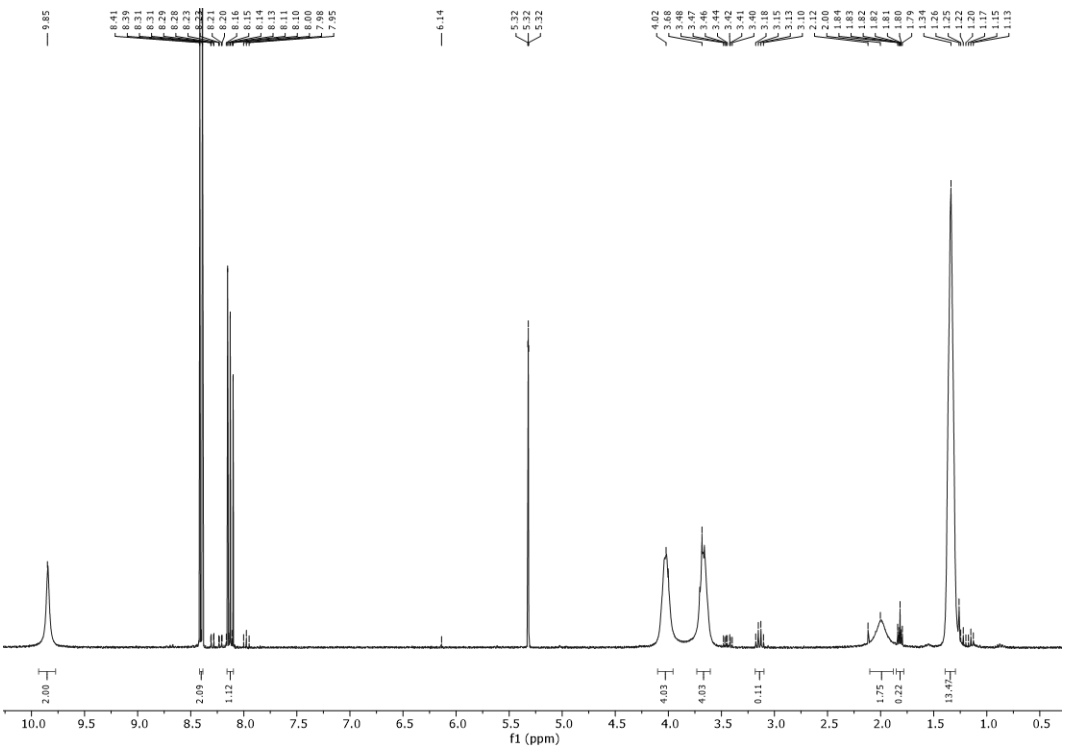

Figure A 85: ^1H NMR spectrum of **$L_{NN}1$** (CD_2Cl_2, 300 MHz, 298.0 K).

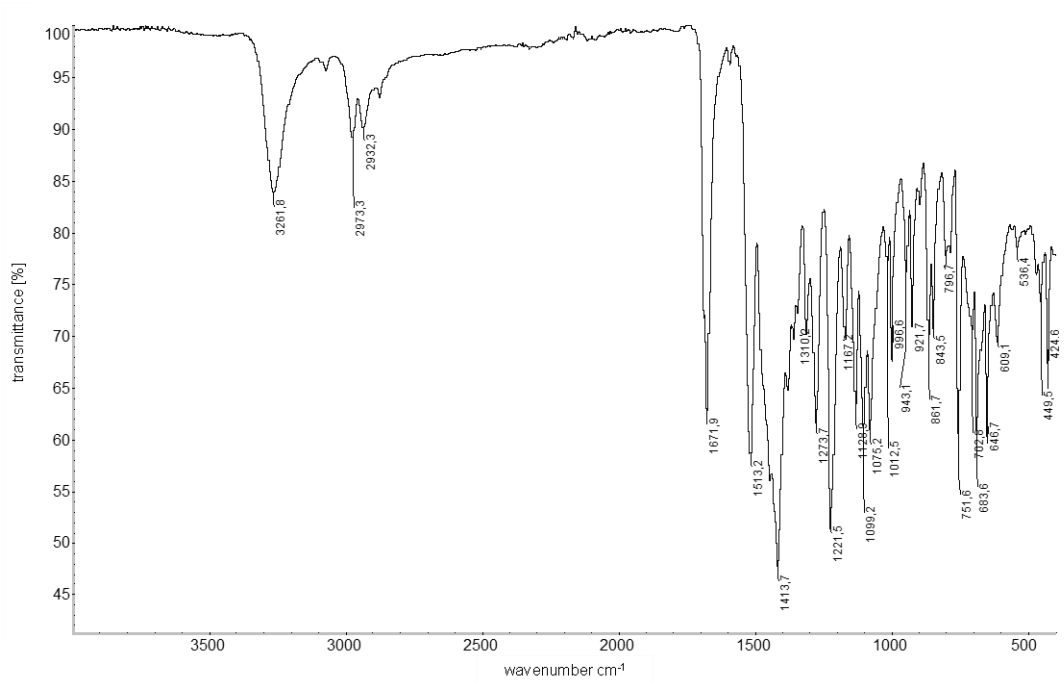

Figure A 86: ATR IR of $\mathbf{L_{NN}1}$.

A-4.2 Complex 1

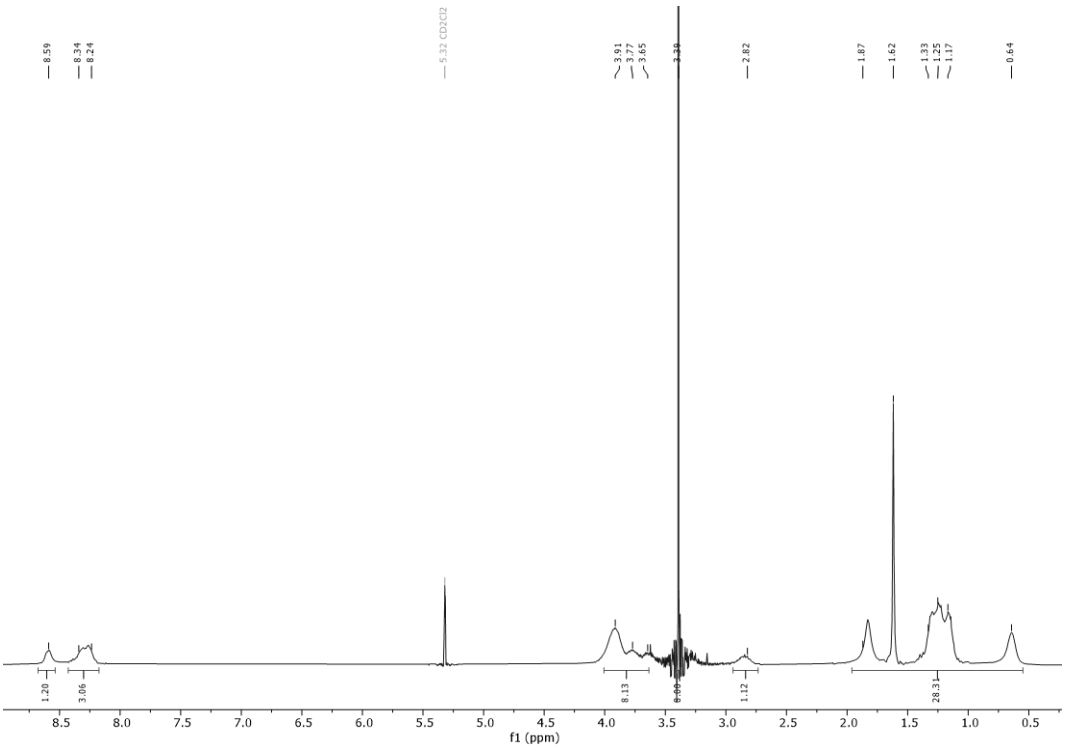

Figure A 87: ^{1}H NMR spectrum of complex **1** (CD_2Cl_2, 300 MHz, 298.0 K).

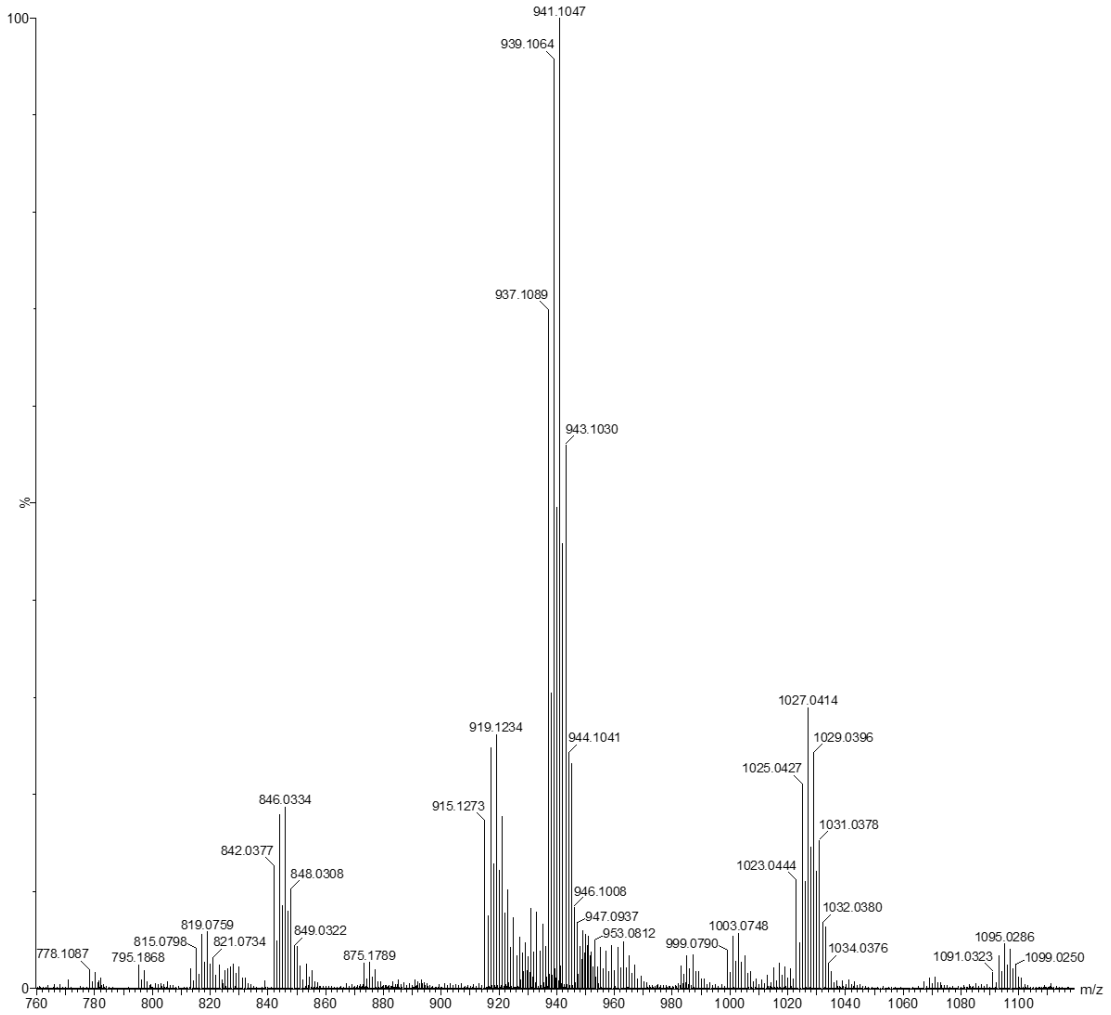

Figure A 88: HRMS of complex **1** (ESI^+, MeOH/0.1% HCOOH in H_2O).

X-ray crystal structure analysis of complex **1**:

Data were collected on a Bruker Kappa APEX II Duo diffractometer. The structure was solved by direct methods (SHELXS-97: Sheldrick, G. M. *Acta Cryst.* **2008**, *A64*, 112.) and refined by full-matrix least-squares procedures on F^2 (SHELXL-2018: Sheldrick, G. M. *Acta Cryst.* **2015**, *C71*, 3.). XP (Bruker AXS) was used for graphical representation. Contributions of further disordered solvent were removed from the diffraction data using the SQUEEZE procedure in PLATON (Spek, A. L. *Acta Cryst.* **2009**, *D65*, 148).

Crystal data of **1**: $C_{39.6}H_{58.4}N_{10}O_{9.6}S_4Zn_3$, M = 1152.51, monoclinic, space group Pc, $\bar{1}a$ = 17.3256(6), b = 16.7889(6), c = 20.1778(7) Å, β = 100.2946(12)°, V = 5774.8(4) Å^3, T = 150(2) K, Z = 4, 130292 reflections measured, 26531 independent reflections (R_{int} = 0.0275), final R values ($I > 2\sigma(I)$): R_1 = 0.0413, wR_2 = 0.1037, final R values (all data): R_1 = 0.0444, wR_2 = 0.1054, 1236 parameters.

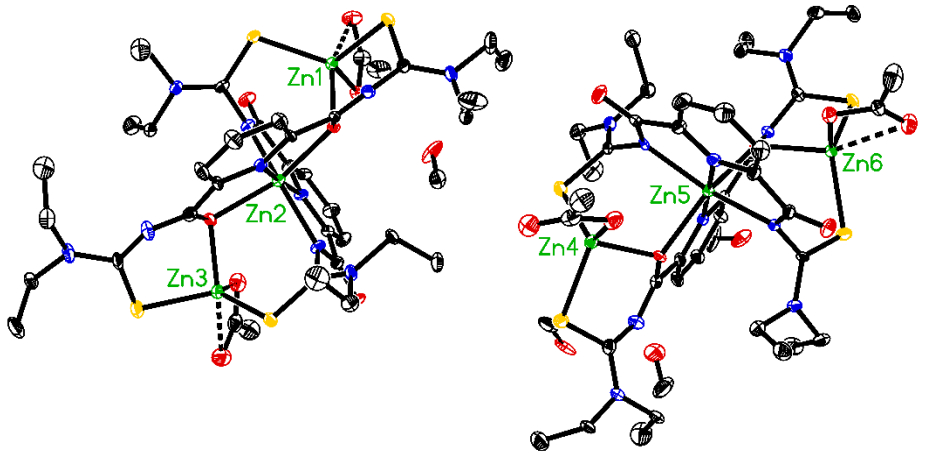

Figure A 89: Molecular structure of complex **1**. Displacement ellipsoids correspond to 30% probability. Hydrogen atoms are omitted for clarity.

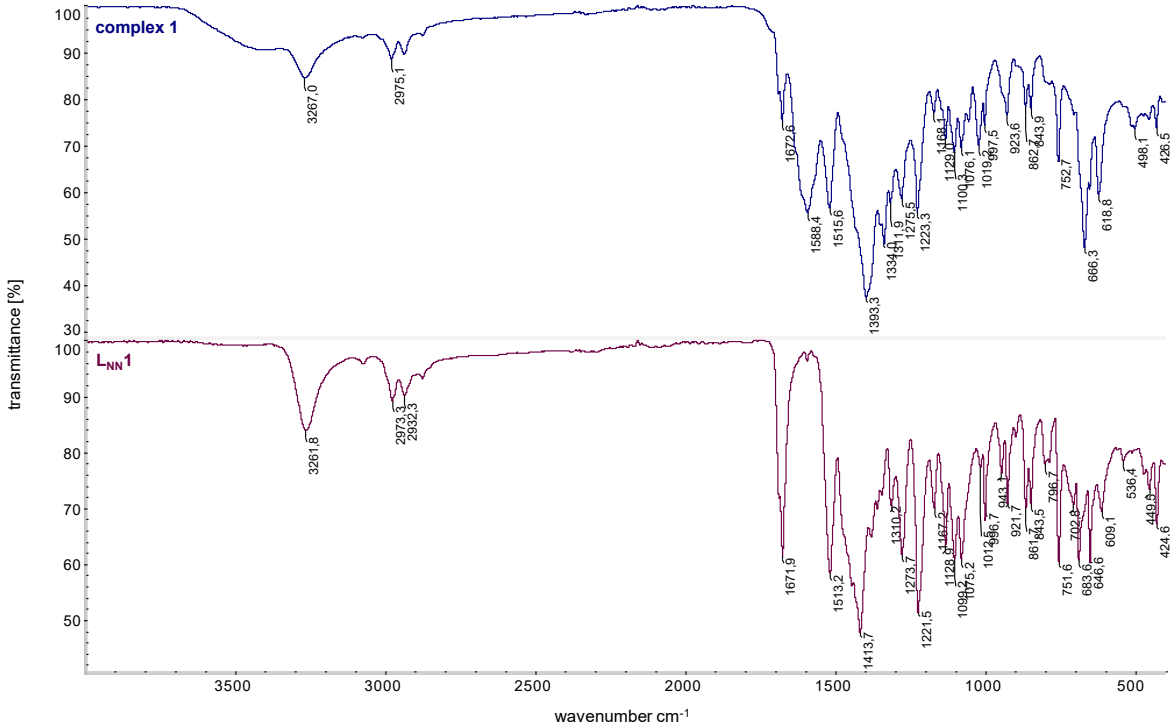

Figure A 90: ATR IR of complex **1.**

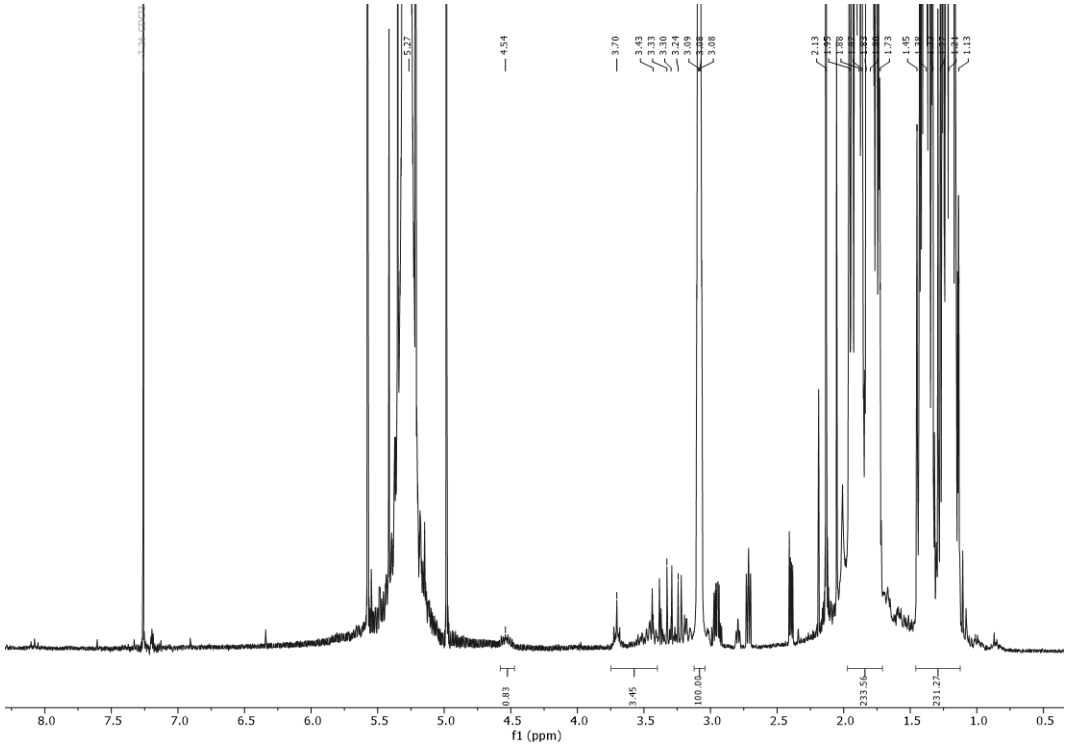

Figure A 91: ^{1}H NMR spectrum of CHO/CO_2 copolymer before workup using complex **1** ($CDCl_3$, 300 MHz, 297.5 K).

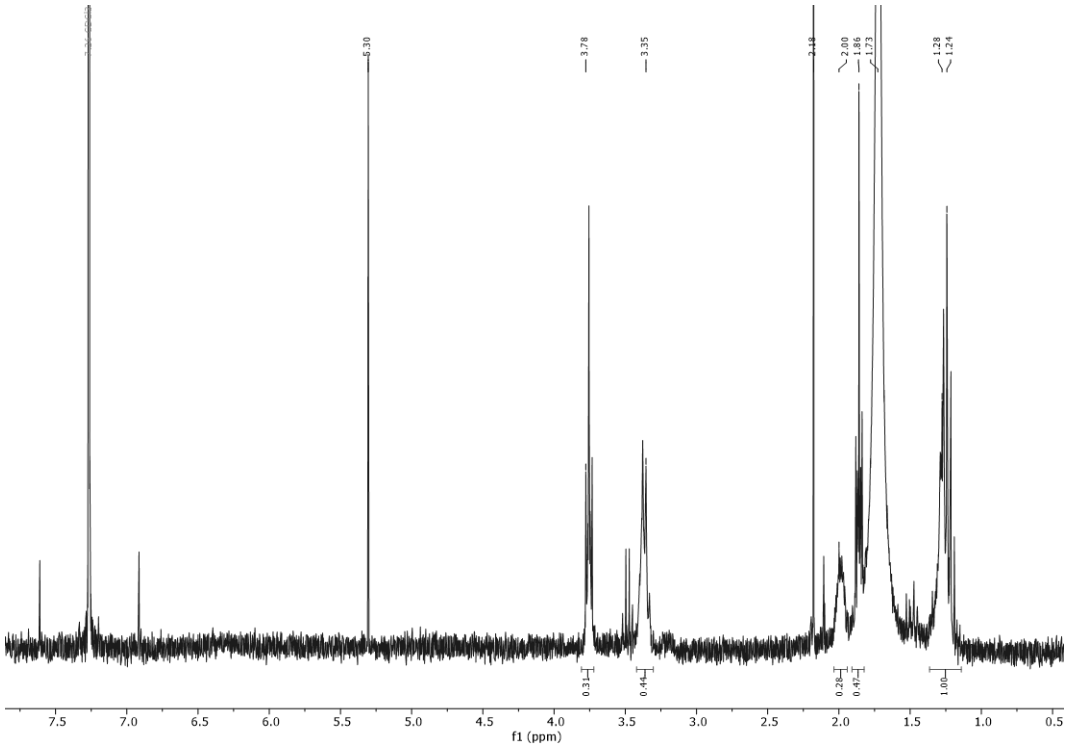

Figure A 92: ^{1}H NMR spectrum of CHO/CO_2 copolymer after workup using complex **1** ($CDCl_3$, 300 MHz, 297.5 K).

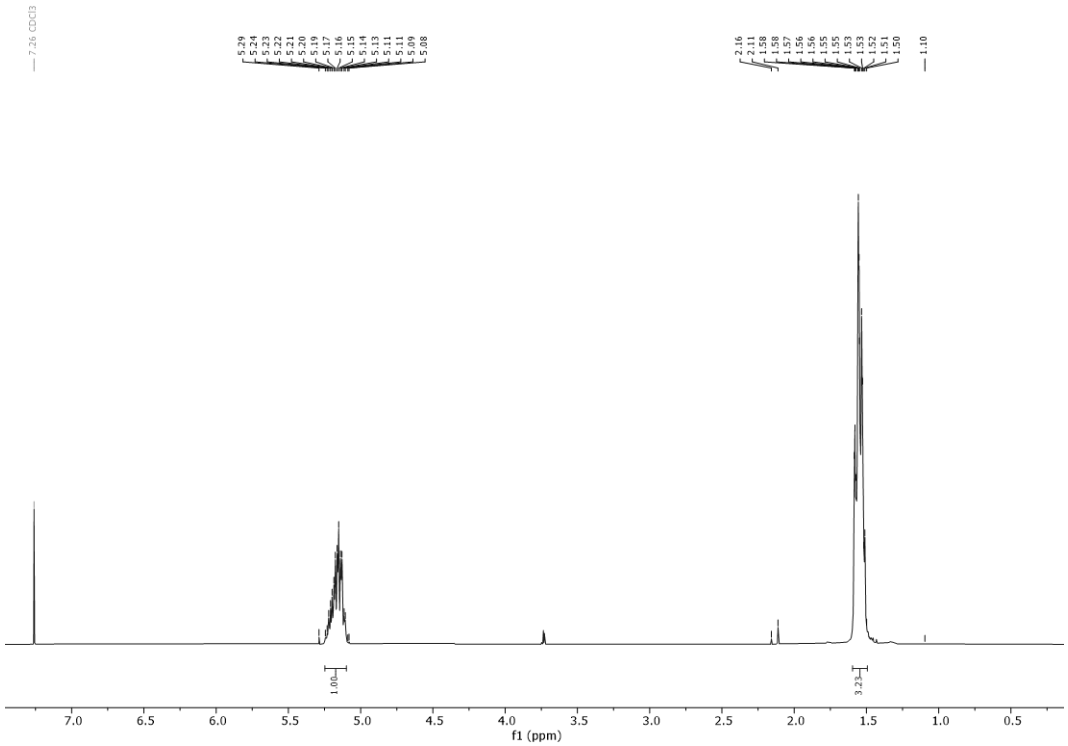

Figure A 93: ^{1}H NMR of PLA prepared using 1 mol% complex **1** ($CDCl_3$, 300 MHz, 298.0 K).

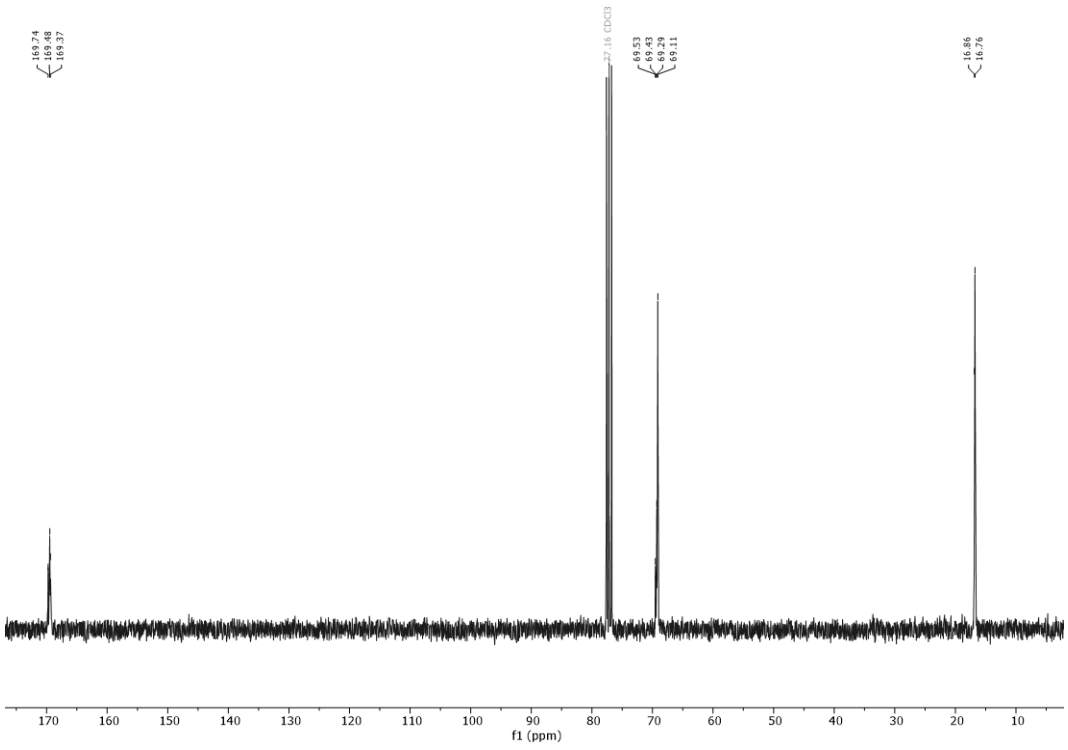

Figure A 94: ^{13}C NMR of PLA prepared using 1 mol% complex **1** ($CDCl_3$, 75 MHz, 298.0 K).

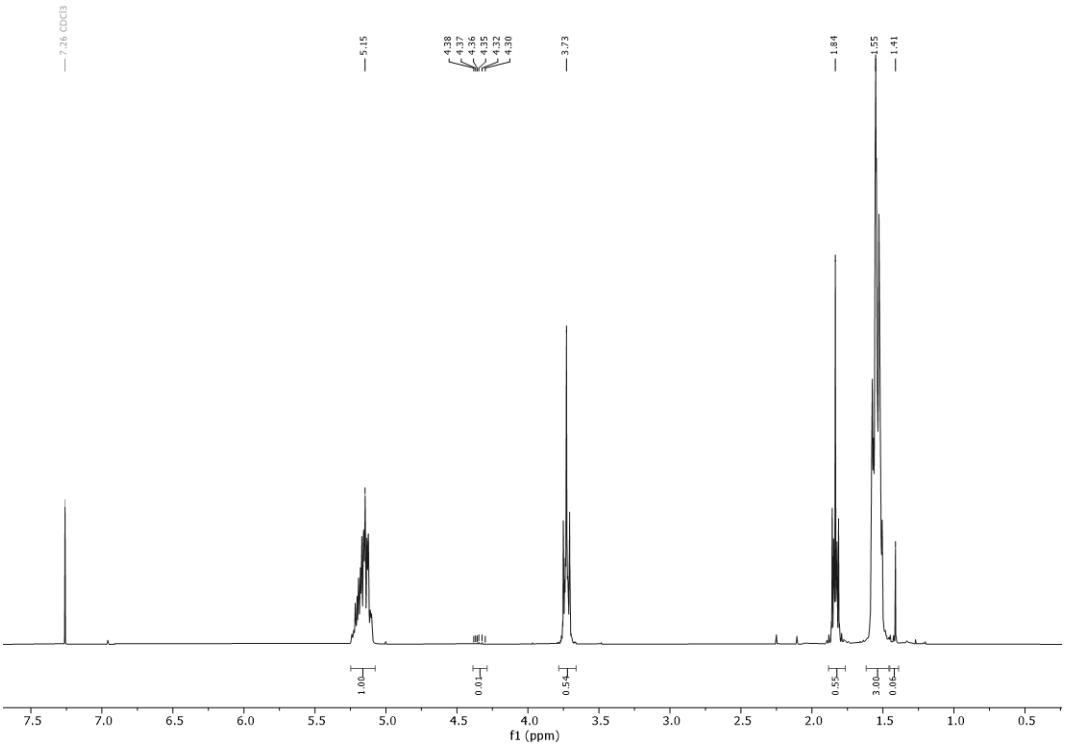

Figure A 95: ^{1}H NMR of PLA prepared using 3 mol% complex **1** ($CDCl_3$, 300 MHz, 298.0 K).

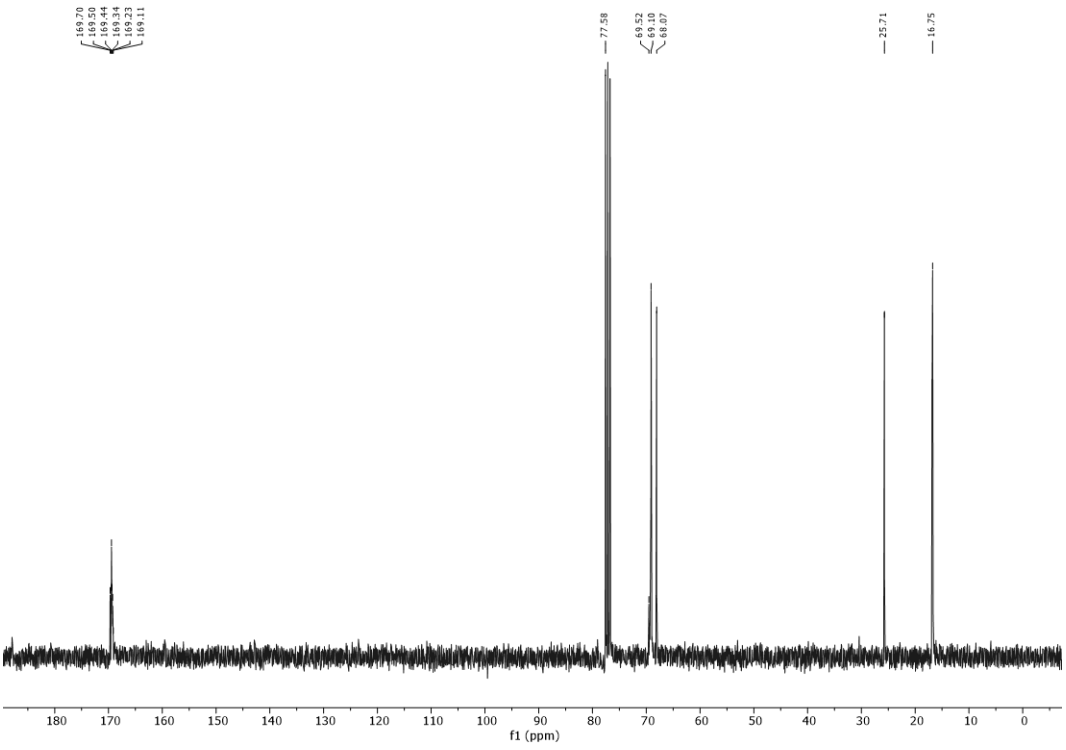

Figure A 96: ^{13}C NMR of PLA prepared using 3 mol% complex **1** ($CDCl_3$, 75 MHz, 298.0 K).

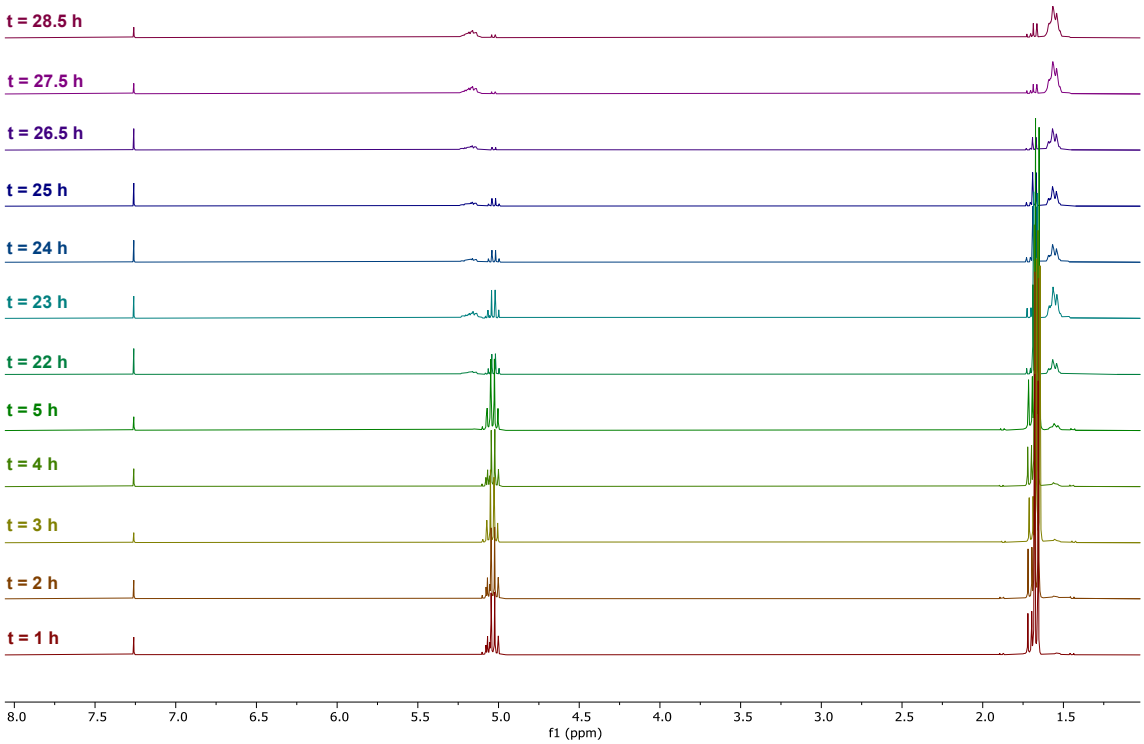

Figure A 97: ^{1}H NMR monitoring of the PLA polymerization using complex **1** ($CDCl_3$, 300 MHz, 298.0 K).

A-4.3 Complex 2

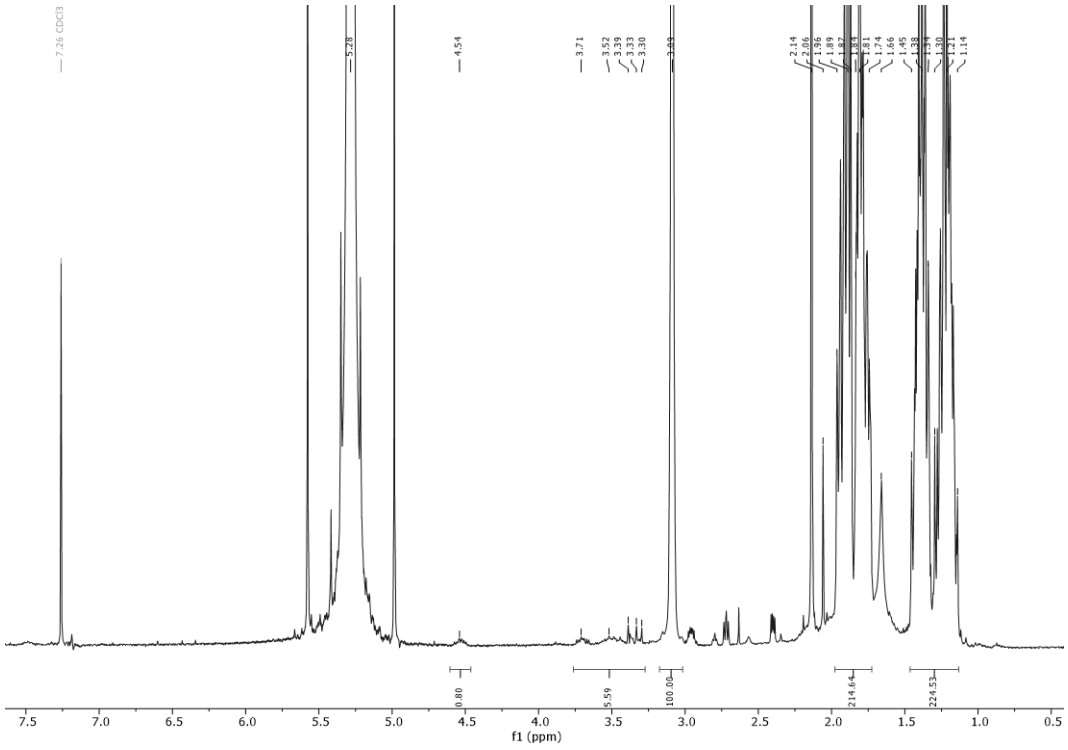

Figure A 98: ^{1}H NMR spectrum of CHO/CO_2 copolymer before workup using complex **2** ($CDCl_3$, 300 MHz, 297.5 K).

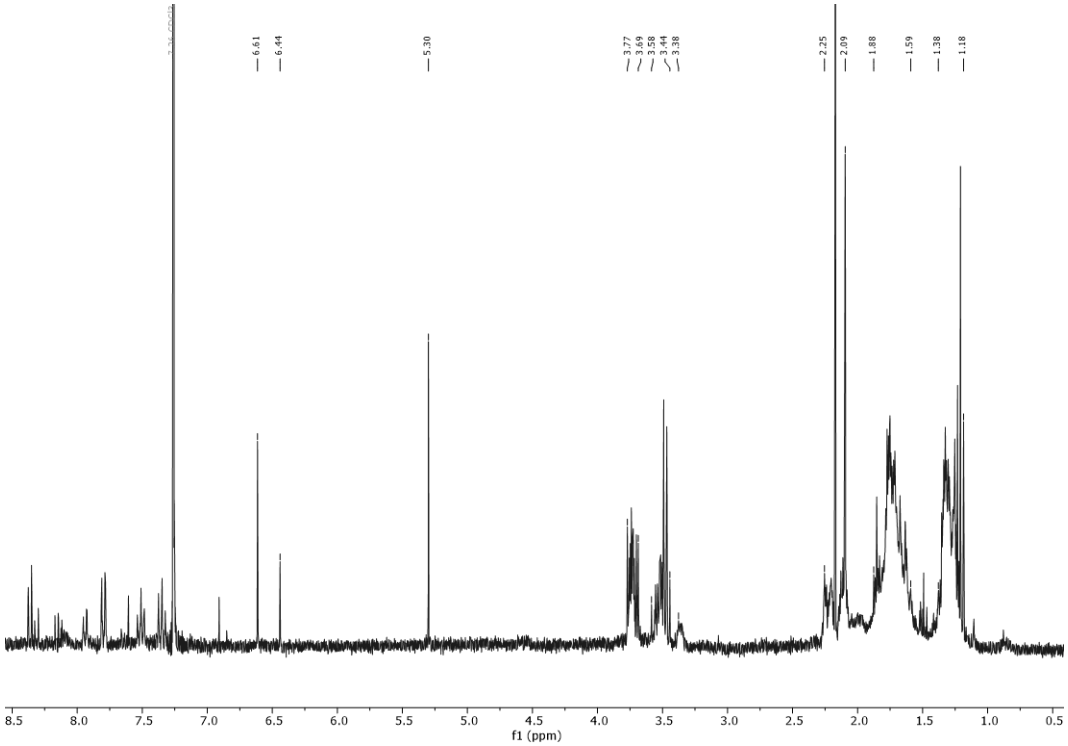

Figure A 99: ^{1}H NMR spectrum of CHO/CO_2 copolymer after workup using complex **2** ($CDCl_3$, 300 MHz, 297.5 K).

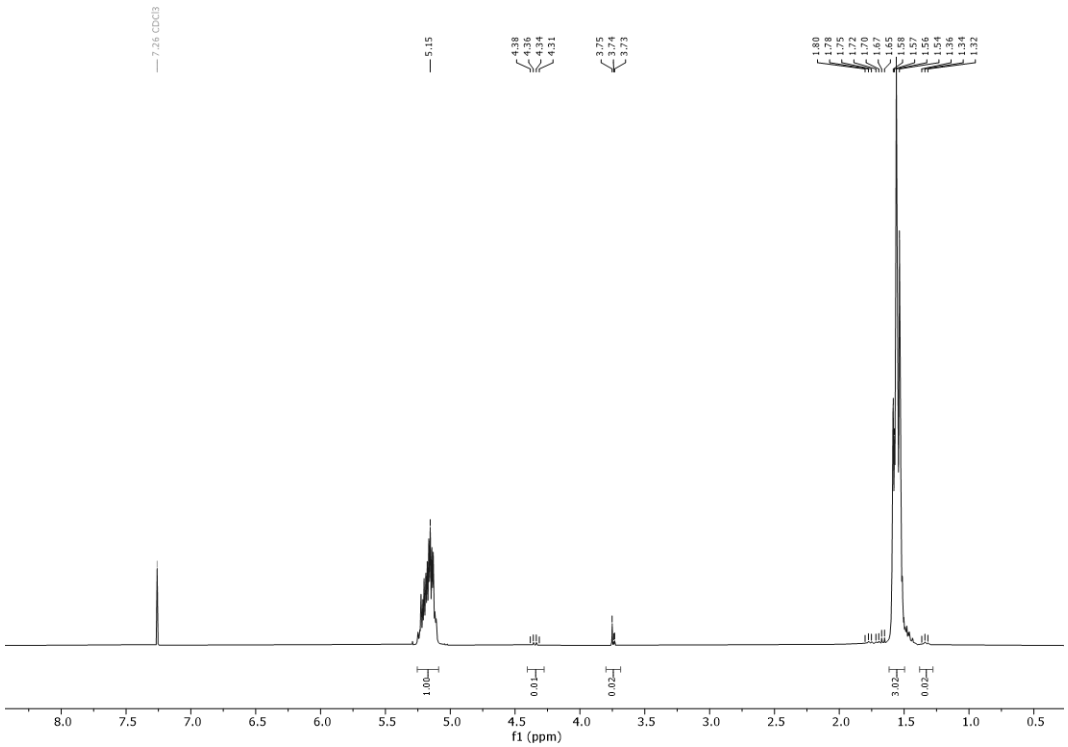

Figure A 100: ^{1}H NMR of PLA prepared using 0.5 mol% complex **2** ($CDCl_3$, 300 MHz, 297.0 K).

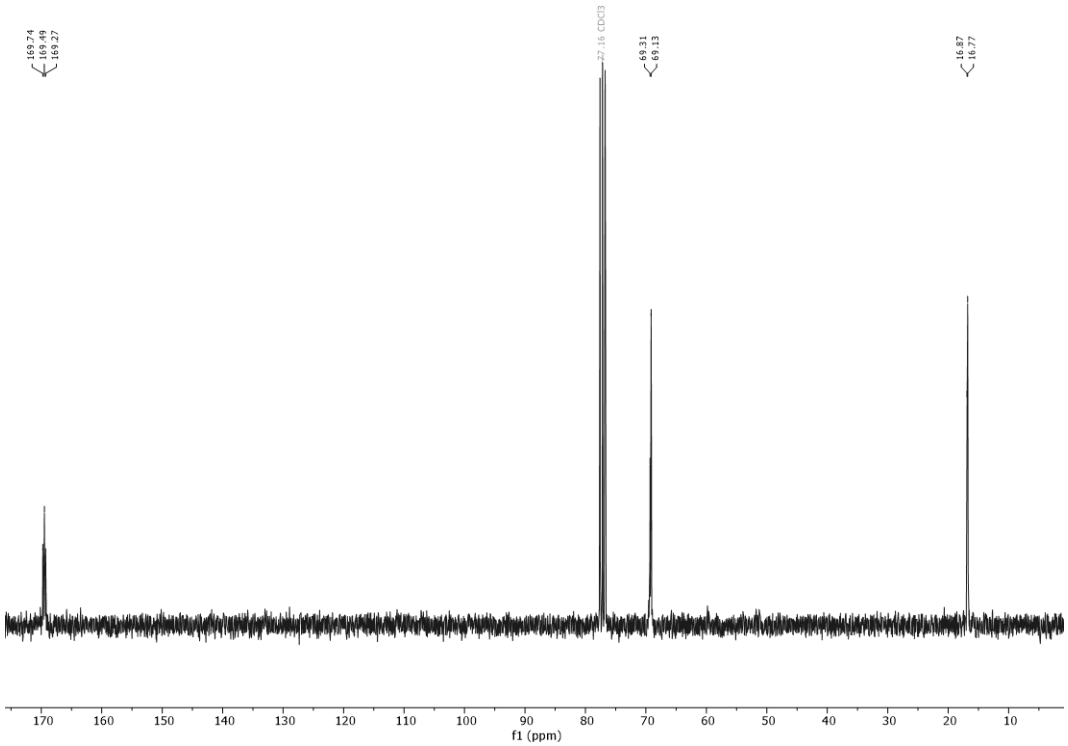

Figure A 101: ^{13}C NMR of PLA prepared using 0.5 mol% complex **2** ($CDCl_3$, 75 MHz, 298.0 K).

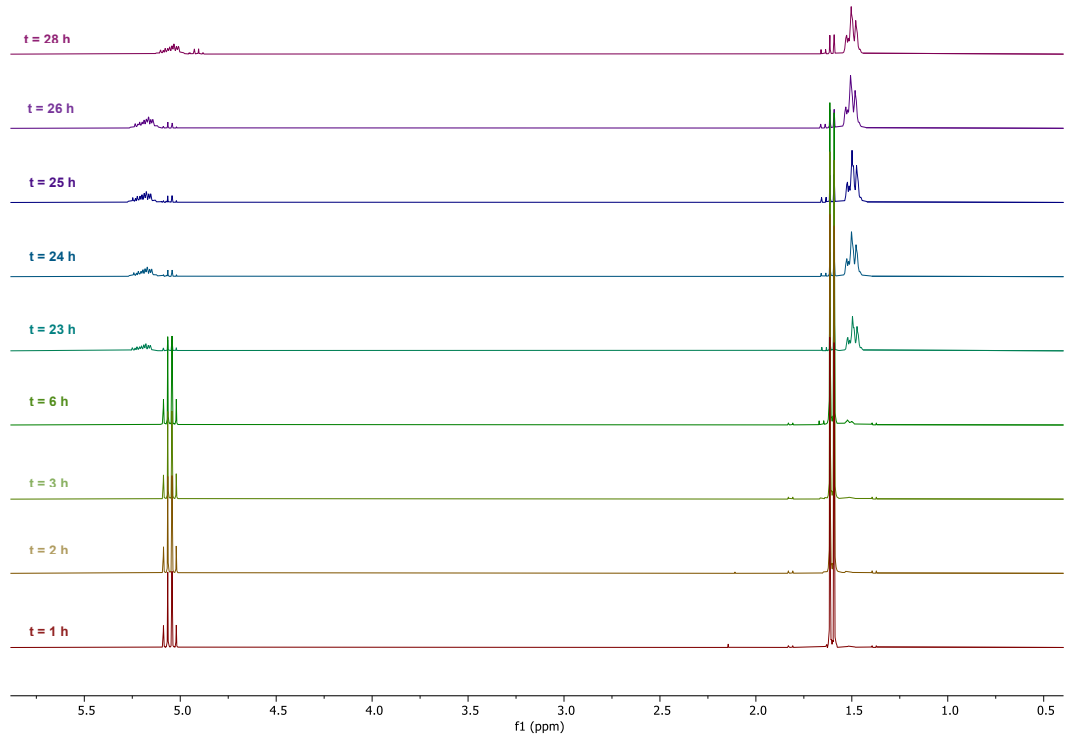

Figure A 102: ^{1}H NMR monitoring of the PLA polymerization using complex **2** ($CDCl_3$, 300 MHz, 298.0 K).

A-4.4 Complex 3

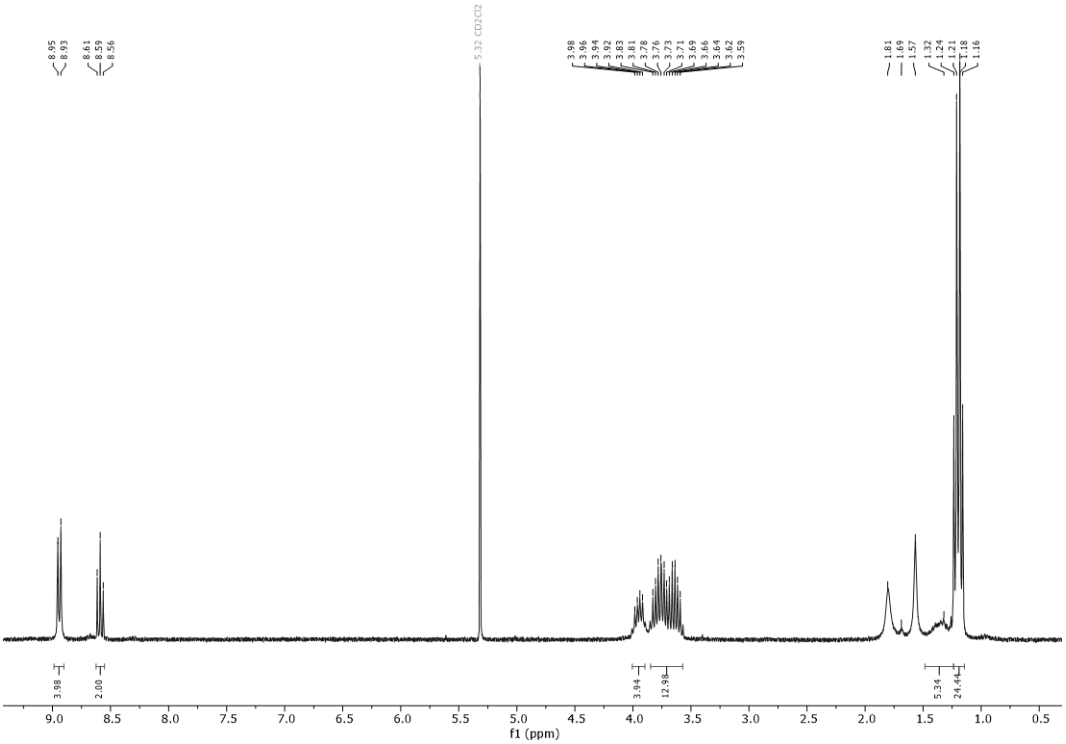

Figure A 103: ^{1}H NMR spectrum of complex **3** (CD_2Cl_2, 300 MHz, 298.0 K).

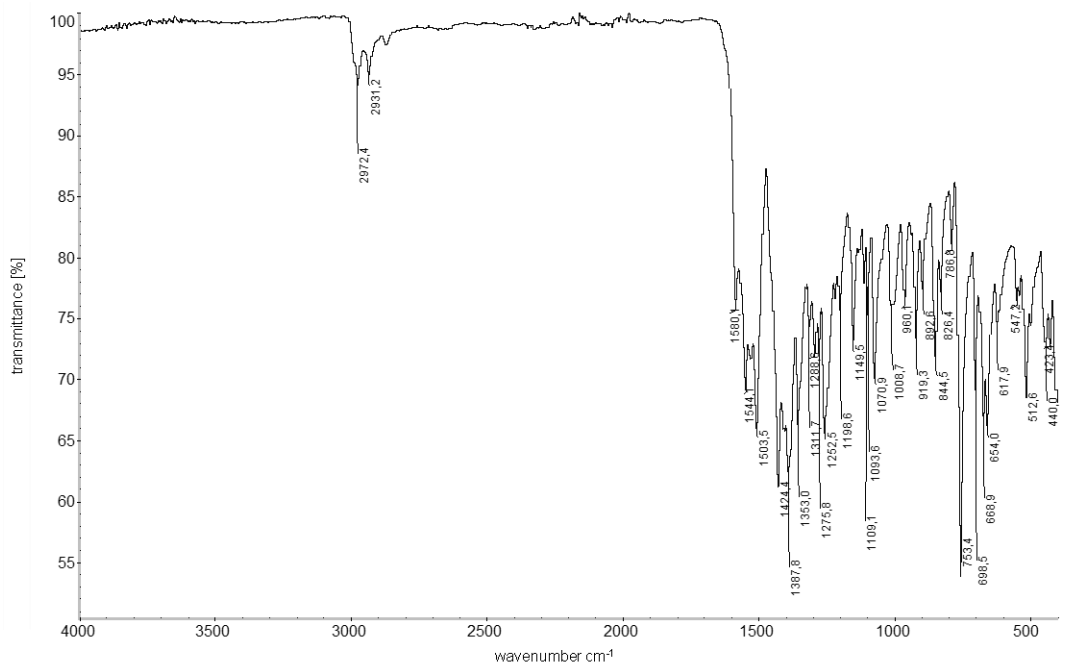

Figure A 104: ATR IR of complex **3**.

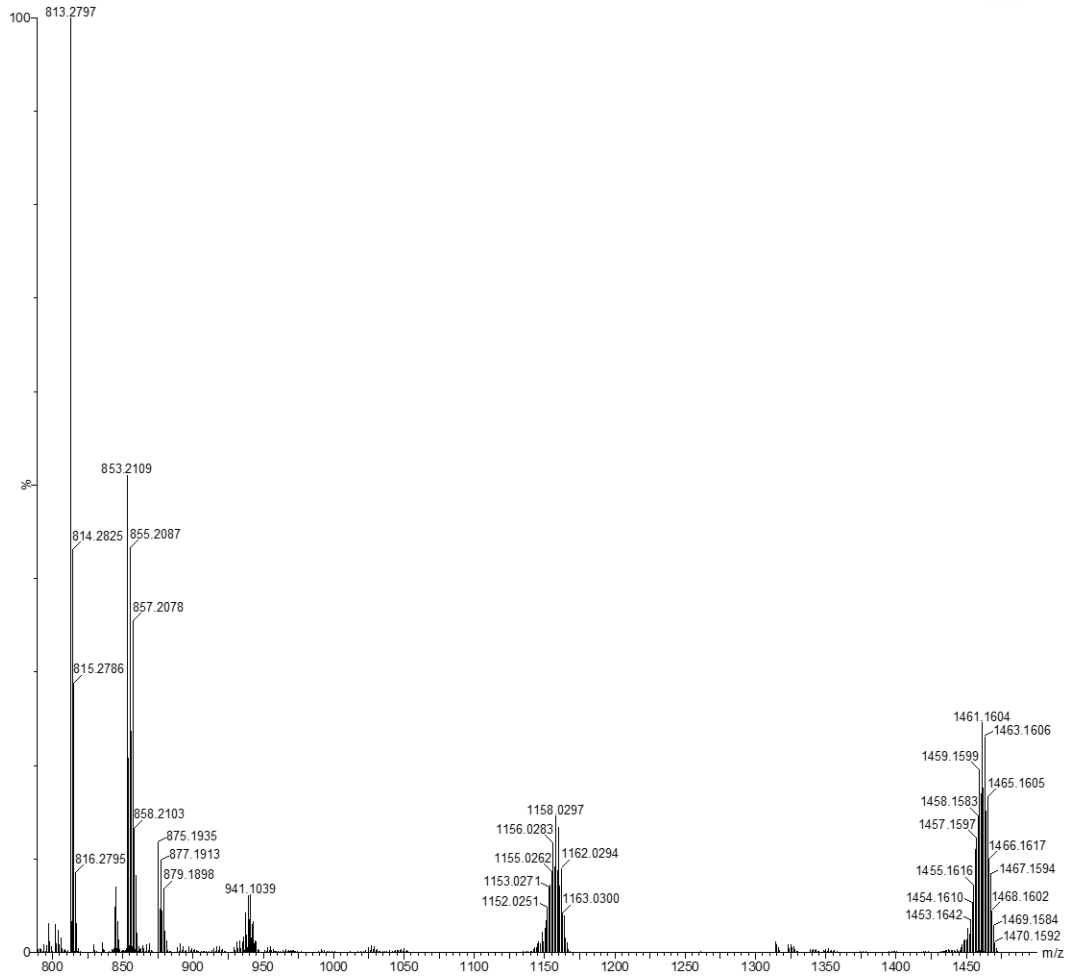

Figure A 105: HRMS of complex **3** (ESI^+, MeOH/0.1% HCOOH in H_2O).:

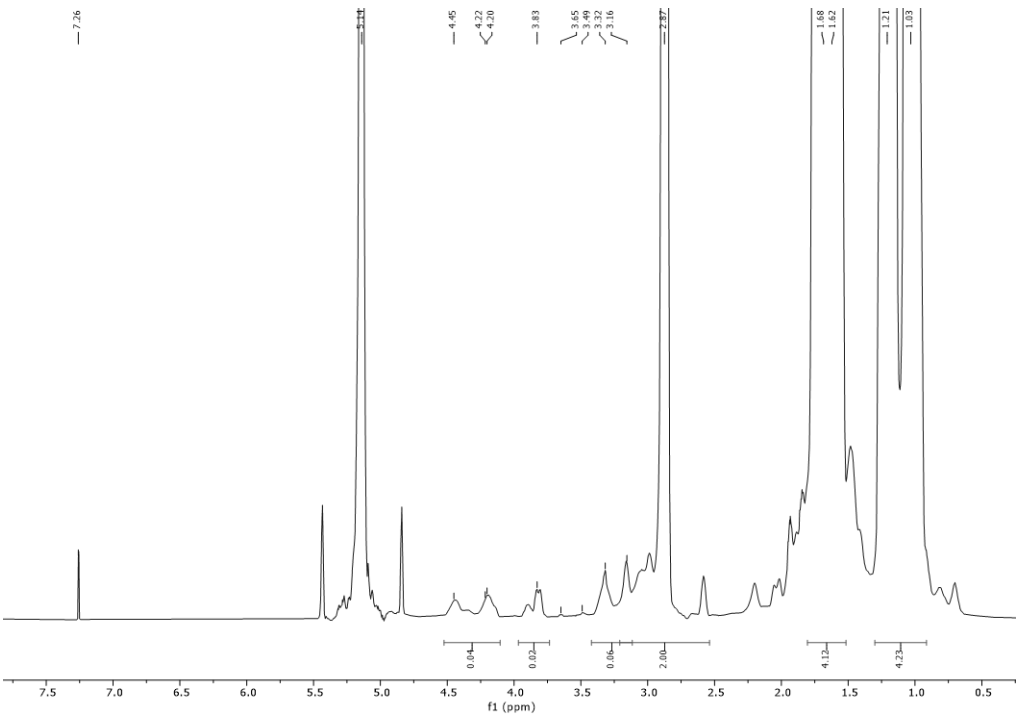

Figure A 106: ^1H NMR spectrum of CHO/CO_2 copolymer before workup using complex **3** ($CDCl_3$, 300 MHz, 297.8 K).

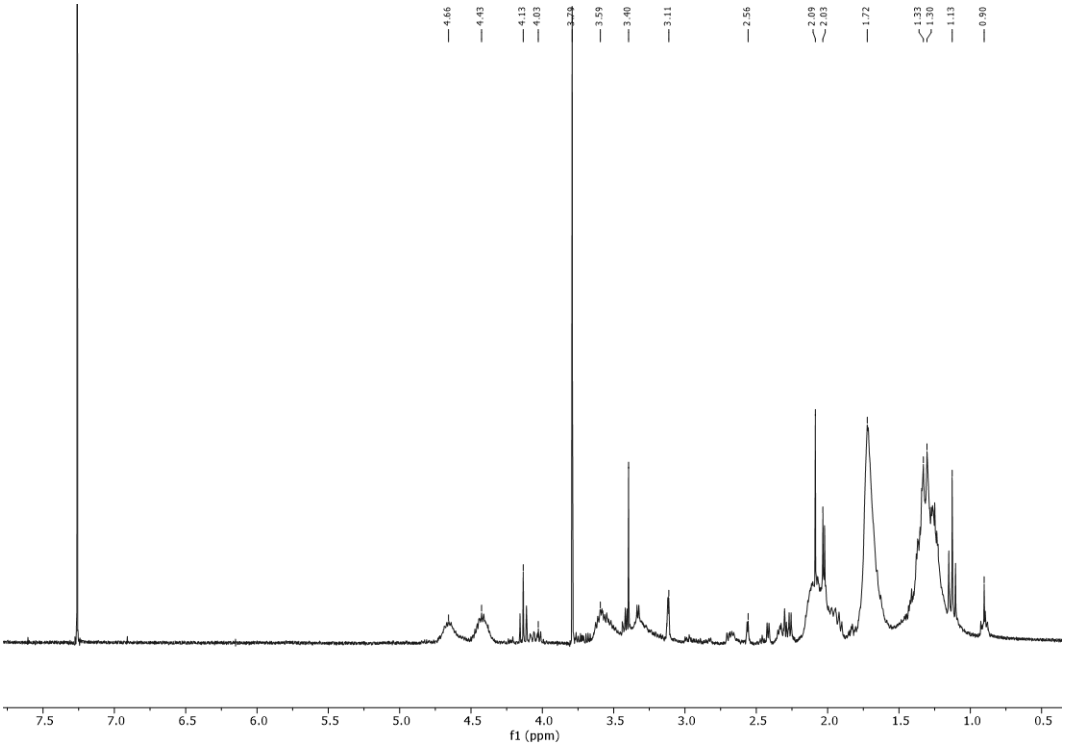

Figure A 107: ^{1}H NMR spectrum of CHO/CO_2 copolymer after workup using complex **3** ($CDCl_3$, 300 MHz, 300.0 K).

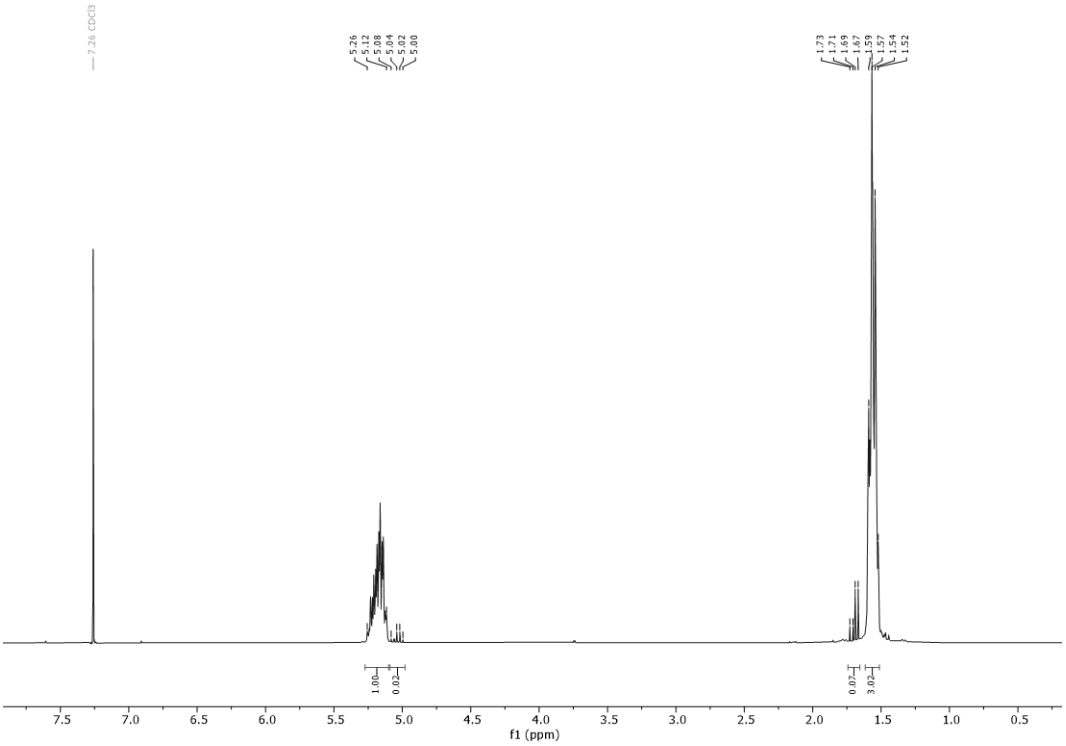

Figure A 108: ^{1}H NMR of PLA prepared using 0.5 mol% complex **3** ($CDCl_3$, 300 MHz, 297.5 K).

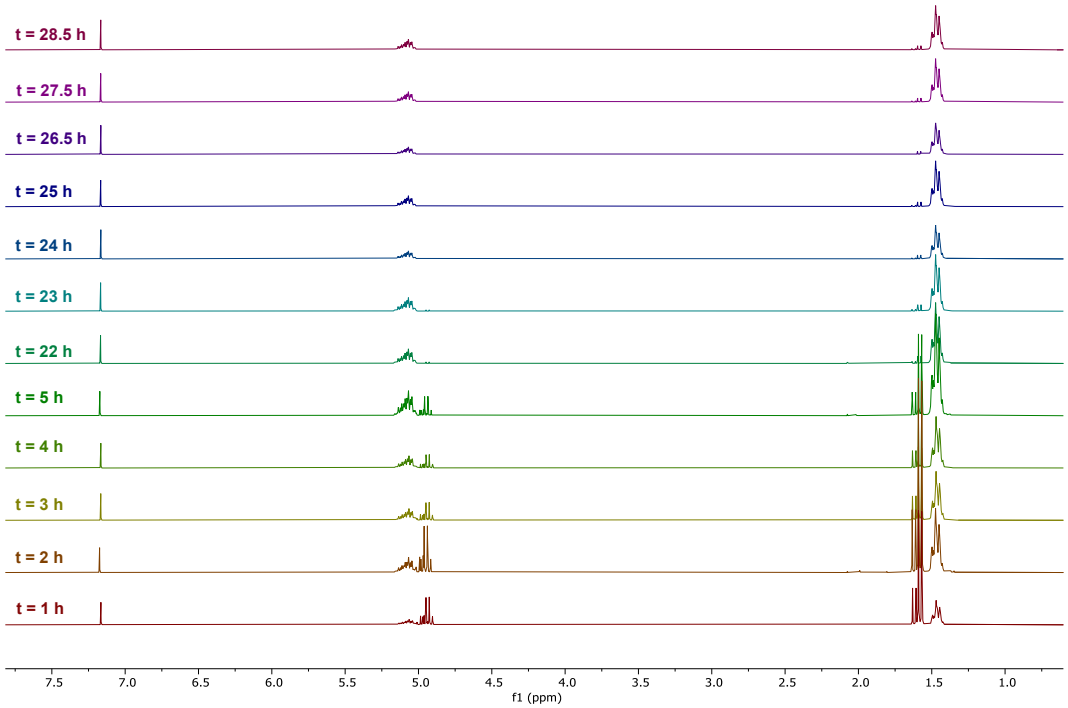

Figure A 109: ^{1}H NMR monitoring of the PLA polymerization using complex **3** ($CDCl_3$, 300 MHz, 297.5 K).

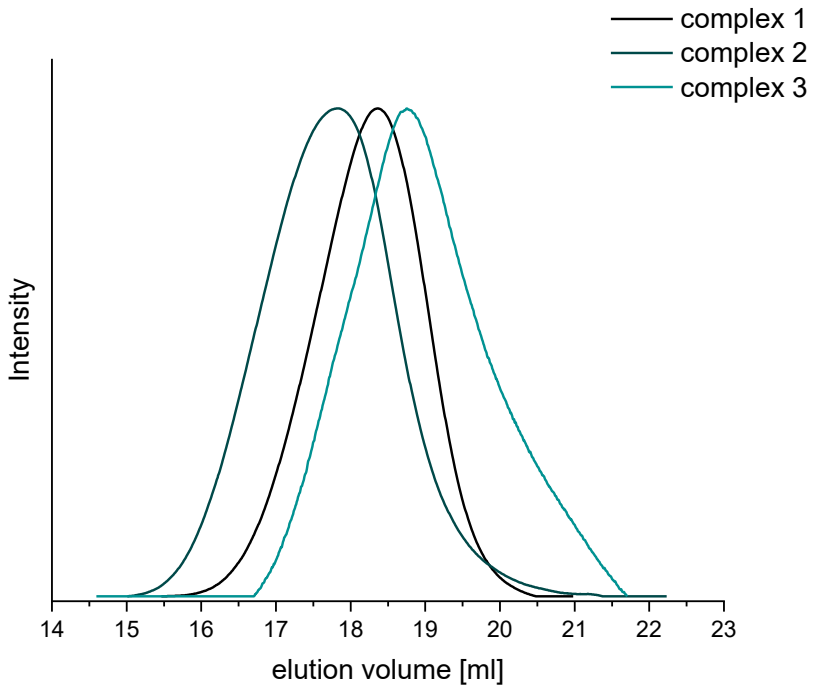

Figure A 110: GPC Chromatograms of PLA samples prepared with complex **1**, **2** and **3** (eluent: THF, standard: polystyrene).

A-4.5 Complex 4

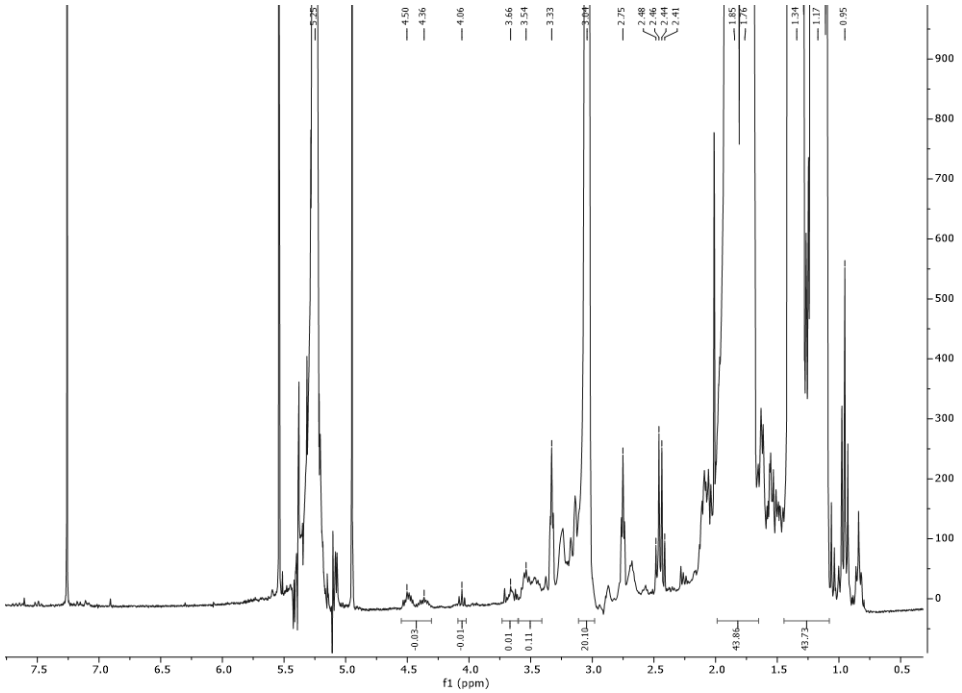

Figure A 111: ^{1}H NMR spectrum of CHO/CO_2 copolymer before workup using complex **4** ($CDCl_3$, 300 MHz, 297.2 K).

A-4.6 Complex 5

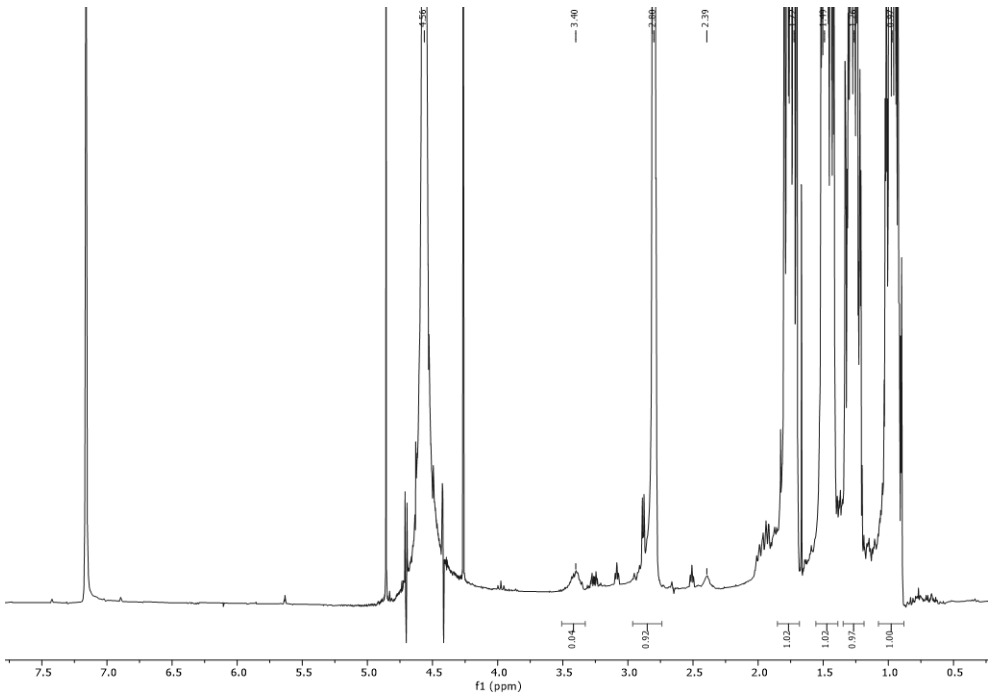

Figure A 112: ^{1}H NMR spectrum of CHO/CO_2 copolymer before workup using complex **5** (C_6D_6, 300 MHz, 297.6 K).

A-4.7 Complex 6

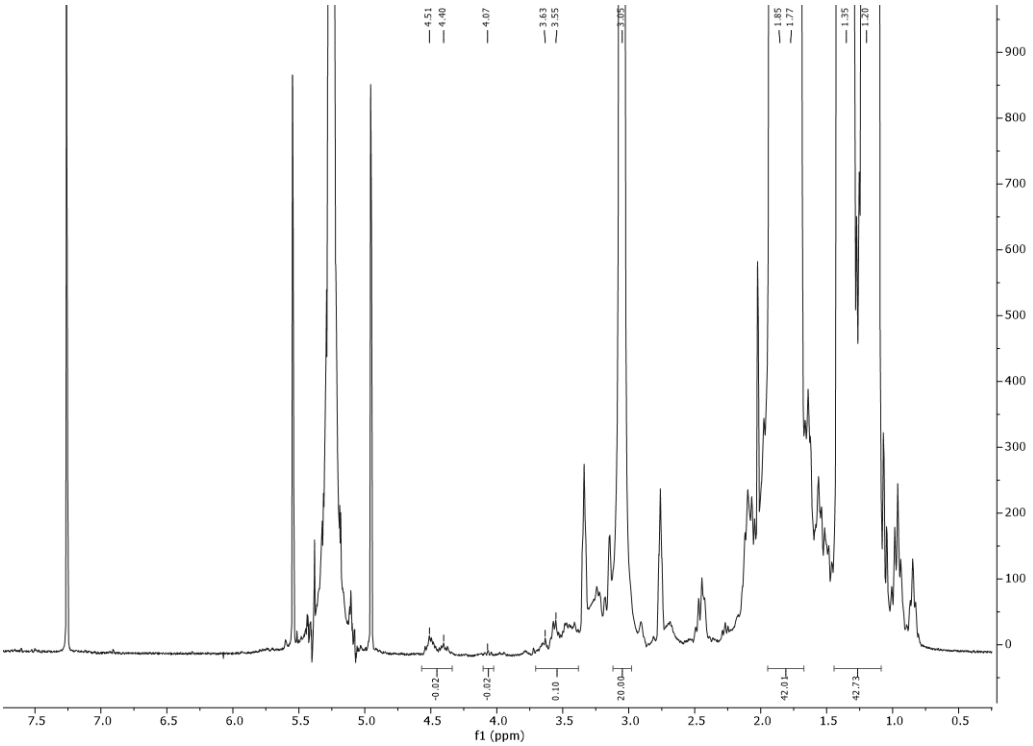

Figure A 113: ^{1}H NMR spectrum of CHO/CO_2 copolymer before workup using complex **6** ($CDCl_3$, 300 MHz, 297.4 K).

A-5 References

[1] B. M. Fung, A. K. Khitrin, K. Ermolaev, *J. Magn. Reson.* **2000**, *142*, 97-101.
[2] J. H. Scofield, *J. Electron Spectrosc. Relat. Phenom.* **1976**, *8*, 129-137.
[3] L. Zander, C. Kunze, J. Klein et al., EP2694210B1, Henkel AG & Co KGaA, **2014**.
[4] C. T. Pham, H. H. Nguyen, A. Hagenbach, U. Abram, *Inorg. Chem.* **2017**, *56*, 11406-11416.
[5] M. Yokoyama, T. Ikuma, N. Obara, H. Togo, *J. Chem. Soc., Perkin Trans. 1* **1990**, 3243-3247.
[6] J. C. Wojdeł, S. T. Bromley, F. Illas, J. C. Jansen, *J. Mol. Model.* **2007**, *13*, 751-756.
[7] J. P. Perdew, Y. Wang, *Phys. Rev. B* **1992**, *45*, 13244-13249.